Aalborg Universitet

Harmonic State Space (HSS) Modeling for Power Electronic Based Power Systems

Kwon, Jun Bum

Publication date:
2017

Document Version
Publisher's PDF, also known as Version of record

Link to publication from Aalborg University

HARMONIC STATE SPACE (HSS) MODELING FOR POWER ELECTRONIC BASED POWER SYSTEMS

BY
JUN BUM KWON

DISSERTATION SUBMITTED 2017

AALBORG UNIVERSITY
DENMARK

HARMONIC STATE SPACE (HSS) MODELING FOR POWER ELECTRONIC BASED POWER SYSTEMS

by

Jun Bum Kwon

AALBORG UNIVERSITY
DENMARK

Dissertation submitted to Faculty of Engineering and Science

at Aalborg University

.

ABSTRACT

The increasing number of renewable energy sources in the distribution grid is becoming a major issue for utility companies since grid-connected converters are operating at different operating points due to the probabilistic characteristics of the renewable energy system. Especially, wideband harmonics and resonances are challenging the stability and power quality of emerging power electronic based power systems. Usually, the harmonics and impedance from other renewable energy sources are not taken carefully into account in the installation and design phase of the systems. However, it can bring an unknown harmonic instability into a multiple power sourced system and make the analysis difficult due to the complexity of the grid network. Hence, harmonic modeling and analysis of power converters are becoming important. Furthermore, the complex interactions on both ac and dc sides of a converter, and the propagated interaction to other systems have been a big challenging task for modeling of the power converter.

This thesis is divided into five parts. The modeling challenge in power electronic systems and the general tools for verification are explained in Chapter 1. The Harmonic State Space (HSS) modeling method is introduced to solve the modeling challenge of power converters in Chapter 2. Additionally, the properties of HSS modeling are compared with several well-known modeling methods in power electronics. For instance, the state-space averaging, the generalized averaging, the dq-domain modeling and the harmonic linearization method are investigated to map their basic properties, modeling procedure and limitation. Based on the theory of HSS modeling, the Voltage Source Converter (VSC) based grid connected system is applied to the first application in Chapter 3 in order to investigate the steady-state and dynamic harmonic interaction between ac and dc side, or ac and ac side. Other power electronic based systems are considered in Chapter 4 in order to analyze the procedure of harmonic transfer, which can be generated from the ac grid and in dc micro grid systems. Furthermore, the diode rectifier is also modeled, where the diode rectifier circuit has been a difficult topology to achieve the frequency response due to their Switching Instant Variation (SIV) as well as the frequency coupling between ac and dc side. Finally, the HSS modeling is applied to analyze the Linear Time-varying Periodically (LTP) stability in Chapter 5 in order to identify some hidden stability regions.

The main contributions of this thesis are the development of HSS (LTP) model for power electronic based systems. The models can be used for the analysis of harmonic interaction between source and loads, and their power converter. The results are verified by the time-domain simulations as well as the experimental setup to investigate how the harmonics are dynamically coupled and transferred with each other. Furthermore, the developed HSS model allows showing the different stability regions, which can not be found in the Linear Time Invariant (LTI) model, which is typical used.

DANSK RESUME

Det stigende antal af vedvarende energikilder med effektelektroniske konvertere i distributionsnettet er ved at blive et problem for forsyningsselskaber, idet nettilsluttede konvertere opererer i forskellige arbejdspunkter på grund af de probabilistiske egenskaber ved de vedvarende energisystemer og interagerer med hinanden. Især harmoniske spændinger og resonanser udfordrer stabiliteten i et bredt frekvens-område og dermed spændings-kvaliteten af de nye effekt elektroniske baserede elsystemer. Normalt er de harmoniske interaktioner og impedansen fra andre vedvarende energikilder ikke taget i betragtning ved design og installation af de vedvarende energisystemer. Men det kan medføre harmonisk ustabilitet i el-systemet og analysen er vanskelig på grund af kompleksiteten af el-systemet. Derfor er harmonisk modellering og analyse af effektkonvertere blevet vigtigt. Desuden har de komplekse interaktioner på både AC og DC siden af en konverter også en indflydelse på de andre systemer, hvilket udvider kompleksiteten.

Denne afhandling er opdelt i fem dele. Modellerings-udfordringerne ved effektelektroniske systemer og de generelle værktøjer til verifikation af modellerne forklares i kapitel 1. Harmonic State Space (HSS) modelleringsmetoden er introduceret i kapitel 2 for at løse modelleringsudfordringerne. Derudover er HSS modellerings egenskaberne sammenlignet med en række kendte modelleringsmetoder anvendt indenfor effektelektronik. For eksempel er state-space modellering, en generaliseret middelværdimetode, DQ-domæne modellering og harmoniske linearisierings metode undersøgt for at kortlægge deres grundlæggende egenskaber, deres modellerings procedure og deres begrænsninger. Baseret på teorien omkring HSS modellering, er Voltage Source Converteren (VSC) anvendt i et nettilsluttet system og i kapitel 3 er de stationære og de dynamiske harmoniske interaktioner mellem AC og DC siden, samt til nettet analyseret. Et anden effekt-elektronisk baseret system er undersøgt i kapitel 4 for at analysere sammenhængen i den harmoniske overførsel imellem systemerne, som kan genereres både fra AC nettet og i et DC net. Endvidere er diode-ensretter systemer også modelleret, idet diode-ensretterkredsløbet er en vanskelig topologi at opnå frekvenskarakterstik omkring grundet dens variation i tænde-tider og som gør det vanskelig at finde frekvens-koblingen mellem AC og DC siden. Endelig anvendes HSS modelleringen til at analysere den Lineære Tidsvarierende Periodisk (LTP) stabilitet i kapitel 5 for el-systemer, hvor hensigten er at identificere nogle skjulte stabilitets regioner.

De vigtigste bidrag fra denne afhandling er udvikling af nye HSS og LTP modeller for effekt-elektroniske systemer. Modellerne kan anvendes til analyse det harmoniske samspil mellem effekt-generatorerne (vedvarende energi-kilder) og belastningerne. Resultaterne er afprøvet med tids-domæne simuleringer, samt på forsøgsopstillinger for at undersøge, hvordan harmoniske er dynamisk koblet og overføres til hinanden i et el-system. Endvidere giver den udviklede HSS model

mulighed for at afsløre forskellige stabilitet regioner, der ikke kan findes i de lineære tidsinvariante (LTI) modeller, som typisk er brugt i dag til effekt-elektroniske systemer.

ACKNOWLEDGEMENTS

I would like to express my sincere gratitude and appreciation to my supervisor Prof. Frede Blaabjerg for his valuable guidance, patience, kindness, suggestions and encouragement throughout whole PhD study. His invaluable support, understanding and expertise have been very important in completing this work.

I also want to express my sincere gratitude and appreciation to my co-supervisor Prof. Claus Leth Bak, who gave me a lot of advices in terms of power system studies and their harmonic behavior as well. Your attitude and mind on work and life will be always in my mind.

I also would like to appreciate Associate Prof. Xiongfei Wang for his advice, continuous support, and friendship while I work in the Harmony group. I hope you do not struggle anymore because of my publications.

I also would like to represent many thanks to all Harmony members for their passion and discussion to the projects and publications. Especially to Remus Narcis Beres, Changwoo Yoon, Zhen Xin, Haofeng Bai, Minghui Lu, and Dapeng Lu. Additionally, Esmaeil and Kazem. Special thanks to Miguel Esparza, who was the guest researcher in AAU for 1 year. It was really glad to have a chance to discuss with you regarding the same research topic.

I also would like to express additional gratitude to all Frede`s group members, especially, Huai, Yongheng, Pooya, Dao, Zian, Hamid, Busca and Vasile, for their continuous help and assistance for 3 years. Especially, thanks to Feng yang for his collaboration and effort on the work.

I also would like to show my gratitude to all staffs and people at Department of Energy Technology. Especially, thanks to Anna and Casper for their help and efforts to manage the Harmony project.

TABLE OF CONTENTS

CHAPTER 1. INTRODUCTION

This chapter presents the background and motivation of this research project followed by its objectives. Then, the thesis ouline is prsented. Finally, all publications related to this research work are listed at the end of the chpater.

1.1. "HARMONY" IN POWER ELECTRONICS

The global consumption of electrical energy is drastically growing and it is forecasted that it will be more than doubled within 20 years. The cost to generate electric power is therefore also expected to increase. Hence, it is urgently required that the production, distribution and the use of electrical energy should be managed efficiently, and the price should also be done cheaper than today. Additionally, advanced technology is also required to satisfy the requirement of the consumer. One of the main technologies to achieve this goal is to use "power electronic based systems" which can efficiently convert electrical energy from the source level to the load level by using power semiconductors and control technologies. Hence, the power electronic based systems are key technologies of the future power systems. The traditional fossil based energy system will continuously be changed to renewable energy based system in the future as depicted in Figure 1-1. In such a case, the energy conversion technology to improve the reliability and efficiency as well as the analysis technique to avoid the interaction between them will be a major issue in the future, since the grid is becoming much more power electronics interfaced with many energy devices. Especially, modeling, mitigation, detection and analysis of the harmonics and resonances among the interfaced devices are critically required in order to make them operate safe in "Harmony" with each other.
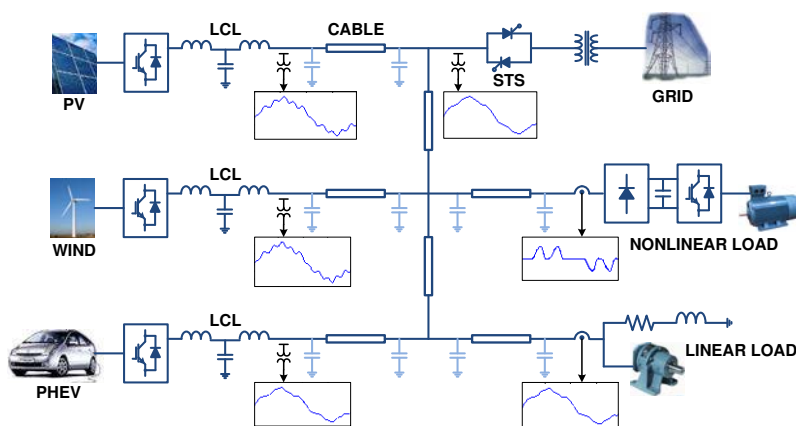
Figure 1-1. Harmonic propagation at system level [1] in a power electronic based power systems

1.2. PROBLEMS & BACKGROUND

As the installation rate of the renewable energy is rising, the local power system might experience challenges like unexpected harmonics, resonances and stability problems. The traditional energy source was mainly dependent on the generator, and the problems which were needed to take care of were mainly at very low frequency below 1 Hz in order to manage the oscillation from prime mover as well as excitation control. On the other hand, the future trends are moving into power electronic based systems in order to achieve more efficiency from renewable energy source and the flexibility of the control of energy. However, the new systems bring more complex situations which need to be solved because of the switch in network and their high frequency switching during the operation. Furthermore, the interaction between multiple power electronic based systems gives more challenges (see Figure 2-1) because of their wideband operation from 0.1 Hz to over 3 kHz. The different control bandwidths from different control structure and their multi connection at the same nodes might increase the wideband harmonics as well as the dynamic interaction between them. The phenomena mainly appear as unexpected harmonics, resonances and also an unstable behavior of the systems.

Several challenges can be found in the real world. The Danish transmission grid from Grenaa to Anholt experiences unexpected harmonics and also damped resonances on both sides, and they can affect the overall power quality as well as to the stable operation [2] of the system. The world largest wind farms in Gansu province, China are also experiencing similar problems in respect to high frequency resonances and the unexpected low frequency harmonics [3]. Furthermore, the bidirectional operation of locomotive systems in Switzerland as well as the interaction between the offshore power converters and the wind turbines in Germany [4] have demonstrated some of the same phenomena, and they have shut down the whole system at the end. Conclusively, a proper way to analyze the resonance and harmonics are urgently required in order to stabilize the power electronic based systems.
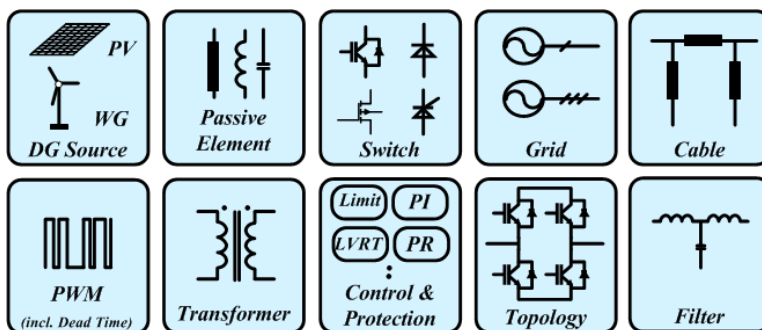
Figure 1-2. Possible Harmonic Sources in a DG System

1.3. MODELLING CHALLANGES

Several modeling methods have already been introduced to analyze the harmonics and resonance interaction between systems. The results from them can be classified into two categories as being in time-domain or in frequency-domain. Even though the analysis from the result of time-domain simulation is an easy way to investigate the phenomena, the problem is that each simulation will take longer in the time-domain as the number of circuits is increasing. Furthermore, it does not give any analytical results at the end. However, the resonance and harmonic analysis from the frequency domain can give more analytical results as well as give intuitive answers to the users. Hence, it is important to use a proper modeling method in order to get more accurate frequency responses.

Power electronic based systems are fundamentally composed by several components as shown in Figure 1-2. Most of them have nonlinear and time-varying characteristics. The average based methods have been widely used to achieve the linear frequency response from the nonlinear – time-varying systems. The approaches are simple and easy to get the simple responses. However, the results can only be obtained based on several assumptions, where the dc-side of the power converter is always constant and the effects of ripples on the outputs are very small and will be neglected for the simplification.

The importance of the neglected information from the averaged model may be more crucial as the number of the considered systems is increasing in the analysis, while it could be enough to use in the analysis of a single converter. The main behavior that we need to take into account in the analysis can be found in the real operation of power converter as shown in Figure 1-3. The generated power from source side is transferred to the load side through the switching. However, it is worth to note that the direction of power is bi-directionally exchanging on both ac- and dc-side through the switching as depicted in Figure 1-3, where it means that the impedance behind the switches affect the frequency response in the ac-side as well. Hence, the consideration of the introduced behavior in the modeling procedure can be very important to achieve more accurate frequency responses. The detailed comparison between the conventional modeling methods and the proposed method will be described in Chapter 2 in the thesis.

As discussed in Figure 1-2, there are many components that we need to consider to obtain the real frequency response. However, "Frequency Coupling" and "Switching Instant Variation (SIV)", two particular challenges of the traditional modeling approach are mainly discussed in this chapter in order to emphasize the frequency shift and their effect on the resonance analysis. The neglection of the nonlinear characteristics of the inductor or transformer is available based on the assumption, that the converter only operates in the linear region. However, the effect of two selected components can not be neglected because it always exists in the converter operation. The procedure by which these challenges can be met is discussed in the next section.
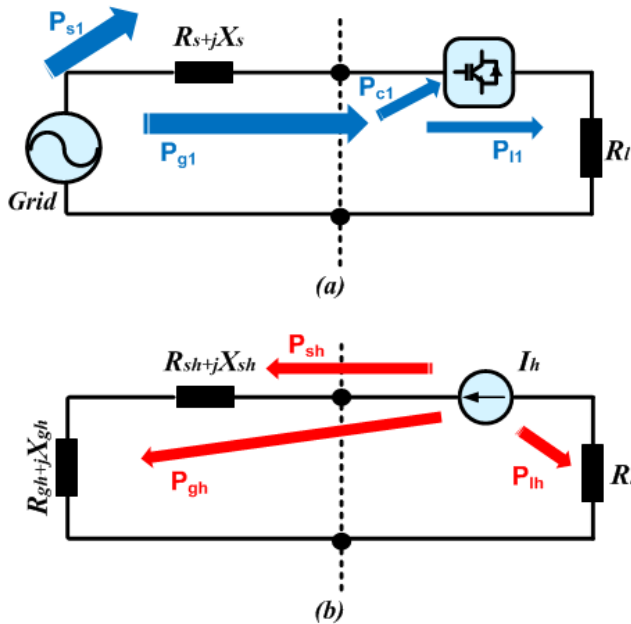
Figure 1-3. Block diagram of harmonic power flow in a DG System[5], where P_{g1} is the generator power supply, P_{s1} is additional power losses, P_{c1} is a small part converted to the power converter, R_l is purely resistive load, R_s+jX_s is the line with its impedance, P_{l1} is the transferred energy to the load and the total power losses are the sum of them ($P_{sh}+P_{lh}+P_{gh}+P_{s1}$), (a) Power flow at the fundamental frequency, (b) harmonic power flow

1.3.1. FREQUENCY (HARMONIC) COUPLING

The voltage and current source power converters used in the grid are usually composed of four parts; the dc network, ac network, controller, and switching network. The power flow and coupling of the frequencies can simply be described as shown in Figure 1-4-(a). Firstly, the ac current (i_{ac}) from the ac network is modulated by switches (IGBTs or MOSFETs) which results in a dc current (i_{dc}). Secondly, the dc network converts the dc current to the dc voltage (v_{dc}) and the dc voltage is converted to the ac side voltage (v_{ac}). The ac voltage interacts with the ac system source and the impedance results in an ac current change. This process (along with the controller coupling and response) creates a feedback loop, which governs the overall system response. If it is assumed that the dc side voltage is independent of the dc side current, the model can be simplified for linearization and analysis. However, for harmonic and stability analysis, this simplification is not easily correct. For instance, if the ac grid current has a small component at f_g and the converter modulation frequency components include f_m, at least one of the two frequencies $f_g + f_m$ and $f_g - f_m$ will be seen on the dc side. If this current results in voltage on the dc side, that will be transferred back to the originating frequency (and

others) on the ac side, closing a feedback loop that includes the dc side impedance at a different frequency. These frequencies may be transferred to an other connected converter and then be involved in another frequency coupling. These frequency couplings are not only necessary for harmonic analysis, but also the frequency coupling may trigger instability by changing the location of the original dominant poles [4]. This behavior is caused by the coupling between many frequencies on both sides of the converter, the frequency dependent impedances on both sides of the converter, and of course the control system contribution.
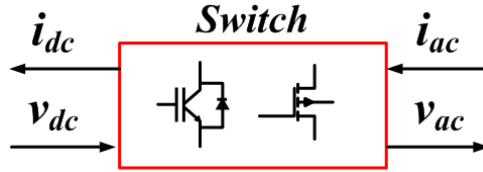
(a)
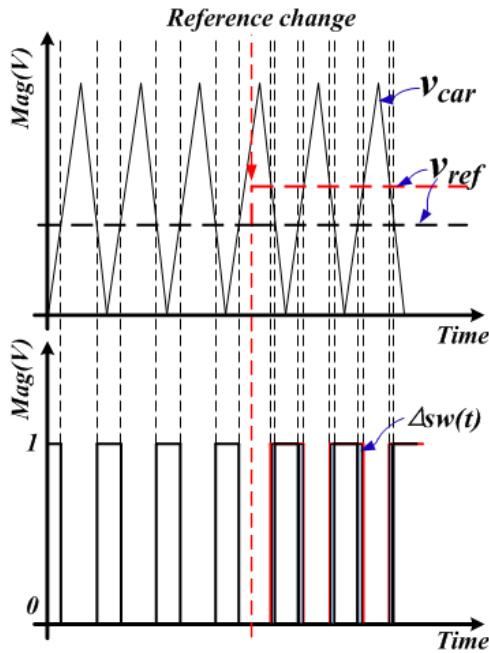
(b)

Figure 1-4. Difficulties in the modeling procedures of power electronic based systems, (a) Frequency (harmonic) coupling of ac-dc power converter, (b) Switching Instant Variation (SIV) because of the modulation procedure and the change of reference from the control systems.

1.3.2. SWITCHING INSTANT VARIATION (SIV)

In general, any distortion during circuit operation will cause Switching Instant Variations (SIV). The simple behavior of SIV in the voltage source converter is shown in Figure 1-4-(b), where a carrier waveform (v_{car}) is compared with the reference voltage (v_{ref}) from the controller. The change of reference due to the distortion as well as the behavior from the controller may yield a small variation of the switching (Δsw) as shown in Figure 1-4-(b) and it brings the variation of harmonic elements that will affect to the dc and ac circuits as well according to the procedure of frequency coupling. Distortions may come from a transient, and include non-harmonic frequencies. These frequencies are introduced into the switching functions through SIV, which strongly changes the frequency couplings around the converter, particularly by adding frequency components associated with the distortion frequencies. It is very important that SIV is considered in order to reflect these interactions.

SIV can be divided by two categories. The first, here called active SIV, results from control action based on the measured variables, or variables derived from these. Any distortion in any measured variables will propagate through the control response and result in varying switching instants in the controlled converter. These variations generate many frequencies, and in general the control response should be optimized by taking all these frequencies into account. The control systems through which these variations are transferred will include the PLL (Phase Locked Loop) [6], [7], current control and dc-voltage control loop which are normally involved with the reference signal of their controllers. The second, here called passive SIV, is applied particularly to diode and thyristor based converters, where some of the switching instants are not directly controlled, but they are dependent on the circuit state variables. An example is that diodes and thyristors only turn off when their current drops to zero. As a result, time-dependent state variables as well as input and control variables make the modulation procedure time-variant over a comprehensive range of frequencies.

1.4. RESEARCH QUESTIONS AND THESIS OBJECTIVES

This PhD thesis mainly investigates the harmonic models for the analysis of the generators and loads as discussed previously. The main research questions are :

1. Can the HSS model be used to identify unforeseen resonances in power electronic based power systems?

2. Are the frequency responses from the conventional modelling methods still enough to represent all the behaviour of power electronic converters?

3. Can we include the time-varying components as well as the nonlinear components in the frequency response in order to achieve an accurate model?

4. Can we explain the procedure of the harmonic transfer inside the converter and the effect on other connected devices through the frequency responses?

5. Can the harmonics and the frequency coupling effect be used for stability analysis of a single system as well as for multiple connected systems?

6. Can unexpected harmonics and the resonances be estimated if the time-varying behaviour is included in the frequency response?

7. Can we obtain an accurate frequency response of a diode rectifier through the conventional methods and investigate their phase dependency from them as well?

Therefore, this thesis will model the power electronic interfaced generators and loads by using the proposed new modeling method, which is considering the time-varying behavior in the modeling procedure. Firstly, the conventional modeling approaches are compared in order to identify their differences and also why the time-varying components should be considered with. Secondly, the Voltage Source Converter (VSC) based systems are modeled as applications of the proposed method. Additionally, other applications like dc-micro grid and diode rectifier are also modeled to investigate the effect of frequency coupling and their influence on the accuracy of the analysis result in the time-domain. The overall applications are studied by simulations as well as in experimental set-ups with detailed discussions on how the coupled frequency response affect the stability and transient behavior. Finally, the final goal is to obtain "Harmony" between the increasing distributed generation sources and the various power loads by using the proposed method in order to mitigate harmonics and to keep stability in the inner/outer side of the power electronic devices or in the whole grid network.

1.5. METHODOLOGY

1.5.1. SMULATION AND MATHEMATICAL ANALYSIS

MATLAB and PSCAD are considered as the main tools for the modelling and its verification in time-domain. In the case of a single system, PLECS is used to analyse the stability and controllability of the system. Furthermore, the matrix calculations, the state-space modelling and the frequency domain analysis are performed by using the MATLAB-Linear analysis toolbox. However, in the case of the multiple connected systems, the PSCAD is used to reflect the real grid network including cable model and other frequency dependent models. Additionally, the mathematical calculations and their analysis are also performed in MathCad, and Maple depending on the purpose of analysis.

1.5.2. SMALL SCALE EXPERIMENTAL SETUP

To verify the simulation results by experiments, 6 PWM voltage source converters and inverters are used as shown in Figure 1-5. PWM Rectifier with LCL filter is regarded as the dc source of each grid connected inverter. Occasionally, the single dc source is connected to validate the system having a common dc-bus bar. Additionally, the dSPACE platform (DS1007) is used to control the PWM converters individually in real time. A comparison between the simulation analysis and the experimental results are performed in the time domain to verify the modelling results from the frequency domain calculations.
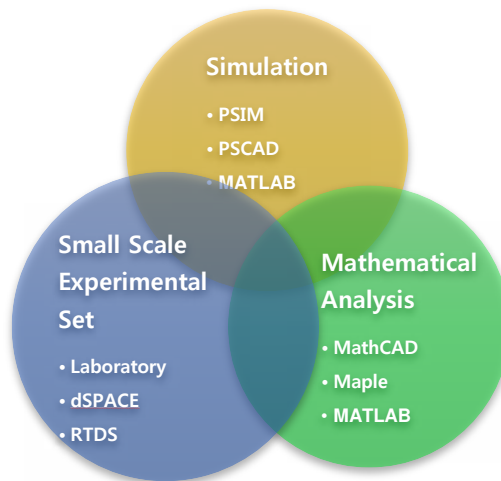
(a)

(b)

Figure 1-5. (a) Methodology overview of the PhD Thesis, (b) Experimental setup for validation of the modeling

1.6. PROJECT LIMITATIONS AND ASSUMPTIONS

In this project, the new model is developed by using the HSS modeling methods. However, the model accuracy is dependent on the number of the selected harmonics in the procedure. Hence, the accuracy of model results can be different according to the target of interest.

The HSS model basically starts from the assumption, where all signals in the power converter and grid are periodically varying. Hence, the analysis can not be properly applied for the systems having the asynchronous behavior as well as the non-periodic operation.

Additionally, the considered time-varying behaviors in the developed model are restricted into two categories as frequency coupling, which is driven by the switching between the ac- and dc-sides, and switching instant variation during the disturbance. The nonlinear elements, which can be found in the inductor, transformer and limiter, are not considered in this thesis.

1.7. OUTLINE OF THE THESIS

The PhD dissertation consists of five chapters and it is organized as follows:

Chapter 1 : Introduction

The background and motivation for the research project are presented including the methodologies, which are used for the validation of research results. Based on research questions given from the background and problems identified, the objective of the project are described as well. Finally, the outline of each chapter and the list of publications are also given.

Chapter 2: Review of modeling methods

A detailed review of the modeling methods are presented in this chapter. The difficulties in the modeling procedure are explained to discuss the limitations of the traditional methods. It can be found that the frequency-coupling as well as the Switching Instant Variation (SIV) are the main concerns of the modeling procedure. Hence, the traditional modeling approaches have advantages and disadvantages according to their application and usage. Finally, the Harmonic State Space (HSS) modeling methods are introduced in details with their structure and the difference are discussed with other modeling methods. The simulation results for the comparison are also presented in order to clarify the limitations of each modeling methods and to emphasize the importance of including both the frequency-coupling and the SIV in the model.

Chapter 3: HSS modeling of VSC based systems

The HSS modeling can include the time-varying components in their procedure and it shows the different behavior with conventional approaches. Hence, the HSS modeling is adapted to develop various power electronic based systems. The single-phase Voltage Source Converter (VSC), 3-phase VSC, Back-to-Back VSC for wind power generation, multiple connected VSC are modeled as applications of the HSS model. The theoretical procedure how to make a model by using this method is also provided in this chapter. A comparison is also done with the time-domain simulations using a commercial tool. Also time-domain results from frequency response are shown and compared with the experiments.

Chapter 4: HSS modeling of other power electronic based systems

The special topologies, which can not accurately be modeled by conventional approaches, are considered in this chapter. The main difficulties in the traditional ways are due to both Switching Instant Variation (SIV) and Frequency Coupling (FC) between ac and dc –sides. The two introduced criteria affect mainly the impedance that is needed to get in order to analyze the system. Furthermore, the phenomena can easily be found in the applications of thyristor or diode where the averaged modeling can not be taken into account in the model. Hence, the HSS modeling is adapted to develop the multiple-frequency response of the diode rectifier. Additionally, the dc-grid is also considered in order to investigate the coupling effects from ac-dc converter to dc-dc converter in order to know how they will affect the quality of dc-output voltage as well as the current. Hence, the DC-grid based on the dc-dc converter and diode rectifiers are modeled as applications of the HSS model. The theoretical procedure on how to make a model by using this method is provided in this chapter. A comparison with the time-domain simulation and the experimental validations is also described.

Chapter 5: Analysis of harmonic instability

The stability issue in power electronic based system is described in this chapter. The traditional approach is based on a Linear Time Invariant (LTI) system. It provides a simple way to investigate the stability of power electronic system by using the Nyquist plot, etc. However, the LTI model can not consider the effect of the time-varying behavior in the stability analysis. However, basically, the HSS modeling method is based on the theory of Linear Time Periodically-varying (LTP) systems, which can take the time-varying behavior into account. The stability of the LTP model is judged by means of the generalized Nyquist plot. The difference between the two models is compared in the simulation as well as in the analytical model. Additionally, a special condition, which can not be analyzed in the LTI model, is also described in this chapter.

Chapter 6: Conclusion and future work

This chapter presents the summary, main findings and conclusion of this thesis. Topics for future research are also discussed. In the end of the thesis, the published papers during the PhD study period are attached.

1.8. LIST OF PUBLICATIONS

A list of the papers, which are published or have been submitted during the PhD study, is given as follows:

Papers related to thesis

A. Journal paper

[J.1] **J. Kwon**, X. Wang, F. Blaabjerg and C. L. Bak, "Frequency Domain Modeling and Simulation of DC Power Electronic Systems", IEEE TRANSACTIONS ON POWER ELECTRONICS, Vol. 32, No. 2, Feb 2017, pp. 1044-1055.

[J.2] **J. Kwon**, X. Wang, F. Blaabjerg, C. L. Bak, A. R. Wood and N. R. Watson, "Harmonic Instability Analysis of Single-Phase Grid Connected Converter using Harmonic State Space (HSS) modeling method", IEEE TRANSACTIONS ON INDUSTRY APPLICATIONS, Vol. 52, No. 5, Sept/Oct 2016, pp. 4188 – 4200.

[J.3] **J. Kwon**, X. Wang, F. Blaabjerg, C. L. Bak, V. S. Sularea and C. Busca, "Harmonic Interaction Analysis in Grid-Connected Converter using Harmonic State Space (HSS) modeling", IEEE TRANSACTIONS ON POWER ELECTRONICS, (Accepted in Press – Open Access) 2016.

[J.4] **J. Kwon**, X. Wang, F. Blaabjerg, C. L. Bak, A. R. Wood and N. R. Watson, "Linearized Modeling Methods of AC-DC Converters For an Accurate Frequency Response" IEEE JOURNAL OF EMERGING AND SELECTED TOPICS IN POWER ELECTRONICS, (Submitted and under Review) 2016.

[J.5] M. Esparza, J. Segundo-Ramirez, **J. Kwon**, X. Wang and F. Blaabjerg, "Modeling of VSC-Based Power Systems in The Extended Harmonic Domain" IEEE TRANSACTIONS ON POWER ELECTRONICS, (Submitted and under Review) 2016.

B. Conference paper

[C.1] **J. Kwon**, X. Wang, C. L. Bak and F. Blaabjerg, "Modeling and Grid impedance Variation Analysis of Parallel Connected Grid Connected Inverter based

on Impedance Based Harmonic Analysis" In Proceedings of the 40th Annual Conference of IEEE Industrial Electronics Society, IECON 2014, pp. 4967-4973.

[C.2] **J. Kwon**, X. Wang and F. Blaabjerg, "Impedance Based Analysis and Design of Harmonic Resonant Controller for a Wide Range of Grid Impedance" In Proceedings of the 5th IEEE International Symposium on Power Electronics for Distributed Generation Systems, PEDG 2014, pp. 1-8.

[C.3] **J. Kwon**, X. Wang, C. L. Bak and F. Blaabjerg, "The Modeling and Harmonic Coupling Analysis of Multiple-Parallel Connected Inverter Using Harmonic State Space (HSS)" In Proceedings of the 2015 IEEE Energy Conversion Congress and Exposition, ECCE 2015, pp. 6231-6238.

[C.4] **J. Kwon**, X. Wang, F. Blaabjerg and C. L. Bak, "Precise Model Analysis for 3-phase High Power Converter using the Harmonic State Space Modeling" In Proceedings of the 2015 9th International Conference on Power Electronics and ECCE Asia, ECCE Asia 2015, pp. 2628-2635.

[C.5] **J. Kwon**, X. Wang, C. L. Bak and F. Blaabjerg, "Modeling and Simulation of DC Power Electronics Systems Using Harmonic State Space (HSS) Method" In Proceedings of the 16th Annual IEEE Workshop on Control and Modeling for Power Electronics, COMPEL 2015, pp. 1-8.

[C.6] **J. Kwon**, X. Wang, C. L. Bak and F. Blaabjerg, "Harmonic Interaction Analysis in Grid Connected Converter using Harmonic State Space (HSS) Modeling" In Proceedings of the 30th Annual IEEE Applied Power Electronics Conference and Exposition, APEC 2015, pp. 1779-1786.

[C.7] **J. Kwon**, X. Wang, C. L. Bak and F. Blaabjerg, "Harmonic Instability Analysis of Single-Phase Grid Connected Converter using Harmonic State Space (HSS) modeling method" In Proceedings of the 2015 IEEE Energy Conversion Congress and Exposition, ECCE 2015, pp. 2421-2428.

[C.8] **J. Kwon**, X. Wang, C. L. Bak and F. Blaabjerg, "Comparative Evaluation of Modeling Methods for Harmonic Stability Analysis of Three-Phase Voltage Source Converters" In Proceedings of PCIM Europe 2015; International Exhibition and Conference for Power Electronics, Intelligent Motion, Renewable Energy and Energy Management, PCIM 2015, pp. 1-9.

[C.9] **J. Kwon**, X. Wang, C. L. Bak and F. Blaabjerg, "Analysis of Harmonic Coupling and Stability in Back-to-Back Converter Systems for Wind Turbines using Harmonic State Space (HSS)" In Proceedings of the 2015 IEEE Energy Conversion Congress and Exposition, ECCE 2015, pp. 730-737.

[C.10] **J. Kwon**, X. Wang, C. L. Bak and F. Blaabjerg, "Comparison of LTI and LTP Models for Stability Analysis of Grid Converters" In Proceedings of the 17th Annual IEEE Workshop on Control and Modeling for Power Electronics, COMPEL 2016, pp. 1-8.

[C.11] **J. Kwon**, X. Wang, C. L. Bak, F. Blaabjerg, M. Hwang, A. R. Wood, N. R. Watson and M. Esparza "Measurement of Phase Dependent Impedance for 3-phase Diode Rectifier" In Proceedings of the 42nd Annual Conference of IEEE Industrial Electronics Society, IECON 2016. (will be presented)

C. Other paper

[O.1] Y. Chung, **J. Kwon**, T. Jung, Y. Kim, W. Song, J. Lee, S. Baek, B. Han and E. Nho, "New Synthetic Test Circuit for the Operational Test of HVDC Thyristor Valve" In Proceedings of the 45th 2014 CIGRE Session, Paris, CIGRE, 2014.

CHAPTER 2. MODELING METHODS OF POWER ELECTRONIC CONVERTERS

AC-dc power converters are found in a vast number of applications, ranging from line-commutated converters such as diode rectifiers in various energy-efficient power loads and thyristor converters in flexible power transmission/distribution systems [8], [9] to self-commutated converters in renewables and regenerative drive systems [10], [11]. With the increasing use of ac-dc converters, stability analysis and optimal design have been an issue for decades. However, the converter is a nonlinear time-varying system due to the control and switching behavior. It is needed to linearize the converters in order to allow the use of Linear Time Invariant (LTI) analysis tools. Otherwise, the system should be analyzed by using the Lyapunov stability criterion based on the nonlinear equations and that is typical difficult to follow it.

The linearization of ac-dc converters has been an important topic in the past decades. The state-space averaging method was first developed for the linearization of dc-dc converters [12]–[15] and it was extended to ac-dc converters to remove the time-discontinuous switching behavior of ac-dc converters. However, the averaged converter model is nonlinear and time-varying, owing to its sinusoidal operating trajectory. Only when the ac-side filter is studied, the ac-dc converter can be approximately linearized like the dc-dc converters [15], [16]. The dq-modeling was developed to transform the time-varying model into a time-invariant model [7] by using the Park transformation. This modeling procedure has been commonly used for stability analysis and controller design of ac-dc converters. However, it is assumed that the switching ripple is low enough to be neglected, and the ratio of the switching frequency to fundamental frequency is high (i.e. high pulse-ratio) such that the sideband harmonics have no influence on the control system dynamics. This assumption may yield an inaccurate model, overlooking the dynamic frequency interactions of low pulse-ratio converters. In [17], the average model, which takes the influence of time-varying modulation into account, shows better results than the original state-space averaging model. Hence, it is important to linearize the time-varying behavior in the model in order to analyze accurately both the dynamic control interactions and the steady-state frequency coupling characteristics.

The importance of including the time-varying behavior in the model can be found in several cases. For instance, some unexpected instability phenomena have been reported over the past few decades [8], [9], [18]. Low-order harmonic frequency oscillations have occurred in the thyristor-based static VAr compensators and high-voltage direct current systems [19], [20]. It is partly because of the resonant behavior of the ac system, where the low order harmonics of current may be magnified by the high impedance of the ac system. Those magnified low-order harmonics may prevent a stable operation of the converters. In recent years, the

widespread use of voltage-source converters in electric railway networks, renewable power plants, and microgrids tend to cause unexpected oscillations and even unstable oscillations at higher frequencies, ranging from hundreds of Hertz to kHz [4], [8], [9]. These phenomena are mainly due to the control and switching interactions between voltage-source converters and passive components in a converter-dominated power grid. Linearization including the time-varying behavior is a useful modeling goal in such ac-dc converter applications.
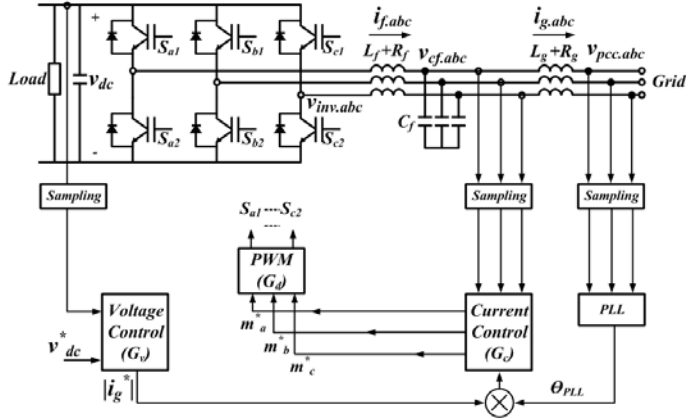
(a)
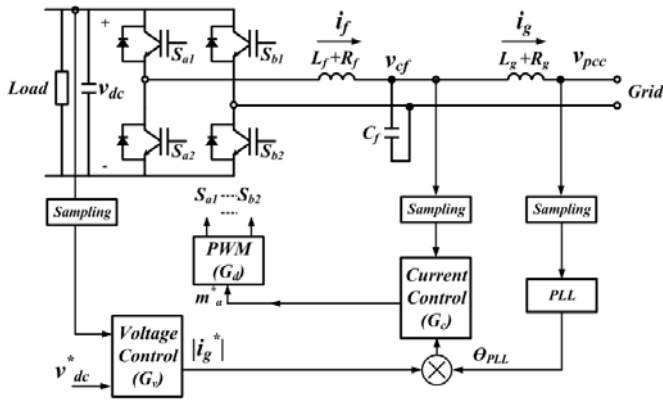
(b)

Figure 2-1. Circuit diagram of grid connected - voltage sourced converters, (a) 3-phase grid-connected converter with controller (L_f=converter side filter inductor, R_f=converter side filter inductor-parasitic resistance, L_g=grid side filter inductor, R_g= grid side filter inductor-parasitic resistance, C_f=filter capacitor, G_c=current controller, G_d=PWM delay), (b) 1-phase grid-connected converter with controller, where the acronyms have the same meaning as in the 3-phase case.

Several modeling methods have been developed to include the effect of time-variance in converter models. Generalized averaging (also known as dynamic phasor) methods and the multi-frequency averaging technique were developed to include the influence of switching harmonics [17], [21]–[25]. However, they still overlook the full range of frequency coupling in the process of linearization. A harmonic linearization model was recently introduced to improve accuracy by including the time-varying modulation in the model [26], [27]. Though it provides an efficient method for obtaining the effective impedance of converters, the coupling of multiple harmonic components and their dynamic interactions in converter-dominated systems are not considered. Harmonic Domain (HD) based models were introduced to linearize all time-varying components of the ac- dc converter, e.g. pulse width modulation, nonlinearities of passive components, and ac/dc disturbances [4], [28]–[31]. It explicitly models how frequencies are coupled with each other and how they interact with the controller dynamics and the passive components. However, these models tend to be quite complex. Modeling methods should be selected according to the details required, and model complexity may become critical for both controller design and stability analysis of the power system.

This chapter presents a comparative review of linearized modeling methods for ac-dc converters, with a particular attention to the linearization of the time-varying behaviour. The modeling accuracy and the importance of frequency coupling for harmonic resonance and stability analysis are considered as the main criteria. The chapter is organized as follows. First, the difficulties in the modeling procedures are explained to identify, what are difficult to be linearized. Secondly, three basic linearised modeling methods, which consider the time-varying components, (traditional averaging, generalized averaging, and harmonic-domain) are compared. Lastly, the advantages and the limitations for both harmonic studies and model accuracy are discussed showing some simulation results.

2.1. MODELING METHODS FOR AC-DC CONVERTERS

Practical AC-DC converters have nonlinear time-variant characteristics. It is difficult to solve the full non-linear differential equation set. The purpose of each modeling approach is to make a Linear Time Invariant (LTI) model by transforming it into different domains, linearizing, and truncating. This section provides a comprehensive comparison of the principal modeling methods. The advantages and the limitations of each modeling method are described, and how they manage the time-varying components of practical systems are also explained. At first, the widely used state-space averaging method [12]–[16], [32], [33] is briefly described. The dq-model is also briefly introduced to show how the model is related to the averaging model. Then, the generalized average model and the dynamic phasor model [17], [19], [21]–[25] are compared since these methods are proposed to enhance the validity of state-space averaging modeling method. The importance of the time-varying elements will also be described. Finally, the HD (Harmonic Domain) [34], [35], EHD (Extended Harmonic Domain), DHD (Dynamic Harmonic Domain) [28] and HSS (Harmonic State Space) modeling methods [30], [31], [36] will be

compared to demonstrate the effectiveness of the modeling in terms of harmonics stability analysis and time-domain waveforms. The overall procedure for the linearization is described in respect to the circuit diagram in Figure 2-1.
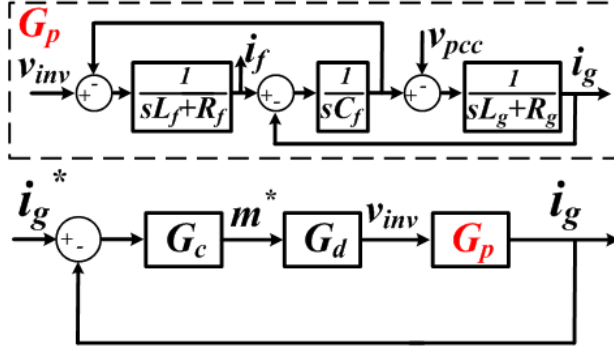
(a)
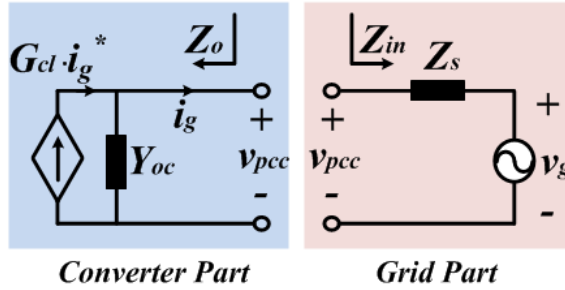
(b)

Figure 2-2. State-space averaging model for grid connected converter (a) Block diagram of the state-space averaging based small signal model, (b) Equivalent controlled Norton circuit (Converter part) and equivalent grid voltage source (Grid part), where Y_{oc} is the output admittance derived from (a), Z_s = grid impedance, Z_o=output admittance seen from the PCC voltage (v_{PCC}) Z_{in}=input impedance seen from the PCC voltage (v_{PCC}).

A. State-space averaging (SSAV) and dq-modeling

The state-space averaging model was originally proposed to simplify the modeling of the discontinuous characteristic of the switching in the dc-dc converter application [12]–[16], [32], [33]. In this process, a moving average filter in (2-1) is used to eliminate the switching ripple component over one switching period (T). It works well for simple dc-dc converters, although simple averaging does not work well for dc-ac converters, and more modern topologies like resonant converters [13]. They also depend on the linearization around an operating point.

$$\bar{x}(t) = \frac{1}{T} \int_{t-T}^{t} x(s)ds \qquad (2\text{-}1)$$

To linearize the dc-dc converter, a small signal perturbation is applied to excite a small variation in the output. The converter is represented by a transfer function between the input and the output. This transfer function makes it possible to use the LTI system based analysis methods, such as Bode diagrams and Nyquist plots [12], [13].

The basic 3-phase grid-connected converters with an *LCL*-filter topology shown in Figure 2-1 are used as an example of an AC-DC converter. Based on three assumptions, SSAV can be used to analyze the overall stability of a system with any filter input impedance [15], although this can be extended to include ac and dc system impedances through superposition. The first assumption is that, if the control bandwidth is sufficiently lower than the switching frequency, the nonlinear discontinuous characteristic of the switching can be restricted to be within the control bandwidth. Secondly, the 3-phase impedances are assumed to be balanced. Thirdly, by assuming a constant dc voltage at a fixed operating point, the switching sequence of the converter can also be represented as a PWM delay function (G_d). By using these assumptions, the block diagram of the transfer function can be derived as shown in Figure 2-2 and by (2-2), where Y_{oc} includes the open loop impedance (T_c) and the admittance between grid current (i_g) to the PCC voltage (v_{pcc}). The role of Y_{oc} is as below according to [15].

$$i_g(s) = G_{cl}(s)i_g^*(s) - Y_{oc}(s)V_{pcc}(s) \qquad (2\text{-}2)$$

where,

$$G_{cl}(s) = \frac{T_c(s)}{1 + T_c(s)}, Y_{oc}(s) = \frac{Y_o(s)}{1 + T_c(s)}$$

$$T_c(s) = G_c(s)G_d(s)Y_{gi}(s)$$
$$Y_{gi}(s) = \frac{i_g(s)}{V_{inv}(s)}, Y_o(s) = \frac{i_g(s)}{V_{pcc}(s)}$$

This transfer function can be represented by either a controlled or uncontrolled Norton current source model (Y_{oc}, G_{cl}) to analyze the interaction between the converter admittance and filter impedance [15] as shown in Figure 2-2-(b). However, the traditional state-space averaging modeling can not be used properly in the case of a low switching frequency (large ripple), low pulse ratio, and the ac voltage (grid) dependent switching [18]. Because, the sideband frequency of the low switching frequency can affect the control bandwidth through the frequency coupling between ac- and dc-side impedance. Furthermore, parameter dependent switching can be affected by input parameter (i.e grid voltage) or the dc-side impedance, and it can not be considered in the average model.

All signals of 3-phase converters are still time-varying signals after the averaging procedure in (2-1). Time invariant signals can be obtained by observing the 3-phase signals from a rotating reference frame using Park's transformation. However, the derived dq-signals must be linearized by assuming that the operating points of dq-

signals are fixed and the variation of input and output signals are very small. The final dq-model, being linearised, is useful to design PI (Proportional Integrator) controllers by using the traditional control theory (Root-Locus, Bode plot, etc). Furthermore, the transformation makes it convenient to control the ac system using stationary signals. However, if the coupling of the d - and q - axis is significant, analysis using Single Input Single Output (SISO) methods such as Nyquist plots and Bode diagrams are difficult. Figure 2-3 shows a model to use when the d - and q - axis coupling should be modeled. Furthermore, this same model is derived based on balanced 3-phase systems, which means that it is less well suited to model single-phase grid connected sources or loads.
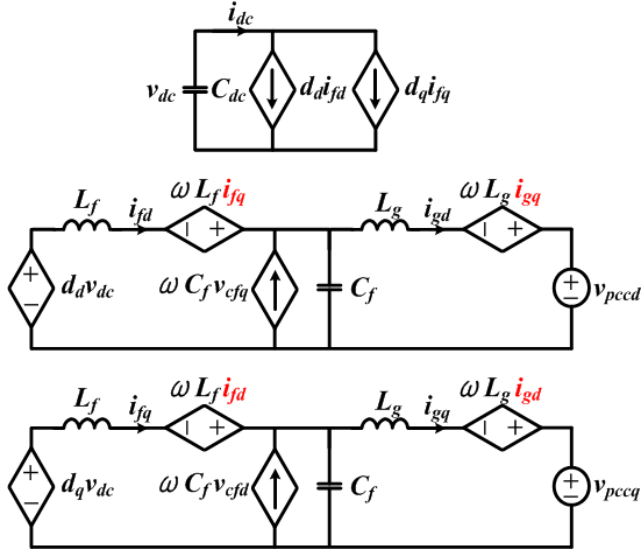
Figure 2-3. Block diagram of dq-reference frame model for 3-phase grid connected converter, where subscripts "d" mean d-axis and subscripts "q" mean q-axis of the dq frame

B. Generalized averaging (Dynamic phasor) modeling

The state-space averaging method can make the model simple since this approach captures average values, and simply averages the switching ripple. However, it is restricted to circuits, which operate at high switching frequency and have small ripple. As mentioned, the impedance of 3-phase circuits should be balanced. To deal with the limitations of the state-space averaging based model, the generalized averaging model, and the dynamic phasor model are introduced [19], [21]–[25], [37]–[39] and given by the following Fourier series.

$$\langle x \rangle_k(t) = \frac{1}{T} \int_0^T x(t - T + \tau) e^{-jk\omega_s(t-T+\tau)} d\tau \qquad (2\text{-}3\text{-}(a))$$

$$x(t - T + \tau) = \sum_k \langle x \rangle_k(t) e^{jk\omega_s(t-T+\tau)} \qquad (2\text{-}3\text{-}(b))$$

The Fourier coefficients of a periodic signal are stationary, and averaging the Fourier coefficients extends the concept of state-space averaging to dc/ac converters. If an arbitrary signal ($x(t)$) is decomposed into a Fourier series in the periodic range

(*T*), each Fourier coefficient can be obtained. The summarized procedure is as follows.

First, (2-3) is obtained from the steady-state operation, where the high-frequency switching components are averaged using a moving average filter (2-1). Secondly, (2-4) is written as

$$\frac{\mathrm{d}}{\mathrm{dt}} x(t) = f\big(x(t), u(t)\big) \tag{2-4}$$

where, *x(t)*, *u(t)* are the state variables and input signals. At this point, the Fourier coefficient vector (2-3) can be substituted directly into (2-4) to describe the dynamic relationships between the harmonic components. Then, the time-domain equation describing the dynamic variation of the Fourier coefficients can be taken as given in (2-5), where $\langle d/dt\, x \rangle_k, \langle f(x, u) \rangle_k$ are the differentiated Fourier coefficients of the state vector and the Fourier coefficients of the input vector.

$$\left\langle \frac{d}{dt} x \right\rangle_k = \langle f(x, u) \rangle_k \tag{2-5}$$

It is required to unfold (2-4) in order to solve it as given in (2-6).

$$\frac{\mathrm{d}}{\mathrm{dt}} \langle x \rangle_k(t) = \left\langle \frac{d}{dt} x \right\rangle_k (t) - jk\omega_s \langle x \rangle_k(t) \tag{2-6}$$

If the state variable vector $\langle x \rangle_k$ is differentiated in the time domain, the differentiated state variable vector ($\langle d/dt\, x \rangle_k$) and complex vector information ($jk\omega_s \langle x \rangle_k$), which is obtained from the Fourier coefficients, can be obtained as given by (2-6). Equation (2-7) can be calculated by substituting (2-3) into (2-6). This procedure is also directly used in the output state-space equation (*y(t)=g(x,u)*).

$$\frac{\mathrm{d}}{\mathrm{dt}} \langle x \rangle_k = -jk \langle x \rangle_k + \langle f(x, u) \rangle_k \tag{2-7}$$

Equation (2-7) is identical to the conventional state-space averaging, when the index of harmonic order k is equal to 0. However, if the dc terms are not sufficient to describe the converter, it is also possible to include other harmonic components. Usually only the most significant harmonic components are considered. Simulation results for a single-phase grid-connected converter, which is referred to Figure 2-1-(b), are shown in Figure 2-4 based on the generalized averaging method. The dc-side volt age and ac-side current are compared in the simulation, where, for the generalized averaging model, the 2nd order harmonics is chosen as the largest harmonic in the dc-circuit and the 1st order harmonic is selected as the largest component in the ac circuit. The results show that including the harmonics is important in order to achieve an accurate result, where the generalized averaging, state-space averaging, and time-domain model are compared in one domain. It is worth to note that the accuracy of modeling may be limited depending on the applications because of the selected significant harmonics and the describing function, where it enforces the response as a SISO (Single Input Single Output) system.

If multiple harmonic components should be considered, equation (2-7) becomes nonlinear [21] due to the linearization procedure. The number of state variable vectors and the number of inputs are different. Hence, the structures of model equations become the nonlinear model. As a solution to this problem, the describing

functions can also be applied to linearize the relationships between the Fourier coefficients of the inputs and variables around the converter. This approach results in a simplified system for system analysis. However, it is worth to note that the higher order harmonics as well as the frequency coupling between low and high frequency range are all neglected due to the characteristic of the describing function. The describing function linearizes the procedure according to the assumption that the system has low-pass filter characteristics. Hence, the systems are considered to filter out all high frequency components, but do not affect the control bandwidth. Even though the results can be more accurate than the SSAV model, they neglect the possibility of frequency coupling between high frequencies and low frequencies. This assumption can lead to inaccurate modeling results.

(a)   (b)
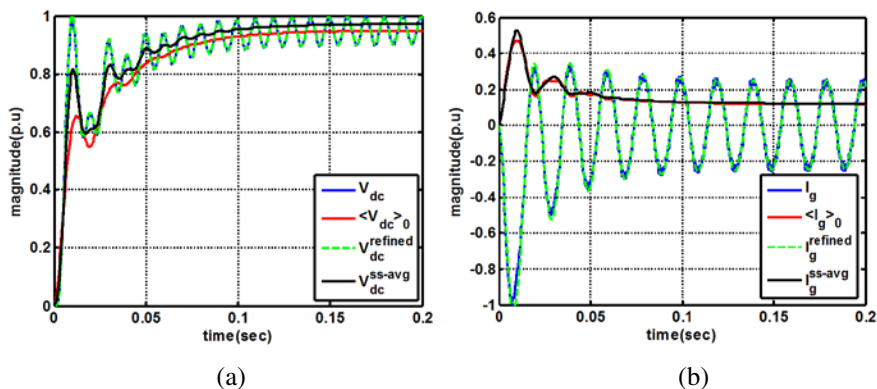
Figure 2-4. Simulation result of the grid connected converter of Figure 2-1-(a) in the time domain, when the converter starts to operate from initial condition, (a) Comparison of the generalized averaging model ($V_{dc}^{refined}$) with traditional state-space averaged model (V_{dc}^{ss-avg}), dc components of the Fourier series ($<V_{dc}>_0$), and non-linear time domain model (V_{dc}), (b) Comparison of generalized averaging model ($I_g^{refined}$) with traditional state-space averaged model (I_g^{ss-avg}), dc components of the Fourier series ($<I_g>_0$) and non-linear time domain model (I_g)

C. Harmonic Domain (HD) based modeling and Harmonic State Space (HSS) modeling

The Harmonic Domain (HD) based models are introduced in [34], [35] with several names, such as the Extended Harmonic Domain (EHD) / Dynamic Harmonic Domain (DHD) [28] and the Harmonic State Space (HSS) [30], [31] to obtain accurate models for the analysis of frequency coupling and its contribution to the system dynamics. If the relationships between signals are predominantly periodic, and are able to be linearized, all of these approaches are useful. For the steady-state analysis, the traditional HD [34], [35] is sufficient to describe the harmonic components and the frequency coupling in the system, where every periodic signal can be represented as the Fourier series expansion. The rotation of each Fourier series component at each frequency and the summation of those bring the same results as the time domain response.

However, this method can not do a transient analysis because it only derives the steady-state frequency components which are often obtained by an iterative process. To include the system dynamics, the Harmonic State-Space (HSS) modeling is a more useful solution, where the Exponentially Modulated Periodic (EMP) signal can be used instead of the periodic signals only. This approach models the transient response of each harmonic component, where the summation of all transient harmonic components is equal to the time domain transient response. The HSS model is based on the LTP theory [40] developed for time-periodic systems in control engineering. The LTP models have the same structure as the LTI-MIMO (Multiple Input Multiple Output) models, and they are an extension of the simpler LTI-SISO (Single Input Single Output) models. The main differences can be described in the following equations, which are based on the standard state-space equation in the form of (2-8).

$$\dot{x} = Ax + Bu \tag{2-8}$$

$$\dot{x}(t) = Ax(t) + Bu(t) \tag{2-9}$$

$$\dot{x}(t) = A(t)x(t) + B(t)u(t) \tag{2-10}$$

$$\dot{X}(\omega, t) = A(\omega) \otimes X(\omega, t) + B(\omega) \otimes U(\omega, t) \tag{2-11}$$

$$(s + jm\omega_0)X_n = \sum_{-\infty}^{\infty} A_{n-m}X_m + \sum_{-\infty}^{\infty} B_{n-m}U_m \tag{2-12}$$

The formulation can be represented as the LTI model (2-9), if the system is linearized at an equilibrium point, where the relationships (A, B) between signals are time invariant but the signals themselves (x, u) can vary. (2-8) can also be extended to (2-10), as in the Linear Time-Variant (LTV) case, if the system parameters (A, B) are time variant. With the assumption that the relationships between variables are time-periodic (*i.e* A and B are time-periodic) (2-10) can be expanded into its Fourier components, and re-written as (2-11). It is worth to note that the system parameters (A, B) of (2-11) are time invariant (they are the Fourier coefficients of the relationships between variables) and the variables (X, U) are Fourier coefficients that vary in time. The convolution of (2-11) can be rewritten as the multiplication of (2-12). This multiplication and summation are practically achieved by a matrix multiplication, as shown in (2-15) and (2-16). The detailed procedure can be explained as follows.

The basis of HSS modeling is a periodic signal, which can be represented in the time interval $[t_0, t_0 + T]$ by its Fourier series.

$$x(t) = \sum_{k \in \mathbb{Z}} X_k e^{jk\omega_0 t} \tag{2-13}$$

where each Fourier coefficient can be calculated by

$$X_k(t) = \frac{1}{T} \int_{t_0}^{t_0+T} x(t)e^{-jk\omega_0 t} dt$$

where $\omega_0 = \frac{2\pi}{T}$ and $t \in [t_0, t_0 + T]$.

It can be written more compactly as a matrix

$$x(t) = \Gamma(\text{t})X$$

where,

$$\Gamma(\text{t}) = [e^{-jh\omega_0 t} \cdots e^{-j2\omega_0 t}, e^{-j\omega_0 t}, 1, e^{j\omega_0 t}, e^{j2\omega_0 t} \cdots e^{jh\omega_0 t}]$$
$$X = [X_{-h}(t) \cdots X_{-1}(t) X_0(t) X_1(t) \cdots X_h(t)]^{\text{T}}$$

Based on the fundamental representation of the EMP signal characteristics, it is also possible to derive mathematical expressions like the derivative, integral and product of two signals to make a time-varying differential equation of the power converter. The differentiation of the time varying signal ($x(\text{t}) = \Gamma(t)X$) is

$$\dot{x}(t) = \dot{\Gamma}(t)X + \Gamma(t)\dot{X} \qquad (2\text{-}14)$$

Based on the principle of these transformations, the state-space equation having a time-varying state transition matrix and a time-varying state variable can be represented as the product of the matrix as

$$(s + jm\omega_0)X_n = \sum_{-\infty}^{\infty} A_{n-m}X_m + \sum_{-\infty}^{\infty} B_{n-m}U_m \qquad (2\text{-}15)$$
$$Y_n = \sum_{-\infty}^{\infty} C_{n-m}X_m + \sum_{-\infty}^{\infty} D_{n-m}U_m$$

In the s-domain, it can also be represented as

$$sX = (A - N)X + BU \qquad (2\text{-}16)$$
$$Y = CX + DU$$

where, $N(= \text{diag}(jm\omega_0))$ is a matrix that represents the differentiation of the steady-state component of each Fourier coefficient. The structure of the matrix given by (2-15), (2-16) makes it possible to analyze the frequency coupling and the interaction as each signal is already decomposed into a harmonic component in the time domain. It also results in an output, which is decomposed into harmonic components.

The Harmonic Transfer Function (HTF) can be derived by transforming (2-16) into (2-17)

$$H_k(s) = \sum_l \hat{C}_{k-l} \left((s + jl\omega_0)I - \hat{A} \right)^{-1} \hat{B}_l + \hat{D}_k \qquad (2\text{-}17)$$

where, $\hat{B}_k$, $\hat{C}_k$, and $\hat{D}_k$, are the Fourier coefficients of the periodic functions $\hat{B}(t)$, $\hat{C}(t)$, and $\hat{D}(\text{t})$, respectively. The results can explicitly be represented as (2-18)

$$Y(\text{s}) = \sum_{k=-\infty}^{\infty} H_k(s - jk\omega_0)U(s - jk\omega_0) \qquad (2\text{-}18)$$

where

$$U(\text{s}) = [\dots U(s - jk\omega_0), U(s), U(s + jk\omega_0) \dots]^T = [\dots U_{-1}(s), U_0(s), U_1(s) \dots]^T$$

$Y(s)$ can also be represented analogously, and $H(s)$ is a double infinite matrix, which is called the Harmonic Transfer Function (HTF). The final models can be divided into two categories as given in (2-19) and (2-20), where (2-19) shows the format of $H_{lti}(s)$ for an LTI system without coupling between harmonics, and (2-20) shows the format of $H_{ltp}(s)$ for an LTP system with coupling within the harmonics.

$$H_{lti}(s) = diag[\ldots \quad H_0(s - j\omega) \quad H_0(s) \quad H_0(s + j\omega) \quad \ldots] \qquad (2\text{-}19)$$

$$H_{ltp}(s) = \begin{bmatrix} \ddots & \vdots & \vdots & \vdots & \\ \ldots & H_0(s - j\omega) & H_{-1}(s) & H_{-2}(s + j\omega) & \ldots \\ \ldots & H_1(s - j\omega) & H_0(s) & H_{-1}(s + j\omega) & \ldots \\ \ldots & H_2(s - j\omega) & H_1(s) & H_0(s + j\omega) & \ldots \\ & \vdots & \vdots & \vdots & \ddots \end{bmatrix} \qquad (2\text{-}20)$$

The HTF derived from HSS modeling is a MIMO (Multiple Input and Multiple Output) system which can be characterized by multiple LTI transfer functions. Hence, $H_0(s - j\omega)$ and $H_0(s + j\omega)$ in (2-19) are the transfer functions from the inputs $U_0(s + j\omega)$ and $U_0(s - j\omega)$ to the outputs $Y(s + j\omega)$ and $Y(s - j\omega)$. Similarly, $H_{-1}(s + j\omega)$ and $H_{-1}(s)$ in (2-20) are the transfer functions from $U_0(s - j\omega)$ and $U_0(s)$ to $Y(s)$. Hence, [$\ldots H_{-1}(s), H_0(s), H_1(s) \ldots$], being transferred from $U_0(s)$ to all the resultant output frequencies are useful to analyze system stability. It is worth to note that an average model considers only $H_0(s)$ for the analysis while the HSS model considers all transfer functions ($[\ldots H_{-1}(s), H_0(s), H_1(s) \ldots]$).

2.2. SIMULATION COMPARISON WITH HD-BASED METHOD

To demonstrate the frequency coupling and the significance of the harmonics, different simulation results are compared. The average model is compared with the HSS model in order to investigate the detailed dynamics of the low-order harmonics in the model. Though the generalized-averaging model and dq-reference model can also be considered for the comparison, the averaged model is compared to demonstrate the frequency coupling and switching instant variation since they can also take those effects partially into account by involving the fundamental component or the largest harmonics in the model. The provided simulation focuses on how two simulations can show the difference between steady-state and dynamics in the frequency domain as well as in the time domain, where the parameters in [41], [42] are considered for the simulation of three phase and single phase systems.

The simulation results obtained from the HD-based modeling approach are shown in Figure 2-5 and Figure 2-6. The 3-phase grid-connected converter in Figure 2-1-(a) is modeled, and the coupling between the reference dc-voltage and the measured dc voltage is shown in Figure 2-5-(a) and (b). The model has the structure shown in (2-20) and only the -6th, -1th, 0, 1th, 6th, harmonic transfer functions are shown. For instance, a 300 Hz (+/- 6th) input frequency may generate three different frequencies with three different responses. Figure 2-5-(a) shows that the harmonic response of dc-component (H_0) is dominant when the harmonic input vector is dc (0 Hz).

However, it can be found in Figure 2-5-(b) that the 6th harmonic response is dominant when the input is assigned as the -6th order harmonic and it happens as well in the +6th harmonic response. In Figure 2-5-(c) and (d), the dc voltage reference is changed at 0.5 sec from 750 V to 650 V, and each harmonic shows a different transient response according to the frequency response in Figure 2-5-(a) and (b). Each harmonic component is governed by its own harmonic transfer function as shown in Figure 2-5 and it gives a different transient time response as shown in Figure 2-5-(d). It is noted that the rotation and summation of the harmonic vector in Figure 2-5-(d) using (2-13) is the same as the time-domain response in Figure 2-5-(c). Furthermore, it means that the involvement of different dynamics from the harmonics demonstrate the correct response. Hence, taking only a fundamental component or averaged value may bring problems of the accuracy.
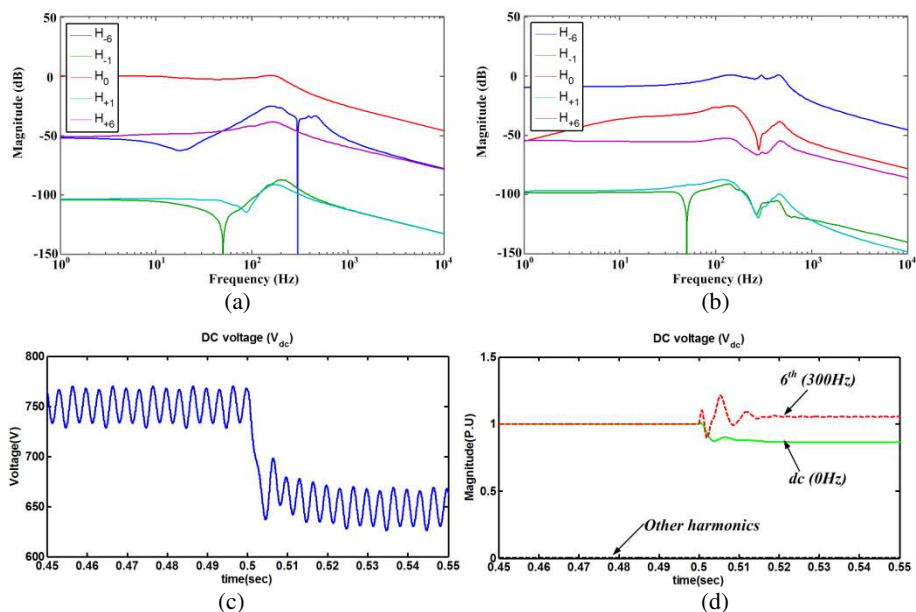
Figure 2-5. Simulation of the converter in Figure 2-1-(a) by using HSS, (a) HTF (v_{dc}/v_{dc}^*), where -6th, -1st, 0, 1st, 6th HTF are only depicted individually (when input harmonic vector = dc (0 Hz)), (b) HTF (v_{dc}/v_{dc}^*), where -6th, -1st, 0, 1st, 6th HTF are only depicted for the visibility (when input harmonic vector = -6th), (c) Time-domain response of dc-link voltage, where the reference is changed from 750 V to 650 V at 0.5 sec, (d) Individual harmonic response from HTF, where the response of -6th, -1st, 0, 1st, 6th are depicted individually.

The importance of harmonics and their coupling in the modeling can also be found in the single-phase application as shown in Fig. 7, where the single-phase grid-connected converter is simulated by using the state-space averaging method and the HSS method. The transient simulation is performed to figure out the dynamics when the reference for the dc-link voltage controller is changed. The dc-link voltage is changed from 450 V to 400 V and the current in the ac-circuit is changed as well according to the behavior of controller.
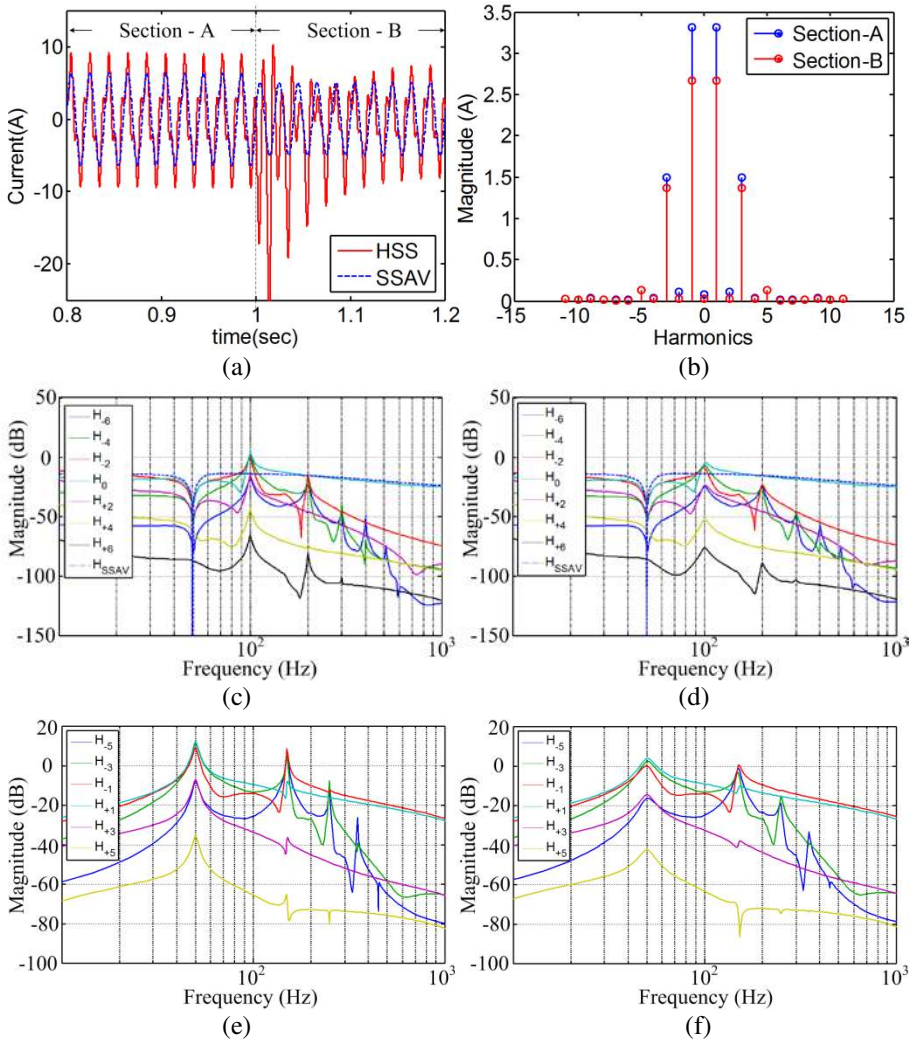
Figure 2-6. Simulation results of single-phase grid-connected converter (see Figure 2-1-(b)) using Harmonic Domain (HD)-based simulation [43], when the reference of grid current is changed at 1 sec, (a) Comparison of HSS simulation and average-based simulation, (b) FFT results of Section-A and Section-B, (c), (d) Frequency responses (admittance) between ac-input current and ac-line voltage (i_{ac}/v_{line}) of Section-A/Section-B, (e), (f) Frequency responses (admittance) between ac-input current and dc-link voltage reference (i_{ac}/v_{dc}^*) of Section-A/Section-B.

It is noted that the dynamics of the HSS model and the averaged model show differences as shown in Figure 2-6-(a), where the dynamics of harmonic are not reflected in the averaged model since it does not consider the frequency coupling. The variation of the harmonic components and their involvement in the dynamic behavior can be seen in Figure 2-6-(b)-(f). The low-order harmonics are changed in

the current waveform, where "Section-A" and "Section-B" of Figure 2-6-(b) mean the same period with Figure 2-6-(a). Even though the fundamental component is mainly affected by the operation, the magnitude and phase of other harmonics also change according to the frequency response in Figure 2-6-(c)-(f). The frequency responses (admittance) between ac-input current and ac-line voltage (i_{ac}/v_{line}) are depicted in order to show the difference of the two models, where the dotted lines in Figure 2-6-(c), (d) mean the average-based model and the other lines are derived from the HSS model. It is noted that the responses from the HSS model are dominant at 100 Hz and 200 Hz and they govern the response of 2nd and 4th order harmonics. Additionally, Figure 2-6-(c) is the response of "Section-A" and Figure 2-6-(d) is the response of "Section-B", where two frequency responses are obtained at different operating points according to the change of reference. The different magnitudes of the two cases affect the different magnitude of harmonics when the transient happens at 1 sec. It is noted that the changed harmonic response is because of the frequency coupling and the switching instant variation, which can not be considered in the average-based model. Though the response of dc-component in the HSS model (H_0) is similar to the average-based model, the response is affected by the other harmonic transfer functions and it shows peaks at 100 Hz and 200 Hz. Figure 2-6-(e), (f) are shown in order to show the frequency response between ac-line current and dc-voltage reference (i_{ac}/v_{dc}^*), where (e) is the response of "Section- A" and (f) is "Section-B". They show the dominant frequency response at 50 Hz and 150 Hz, which are mainly the odd-order harmonics. The responses are reflected in the ac-line current, where the odd-order harmonics mainly appear in the ac-line current and it matches with the time-domain response. Furthermore, the frequency responses of each harmonic can trigger the unstable behavior of a system when they are dominant at the resonant frequency [4], [44], [45].

As given in the simulation results in Figure 2-5 and Figure 2-6, harmonics should be included in the modeling procedure in order to do accurate analysis. It has been shown in the literature that these multiple harmonic frequency responses can show different dynamics and stability results in locomotive applications [4], [46]. Also HVDC, FACTS and other thyristor-based applications have been studied in [20], [31], [36], [47], [48] and they show how low order harmonics can be strongly involved in the transient response through both frequency coupling and SIV.

2.3. DISCUSSION AND SUMMARY

Power electronic based systems are being employed in many fields such as electrical networks, wind farms, photovoltaic plants, and traction applications. Analysis of complex dynamics and harmonic coupling is essential in order to maintain both stable operation and good power quality. Problems related to the frequency coupling are an issue since instability can arise and unexpected frequencies can appear in complex networks. An accurate model, which can cover all the components in one domain and provide some insight into system interactions, is required because the time-varying behaviors and trajectories can not be considered in the traditional way. Four aspects are discussed as follows :

Table 2-I. Performance comparison of modeling for voltage source converter

	State-space Averaging	**Generalized Average (=Dynamic Phasor)**	**Harmonic State-space (= Harmonic Domain Base)**
Time-varying behavior	Averaging	Averaging + Fourier Series	Full consideration
AC-DC control frequency coupling	X	Δ	O
Analysis of an unbalanced system	X	Δ	O
Modularity for a large network harmonic analysis	X	Δ	O
Purpose	Stability analysis, Control design	Stability analysis, Control design (with relatively large harmonics)	Stability analysis, Control design, Harmonic analysis

O= Possible, X=impossible, Δ=Partially possible

A. Time-varying behavior

Each modeling approach deals with the time-varying elements in different ways. The key time variation that has to be modeled is the switching pattern of the converter, which interconnects the dc and dc, or dc and ac sides in power converters. This switching pattern (referred to inputs, outputs or state variables) can be reduced to average values, suited to dc/dc converters, or to an average value and a fundamental frequency value, suited to dc/ac converters, or to harmonics of the actual values, which are suitable for most converters. The moving average window of the state-space averaging is a sufficiently short duration which captures the system dynamics, while filtering out most of the higher switching frequencies. Dynamic phasors consider the fundamental frequency component (and the dc component of the dc side, if there is one), but neglects the switching frequencies. The HSS model captures all the frequencies up to the maximum frequency of a truncated harmonic spectrum. All the models describe the relationships that govern the system transient behavior, and all the components described are allowed to vary transiently.

B. AC-DC-control frequency coupling

All ac/dc converters use switches to couple the dc and ac side. As there is usually a direct connection between the ac and dc sides by a combination of switches, the ac side transients are coupled to the dc side, and vice-versa. In fact, any transient will involve the ac side, the dc side, and the control feedback system. In general, it is important to include the properties of all these systems in a network model. State-space averaging was originally derived from the assumption that the dc voltage is always constant, although this is not a necessary assumption. In general, any

contribution in this area must be studied carefully, to ensure that ac system dynamics, dc system dynamics, and control dynamics are all included. While ac and dc systems around a converter are designed to act as low pass filters, the frequency coupling of the converter itself can move high frequencies to low frequencies and back again, creating significant cross-coupling between the frequency components around the converter. It is a mechanism by which the high-frequency resonances (typically on the ac side of the converter) can be coupled to frequencies within the converter control bandwidth, leading to stability issues. Only the HSS explicitly describes this mechanism.

C. Analysis of an unbalanced system

This aspect is also quite important in practical systems. The main reason is that different cable lengths and unbalanced overhead lines often exist and, the mutually coupled impedances between the phases are not balanced. To analyze the impact of such unbalanced impedances on harmonics the selection of modeling method is quite critical. In the state-space averaging method it is not possible to consider these because it is always regarded as a 3-phase balanced system. In the case of harmonic linearization, the original basic concept is from the state-space averaging model. It does not include the time-varying modulation, which comes from the unbalance, and means that the modeling starts from the assumption that all 3-phase passive elements are balanced. Hence, even though several studies discuss the harmonics driven by the unbalanced grid, they cannot take into account the unbalanced passive parameters in the model. However, the generalized averaging and the HSS have the formulation to treat the unbalanced passive elements and voltage in the model. HD-based models have already been used for the analysis of the unbalanced harmonics [49]. However, the generalized averaging method is not used for this purpose in the research due to the number of harmonics considered in the model.

D. Modularity for large network harmonic analysis

This aspect is important in order to allow the expansion of the analysis to a large network. With the increasing number of converter system in the grid the analysis of unexpected frequencies is getting more difficult. The inclusion of the dc circuit, switching and control is essential to model the frequency coupling and harmonic flow between the systems and the grid. The state-space averaging and harmonic linearization methods have difficulties in being connected with other dc side connected converters, as they assume a constant dc voltage, which de-couples any connected dc circuit. However, the generalized averaging and HSS modeling methods considering the dc circuit and switching are easy to connect with other models due to the matrix formulation. Although the HSS is suited to be an efficient solution for large networks, it does suffer from the number of state variables that it generates.

A comparison of the different methods is summarized in Table 2-I indicating that the HSS modeling will give most possibilities.

CHAPTER 3. HSS MODELING OF VSC BASED SYSTEMS

With the increased use of power electronic based Distributed Generation (DG) Systems, the stability and the dynamic performance of the system are important issues today [8], [9], [67], [72], [73]. Particularly, various DG systems are gathered into the same grid network, where complex connections, active control and bidirectional current flow can make it difficult to analyze the dynamics and interaction of the power electronic based systems [8], [74]–[78]. Besides that, even if "N" identical power converters, which operate simultaneously or independently, are connected to the same bus, the cancellation, generation, attenuation and magnification of harmonics are available depending on the randomness [79].

Furthermore, the installation ratio of renewable energy is drastically increasing for home appliances as well as in large factories [50]–[52]. Especially photovoltaic systems, which have been installed on the rooves of houses as well as in windows of buildings, are rapidly increasing [50], [53]–[56]. The single-phase grid-connected converter having a small power rating was not an issue for the grid in few years ago. However, power quality and stability [51], [57]–[59] have now become more critical issues because many units are now connected to the same network with variable operation according to conditions of network. For instance, low-order harmonics are being an issue since the ESS (Energy Storage System) is also being more installed in home applications by using single phase boost rectifiers. The main problems are that the lifetime of batteries can be reduced by harmonics in the dc network and it may increase the losses of ESS [60], [61] as well. Additionally, ESS, which is having both boost and inverter operations, requires a bi-directional operation to perform charge and discharge of batteries. ESS thus does not have only one fixed operating point, where the variable frequency response or model should be considered to analyze the system precisely. Thus, more progressed modeling ways are essentially required to look into the harmonic propagation on both sides as well as to the other connected ESS or renewable energy converters.

Additionally, the installation ratio of wind turbines in onshore / offshore wind farms are also drastically increasing. Furthermore, most of their converter technologies are now moving to become back-to-back converters because of more flexible controllability and to fulfill the grid code [90]. However, the power quality of wind turbines are now giving new challenges since the harmonic coupling and their interaction in both steady-state and dynamic are getting severe as the number of wind turbine is increasing. Hence, it is required to find a solution or a tool to figure out the origin of the harmonics and their instabilities [67]. The critical issues can be classified into two categories. Firstly, the resonance or unexpected harmonics are appearing in the grid current because most back-to-back converters are connected to

a substation through a submarine cable having a large capacitance, and the impedance of the cable is coupled with switching behavior in the converter. Secondly, each wind turbine in the wind farm is working at different operating points, because of the wind direction, wind speed and their control strategy. The varying operation is continuously changing the impedance of wind turbine and it brings unexpected behaviors as like cancelation, reduction and magnification of certain harmonics. Furthermore, the non-linearity of components and coupled behavior within the converters make harmonic analysis difficult for such systems. As a result, the time-varying behavior and their nonlinearity may change the output impedance of the converters continuously [8], [9]. Additionally, a large wind farm can affect to the impedances of other wind farms, which are connected by MV or HV network, through an unpredicted harmonic or a resonance. Hence, an accurate analysis method and modeling approach, which can include the properties of time-varying and nonlinear components, are required to avoid the unexpected interactions.

Besides, the trends for harmonic and stability analysis of power converter are now moving from a single device to multi-connected devices [67]. Hence, it has been an important topic to find proper modeling ways and analysis methods. Furthermore, each converter has their own time-varying components and they are varying continuously according to the operating point. Additionally, the time-varying components can not be simplified as a single constant value. The consideration of time-varying behavior in the modeling could be very significant depending on the system conditions and it can be more severe for a complex systems. For instance, the power converters in a wind farm, which have experienced such phenomenon due to the wake effect of the wind, have experienced unexpected resonances and harmonics due to the different varying components in each converter, and they disconnect to the systems triggered by the protection [97]. Hence, the varying operations of converters may still bring uncertainties in the analysis [98]. Furthermore, such phenomenon can make the harmonic and resonance analysis difficult and inaccurate. Hence, it is urgently required to develop the advanced models, which can consider the time-varying components for an accurate analysis.

The introduced harmonic interactions mainly occur in power converters, because the ac - side impedance is coupled with dc - side impedance through the frequency coupling, which is generated by the switching modulation. The variation of harmonics with their negative impact on distribution losses and the possibility of interruption to other customers are main concerns of the network operator [52]. Furthermore, these coupled operations of the system may invoke instability problems in the power electronic based systems [67], [80]. Hence, an accurate harmonic analysis of the steady-state and dynamic behaviors is important in order to obtain a stable operation of the power systems.

"*Switching method and modulation*" of the power converter, which is the time-varying component in the power converter, should be considered in order to get the accurate frequency response. However, it is typically neglected or simplified as an averaged duty value in the LTI model with the assumptions where the switching may not affect the behavior of controller due to the high switching frequency. However, it has been shown in generalized averaging and other advanced averaging methods [17], [19], [21] that the modulation should be taken into account with its phasor in order to achieve an accurate modeling. Additionally, the phasor information of the switching and its sideband frequency should also be considered in both low switching frequency (< 2 kHz) and grid dependent switching application (e.g diode, thyristor application) in order to investigate their effect on the controller or the interaction with other elements [31], [48]. Hence, the switching components and modulation should be modeled together with other components.

Several methods, which are derived from average based models, are introduced in [26], [67], [81], [82] to investigate these problems. However, these Linear Time Invariant (LTI) based models are not enough to analyze these complex and bidirectional phenomena, because of the time-varying properties of power converter operation and the typically neglected switching modulation during the modeling procedure. For instance, the breaking and normal operation of the converter in railway applications, the discharging and charging of the batteries in Energy Storage Systems (ESS), and the different operating point of the converter in renewable energy applications, can be the challenges in the analysis of the system using the conventional modeling approaches. As a result, it is found that the frequency couplings, which are driven by the switching modulation, harmonics and time-varying properties of signals, are the main reasons for the difficulties to analyze the bidirectional systems correctly. Hence, the developments of an accurate model including time-varying signals are important in order to understand the harmonic interaction and the frequency coupling of converters [67], [73], [80]. To solve the problems, new modeling approaches considering the periodic signals have been proposed. A harmonic linearization method is introduced in [83], [84] to calculate the input-output impedance of 3-phase systems according to linearized sequence components. Besides, a steady-state analysis of a Modular Multilevel Converter (MMC) is performed to analyze the circulating current by using Fourier series expansion and small-signal modeling [85], [86]. However, the harmonic interaction in the system with an overall picture of the other components has not been studied. Furthermore, the harmonic interaction problem inside the voltage source converter is also typically overlooked due to a simplified modeling approach [87].

As an alternative to analyze the harmonic couplings at the transmission level, Harmonic Domain (HD), Extended Harmonic Domain (EHD) and Harmonic State Space (HSS) modeling methods were introduced in the analysis of power system. For the steady-state harmonic coupling investigations in symmetrical and unsymmetrical grid conditions, the harmonic domain method has been developed

[35]. However, this approach is not enough to derive the dynamic behavior in the time-domain. Hence, the EHD modeling is introduced to explore the dynamic performance in the harmonic domain, where pre-calculated harmonic domain values are used as initial values [88]. Furthermore, the Dynamic Harmonic Domain (DHD) is also developed in order to consider a nonlinear characteristic of inductor and transformer in the dynamic model e.g. in FACTS applications. The HSS modeling and Harmonic Transfer Function (HTF) method are further used to analyze the bi-directional harmonic coupling in the Swiss railway system [46] and to meet the overall requirement including harmonic interaction and inter-harmonic analysis [4], [30], [31], [47].

This chapter presents the HSS modeling of the VSC applications. Four different applications are considered and the background and previous research work are also reviewed for demonstrating that the time-varying behavior is important and how those can be included in the HSS model. The achieved models show also how harmonics of the VSC converter are involved in the performance at the steady-state as well as the dynamic behavior. All modeling results of each applications are implemented by using MATLAB and compared with nonlinear time-domain simulations. Futhermore, the obtained results are verified in the experimental set-up by using dSPACE.

3.1. HSS MODELING OF SINGLE PHASE VSC SYSTEMS

This section represents the LTP modeling and their analysis of a single phase grid-connected rectifier for renewable energy by means of the HSS modeling. The detailed modeling procedure is described with the background of the LTP system. Furthermore, the dynamic influences of harmonics to the systems are analyzed by using the harmonic transfer function and eigenvalue. The harmonic impedance matrix from HSS modeling is also used to represent the coupling of steady-state harmonic impedance. As a result, all analysis are verified by time-domain simulation as well as experiments to validate the obtained harmonic transfer function.

3.1.1. MODELING PROCEDURE

A single-phase grid-connected converter is studied in the modeling procedure, and the fundamental structure of the converter is shown in Figure 3-1, where L_f, C_f, L_g, C_{dc}, Z_{grid} are the converter-side inductor, capacitor filter, grid-side inductor, dc-link capacitor and grid impedance, respectively. A PI controller (PI(s)) controls the dc-link voltage (v_{dc}) by using the low-pass filtered signal ($H_2(s)$). A PI controller also controls the obtained current reference (i_g*), where the dq-transformed grid current, which are obtained by delaying the reference angle from PLL, is filtered by a low-pass filter ($H_1(s)$). The output of the current controller is divided by the dc voltage ($v_{dc-sense}$) to be compared with the carrier signal in order to generate the PWM signals. The detailed procedure to achieve the LTP model is as follows:

Figure 3-1. "Block diagram of single-phase grid connected PWM converter" [43].

A. Converter Modeling

The HSS model of the circuit in Figure 3-1 can be obtained as shown in (3.1-3) and Figure 3-2 based on (2-15) ~ (2-18) and the introduced theory given in Chapter 2. Firstly, Figure 3-1can be converted into a differential equation as given in (3.1-1).

$$\dot{i}_g(t) = -\frac{R_g}{L_g}i_g(t) + \frac{1}{L_g}v_{pcc}(t) - \frac{1}{L_g}v_{cf}(t) \qquad \text{(3.1-1-(a))}$$

$$\dot{i}_f(t) = -\frac{R_f}{L_f}i_f(t) + \frac{1}{L_f}v_{cf}(t) - \frac{1}{L_g}v_{inv}(t) \qquad \text{(3.1-1-(b))}$$

$$\dot{v}_{cf}(t) = \frac{1}{C_f}i_g(t) - \frac{1}{C_f}i_f(t) \qquad \text{(3.1-1-(c))}$$

$$\dot{v}_{dc}(t) = \frac{1}{C_{dc}}i_{dc}(t) - \frac{1}{R_{dc}C_{dc}}v_{dc}(t) \qquad \text{(3.1-1-(d))}$$

$$v_{inv}(t) = sw(t)v_{dc}(t) \qquad \text{(3.1-1-(e))}$$

$$i_{dc}(t) = i_f(t)sw(t) \qquad \text{(3.1-1-(f))}$$

where all signals in (3.1-1) are nonlinear and time-varying. (3.1-1) can then be linearized based on the assumption that the operating trajectory (o) of the converter is not changed too much even if there are small perturbations (Δ) in the steady-state. As a result, (3.1-2) can be obtained by using the linearization.

$$\Delta\dot{i}_g(t) = -\frac{R_g}{L_g}\Delta i_g(t) + \frac{1}{L_g}\Delta v_{pcc}(t) - \frac{1}{L_g}\Delta v_{cf}(t) \qquad \text{(3.1-2-(a))}$$

$$\Delta\dot{i}_f(t) = -\frac{R_f}{L_f}\Delta i_f(t) + \frac{1}{L_f}\Delta v_{cf}(t) - \frac{1}{L_g}\Delta v_{inv}(t) \qquad \text{(3.1-2-(b))}$$

$$\Delta\dot{v}_{cf}(t) = \frac{1}{C_f}\Delta i_g(t) - \frac{1}{C_f}\Delta i_f(t) \qquad \text{(3.1-2-(c))}$$

$$\Delta \dot{v}_{dc}(t) = \frac{1}{C_{dc}} \Delta i_{dc}(t) - \frac{1}{R_{dc}C_{dc}} \Delta v_{dc}(t) \qquad \text{(3.1-2-(d))}$$

$$\Delta v_{inv}(t) = sw_0 \Delta v_{dc}(t) + v_{dc0} \Delta sw(t) \qquad \text{(3.1-2-(e))}$$

$$\Delta i_{dc}(t) = i_{f0} \Delta sw(t) + sw_0 \Delta i_f(t) \qquad \text{(3.1-2-(f))}$$

where sw_0, i_{f0}, v_{dc0} mean constant trajectories and Δ means a small variation around the trajectory of signal. Equation (3.1-2) can be reorganized by substituting (3.1-2-(e)) and (3.1-2-(f)) into (3.1-2-(a)) ~ (3.1.2-(c)). The results can be converted into multiple LTI systems by using (2-14) and (2-15) when all signals of the converter are periodically time-varying.
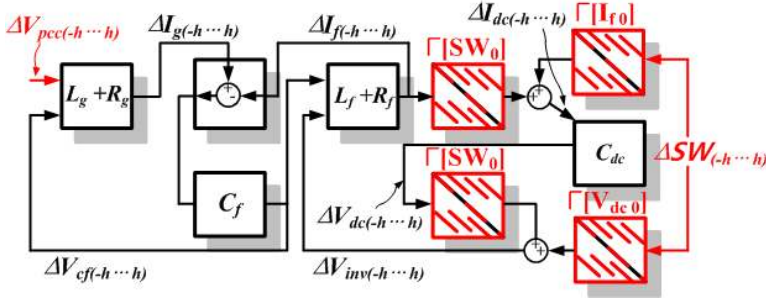
Figure 3-2. "Block diagram of LTP topology model, where the red-box means the Toeplitz matrix" [43]

It is worth to note that the multiplication of two time-domain signals is equal to the convolution of two signals in frequency domain. Hence, the multiplication of steady-state operating trajectory (0) and small variation of signal (Δ) in the LTP system can be found by using the Toeplitz matrix (Γ), where the method shows identical results using the convolution. As a result, (3.1-3) can be obtained through the introduced procedure as given below

$$\begin{bmatrix} \Delta \dot{I}_g(t) \\ \Delta \dot{I}_f(t) \\ \Delta \dot{V}_{cf}(t) \\ \Delta \dot{V}_{dc}(t) \end{bmatrix} = \begin{bmatrix} \frac{-R_g}{L_g}I - N & Z_M & \frac{-1}{L_g}I & Z_M \\ Z_M & \frac{-R_f}{L_f}I - N & \frac{1}{L_f}I & -\frac{\Gamma[sw_0]}{L_f} \\ \frac{1}{C_f}I & \frac{-1}{C_f}I & -N & Z_M \\ Z_M & \frac{\Gamma[sw_0]}{C_{dc}} & Z_M & -\frac{1}{R_{dc}C_{dc}}I - N \end{bmatrix} \begin{bmatrix} \Delta I_g(t) \\ \Delta I_f(t) \\ \Delta V_{cf}(t) \\ \Delta V_{dc}(t) \end{bmatrix} + \begin{bmatrix} \frac{1}{L_g}I & Z_M \\ Z_M & -\frac{\Gamma[V_{dc0}]}{L_f} \\ Z_M & Z_M \\ Z_M & \frac{\Gamma[I_{f0}]}{C_{dc}} \end{bmatrix} \begin{bmatrix} \Delta V_{pcc}(t) \\ \Delta SW(t) \end{bmatrix}$$

(3.1-3)

where, the acronyms in (3.1-3) match with Figure 3-1. "*I*" means the identity matrix, "*N*" is came up with differentiation based on (2-15) - (2-18), "Z_M" is the zero square matrix and "$\Gamma[\cdot]$" means a transformation row or column vector into a Toeplitz matrix. Furthermore, "Δ" term means the small variation of each signal in Figure 3-1 based on the assumption that signals may change slightly according to the disturbance. Hence, the letter with a subscript "0" means a nominal value from Figure 3-1. The small letter in Figure 3-1 points out the time domain signal. The capital letters in (3.1-3) represents the harmonic vector in Figure 3-1, which came up

with the Fourier series (2-13). The results from (3.1-3) can be converted into the time-domain signals by using (2-13) ~ (2-15). Besides, the size of each matrix depends on the number of harmonics considered in the modeling. In this section, the -20th ~20th harmonics, the switching harmonics, and the sideband harmonics are only considered as given in (3.1-4) and it determines the size of HSS modeling.

$$h = [\dots, -h_{sw}, -h_{sw+1}, -20, \dots, -1, 0, 1, \dots, 20, \dots h_{sw-1}, h_{sw}, \dots] \tag{3.1-4}$$

Depending on the PWM method used, e.g., Space Vector Modulation (SVM), Sinusoidal PWM (SPWM), Discontinuous PWM (DPWM), the frequency and the magnitude of switching harmonics can be decided. The switching function in the time-domain can be transformed into a Toeplitz (Γ) matrix as given by (3.1-5) to do a convolution, where the Fourier coefficient of the switching ($SW_0 = [\dots SW_{-2}, SW_{-1}, SW_0, SW_1, SW_2 \dots]$) in steady state can be achieved by using the DFT (Discrete Fourier Transform) of the time domain signals or an analytical model.

$$\Gamma[SW_0] = \begin{bmatrix} SW_0 & SW_{-1} & SW_{-2} & \dots \\ SW_1 & SW_0 & SW_{-1} & \dots \\ SW_2 & SW_1 & SW_0 & \dots \\ \vdots & \vdots & \vdots & \ddots \end{bmatrix} \tag{3.1-5}$$

The variation of the modulation can be reflected by adding a small variation (Δ) of switching into the previous state (SW_0) as given in (3.1-8).

B. Controller modeling

A low-pass filter and PI-controller can also be converted into the HSS model formulation and take into account the effect of harmonics in the controller by using the frequency shift as given in (3.1-6) and (3.1-7).

$$PI = \text{diag}[PI(s - jh\omega_0) \cdots PI(s) \cdots PI(s + jh\omega_0)] \tag{3.1-6}$$

where, $PI(s) = K_p + K_i/s$, K_p is the proportional gain and K_i is the integrator gain.

$$H_1, H_2 = \text{diag}[H(s - jh\omega_0) \cdots H(s) \cdots H(s + jh\omega_0)] \tag{3.1-7}$$

where, $H(s) = 1/(s \cdot K_{lpf} + 1)$; K_{lpf} is the bandwidth of the low-pass filter. This transfer function "H" and "PI" means the frequency response of the filter at each harmonic frequency ($h\omega_0$).

It is thus needed to substitue the small variation of the switching ($\Delta[SW]$) into the base operating point ($\Gamma[SW_0]$) in order to consider the small variation of the controller into (3.1-3). If there is not a variation of the reference, the small variations in the controller output are zero. As a result, the small variation ($\Delta[SW]$) from the controller should be multiplied and added with the previous state of dc voltage (V_{dc0}) and ac current (I_{f0}) through (3.1-3) and (3.1-8).

$$\Delta V_{inv} = \Gamma[SW_0]\Delta V_{dc} + \Gamma[V_{dc0}]\Delta[SW] \tag{3.1-8}$$

$$\Delta I_{dc} = \Gamma[SW_0]\Delta I_f + \Gamma[I_{f0}]\Delta[SW]$$

where, "Δ" term is the small variation of each signal from the partial differential equation of Figure 3-1 and "$\Gamma[\cdot]$" means a transformed Toeplitz matrix from row or column vector. The convolution between the controller output and the partial differential equation of the switching matrix produce a small variation of the switching harmonics ($\Delta[SW]$). The acronym in each equation "-0" means the previous state from (3.1-3). Hence, the small variation of nonlinear-discontinuous signal (sw(t)) can be taken into account in the frequency domain as given in (3.1-8).
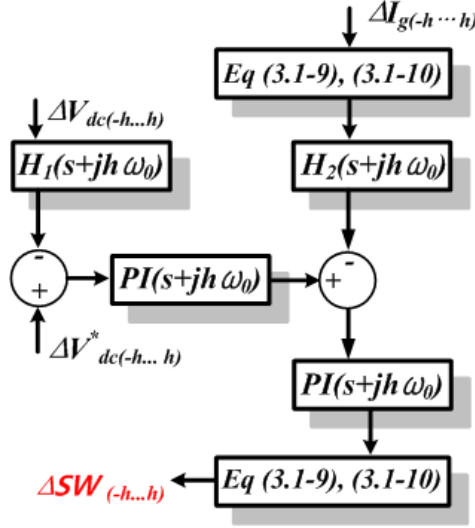
Figure 3-3. "Block diagram of LTP controller model"[43] used in the single phase converter

The reference frame in time domain simulation is usually synchronized with the grid voltage by using the PLL (Phase Locked Loop), which is defined as the α term. To achieve the αβ and dq signals, α should be delayed by 90 deg through an all-pass filter to achieve β signal. However, the measured grid current (i_g) in the case of HSS model can have the same function with αβ frame in the time domain by multiplying the complex number (j) to the harmonic vector (I_g) of the grid current as given by (3.1-9).

$$I_\beta = [j \cdot I_{\alpha(-h)}, -j \cdot I_{\alpha(h)}] \tag{3.1-9}$$

The αβ-dq transformation can also be achieved by using the same manner. The decomposed Park transformation in the frequency domain is given in (3.1-10) as :

$$Park_{HSS} = \begin{bmatrix} \Gamma\begin{bmatrix} \frac{1}{2} & 0 & \frac{1}{2} \end{bmatrix} & \Gamma\begin{bmatrix} -\frac{1}{j2} & 0 & \frac{1}{j2} \end{bmatrix} \\ -\Gamma\begin{bmatrix} -\frac{1}{j2} & 0 & \frac{1}{j2} \end{bmatrix} & \Gamma\begin{bmatrix} \frac{1}{2} & 0 & \frac{1}{2} \end{bmatrix} \end{bmatrix} \tag{3.1-10}$$

$$\text{i.e)} \ \ \text{Park}_{\text{HSS}} \cdot \begin{bmatrix} 0.5n \\ 0 \\ 0.5n \\ j0.5n \\ 0 \\ -j0.5n \end{bmatrix} = \begin{bmatrix} 0 \\ n \\ 0 \\ 0 \\ 0 \\ 0 \end{bmatrix}, \text{ where n=peak value of i}_g$$

The structure of the transformation has a Toeplitz format depending on the convolution rules. If the final results from (3.1-10) are transformed into the time domain by using (2-13) – (2-15), the obtained results have the same signal in the time domain. As an alternative of the introduced method, the dq information in the frequency domain can be achieved by adding the fundamental component of the grid current ($I_d = I_{g1} + I_{g-1}, I_q = 0$), if the q-axis component is assumed to be controlled to be "0". The dynamics of PLL part are not considered in order to focus on the effect of the linearized PWM. Hence, the angle information from the PLL is assumed to be synchronized with the ideal grid voltage. According to the introduced theory and procedure, an HSS model for single phase grid connected converter can be achieved.

3.1.2. SIMULATION AND EXPERIMENTAL RESULTS

MATLAB is used to compare the HSS model with non-linear time domain simulation done in PLECS. The final HSS model from (3.1-3)-(3.1-10) is compiled by using an m-file script. A single-phase voltage source converter is considered as a grid-connected converter with an LCL-filter to perform a laboratory test in an experimental set-up. The DS1007 dSPACE system is used to implement the control algorithms in the experiments. The parameters used in both the simulations and the experiment are shown in Table 3-I.

Table 3-I. "Parameters for simulation"[43] and test of HSS modeling

Parameters	Value
Power rating (P_w)	1 kW
Grid side inductor (L_g)	1 mH
Converter side inductor (L_f)	3 mH
Filter capacitor (C_f)	4.7 uF
DC link capacitor (C_{dc})	450 uF
DC voltage reference (V^*_{dc})	450 V
DC controller gain ($K_{p(dc)}$ / $K_{i(dc)}$)	0.2 / 20
AC controller gain ($K_{p(ac)}$ / $K_{i(ac)}$)	5 / 500
Low pass filter (K_{lpf})	0.001
Switching frequency (f_{sw})	10 kHz
Grid voltage (v_{pcc})	220 V_{rms}

* Parasitic resistance of inductor is assumed to be 1 μΩ

A. Discussion about the steady-state of harmonics

The output harmonics at steady state can be achieved by using (2-20) when "s" is equal to "0". The identical results can also be calculated by using (2-17) as well. The procedure to calculate the frequency coupling inside the converter is shown in (3.1-11).

$$v_{inv}(t) = sw(t) \cdot v_{dc}(t) \qquad (3.1\text{-}11)$$
$$\mathrm{i}_{dc}(t) = sw(t) \cdot i_{ac}(t)$$

where,

$$\mathrm{sw(t)} = \sum_{k=-h}^{h} SW_i e^{-jk\omega_{sw}}, \mathrm{v_{dc}}(t) = \sum_{m=-h}^{h} V_{dc} e^{-jm\omega_{vdc}}$$

$$\mathrm{i_{ac}}(t) = \sum_{n=-h}^{h} I_{ac} e^{-jn\omega_{iac}}, \mathrm{i_{dc}}(t) = \sum_{p=-h}^{h} I_{dc} e^{-jp\omega_{idc}}$$

$$\mathrm{v_{inv}}(t) = \sum_{q=-h}^{h} V_{inv} e^{-jq\omega_{inv}}$$

The acronyms with small and large letter in (3.1-11) have the same meaning as in Figure 3-1. Equation (3.1-11) is reasonable since "$e^{st} = 1$" when "s=0" in the steady state harmonic analysis. As a result, (3.1-12) can simply represent the frequency coupling of (3.1-11), where the frequency of the dc-current (i_{dc}) depends on the frequency of the modulation (ω_{sw}) as well as the frequency of the ac-current (ω_{iac}). Similarly, the frequency of the inverter output (ω_{inv}) is relevant to both the frequency of dc voltage (ω_{vdc}) but also the modulation frequency (ω_{sw}).
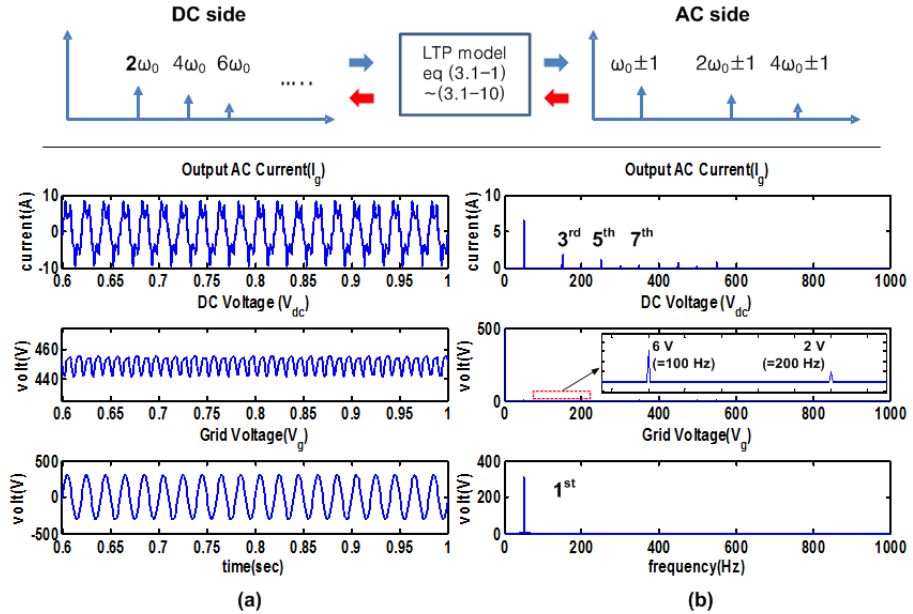
Figure 3-4. "Simulation result of single phase grid converter in steady state (1 kW)"[43]using MATLAB, (a) Time domain simulation results of HSS model, (b) FFT results of HSS model

$$\omega_{idc} = \omega_{sw} \pm \omega_{iac} \qquad (3.1\text{-}12)$$
$$\omega_{inv} = \omega_{sw} \pm \omega_{vdc}$$

Furthermore, the frequency component of the dc-current (ω_{idc}) is multiplied with the frequency component of dc network ($Imp_{dc} = diag \left[\frac{1}{-jh\omega_o C_{dc}} \dots \infty \dots \frac{1}{jh\omega_o C_{dc}} \right]$) to calculate the frequency of dc voltage (ω_{vdc}), and it will be combined with the modulation frequency (ω_{sw}) in order to calculate the frequency of inverter output voltage (ω_{inv}). Additionally, it will generate the frequency of the grid current (ω_{iac}) with the grid frequency as well as ac side admittance $Imp_{ac} = diag \left[-jh\omega_o L_{ac} \dots 0 \dots -jh\omega_o L_{ac} \right]$ with a same manner used in dc side. As a result, 2nd, 4th … even order harmonics can be investigated at the dc side and 1st, 3rd… odd order harmonics can be studied at the ac side based on the coupling behavior, which has been explained in (3.1-11) – (3.1-12). It is available when the grid voltage is purely sinusoidal and there is no additional impedance in the ac and dc network. However, the analysis of the frequency coupling by using (3.1-11) – (3.1-12) may become more difficult as the complexity of network increase. On the contrary, the HSS model can include all mathematical relationships, which are described in (3.1-11) – (3.1-12) and give a lot of information. The simulation result of frequency coupling is shown in Figure 3-4, where the parameters in Table 3-I are used in the HSS simulation.
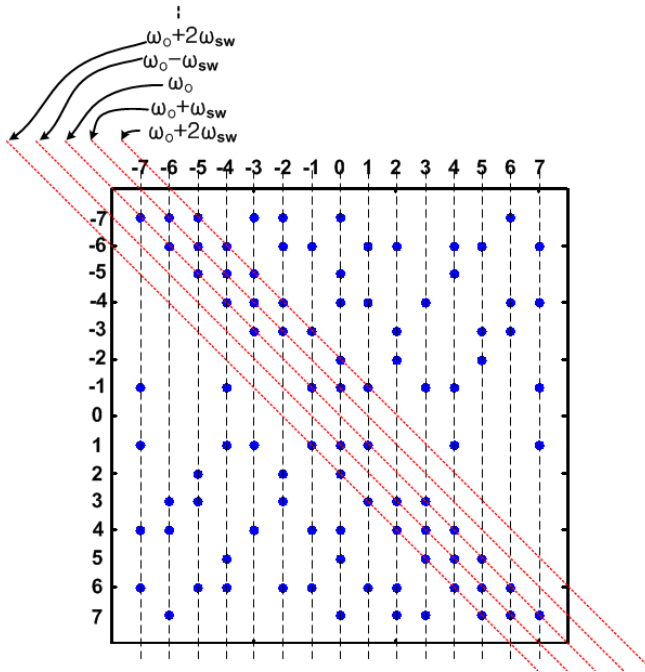
Figure 3-5. "Harmonic admittance map derived from the HSS model (s=0), where the x-axis is the harmonic vector (-7th ~7th) of v_g and the y-axis is harmonic vector (-7th ~ 7th) of i_g"[43].

The grid current shows a distorted waveform even if the input grid voltage is not distorted because both the modulation and the dc-side harmonics are involved in the coupling of harmonics as shown in Figure 3-4, where ω_0 is the fundamental frequency of the harmonics. The generated harmonics on both the ac- and the dc-side shows identical results. It is noted that the simulation results in Figure 3-4 are from the direct HSS simulation (s=0). For instance, the sparse matrix of the harmonic admittance is plotted in Figure 3-5 by using MATLAB, where the "blue dot" implies the important admittances (> 0.000001), which is obtained by (2-20) and considers all harmonic impedances in steady state. The grid currents (i_g) in the time domain and the FFT results are extracted by the matrix in Figure 3-5. It is worth to note that main diagonal axis (ω_0) of the matrix in Figure 3-5 is the grid frequency, and it is mutually coupled with off-diagonal axis ($...\omega_0 - \omega_{sw}, \omega_o + \omega_{sw}, ...$). Additionally, the output harmonic vectors (column) do not have a meaning if the input harmonic vectors (row) are multiplied with harmonic admittance having "0". On the contrary to this characteristic, the harmonics from the grid voltage (row) may not have a distorted grid current according to the coupled admittance from circuit and controller parameter. As a conclusion, the steady state matrix from (2-20) can give an accurate coupling map to describe how the harmonics are coupled, generated, reduced, and canceled.
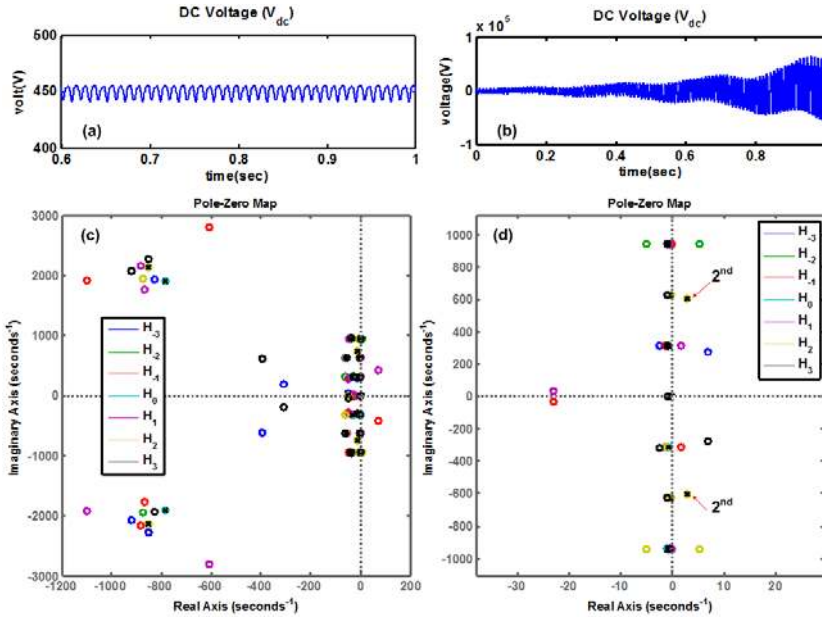
Figure 3-6. "Dynamic simulation result of a single phase grid connected converter (1 kW), where $H_k(s)$ is the harmonic transfer function (k= -3~3)"[43]

(a) Time domain result of the HSS model (Kp=0.5), (b) Time domain result of the HSS model (Kp=3), (c) Pole Zero map of the HSS model (stable case, Kp=0.5), (d) Pole Zero mapping of the HSS model (unstable case, Kp=3)

B. Discussion about the dynamic of harmonics

The dynamic operation of each harmonic can also be simulated by means of the HSS model. $-3^{rd} \sim 3^{rd}$ harmonics are considered in Figure 3-6 for the simplicity. As shown in Figure 3-6-(a), the dc voltage (v_{dc}) is stable when the gain of voltage controller is $K_p = 0.5$. The result in the time-domain shows the same behavior in the pole-zero map as shown in Figure 3-6-(c), where all poles (X) of the harmonic transfer function are located in the Left Half Plane (LHP). However, the system is being unstable if the proportional gain (K_p) is increased as shown in Figure 3-6-(b). Furthermore, the results of the pole-zero map show an unstable state since two poles (X) of the 2nd order harmonic transfer function are located in the Right Half Plane (RHP) as shown in Figure 3-6-(d). However, it is worth note that the poles of the other harmonics transfer function are still in the LHP and thereby they are stable.
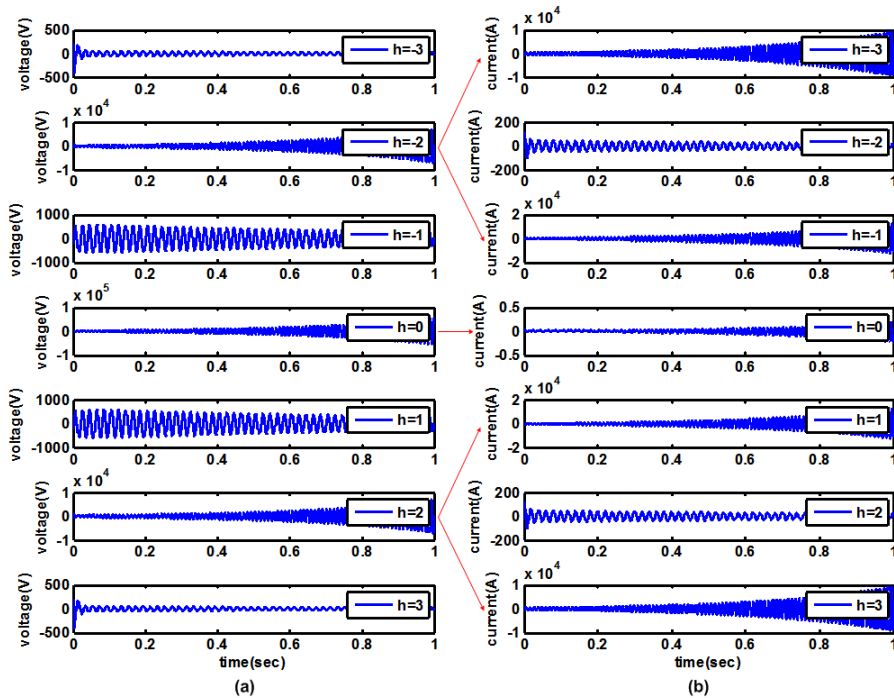
Figure 3-7. "Dynamic harmonic response of single phase grid connected converter in the unstable region (1 kW), where h is the harmonic order (h=-3~3), (a) Harmonic response of dc side from HTF, (b) harmonic response of ac side from HTF"[43]

The dynamic responses of each harmonic in the time-domain are plotted in Figure 3-7 by using (2-20) in order to investigate the movement of pole and zeros, which are shown in Figure 3-6. As shown in the pole-zero map, the time response of the second order harmonics at the dc side shows an unstable waveform as shown in Figure 3-7-(a). However, it is worth to note that the time responses of other

harmonics are still stable, even though they have small oscillations. Additionally, the instability of the 2nd order harmonic may be directly transferred to the ac side because of the frequency coupling between ac and dc side. As a result, it can be investigated whether the time responses of the 1st and 3rd harmonic at the ac-side are unstable. However, the time response of 2nd order harmonic is converging to a steady state value as shown in Figure 3-7-(b).
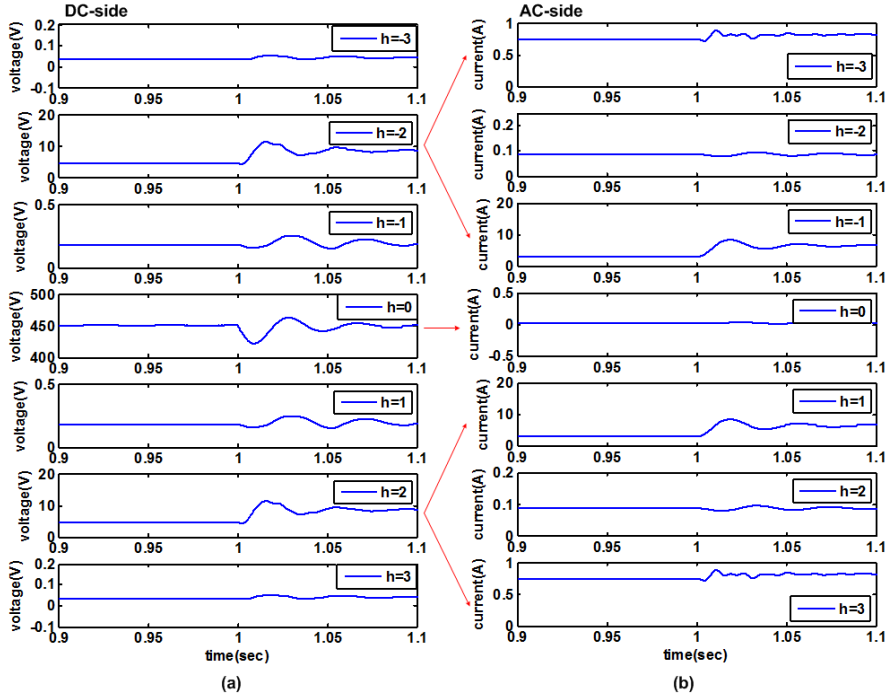
Figure 3-8. "Dynamic harmonic response of single phase grid connected converter at stable region(1 kW to 2 kW), where h is the harmonic order (h=-3~3), (a) Harmonic response of dc side from HTF, (b) Harmonic response of ac side from HTF" [43].

Furthermore, the time responses in the stable region are simulated and shown in Figure 3-8 to investigate the dynamics of each harmonic, where the dc - load is changed from 1 kW to 2 kW at 1 sec. The dc component and second order harmonics (h = -2, 0, 2) have relatively larger transient than other harmonics (h = -3,-1, 1, 3) as shown in Figure 3-8-(a). Even though there are small variations in the odd order harmonics since they are also coupled to others according to the rule in (3.1-11) and (3.1-12), the strength of the coupling is weak compared to the even harmonics. It is worth to note that other harmonics are also coupled with each other in the practical case. Similarly, the odd harmonics (h = -3, -1, 1, 3) in the ac current side show relatively larger transients compared to the even harmonics (h = -2, 2) as shown in Figure 3-8-(b) due to the frequency coupling. However, even harmonics in ac side just have a small variation due to the coupling with other harmonic impedances.

C. Discussion about the difference with the conventional SSAV approach

The state-space averaging (SSAV) method is selected as a conventional approach to compare the difference with the introduced Harmonic State Space (HSS) approach. The current controller is only considered in the SSAV model because the dc-voltage is constant and will not affect the dynamics of the current controller [67]–[70] according to the assumption of SSAV. Hence, the impedance based model from the SSAV method [67] is implemented in order to compare the differences.
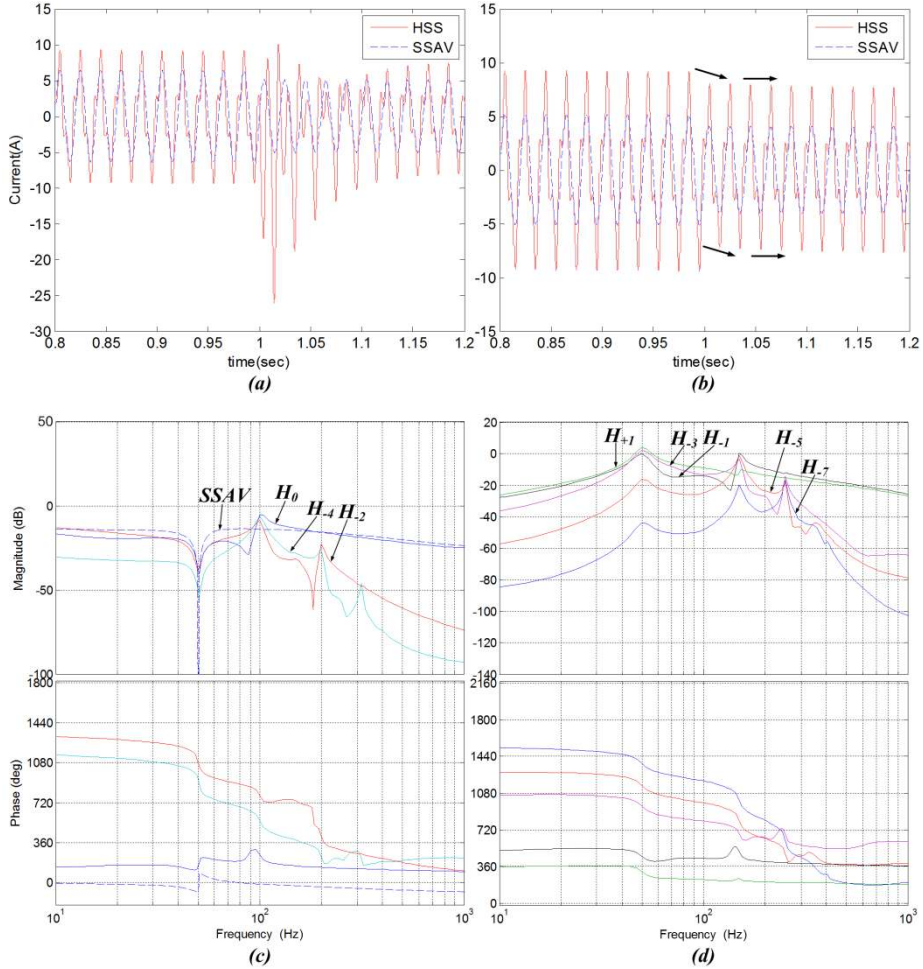
Figure 3-9. "Comparison of HSS and SSAV methods, (a) Grid current (Case #1), (b) Grid current (Case #2), (c) Output admittance (Case #1) $(Y_{oc}(=\frac{i_g}{v_{pcc}}))$, (d) Frequency response of closed loop (Case #1) $(G_{cl}(=\frac{i_g}{v_{dc}^*}))$"[43].

Equation (3.1-13) is derived from the current-controlled grid-connected converter [67], where $G_{cl}(s)$ is the closed-loop transfer function and $Y_{oc}(s)$ is the closed-loop output admittance. Additionally, i_g^* is the reference of the grid current, v_{pcc} is the pcc voltage and i_g is the controlled output current [67].

$$i_g(s) = G_{cl}(s)i_g^*(s) - Y_{oc}(s)v_{pcc}(s) \qquad (3.1-13)$$

As a result the impedance of the SSAV model is also calculated by using MATLAB based on equation (3.1-13). The PCC voltage (Δv_{pcc}) and the reference of the grid current (Δi_g^*) are considered as the input values of the SSAV model, where the parameters used in the HSS simulation are used as well for the simulation of the SSAV model. The dynamics of the HSS model and the SSAV model are compared by two different cases.

- Case #1 : The reference of the dc-voltage controller is changed from 450 V to 400 V at 1 sec.
- Case #2 : The dc-load is changed from 1 kW to 0.8 kW at 1 sec, where the reference of the dc-voltage controller is not changed."[43]

The time responses of Case #1 are shown in Figure 3-9-(a), where "red-line" is from the impedance of HSS model and "blue-line" is from the impedance of SSAV model. It can be seen in Figure 3-9-(a) that the time response from the SSAV model shows explicitly the different dynamics with the time response of the HSS method. The difference is mainly because of the coupled dynamics between the ac and dc network through the switch network which are reflected in "red-line", but they are not taken into account in "blue-line". However, the dynamics of the HSS and the SSAV only show a minor difference in Figure 3-9-(b) since the condition of the dc voltage in HSS model is almost similar with a constant value. The compared results definitely show how the converter or inverter can be analyzed by using the SSAV method. However, the important aspects are that there are still differences in Figure 3-9-(b), and it is due to the dynamics of the coupled harmonics.

The Bode diagram of the HSS model and the SSAV model are also compared in Figure 3-9-(c), (d). In the case of HSS model, the dominant transfer functions are only depicted for the visibility. The closed loop output admittance (Y_{oc}) of the two approaches are only analyzed at the same frequency domain since the frequency coupling as well as the dc-network are included in the closed loop transfer function (G_{cl}) of the HSS model, and it is difficult to directly compare with the closed loop transfer function (G_{cl}) of the SSAV model. The dominant parts of the frequency responses are only depicted in Figure 3-9-(c), (d) to analyze the dynamics of the time responses in Figure 3-9-(a), (b). If the single-input is perturbed at a specific frequency in the HSS model, it gives multiple outputs as shown in Figure 3-9-(c), (d), but a single perturbation in the SSAV model may give only a single output. It is worth to note that the final output of the converter is dominantly governed by a single frequency response. Furthermore, they are also ruled by the multiple

frequency responses from the HSS model. Both the SSAV model and the HSS (H_0) model in Figure 3-9-(c) derive a similar response. However, the transfer function from the HSS model shows a small difference at 100 Hz, which is additionally obtained by the coupling procedure. Furthermore, the frequency responses of the H_{-4}, H_{-2} are dominant in a certain frequency range (around 100 Hz). The harmonic transfer functions from the HSS model also govern the closed loop transfer function based on the range of the input frequency as shown in Figure 3-9-(d).

As a conclusion, the dynamic behaviors of the converters are coupled with each other. Furthermore, the phenomenon can only be estimated through multiple frequency responses (MIMO) like the HSS model. Even though the conventional approach based on some assumptions can approximately estimate the overall stability of the grid-connected converter, the results from HSS model show that the main frequency response is coupled, shifted, transformmed and ruled by other harmonic frequencies in the specific frequency range, and the results from the HSS model shows more accurate results.
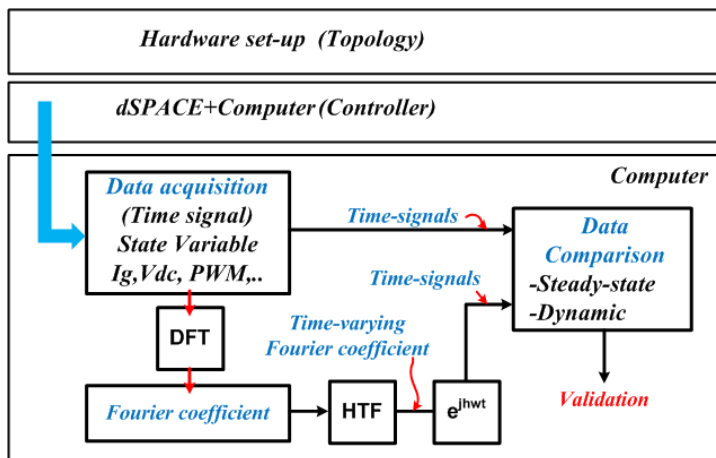
Figure 3-10. "Diagram for the experimental validation of the HSS model (HTF)" [43]

C. Experimental results

The experimental validation is performed by using the signal processing to analyze the signals. Additionally, the harmonic compensators or controllers to eliminate the harmonics are not included in the experiment in order to study the basic coupling of the power converter. Additionally, the current controller is only used for the control of the fundamental frequency. The test set-up for validation is divided into three stages as shown in Figure 3-10. First, a single phase voltage source inverter is used for the hardware platform of single phase grid converter. Second, the converter is mainly controlled by dSPACE platform (DS1107), where the dc voltage (v_{dc}), the grid voltage (v_{pcc}) and the grid current (i_g) are sensed through the sensing board to control the grid connected converter. A number of transfer functions are considered

in the whole model to verify the HTF method in the experiment. The third step is shown in Figure 3-10, where it is emulating the same dynamic performance in the experimental measurement. It can start from the measurement of interesting signals at steady state. The time-domain data are measured from the control desk of the dSPACE platform by using a record function. The measurement simultaneously measures the current of converter-side filter, voltage of capacitor, the state of the PI controller, PWM signals, and the grid voltage. The recorded time-domain signals can be converted into the frequency domain by using the Discrete Fourier Transform (DFT). The same number of harmonics as with the simulation is sorted by using a sorting algorithm. Then, the decomposed Fourier coefficients are inserted into the Harmonic Transfer Function (HTF) in (3.1-3)-(3.1-10) as the initial state variable and the input. Conclusively, the HSS model from (3.1-3)-(3.1-10) can then be verified by using the measured data from the experiments. The output of the HTF is time-varying Fourier coefficients including the information of the experimental set-up. Finally, the time-varying Fourier coefficient from the outputs of HTF can be transformed into the ac signals in the time-domain by rotating the phasor ($e^{jh\omega t}$) and their summation shows the time domain signals. In the final stage, the achieved time-domain signals from the HTF are finally made to compare with the measured signals. The final comparisons are shown in Figure 3-11, where the signals from harmonic matrix are compared with nonlinear time domain simulation and experimental results. The frequency coupling between ac-circuit and dc-circuit through the switching brings harmonic distortions in Figure 3-10 as described in (3.1-11) - (3.1-12). Hence, it is worth to note that the single-phase grid-connected converter with grid side filter itself generates low-order harmonics [52], [71], e.g., the odd-order harmonics in the ac-current side and the even-order harmonics in the dc-voltage side, even if the grid voltage is not distorted. However, if the current reference is increased, the percent ratio of the low order harmonics is relatively lower. Hence, the experiments as well as the simulation are performed at the low power rating to investigate the coupling procedure and their result on both sides.

The results from analytical model match well with the PLECS time domain simulation as shown in Figure 3-11-(a). It means that the coupled harmonics can be modeled by the harmonics transfer function. Furthermore, the simulations results from analytical model are compared with the experimental results shown in Figure 3-11-(b), where the main harmonics of both results matched correctly except for the even order harmonics. The dead time (<1us – 2 us) and the error of the FFT analysis may bring errors into the comparison. As an alternative, the error could be reduced if the resolution of the FFT is increased or the dead time of the converter is linearized at the specific operating point. However, the calculation time to get the HTF model can be increased due to the size of the matrix. Hence, the selection of the number of harmonics and the resolution of the FFT are quite important criteria for the analysis. However, the results show that the model obtained by HSS model has more advantages to analyze the frequency coupling and their effects in the system.
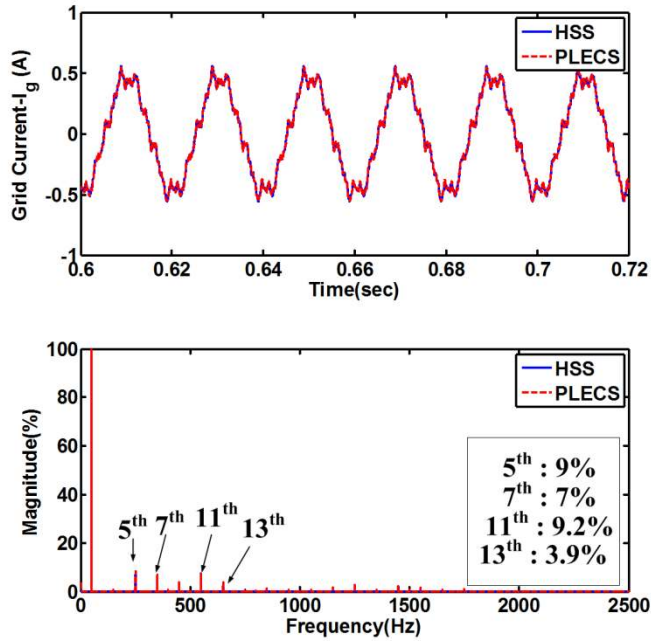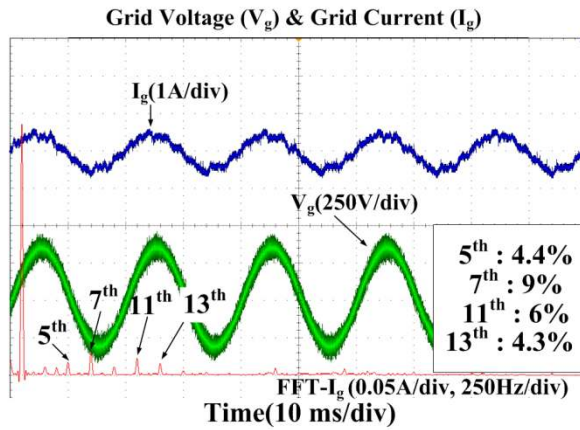
Figure 3-11. "Simulation and experimental results for 1 kW single phase inverter : Converter side inductor L_f = 3 mH, grid side inductor L_g = 1 mH, filter capacitance C_f = 4.7 uF, dc link capacitor = 450 uF, dc link voltage = 450 V, Grid Voltage = 230 V, switching frequency = 10 kHz) – Grid side inductor current simulation (harmonic = $-40^{th} - 40^{th}$) waveform

(a) Simulation by HSS and PLECS (grid side inductor current (Ig) 0.5 A injection), (b) Experimental results of the grid side inductor current (I_g) 0.5 A injection (blue = grid side current, green = grid voltage, red= FFT waveform of grid side current)"[43].

3.1.3. SUMMARY AND CONCLUSION

This section has proposed a new frequency domain model of single-phase grid-connected converter by using the HSS modeling method. The simulation results from the analytical model (HTF) show that the steady-state as well as the dynamics of harmonics are brought by the coupling between the ac and dc circuit. Furthermore, the stable or unstable operation of the single phase grid-connected converter is also strongly relevant with frequency coupling. In the case of a LTI (Linear Time Invariant) based model like SSAV, the coupling and their effects on the operation of converter can normally not be considered in details. However, the LTP (Linear Time varying Periodically) theory and HSS model can take into account the characteristics of MIMO (Multi Input Multi Output) systems and the time-varying behavior. The developed model in this chapter can be expanded into the analysis of frequency coupling with other converters or loads. The unknown stability region in the LTI model can also be investigated by involving HTF in the model, where the frequency response from the LTI model is a part of LTP model.

3.2. HSS MODELING OF 3-PHASE VSC SYSTEMS

This section develops an accurate model of the three-phase grid-connected converter by using the HSS modeling method. First, the model differences between LTI (Linear Time Invariant) and LTP (Linear Time varying Periodically) are reviewed by comparing the structure and their principles. Second, a detailed procedure of the modeling is described by including how the switching component and harmonics can be involved in the modeling procedure through the HSS modeling. Third, the frequency coupling of the converter inside is analyzed by using the developed model. Both dynamic and steady-state harmonic interactions are then analyzed from the grid and load disturbance by using the achieved model. Last, both simulation and experimental results are included in order to validate the proposed method.

3.2.1. HSS MODELING OF GRID-CONNECTED CONVERTER
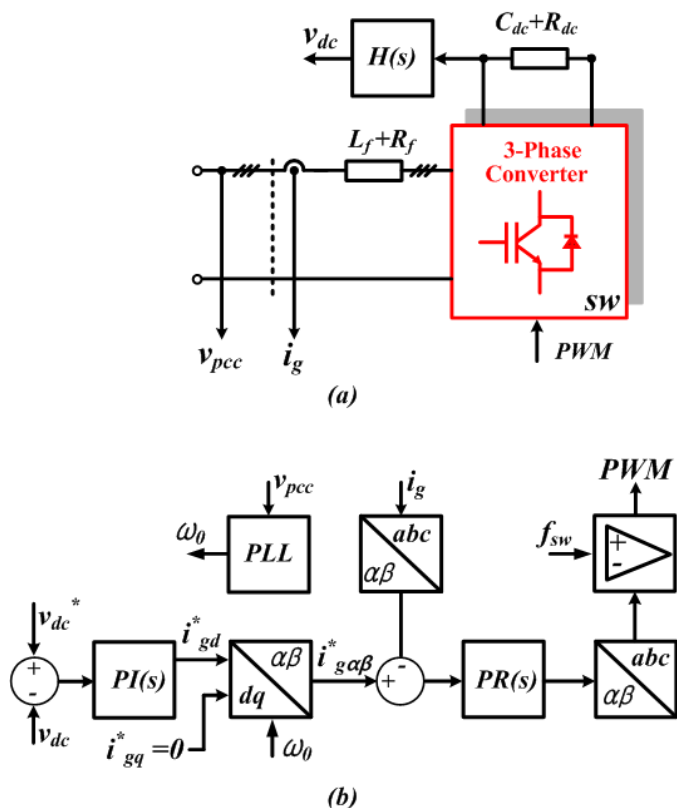
Figure 3-12. Block diagram of a 3-phase grid-connected converter

(a) Topology, (b) Controller.

The block diagram of a 3-phase grid-connected converter is shown in Figure 3-12. The HSS modeling is performed in two separate parts. First, the topology part as shown in Figure 3-12-(a) is considered, where grid-side inductor (L_g+R_g), inverter-side inductor (L_f+R_f) and ac filter capacitor (C_f+R_{cf}) are connected to the ac-side and the dc link capacitor ($C_{dc}+R_{dc}$) is connected to the dc-side circuit through a switch network. Secondly, the controller part in Figure 3-12-(b) is modeled by means of the LTP theory. The dc voltage reference (v_{dc}^*) is compared with a sensed dc voltage (v_{dc}) through a low pass filter ($H(s)$) and the error is controlled by a PI controller ($PI(s)$). The derived d-axis current reference (i_{gd}^*) is transformed into alpha-beta coordinates ($i_{g\alpha\beta}^*$) and the references are compared with the transformed sensing current ($i_{g\alpha\beta}$). The errors are compensated by means of PR controller ($PR(s)$). Finally, the achieved reference frame is re-transformed into abc-coordinates to be compared with a triangle waveform and the results (PWM) are used to operate switches. The modeling procedure is explained by two parts in topology and controller.
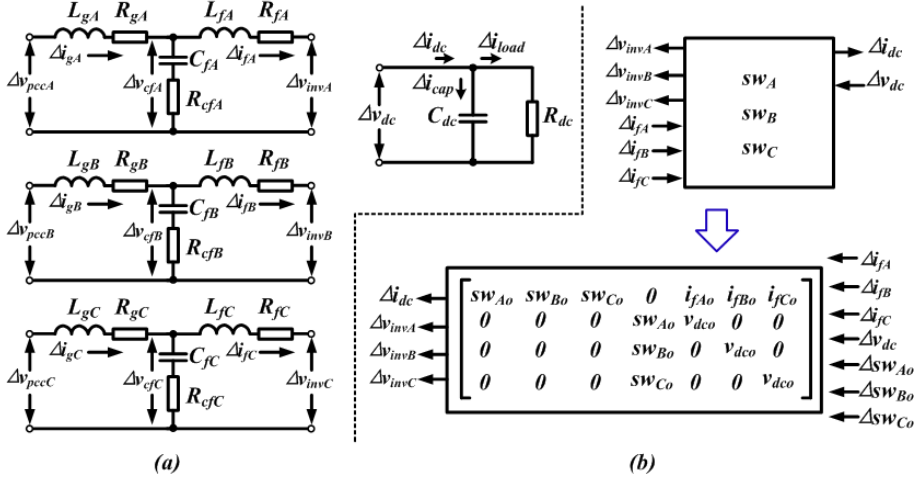
Figure 3-13. Linearization of a 3-phase grid-connected converter (a) ac / dc filter, (b) switching network

A. Topology Modeling

The simple block diagrams in Figure 3-12-(a) can be decomposed as shown in Figure 3-13, where all acronyms in Figure 3-12 have the same meaning as given in Figure 3-12-(a). The small signal representation (Δ) is used in the differential equation to achieve a small signal based HSS model. According to the circuit relation described in Figure 3-13-(a), the ac-side circuit and dc-side circuit can be represented as given in (3.2-1)~(3.2-5), where v_{capABC} is the ac filter capacitor voltage and other acronyms are used from Figure 3-12 ~ Figure 3-13.

$$\frac{d}{dt}\Delta i_{gA} = \frac{\Delta v_{pccA} - \Delta v_{cfA}}{L_{gA}} - \frac{R_{gA}}{L_{gA}}\Delta i_{gA} \tag{3.2-1}$$

$$\frac{d}{dt}\Delta i_{gB} = \frac{\Delta v_{pccB} - \Delta v_{cfB}}{L_{gB}} - \frac{R_{gB}}{L_{gB}}\Delta i_{gB}$$

$$\frac{d}{dt}\Delta i_{gC} = \frac{\Delta v_{pccC} - \Delta v_{cfC}}{L_{gC}} - \frac{R_{gC}}{L_{gC}}\Delta i_{gC}$$

$$\frac{d}{dt}\Delta i_{fA} = \frac{\Delta v_{cfA} - \Delta v_{invA}}{L_{fA}} - \frac{R_{fA}}{L_{fA}}\Delta i_{fA} \tag{3.2-2}$$

$$\frac{d}{dt}\Delta i_{fB} = \frac{\Delta v_{cfB} - \Delta v_{invB}}{L_{fB}} - \frac{R_{fB}}{L_{fB}}\Delta i_{fB}$$

$$\frac{d}{dt}\Delta i_{fC} = \frac{\Delta v_{cfC} - \Delta v_{invC}}{L_{fC}} - \frac{R_{fC}}{L_{fC}}\Delta i_{fC}$$

$$\Delta i_{dc} = \frac{\Delta v_{dc}}{R_{dc}} + C_{dc}\frac{d}{dt}\Delta v_{dc} \tag{3.2-3}$$

$$\Delta v_{cfA} = \Delta v_{capA} + \left(\Delta i_{gA} - \Delta i_{fA}\right)R_{cfA} \tag{3.2-4}$$

$$\Delta v_{cfB} = \Delta v_{capB} + \left(\Delta i_{gB} - \Delta i_{fB}\right)R_{cfB}$$

$$\Delta v_{cfC} = \Delta v_{capC} + \left(\Delta i_{gC} - \Delta i_{fC}\right)R_{cfC}$$

$$\frac{d}{dt}\Delta v_{capA} = \frac{\Delta i_{gA} - \Delta i_{fA}}{C_{fA}} \tag{3.2-5}$$

$$\frac{d}{dt}\Delta v_{capB} = \frac{\Delta i_{gB} - \Delta i_{fB}}{C_{fB}}$$

$$\frac{d}{dt}\Delta v_{capC} = \frac{\Delta i_{gC} - \Delta i_{fC}}{C_{fC}}$$

The switching (*sw*) generated by the PWM and their relationship with the ac- and dc-side circuit can be represented as given (3.2-6) ~ (3.2-7) and Figure 3-13-(b), where the converter side filter currents (i_{fABC}) are multiplied with the switching (*sw*) to generate the dc current (i_{dc}). The generated dc voltage (v_{dc}) is repetitively multiplied with the switching (*sw*) to supply the converter output voltage (v$_{invABC}$). Even though the switching (sw) in (3.2-6) should be $sw_{A,B,C} - (sw_A + sw_B + sw_C)/3$, "$(sw_A + sw_B + sw_C)/3$" is neglected since the summation of the 3-phase switching is zero when the grid-connected converter is operating in balanced conditions. Furthermore, even though the switching does not have state variable information, it is mainly required to linearize the switching property at a specific operating point to include a switching instant variation driven by the controller behavior. The linearized results are given in (3.2-8) ~ (3.2-9) assuming that the switching instant from the controller behavior is very small. The subscript "o" in (3.2-8) ~ (3.2-9) means a previous state value that can be obtained from hand calculation or nonlinear simulation results. The acronym "Δ" means small variations of signals, which are generated from the dynamic controller behavior.

$$v_{invA}(t) = v_{dc}(t)sw_A(t) \tag{3.2-6}$$

$$v_{invB}(t) = v_{dc}(t)sw_B(t)$$
$$v_{invC}(t) = v_{dc}(t)sw_C(t)$$

$$i_{dc}(t) = i_{fA}(t)sw_A(t) + i_{fB}(t)sw_B(t) + i_{fC}(t)sw_C(t) \tag{3.2-7}$$

$$\Delta v_{invA} = sw_{Ao}\Delta v_{dc} + v_{dco}\Delta sw_A \tag{3.2-8}$$
$$\Delta v_{invB} = sw_{Bo}\Delta v_{dc} + v_{dco}\Delta sw_B$$
$$\Delta v_{invC} = sw_{Co}\Delta v_{dc} + v_{dco}\Delta sw_C$$

$$\Delta i_{dc} = sw_{Ao}\Delta i_{fA} + i_{fAo}\Delta sw_A + \tag{3.2-9}$$
$$sw_{Bo}\Delta i_{fB} + i_{fBo}\Delta sw_B +$$
$$sw_{Co}\Delta i_{fC} + i_{fCo}\Delta sw_C$$

The small signal and the differential equation (3.2-1) ~ (3.2-5) can be transformed into state space equation as given (3.2-10) by substituting (3.2-8) and (3.2-9) into (3.2-2) and (3.2-3).

$$\dot{x}_t = A_t x_t + B_t u_t \tag{3.2-10}$$

where,

$x_t = [\Delta i_{gA}\ \Delta i_{gB}\ \Delta i_{gC}\ \Delta v_{capA}\ \Delta v_{capB}\ \Delta v_{capC}\ \Delta i_{fA}\ \Delta i_{fB}\Delta i_{fC}\ \Delta v_{dc}]^T$,

$u_t = [\Delta v_{pccA}\ \Delta v_{pccB}\ \Delta v_{pccC}\ \Delta sw_A\ \Delta sw_B\ \Delta sw_C]^T$, A_t , $B_t$are given in (3.2-11) ~ (3.2-12) as :

$$A_t = \begin{bmatrix}
\frac{-R_{gA}-R_{cfA}}{L_{gA}} & 0 & 0 & \frac{-1}{L_{gA}} & 0 & 0 & \frac{R_{cfA}}{L_{gA}} & 0 & 0 & 0 \\
0 & \frac{-R_{gB}-R_{cfB}}{L_{gB}} & 0 & 0 & \frac{-1}{L_{gB}} & 0 & 0 & \frac{R_{cfB}}{L_{gB}} & 0 & 0 \\
0 & 0 & \frac{-R_{gC}-R_{cfC}}{L_{gC}} & 0 & 0 & \frac{-1}{L_{gC}} & 0 & 0 & \frac{R_{cfC}}{L_{gC}} & 0 \\
\frac{1}{C_{fA}} & 0 & 0 & 0 & 0 & 0 & \frac{-1}{C_{fA}} & 0 & 0 & 0 \\
0 & \frac{1}{C_{fB}} & 0 & 0 & 0 & 0 & 0 & \frac{-1}{C_{fB}} & 0 & 0 \\
0 & 0 & \frac{1}{C_{fC}} & 0 & 0 & 0 & 0 & 0 & \frac{-1}{C_{fC}} & 0 \\
\frac{R_{cfA}}{L_{fA}} & 0 & 0 & \frac{1}{L_{fA}} & 0 & 0 & \frac{-R_{fA}-R_{cfA}}{L_{fA}} & 0 & 0 & \frac{-sw_{Ao}}{L_{fA}} \\
0 & \frac{R_{cfB}}{L_{fB}} & 0 & 0 & \frac{1}{L_{fB}} & 0 & 0 & \frac{-R_{fB}-R_{cfB}}{L_{fB}} & 0 & \frac{-sw_{Bo}}{L_{fB}} \\
0 & 0 & \frac{R_{cfC}}{L_{fC}} & 0 & 0 & \frac{1}{L_{fC}} & 0 & 0 & \frac{-R_{fC}-R_{cfC}}{L_{fC}} & \frac{-sw_{Co}}{L_{fC}} \\
0 & 0 & 0 & \frac{sw_{Ao}}{C_{dc}} & \frac{sw_{Bo}}{C_{dc}} & \frac{sw_{Co}}{C_{dc}} & 0 & 0 & 0 & \frac{-1}{R_{dc}C_{dc}}
\end{bmatrix}$$

$$\tag{3.2-11}$$

$$B_t = \begin{bmatrix} \frac{1}{L_{gA}} & 0 & 0 & 0 & 0 & 0 \\ 0 & \frac{1}{L_{gB}} & 0 & 0 & 0 & 0 \\ 0 & 0 & \frac{1}{L_{gC}} & 0 & 0 & 0 \\ 0 & 0 & 0 & 0 & 0 & 0 \\ 0 & 0 & 0 & 0 & 0 & 0 \\ 0 & 0 & 0 & 0 & 0 & 0 \\ 0 & 0 & 0 & \frac{-v_{dco}}{L_{fA}} & 0 & 0 \\ 0 & 0 & 0 & 0 & \frac{-v_{dco}}{L_{fA}} & 0 \\ 0 & 0 & 0 & 0 & 0 & \frac{-v_{dco}}{L_{fA}} \\ 0 & 0 & 0 & \frac{i_{fAo}}{C_{dc}} & \frac{i_{fBo}}{C_{dc}} & \frac{i_{fCo}}{C_{dc}} \end{bmatrix} \tag{3.2-12}$$

As a result, (3.2-10) ~ (3.2-12) should be converted into the LTP formulation according to the assumption that all signals are varying periodically and they can be linearized in periodic trajectories. Hence (3.2-13) ~ (3.2-15) can be obtained by using the HSS modeling procedure that is introduced in (2-13) ~ (2-16).

$$\dot{X}_f = A_f X_f + B_f U_f \tag{3.2-13}$$

where, $X_f = \begin{bmatrix} \Delta I_{gA} & \Delta I_{gB} & \Delta I_{gC} & \Delta V_{capA} & \Delta V_{capB} & \Delta V_{capC} & \Delta I_{fA} & \Delta I_{fB} & \Delta I_{fC} & \Delta V_{dc} \end{bmatrix}^T$, $U_f = \begin{bmatrix} \Delta V_{pccA} & \Delta V_{pccB} & \Delta V_{pccC} & \Delta SW_A & \Delta SW_B & \Delta SW_C \end{bmatrix}^T$, A_f and B_f are given in (3.2-14) ~ (3.2-15). The small letter in (3.2-10) ~ (3.2-11) means the time-domain signal. The capital letters in (3.2-13) ~ (3.2-15) are the harmonic coefficient component from $[\ldots - h \ldots - 1,0,1 \ldots h \ldots]$, which are derived from the Fourier series. In this chapter, -20th~20th harmonics order are considered to analyze the harmonic interaction by the 20th harmonics.

$$B_f = \begin{bmatrix} \frac{1}{L_{gA}}I & Z_M & Z_M & Z_M & Z_M & Z_M \\ Z_M & \frac{1}{L_{gB}}I & Z_M & Z_M & Z_M & Z_M \\ Z_M & Z_M & \frac{1}{L_{gC}}I & Z_M & Z_M & Z_M \\ Z_M & Z_M & Z_M & Z_M & Z_M & Z_M \\ Z_M & Z_M & Z_M & Z_M & Z_M & Z_M \\ Z_M & Z_M & Z_M & Z_M & Z_M & Z_M \\ Z_M & Z_M & Z_M & \frac{-\Gamma[V_{dco}]}{L_{fA}} & Z_M & Z_M \\ Z_M & Z_M & Z_M & Z_M & \frac{-\Gamma[V_{dco}]}{L_{fA}} & Z_M \\ Z_M & Z_M & Z_M & Z_M & Z_M & \frac{-\Gamma[V_{dco}]}{L_{fA}} \\ Z_M & Z_M & Z_M & \frac{\Gamma[I_{fAo}]}{C_{dc}} & \frac{\Gamma[I_{fBo}]}{C_{dc}} & \frac{\Gamma[I_{fCo}]}{C_{dc}} \end{bmatrix} \tag{3.2-14}$$

$$A_f =
\begin{bmatrix}
\frac{-R_{gA}-R_{cfA}}{L_{gA}}I - N & Z_M & Z_M & \frac{-1}{L_{gA}}I & Z_M & Z_M & \frac{R_{cfA}}{L_{gA}}I & Z_M & Z_M & Z_M \\[4pt]
Z_M & \frac{-R_{gB}-R_{cfB}}{L_{gB}}I - N & Z_M & Z_M & \frac{-1}{L_{gB}}I & Z_M & Z_M & \frac{R_{cfB}}{L_{gB}}I & Z_M & Z_M \\[4pt]
Z_M & Z_M & \frac{-R_{gC}-R_{cfC}}{L_{gC}}I - N & Z_M & Z_M & \frac{-1}{L_{gC}}I & Z_M & Z_M & \frac{R_{cfC}}{L_{gC}}I & Z_M \\[4pt]
\frac{1}{C_{fA}}I & Z_M & Z_M & -N & Z_M & Z_M & \frac{-1}{C_{fA}}I & Z_M & Z_M & Z_M \\[4pt]
Z_M & \frac{1}{C_{fB}}I & Z_M & Z_M & -N & Z_M & Z_M & \frac{-1}{C_{fB}}I & Z_M & Z_M \\[4pt]
Z_M & Z_M & \frac{1}{C_{fC}}I & Z_M & Z_M & -N & Z_M & Z_M & \frac{-1}{C_{fC}}I & Z_M \\[4pt]
\frac{R_{cfA}}{L_{fA}}I & Z_M & Z_M & \frac{1}{L_{fA}}I & Z_M & Z_M & \frac{-R_{fA}-R_{cfA}}{L_{fA}}I - N & Z_M & Z_M & \frac{-\Gamma[SW_{Ao}]}{L_{fA}} \\[4pt]
Z_M & \frac{R_{cfB}}{L_{fB}}I & Z_M & Z_M & \frac{1}{L_{fB}}I & Z_M & Z_M & \frac{-R_{fB}-R_{cfB}}{L_{fB}}I - N & Z_M & \frac{-\Gamma[SW_{Bo}]}{L_{fB}} \\[4pt]
Z_M & Z_M & \frac{R_{cfC}}{L_{fC}}I & Z_M & Z_M & \frac{1}{L_{fC}}I & Z_M & Z_M & \frac{-R_{fC}-R_{cfC}}{L_{fC}}I - N & \frac{-\Gamma[SW_{Co}]}{L_{fC}} \\[4pt]
Z_M & Z_M & Z_M & \frac{\Gamma[SW_{Ao}]}{C_{dc}} & \frac{\Gamma[SW_{Bo}]}{C_{dc}} & \frac{\Gamma[SW_{Co}]}{C_{dc}} & Z_M & Z_M & Z_M & \frac{-1}{R_{dc}C_{dc}}I - N
\end{bmatrix}
\tag{3.2-15}$$

The direct results from (3.2-13) can be re-transformed into the time-domain signal by using (2-13) according to the principle of *LTP*. Additionally, "*I*" denotes the identity matrix, "Z_M" is zero matrices having the same matrix size with the considered number of harmonics and "N = $diag[-jh\omega_0 \dots - j\omega_0, 0, j\omega_0 \dots jh\omega_0]$" is derived from the derivative procedure of (2-15). The previous value of the time-domain switching functions (sw_{ABCo}), ac filter current (i_{fABCo}) and dc voltage (v_{dco}) are reorganized into a Toeplitz (Γ) [31] matrix in order to perform a convolution. The multiplication of two time-domain signals can be implemented into the frequency domain by means of a convolution, where this can be obtained by using the Toeplitz matrix and the harmonic vectors. The derived output harmonic vector from the Toeplitz matrix can be converted into time-domain signals by using (2-13). Conclusively, the topology in Figure 3-12-(a) is modeled as (3.2-13) by using the HSS modeling method. The derived result shows how small variation of the input harmonics ($\Delta V_{pccABC}, \Delta SW_{ABC}$) can be transferred into output harmonic information ($\Delta I_{gABC}, \Delta I_{fABC}, \Delta V_{capABC}, \Delta V_{dc}$).

B. Controller modelling

Based on Figure 3-12-(b), the controller can also be modeled by using a time-domain differential equation to frequency domain differential equation. The small signal representation (Δ) is used to obtain small variations of the switching (ΔSW_{ABC}) from the controller output. The PLL (Phase Locked Loop) is assumed to provide a steady-state angle information (θ_0) to both current controller and park transformation. Additionally, the Clark transformation in the time-domain can be represented as given in (3.2-16) ~ (3.2-17) in the frequency domain as :

$$clark_{abc-\alpha\beta} = \begin{bmatrix} \frac{2}{3} & -\frac{1}{3} & -\frac{1}{3} \\ 0 & \frac{1}{\sqrt{3}} & -\frac{1}{\sqrt{3}} \end{bmatrix} \qquad (3.2\text{-}16)$$

$$CLARK_{abc-\alpha\beta} = \begin{bmatrix} \frac{2}{3}I & -\frac{1}{3}I & -\frac{1}{3}I \\ Z_M & \frac{1}{\sqrt{3}}I & -\frac{1}{\sqrt{3}}I \end{bmatrix} \qquad (3.2\text{-}17)$$

where (3.2-16) is for time-domain transformation and (3.2-17) is for transformation into the frequency domain. The inputs of (3.2-17) are the Fourier coefficient components derived from sensed signals or from other outputs. In a similar way, the park transformation in time and frequency domain can be represented as given in (3.2-18) ~ (3.2-19). The different aspects of Clark transformation are that the park transformation is a multiplication of two time-domain signals. Hence, the convolution theory, which is explained in the previous section, is also used in the transformation.

$$park_{\alpha\beta} = \begin{bmatrix} \cos(\theta_0) & \sin(\theta_0) \\ -\sin(\theta_0) & \cos(\theta_0) \end{bmatrix} \tag{3.2-18}$$

$$PARK_{\alpha\beta} = \begin{bmatrix} \Gamma[\cos(\theta_0)] & \Gamma[\sin(\theta_0)] \\ -\Gamma[\sin(\theta_0)] & \Gamma[\cos(\theta_0)] \end{bmatrix}$$

$$= \begin{bmatrix} \Gamma\left[\ldots\frac{1}{2},0,\frac{1}{2},\ldots\right] & \Gamma\left[\ldots-\frac{1}{j2},0,\frac{1}{j2},\ldots\right] \\ -\Gamma\left[\ldots-\frac{1}{j2},0,\frac{1}{j2},\ldots\right] & \Gamma\left[\ldots\frac{1}{2},0,\frac{1}{2},\ldots\right] \end{bmatrix} \tag{3.2-19}$$

where "Γ" means a Toeplitz matrix to perform a convolution of two signals and components in Toeplitz matrix mean the Fourier coefficient components of "$\cos(\theta_0)$" and "$\sin(\theta_0)$". Through the multiplication with (3.2-17) or (3.2-18), the same results can come out in the frequency domain as well.

$$PI(s) = K_p + \frac{K_i}{s} \tag{3.2-20}$$

$$PR(s) = K_{pPR} + \frac{sK_{iPR}}{s^2+\omega_0^2} \tag{3.2-21}$$

$$H(s) = \frac{1}{K_{LPF}s+1} \tag{3.2-22}$$

where, K_p, K_i are proportional and integral gain used in PI controller, K_{pPR}, K_{iPR} are PR controller gain employed in both α and β axis and K_{LPF} is low pass filter gain used for the sensing and filtering of dc voltage (v_{dc}). As a result, the HSS model for the controller part can be derived as given in (3.2-23) by using Figure 3-12-(b), (3.2-17), (3.2-19) and (3.2-20) ~ (3.2-22), where the capital letter means a Fourier coefficient (+…-) and acronyms in (3.2-13) have the same meaning as the topology modeling in Figure 3-13.

$$\begin{aligned} X'_{fc} &= A_{fc}X_{fc} + B_{fc}U_{fc} \\ Y_{fc} &= C_{fc}X_{fc} + D_{fc}U_{fc} \end{aligned} \tag{3.2-23}$$

where, $X_{fc} = \begin{bmatrix} \Delta X_{LPF} & \Delta X_{PI} & \Delta X_{PR\alpha1} & \Delta X_{PR\alpha2} & \Delta X_{PR\beta1} & \Delta X_{PR\beta2} \end{bmatrix}^T$, $U_{fc} = \begin{bmatrix} \Delta V_{dc} & \Delta V^*_{dc} & \Delta I_{ga} & \Delta I_{gb} & \Delta I_{gc} \end{bmatrix}^T$, $Y_{fc} = \begin{bmatrix} \Delta SW_A & \Delta SW_B & \Delta SW_C \end{bmatrix}^T$, ΔX_{LPF} is the harmonic state variable of a low pass filter (H(s)) shown in Figure 3-12-(a), ΔX_{PI} is state variable of the PI controller (PI(s)) and $\Delta X_{PR\alpha1}$ $\Delta X_{PR\alpha2}$ $\Delta X_{PR\beta1}$ $\Delta X_{PR\beta2}$ are the state variables used in the PR controller (PR(s)) at the α, β axis and A_{fc}, B_{fc}, C_{fc} and D_{fc} are given in (3.2-24) ~ (3.2-27).

$$A_{fc} = \begin{bmatrix} -\frac{1}{K_{LPF}}I - N & Z_M & Z_M & Z_M & Z_M & Z_M \\ -I & -N & Z_M & Z_M & Z_M & Z_M \\ -K_p\Gamma[\cos(\theta_o)] & K_i\Gamma[\cos(\theta_o)] & -N & -\omega_0^2I & Z_M & Z_M \\ Z_M & Z_M & I & -N & Z_M & Z_M \\ -K_p\Gamma[\cos(\theta_o)] & K_i\Gamma[\sin(\theta_o)] & Z_M & Z_M & -N & -\omega_0^2I \\ Z_M & Z_M & Z_M & Z_M & I & -N \end{bmatrix} \tag{3.2-24}$$

$$B_{fc} = \begin{bmatrix} \frac{1}{K_{LPF}}I & Z_M & Z_M & Z_M & Z_M \\ Z_M & I & Z_M & Z_M & Z_M \\ Z_M & K_p\Gamma[\cos(\theta_o)] & -\frac{2}{3}I & \frac{1}{3}I & \frac{1}{3}I \\ Z_M & Z_M & Z_M & Z_M & Z_M \\ Z_M & K_p\Gamma[\sin(\theta_o)] & Z_M & -\frac{1}{\sqrt{3}}I & \frac{1}{\sqrt{3}}I \\ Z_M & Z_M & Z_M & Z_M & Z_M \end{bmatrix} \qquad (3.2\text{-}25)$$

$$C_{fc} = \begin{bmatrix} C_{fc1} & C_{fc2} & K_{iPR}I & Z_M & Z_M & Z_M \\ C_{fc3} & C_{fc4} & -\frac{K_{iPR}}{2}I & Z_M & \frac{\sqrt{3}}{2}K_{iPR}I & Z_M \\ C_{fc5} & C_{fc6} & -\frac{K_{iPR}}{2}I & Z_M & -\frac{\sqrt{3}}{2}K_{iPR}I & Z_M \end{bmatrix} \qquad (3.2\text{-}26)$$

where,

$$C_{fc1} = -K_{pPR}K_p\Gamma[\cos(\theta_0)]$$
$$C_{fc2} = K_{pPR}K_i\Gamma[\cos(\theta_0)]$$

$$C_{fc3} = \frac{1}{2}K_pK_{pPR}\Gamma[\cos(\theta_0)] - \frac{\sqrt{3}}{2}K_pK_{pPR}\Gamma[\sin(\theta_0)]$$

$$C_{fc4} = \frac{\sqrt{3}}{2}K_iK_{pPR}\Gamma[\sin(\theta_0)] - \frac{1}{2}K_iK_{pPR}\Gamma[\cos(\theta_0)]$$

$$C_{fc5} = \frac{1}{2}K_pK_{pPR}\Gamma[\cos(\theta_0)] + \frac{\sqrt{3}}{2}K_pK_{pPR}\Gamma[\sin(\theta_0)]$$

$$C_{fc6} = -\frac{1}{2}K_iK_{pPR}\Gamma[\cos(\theta_0)] - \frac{\sqrt{3}}{2}K_iK_{pPR}\Gamma[\sin(\theta_0)]$$

$$D_{fc} = \begin{bmatrix} Z_M & K_{pPR}K_p\Gamma[\cos(\theta_0)] & -\frac{2}{3}K_{pPR}I & \frac{K_{pPR}}{3}I & \frac{K_{pPR}}{3}I \\ Z_M & D_{fc1} & D_{fc2} & D_{fc3} & D_{fc4} \\ Z_M & D_{fc5} & D_{fc6} & D_{fc7} & D_{fc8} \end{bmatrix} \qquad (3.2\text{-}27)$$

where,

$$D_{fc1} = \frac{\sqrt{3}}{2}K_{pPR}K_p\Gamma[\sin(\theta_0)] - \frac{1}{2}K_{pPR}K_p\Gamma[\cos(\theta_0)]$$

$$D_{fc2} = \frac{1}{3}K_{pPR}I - \frac{1}{\sqrt{3}}K_{pPR}I$$

$$D_{fc3} = -\frac{1}{6}K_{pPR}I + \frac{1}{2\sqrt{3}}K_{pPR}I$$

$$D_{fc44} = -\frac{1}{6}K_{pPR}I + \frac{1}{2\sqrt{3}}K_{pPR}I$$

$$D_{fc5} = -\frac{\sqrt{3}}{2}K_{pPR}K_p\Gamma[\sin(\theta_0)] - \frac{1}{2}K_{pPR}K_p\Gamma[\cos(\theta_0)]$$

$$D_{fc6} = \frac{1}{3}K_{pPR}I + \frac{1}{\sqrt{3}}K_{pPR}I$$

$$D_{fc7} = -\frac{1}{6}K_{pPR}I - \frac{1}{2\sqrt{3}}K_{pPR}I$$

$$D_{fc8} = -\frac{1}{6}K_{pPR}I - \frac{1}{2\sqrt{3}}K_{pPR}I$$

It is worth to mention that all state variables, inputs and output are harmonic vectors and the size of each matrix components is the same as the number of harmonics used in the modeling procedure. Additionally, the switching harmonics and sideband frequency of the switching frequency are used to investigate the effect of harmonic interaction driven by them. As a conclusion for the HSS model of the topology (3.2-13), where the output vector of (3.2-13) can be chosen by the user depending on which signals user wants to investigate, and controller HSS model (3.2-23) can be connected as shown in Figure 3-14 to connect harmonic vector each other. The results of the two combined HSS models are all frequency information. However, the frequency outputs can be converted into time-domain results by using (2-13).
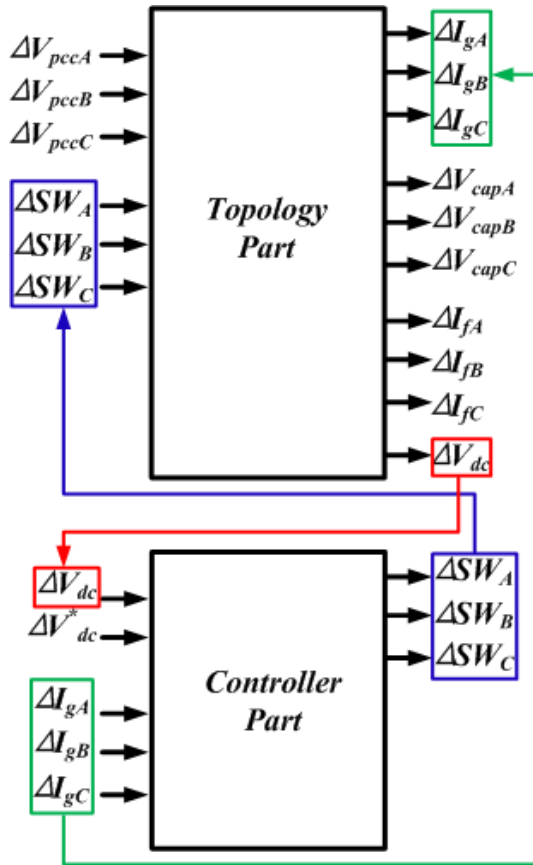

Figure 3-14. Connection of two HSS models (Topology part (3.2-13) and Controller part (3.2-23))

3.2.2. SIMULATION AND EXPERIMENTAL RESULTS

The full HSS model derived from 3.2.1 is simulated and compared with experiments. First, steady-state and dynamic simulations of the HSS method are performed by using the Harmonic Transfer Matrix (HTM), which is also called the Harmonic Transfer Function (HTF), and compared with results from the commercial simulation tool (PLECS) in order to validate the accuracy as well as the harmonic transfer procedure of the HSS model. Also, the results are compared with experiments under the same conditions.

A. Simulation and Experimental conditions

The HSS model is implemented by using an m-file in MATLAB, and laboratory tests are performed in an experimental set-up. The control algorithms are implemented in a DS1007 dSPACE system. A 3-phase voltage source converter is selected as a grid-connected converter at a 3 kW power rating, where the converter-side inductor L_f = 6.25 mH, grid-side inductor L_g = 3.3 mH, filter capacitance C_f = 9.4 uF, dc link capacitor = 450 uF, dc-link voltage = 750 V, line-line grid voltage = 380 V and the switching frequency = 2 kHz are used in both simulations and experiments.

According to the international standard IEC 61000-2-4, which defines the compatibility levels in industrial plants for low-frequency disturbances and applies for low-voltage and medium-voltage at 50 Hz or 60 Hz, a distorted grid voltage is considered in the simulations as well as in the experiments. In the case of the experiment, a programmable ac-source is used to generate a distorted grid voltage condition. The verification of the modeling is also performed under the distorted grid voltage, where a Case-A has 3rd (0.5%), 5th (4.5%), 7th (1.5%) harmonic distortions and Case-B has 3rd (0.5%), 5th (2.5%), 7th (4.5%) harmonic distortions.

The comparison is performed under two specific conditions in order to study the steady-state and the dynamics of the harmonics. First, the steady-state behavior of the harmonics is investigated. Second, the dynamic behavior of the harmonics is investigated by adjusting the reference at a given instant. Additionally, in order to identify the source of distorted current, the converter is controlled without considering the harmonic compensator in both simulations and experiments.

B. Simulation and Experiment results

The dynamic behaviors of harmonics from HSS model are simulated and shown in Figure 3-15. The grid-connected converter operates at the condition of "Case-A" until 0.5 sec, and the harmonics in the grid voltage are adjusted to "Case-B" after 0.5 sec. The low-order harmonics are mainly depicted in Figure 3-15 for the visibility. The grid-current is distorted according to the condition of harmonics in the grid-voltage. The waveform of the grid current is changed due to the harmonic contents

of the grid voltage, where 5th, 7th harmonics are adjusted in "Case-A" and "Case-B" as shown in Figure 3-15-(a). Furthermore, the magnitude of harmonics in the dc-voltage as well as in the dc-current are also changed because of the harmonic components in the grid-current, where the magnitude of 6th harmonics are mainly changed in the simulations. It is noted that the simulation results in the time-domain can also be performed by a commercial simulation tool. However, it is difficult to investigate their coupling by using the conventional tools for modeling. The dynamic couplings are simulated as shown in Figure 3-15-(b). The output results of HSS model at low-order harmonics are mainly drawn for the visibility. The behaviors of the 5th and 7th order harmonics are investigated since the grid voltage is distorted according to "Case-A" and "Case-B". The harmonic components in the 3-phase grid current are depicted by positive-sequence and negative-sequence harmonics according to the relationship given in (3.2-28).

$$V_{inv[P]} = SW_{[P]} * V_{dc[Z]}$$
$$V_{inv[N]} = SW_{[N]} * V_{dc[Z]}$$
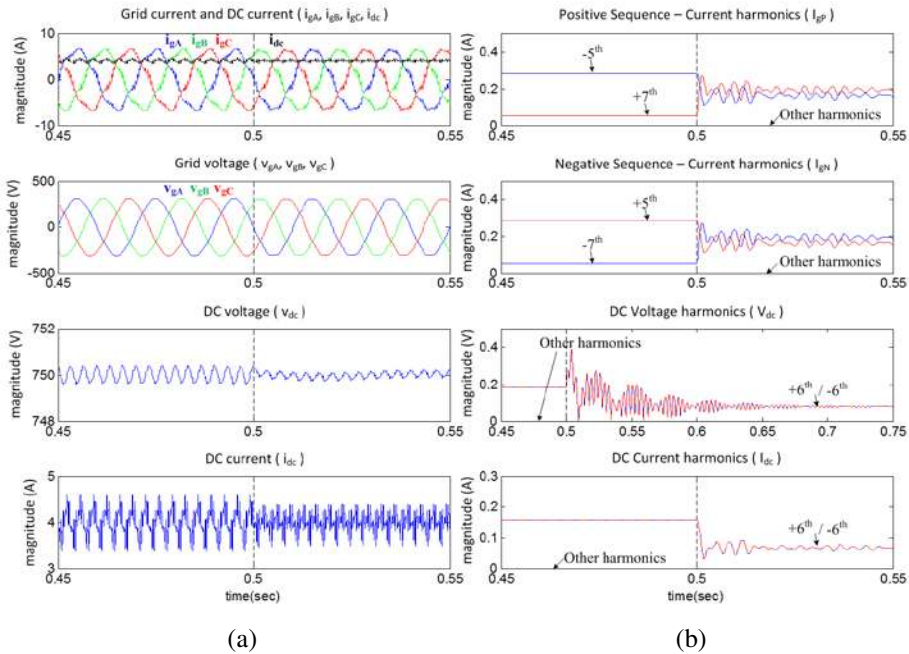$$I_{dc[Z]} = SW_{[P]} * I_{g[N]} + SW_{[N]} * I_{g[P]}$$

(3.2-28)

Figure 3-15. Simulation result for the verification of harmonic interaction, (a) Time-domain simulation using HSS method,

(b) Dynamic response for harmonic interaction in the time-domain

If it is assumed that there are not zero sequence in the grid-side, the procedure of harmonic transfer in the 3-phase converter can simply be explained by using (3.2-28), where "P" is positive sequence harmonics […-17, -11, -5, +1, +7, +13…], "N" is negative sequence harmonics […-13, -7, -1, +5, +11, +17…], "Z" is zero sequence harmonics […-18, -12, -6, 0, +6, +12, +18…], "*" means the convolution in the frequency domain, and the other acronyms are the same as specified in Figure 3-14. The convolution between the zero sequence harmonics in the dc-side and positive sequence harmonics of the switching generates positive sequence harmonics in the input side of the ac-filter, and the negative sequence harmonics behave similarly. They generate a positive and negative sequence harmonics of the grid current through the voltage difference with the positive and negative sequence harmonics of the grid voltage. The negative sequence harmonics of the grid current is convoluted with the positive sequence of switching component, and the summation of the convolution of the negative sequence part generates a zero sequence of the dc-current. It is used to make the zero sequence of the dc-voltage. These procedures happen continuously during the operation.

As a result, the magnitude of the 5th harmonics in positive sequence (-5th) and negative sequence ($+5^{th}$) is decreasing as the 5th harmonics of the grid voltage is varying. Besides, the magnitude of 7th harmonics at the positive sequence ($+7^{th}$) and negative sequence (-7th) are increasing as the 7th order harmonics in the grid voltage is increasing. It is worth to note that the dc-side harmonics are also changing simultaneously since the ac-side of the converter is coupled with the dc-side of the converter through the modulation behavior. The zero sequence harmonics ($+6^{th}/-6^{th}$) at the dc-side are decreasing. Additionally, the harmonic vectors in Figure 3-15-(b) can be converted into Figure 3-15-(a) by using (2-13). Each harmonic has their own impedance and they are coupled with each other since it has then its own transient behavior as shown in Figure 3-15-(b). The simulated characteristics mean that the impedance of harmonics and their transient behaviors are also correlated with the overall behavior of the converter, and the main harmonic impedance should be considered for an accurate analysis.

Table 3-II. Errors between simulation and experiment

		HSS/PLECS (A)	Experiment (A)	$\frac{HSS-Exp}{HSS} \times 100$ (%)
Case - A	5th	0.6	0.58	3.3
	7th	0.08	0.05	37.5
Case - B	5th	0.3	0.29	3.3
	7th	0.4	0.38	5

(a)   (b)

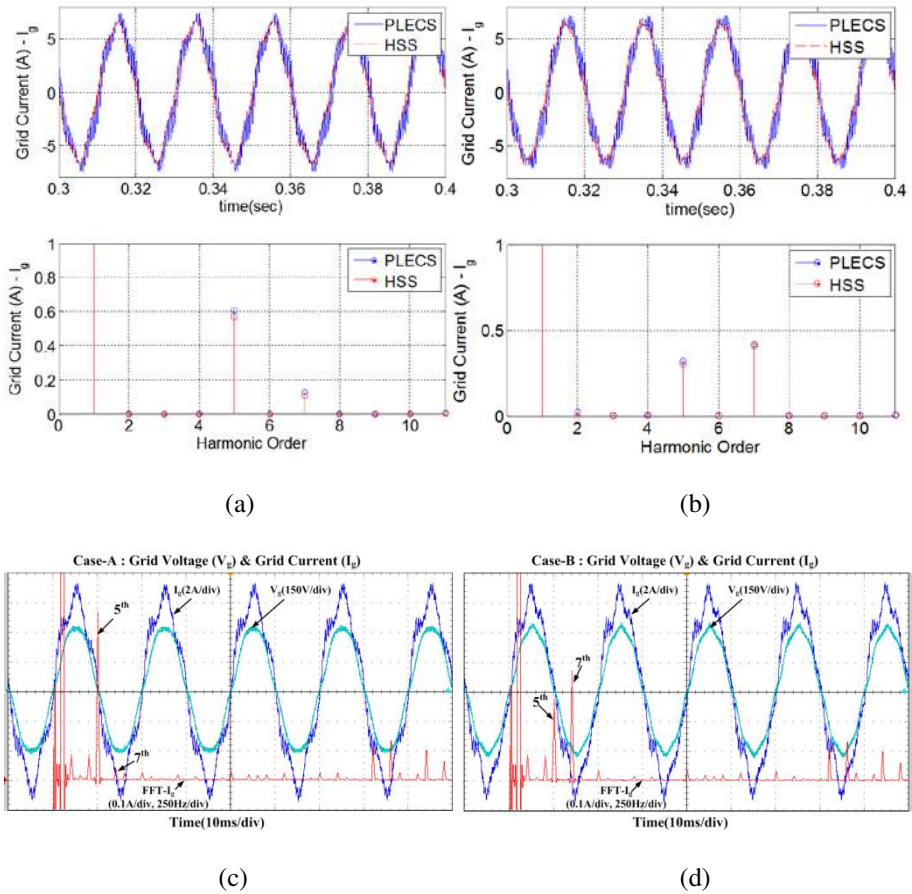(c)   (d)

Figure 3-16. Simulation of three-phase converter (HSS, PLECS), and experimental results

- Grid-side inductor current simulation (harmonic = -40th ~40th) waveform and FFT of the distorted grid voltage (a) Case-A (b) Case-B- (blue=PLECS, red=HSS)

- Grid-side inductor current experimental waveform and FFT from distorted grid voltage (c) Case-A, (d) Case-B - (blue = grid-side current, cyan=grid voltage, red = FFT waveform of grid-side current).

The harmonics in steady-state are compared using HSS model, PLECS and experiments. The results of the HSS model are converted to the time-domain by using (2-13) since the output of HSS model is frequency vectors. The harmonics from -40th to 40th are considered in the HSS model to investigate the low-order harmonics and to show the switching behavior in the time-domain result. The size of the model depends on the harmonics of the modeling procedure. However, it can be reduced according to the requirement. For instance, the positive and negative sequence can only be used for the reduced-order model. As shown in Figure 3-16-(a),

(b), a comparison between the HSS and PLECS seems to be a well match. The small error can be regarded as a calculation error in the computer simulations or a resolution problem (time-step). It is worth to note that the transfer procedure of the harmonics is properly working in the model inside according to the theory of the HSS model. Even though the average model can be used to analyze the harmonic contents of the voltage source converter, when the switching frequency is very high, it can not properly be adapted to the harmonic analysis as the switching frequency is lower (< 2 *kHz*). The switching harmonics can be moved to near the low-frequency range and can affect both the dc and ac harmonic transfer procedure through the frequency coupling [89]. It means that the impedances of each harmonic are coupled with each other, and they can only be analyzed by the modeling methods, which are considering the effect of the time-varying elements.

The simulation results of both models are compared with the experiments as shown in Figure 3-16-(c), (d). Additionally, typical odd order harmonics (5th, 7th) are compared in Table 3-II with their error rate. Even though there are small differences between simulations and experiments, the HSS modeling show the same capability as with the non-linear time-domain simulations. The reason of the mismatch between them is that only the linear components are only implemented in the simulations. Furthermore, the dead-time and the nonlinear characteristic of the passive elements are not considered in the HSS model. Hence, the even-order harmonics, which are normally driven by the dead-time, and the coupling effect of them to other harmonics are not shown in the HSS model and PLECS as well. Also, the frequency at the ac-side is shown in the dc-side as a shifted frequency or a coupled frequency according to the components at switching, ac and dc-side, and it is transferred again to the ac-side. For instance, even-order harmonics in the ac-side will be shown in the dc-side as odd-order harmonics, and they will be shown again as even-order harmonics of the ac-side. However, both odd and even order harmonics move simultaneously in practical systems, and it makes different magnitudes of harmonics. Hence, this coupled behavior makes an error if one component is not considered in the analytical model as well as in the nonlinear time-domain simulations.

3.2.3. SUMMARY AND CONCLUSION

This section analyzes the harmonic interaction between the 3-phase grid-connected converter and the grid voltage by using HSS modeling. First, the full HSS modeling procedure is provided to show the difference to the conventional modeling methods. Second, the output results from the developed model are compared with nonlinear time-domain simulation result to show the validity of the HSS model. As a result, it also shows well-matched results with a commercial simulation tool as well as with experimental results. Third, the HSS model is used as a tool to analyze the steady-state harmonic interaction as well as the dynamic harmonic interaction. The result

shows how harmonics are transferred in the model and which impedances are effective to generate the harmonics.

The result from the HSS model can be used to give accurate results compared to the conventional simulation results. Furthermore, the derived harmonic coupling matrix can be extended to the frequency coupling analysis with other connected devices.

3.3. HSS MODELING OF BACK-TO-BACK VSC SYSTEMS

This section presents an analysis of harmonic coupling for a back-to-back wind turbine converter and their modeling methods including the time-varying behavior. Firstly, the back to back converter is modeled by using the HSS modeling approach. The detailed procedures for a linearization of the back-to-back converter are described to know how the time-varying behavior can be considered in the modeling procedure. The generator side of the wind turbine is assumed as a simple passive filter in order to focus on the analysis of harmonic instability in a full-scale converter. Secondly, the variation of the wind-turbine speed is taken into account in order to investigate their effect on the steady-state harmonic and on their coupling effect. Consequently, the modeling procedures and the analyzed results show that harmonics in the converters as well as harmonics in grid side is interacting with each other based on the operating point of the wind turbine. Furthermore, the impedance characteristic from the HSS model shows the difference with the traditional linearized model in respect to the accuracy. The HSS model and their results are fully verified through the comparisons between time-domain simulation and analytical model, and the results are also compared with the experimental results.
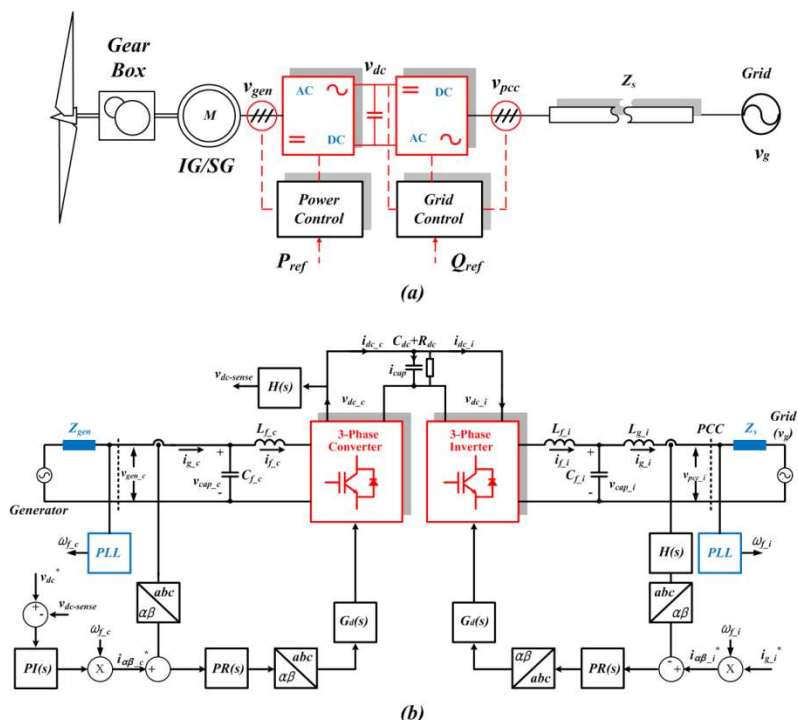

Figure 3-17. "Block diagram for Full-scale back to back (BtB) converter

(a) Structure of wind turbine converter (b) Block diagram of the simplified model of converter"[91].

3.3.1. MODELING PROCEDURE

A. System Description

A single Back to Back Converter is used in this section as shown in Figure 3-17-(a). The Induction Generator (IG) or Synchronous Generator (SG) can be considered as the generator at the rotor side. However, the generator is assumed to have a large inductance ($Z_{gen} = L_{g\_c} + R_{g\_c}$) to limit the range of analysis to the harmonics, which are generated by the input frequency of the generator. The mechanical vibration and their effect from the gear box are also not considered in the analysis. The input frequency of Rotor (Generator) Side Converter (RSC) is defined as the range from 10 Hz to 50 Hz. Furthermore, the controllers for the generator side including the Maximum Power Point Tracking (MPPT), the torque and the speed are assumed as the simplified algorithm of the grid connected converter as shown in Figure 3-17-(b). The PLL is used in the RSC with the Proportional Resonant (PR) Controller to get the same frequency with the generator side frequency. The PLL is also used in the Grid Side Converter (GSC) to synchronize with the grid frequency (50 Hz). Furthermore, the dc link voltage is mainly controlled by the dc voltage controller in the RSC as shown in Figure 3-17-(b). The detail system parameter for the modeling and simulation are given by Table 3-II.

Table 3-III. "System parameter used for study"[91]

Conv.	P_{rate}	L_f (mH)	R_{Lf} (mΩ)	C_f (uF)	R_{Cf} (mΩ)	L_g (mH)	R_{Lg} (mΩ)	V_{dc} (V)	C_{dc} (uF)	R_{dc} (Ω)	f_{sw} (kHz)
RSC	35kVA	0.87	11.4	22	7.5	0.22	2.9	750	1000	10	2
GSC	35kVA	1.2	15.7	15	11	03	3.9	750	1000	10	2

B. HSS modeling of RSC topology

$$\begin{bmatrix} \dot{I}_{g\_c-abc}(t) \\ \dot{I}_{f\_c-abc}(t) \\ \dot{V}_{cap\_c-abc}(t) \\ \dot{V}_{dc\_c}(t) \end{bmatrix} = \begin{bmatrix} \frac{-R_{g\_c}}{L_{g\_c}}I - N & 0 & \frac{-1}{L_{g\_c}}I & 0 \\ 0 & \frac{-R_{f\_c}}{L_{f\_c}}I - N & \frac{1}{L_{f\_c}}I & -\frac{\Gamma[SW^T]}{L_f} \\ \frac{1}{C_{f\_c}}I & \frac{-1}{C_{f\_c}}I & -N & 0 \\ 0 & \frac{\Gamma[SW]}{C_{dc\_c}} & 0 & -N \end{bmatrix} \begin{bmatrix} I_{g\_c-abc}(t) \\ I_{f\_c-abc}(t) \\ V_{cap\_c-abc}(t) \\ V_{dc\_c}(t) \end{bmatrix} +$$

$$\begin{bmatrix} \frac{1}{L_{g\_c}}I \\ 0 \\ 0 \\ 0 \end{bmatrix} [V_{gen\_c-abc}(t)] \quad (3.3-1)$$

A 3-phase grid connected PWM converter is modeled based on the procedure described in [42] by using (2-15). The harmonic state space model of single converter are shown in (3.3-1), where "*I*" is the identity matrix and "*N*" means the derivative terms for dynamics from (2-15). The switching and modulation in time-domain are transformed into a Toeplitz (Γ) [31] matrix in the frequency domain in

order to achieve the same results with the multiplication in a time-domain by using a convolution method described in Figure 3-17. Additionally, the small letter in Figure 3-17 means the time domain signal, but the capital letters in (3.3-1) are the harmonic vectors, which are derived from the linearization of time-domain signals according to the time-varying trajectories.

The final block diagram of the single 3-phase grid connected PWM converter is depicted in Figure 3-18 based on (3.3-1) to describe how the harmonic vectors are correlated with each other in the open loop. The harmonic vectors from the generator ($V_{gen\_c-abc(-h...h)}$) are being the input vector of the harmonic transfer function at LCL-filter side. The output harmonic vector of the inverter side filter current ($I_{f\_c-abc(-h...h)}$) is connected into the harmonic transfer function at the dc-side through the convolution with a linearized switching harmonic vector ($\Gamma[SW_C]$). The summation of the three phase current ($I_{g\_c-ABC(-h...h)}$) is identical with the harmonic vector of dc current ($I_{dc\_c(-h...h)}$). The results are multiplied with the harmonic vector (C_{dc}) at dc network in order to obtain the harmonic vector of dc voltage ($V_{dc1(-h...h)}$). The obtained harmonic vectors are convoluted again with the linearized switching harmonic vector ($\Gamma[SW_C]$) to achieve the harmonic vector at the converter side voltage ($V_{inv\_c-abc(-h...h)}$).
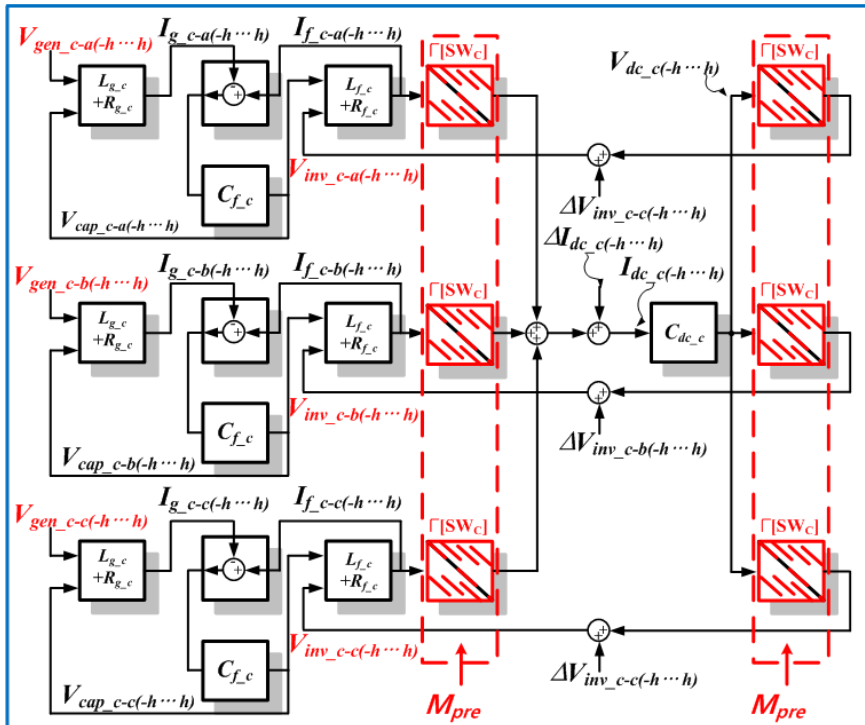

Figure 3-18. "Block diagram for the HSS modeling of RSC and GSC topology"[91].

The harmonic vector of converter side voltage is being the input harmonic vectors of the harmonic transfer function at the LCL filter side to investigate the response of each harmonic vector. Conclusively, the linearized switching harmonic vector ($\Gamma[SW_C]$), which is linearized according to the previous modulation (M_{Pre}), rules the voltage and current data at the initial values of state variables. However, a small perturbation (Δ) should be considered together with the initial conditions to analyze the dynamic response from the operating point. The small variations ($\Delta V_{inv\_c-abc}, \Delta I_{dc\_c}$) can continuously be updated from the controller.

D. HSS modeling of GSC topology

The topology of the GSC can also be transformed into the HSS model using the same method as the RSC. However, a different flow of the harmonic vectors should be taken into account in order to connect the harmonic vectors of RSC and GSC in the same domain. The dc link circuit between the RSC and GSC can be regarded as a single dc circuit by changing the plus sign (+) of dc current in GSC side ($I_{dc\_i(-h...h)}$) into the minus (-) sign. Hence, the opposite direction of harmonic vectors at GSC dc current ($I_{dc\_i(-h...h)}$) can be used as the load current of the RSC ($I_{load(-h...h)}$). Finally, the HSS structure of the two converters (GSC, RSC) can be combined as shown in Figure 3-19. Hence, the harmonic coupling from the RSC to the GSC can have the same characteristics with the time-domain model through the communication of harmonic vector between the RSC and GSC.

The HSS model of the controller can also be connected to each RSC and GSC model. The PI, PR controller are mainly adapted to control the dc link voltage, generator side current and the grid side current as well. The detailed procedure for the linearization of the controller and their transformation into the HSS model are performed by the same methods as described in [42].
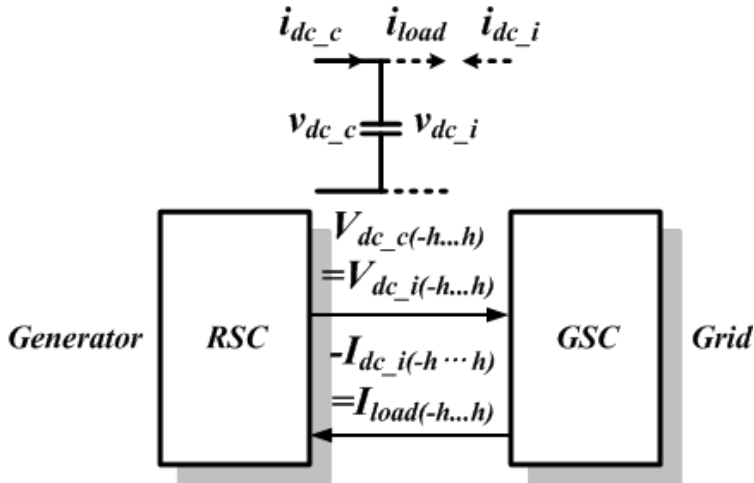

Figure 3-19. "Exchange of harmonic vector information between RSC and GSC"[91].

3.3.2. SIMULATION AND EXPERIMENTAL RESULTS

MATLAB and PLECS are used for time and frequency domain simulation to verify the modeling and analysis of the back to back converters by the two different methods. HSS model and their results are also compared through the laboratory test, where two 3-phase commercial voltage source converters are considered as the RSC and GSC and they are connected through the dc-link to compose the back to back converter. The control algorithms for grid current, dc link voltage and synchronization are implemented by using the dSPACE (DS1107) system to analyze the harmonics and their coupling. The harmonic order from -40th to 40th are considered for the HSS modeling to analyze the harmonic interactions up to 2 kHz.
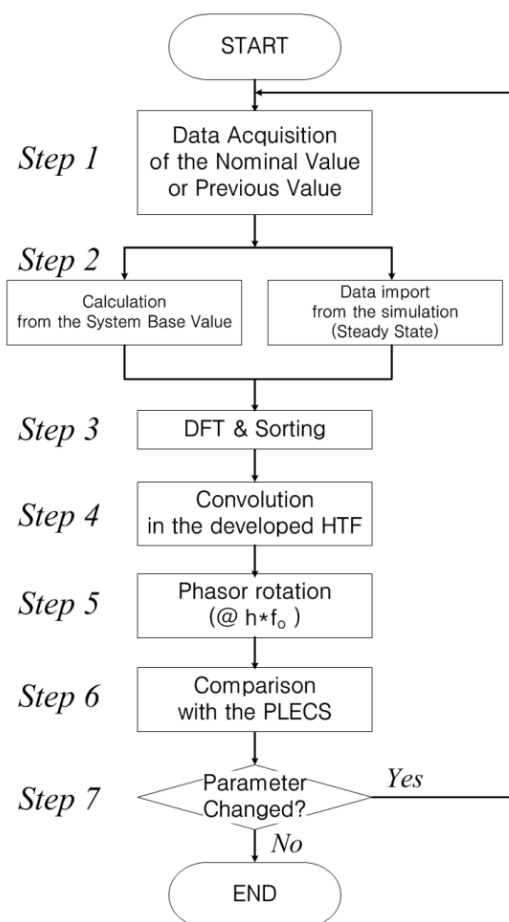

Figure 3-20. "Flowchart for the validation of HSS model with the nonlinear time domain simulation"[91]

A. *Flowchart for the simulation*

A flow chart is shown in Figure 3-20 to verify the developed HSS model and their impedances with the time-domain simulation in PLECS or PSCAD. The overall sequence is as follows:

Step 1) It is first needed to measure the principal waveform in time-domain, for instance, the grid current, and grid voltage, which will be used for the initial value of the simulation or the initial conditions of the state variables.

Step 2) If the initial conditions can be numerically calculated by the base value of the system parameters, the nominal parameters can easily be obtained through the equations. However, if the configuration of the system is complex or the conditions are quite a lot to calculate the initial conditions by hand, a direct measurement from the time-domain simulations could be an easier way to get the initial conditions or state variables.

Step 3) The obtained data from "Step 2" need to be transformed into the frequency domain by using the Discrete Fourier Transform (DFT) in order to use them as the initial conditions of the HSS model. The Fourier coefficients then need to be sorted in order to rearrange them based on the number of harmonics, which is considered in the HSS model.

Step 4) The data from "Step 3" can be the initial conditions of the HSS model. Therefore, the output harmonic vectors can be achieved through the convolution and the transformation into Toeplitz matrix as described in the modeling procedure.

Step 5) The output harmonics from the HSS model can be re-transformed into the time domain signals by rotating the phasor information with an identical frequency $(h \cdot f_o)$ with their harmonics, where "h" is the harmonic vectors and the "f_o" is the fundamental frequency that is considered in the modeling procedures.

Step 6) The time domain signals from the HSS model can then be analyzed with the results from the nonlinear time domain simulation (PSCAD or PLECS) to verify the accuracy of the HSS model and the influences of harmonics in the HSS model.

Step 7) The HSS model should be simulated again from the previous initial conditions, if the system parameters are changed to test the different conditions. The HSS simulation performed at the first conditions can be regarded as the simulation of small harmonic perturbations at that operating point. The HSS model thus should be reformed again if the operating point or the system parameters are changed.

B. *Steady-state and Dynamic performance*

The HSS model of the back-to-back converter from 3.3.1 can be reformed into a Harmonic Transfer Function (HTF) [92] by means of (2-17). It is worth to note that the "$H_0(s)$" of the HTF shows identical results with the frequency response in LTI model. Hence, the LTP model can derive more accurate frequency response than the LTI model since it is containing the frequency responses of other harmonics in a single domain. The obtained HTF can be verified according to the introduced procedure given in Figure 3-20. First, 50 Hz frequency is considered as a main

frequency of both RSC and GSC sides in order to verify the results of the HSS modeling.

(a)

(b)

(c)

(d)
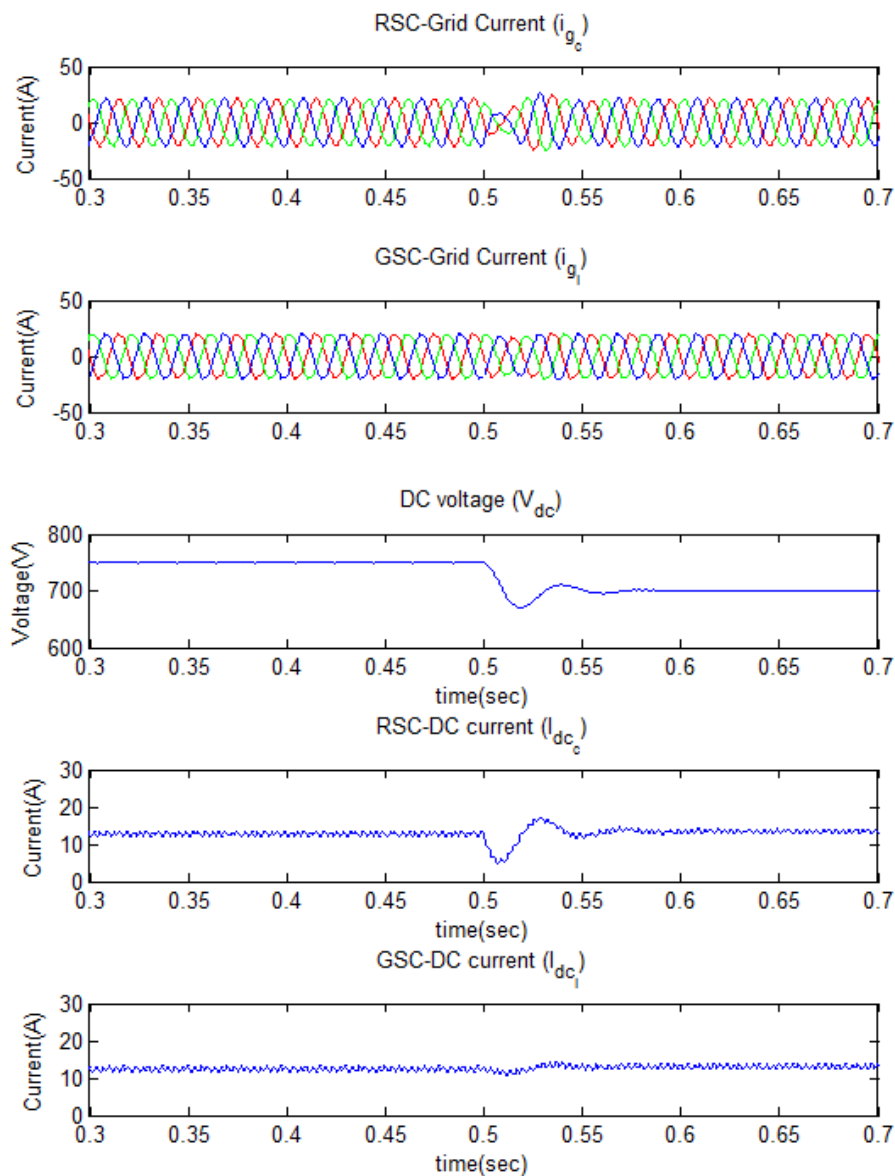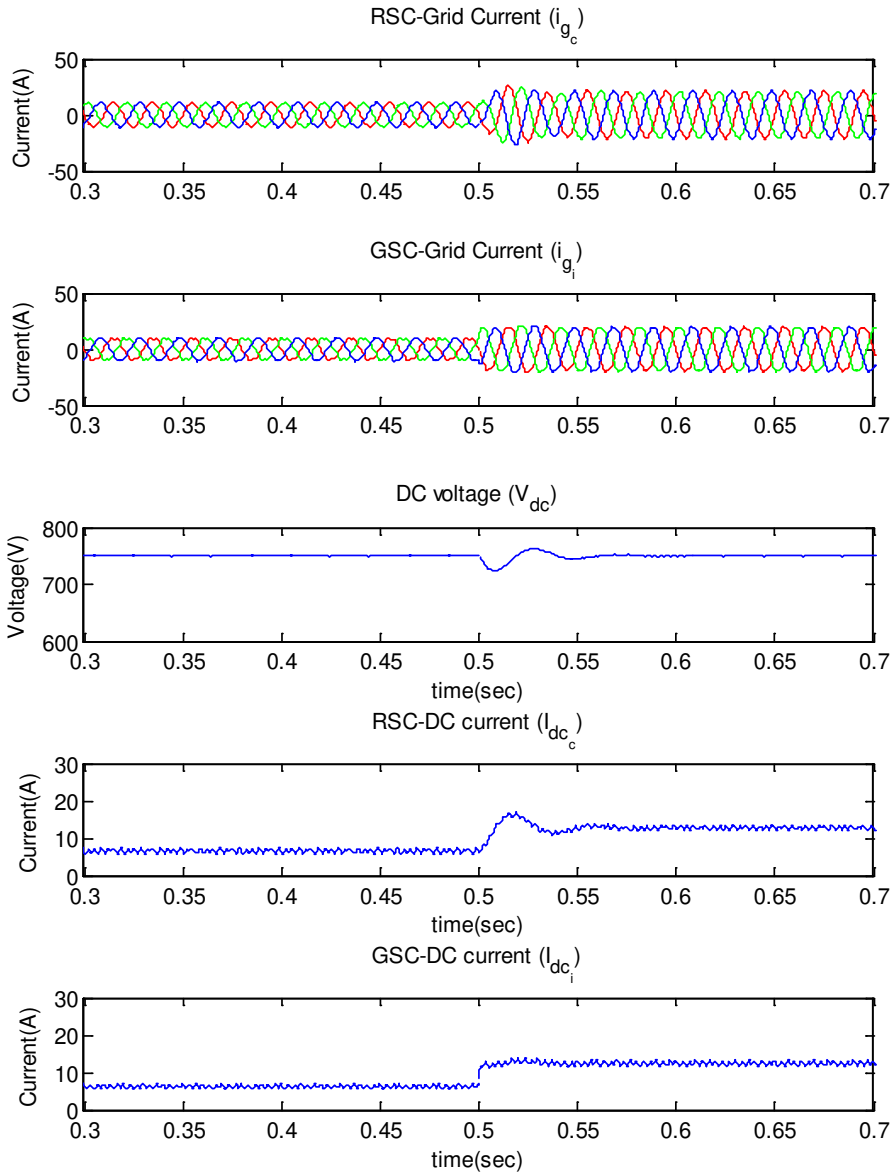
Figure 3-21. "Time domain simulation result and the HTF (RSC=50 Hz, GSC=50 Hz)

(a) DC voltage reference variation at 0.5 sec, (b) Grid current reference variation at 0.5 sec, (c) Admittance response (RSC side input voltage (Phase A) to GSC side grid current (Phase A)), when the harmonics (-11th~11th) are considered, (d) Admittance response (RSC side input voltage (Phase A) to DC link voltage), when the harmonics (-11th~11th) are considered."[91]

(a)

RSC-Grid Current (i_{g_c})

GSC-Grid Current (i_{g_i})

DC voltage (V_{dc})

RSC-DC current (I_{dc_c})
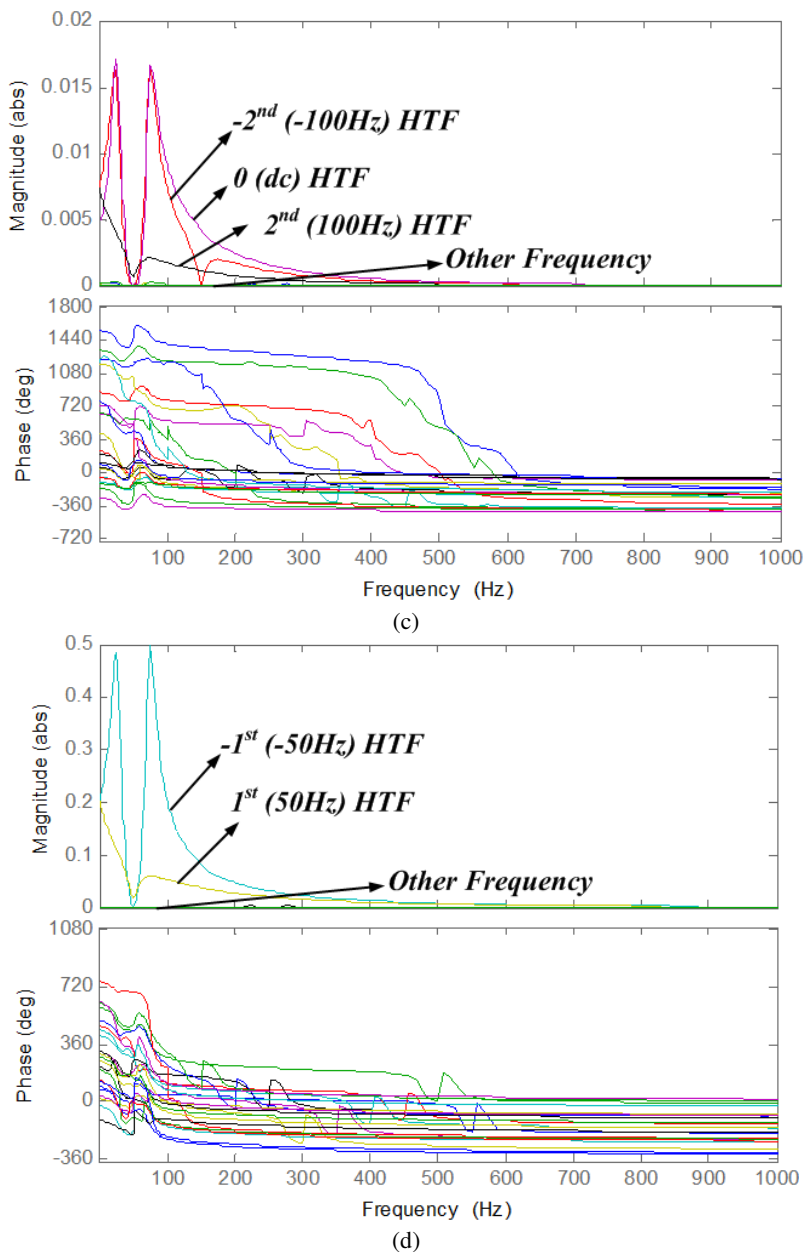
GSC-DC current (I_{dc_i})

(b)
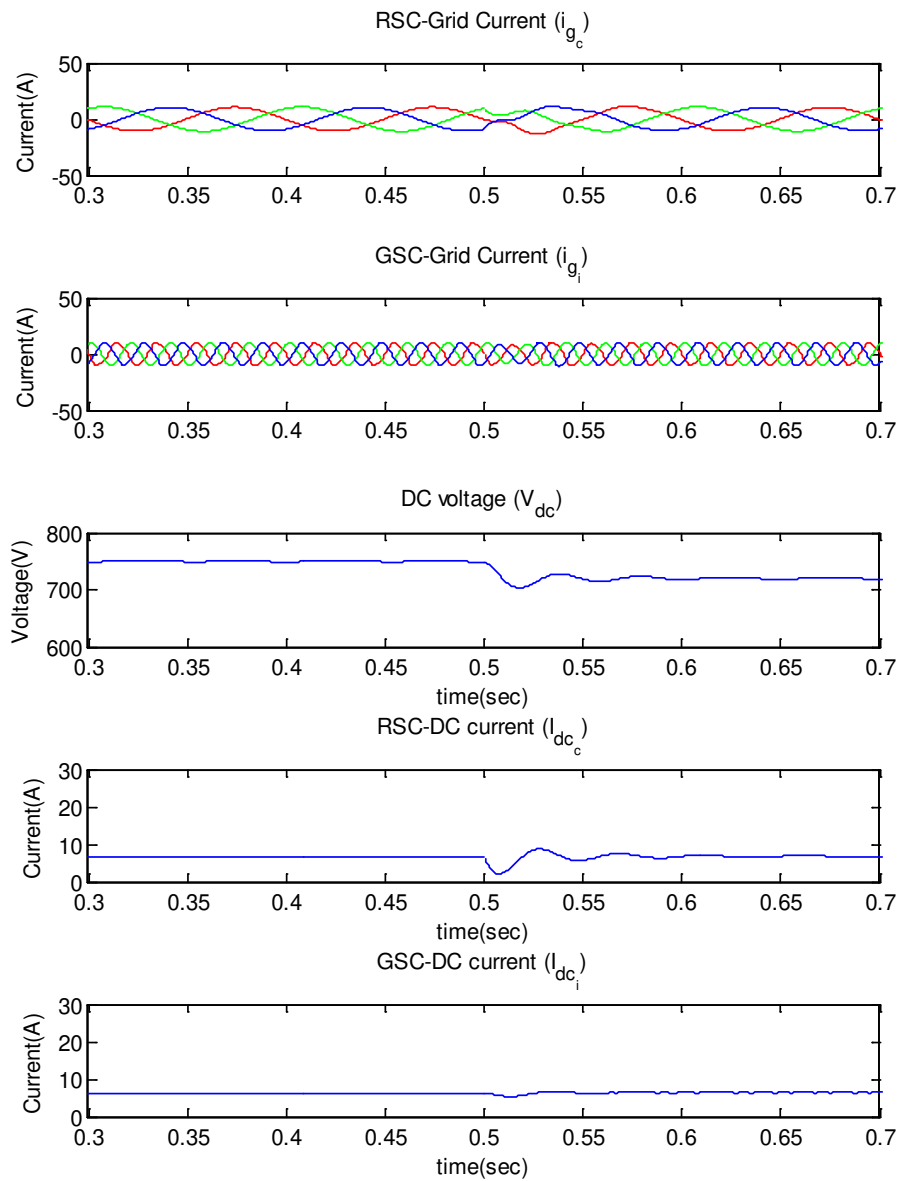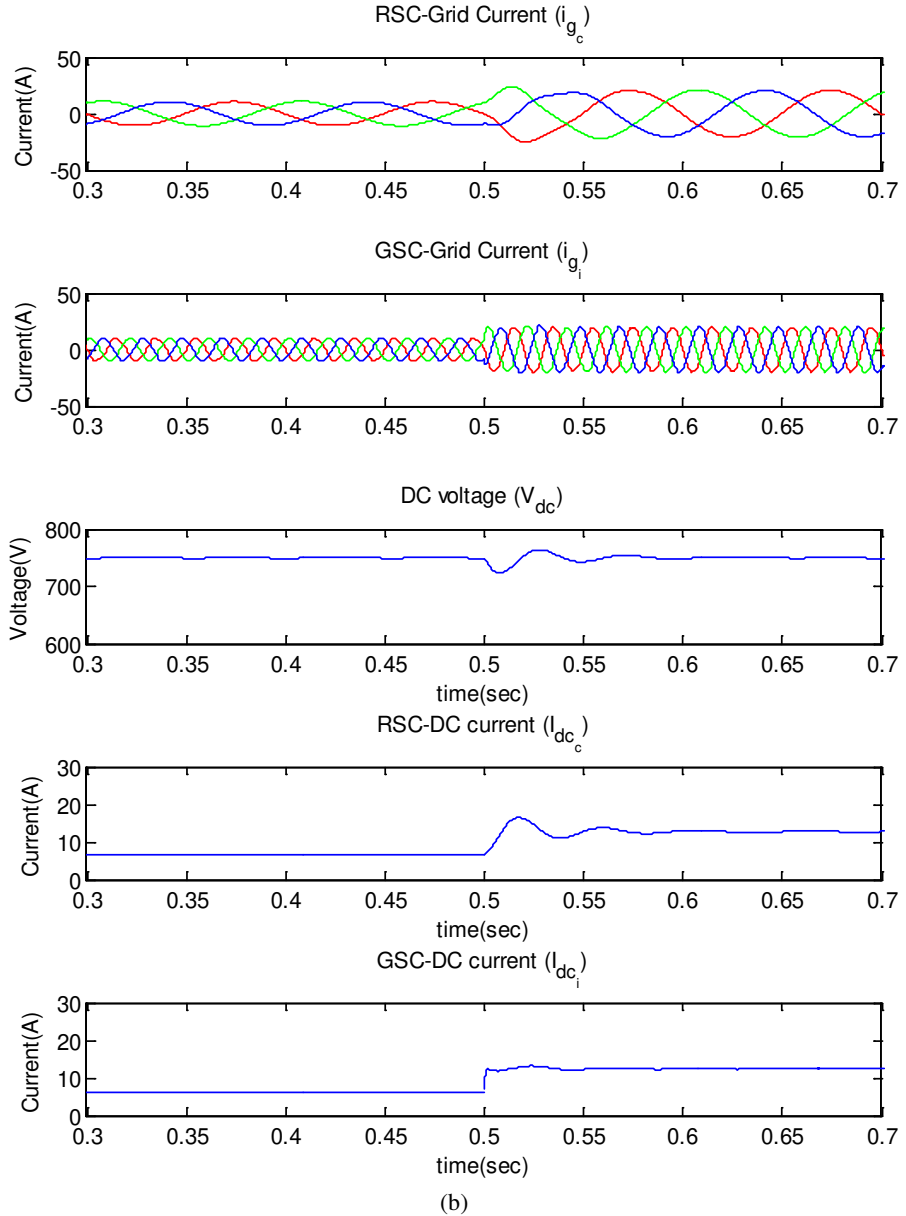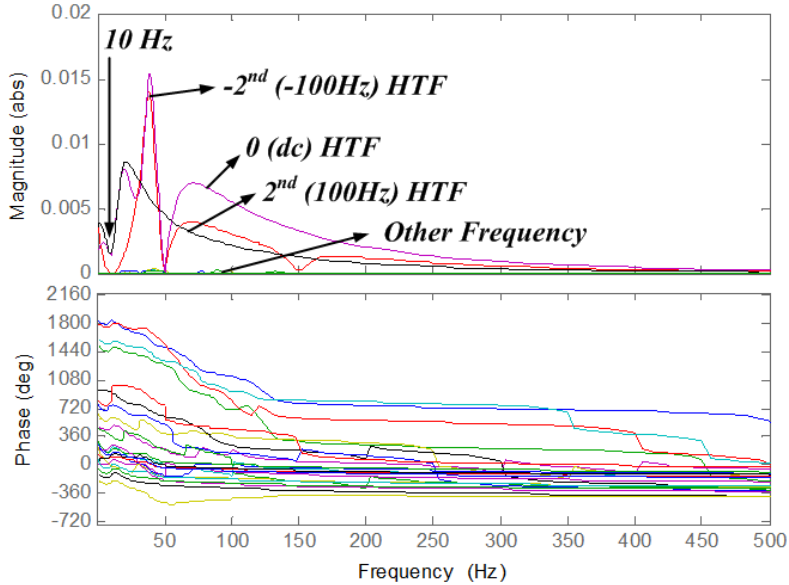
(c)

(d)

Figure 3-22. "Time domain simulation result and the HTF (RSC=10 Hz, GSC=50 Hz) (a) DC voltage reference variation at 0.5 sec, (b) Grid current reference variation at 0.5 sec, (c) Admittance response (RSC side input voltage (Phase A) to GSC side grid current (Phase A)), when the harmonics (-11th~11th) are considered, (d) Admittance response (RSC side input voltage (Phase A) to DC link voltage), when the harmonics (-11th~11th) are considered."[91]
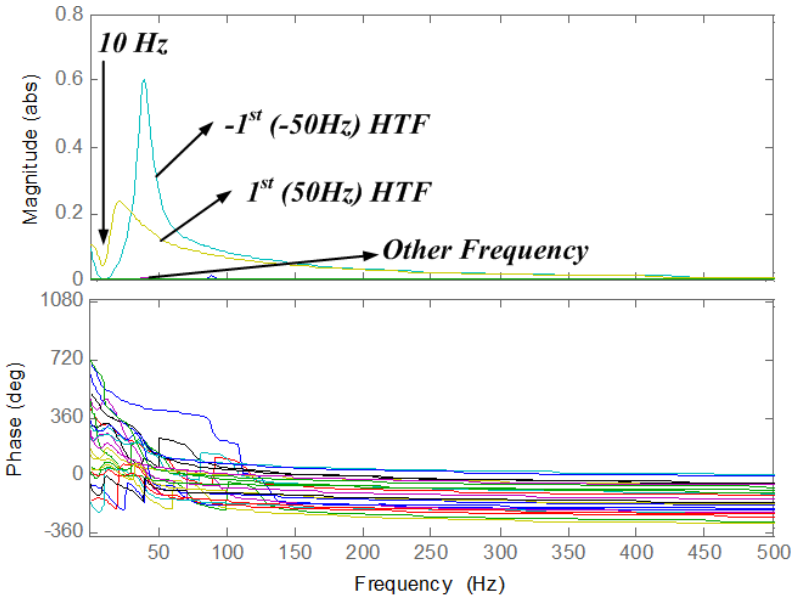
All input, output and state variables in the HTF are composed by harmonic components, and the final results from the HTF are shown in Figure 3-21, where two cases are simulated to analyze the dynamic response of the HTF. Additionally, the grid side current is controlled by the current controller in GSC, but the rotor side current is decided by the dc voltage reference. The simulation results at steady state are controlled by the controller part of the HSS model as shown in Figure 3-21. The dynamics of the HTF are also verified that the dc voltage reference is changed from 750 V to 700 V and the dc voltage is chasing the reference without having a divergence. Simultaneously, it can be seen in the RSC that the ac current (I_{g_c}) is reduced and the dc voltage is also tracing the changed reference, while the ac current (I_{g_i}) at the GSC are converging into the current reference again as shown in Figure 3-21-(a). As a second case, the reference of ac current (I_{g_i}) at the GSC is varied from 10 A to 20A. It comes out by increasing the rotor side current (I_{g_c}) due to the same power rating on both RSC and GSC sides. Furthermore, both the dc current (I_{dc_c}) at RSC and the dc current (I_{dc_i}) at GSC are also increased simultaneously. However, the dc voltage (V_{dc}) keeps the reference voltage with a small transient, even if the current reference is changed in the GSC.

The closed loop HTF are depicted as shown in Figure 3-21-(c), (d) to analyze how each HTF are coupled with each other, where I_{g_i}/V_{g_c} is drawn by two cases. The 11th order harmonics are only drawn in Figure 3-21-(c) individually. It is worth to note that the 2nd / -2nd order harmonics and the dc are more coupled than the others, and it means that the input from 0 Hz to 600 Hz will be influenced by the -2, 2 order and dc HTF. Furthermore, the HTF of +/- 1st order are coupled with the admittance response between the input voltage and the dc voltage at RSC. The derived HTF model for the BtB converter can be used to show how the frequency is coupled with each other. Additionally, the HTF response of other harmonics can also have the possibility to be coupled with HTF of the connected other devices. More precise frequency components can be used as a base harmonic vector in order to consider the varying input frequency of the RSC. In this chapter 5 Hz is selected as the base frequency (f_b) of harmonic components (-40th ~40th), and it can decompose each signal by a 5 Hz unit as shown in (3.3-2),

$$\frac{f_o}{f_b} = m \quad , \qquad \frac{f_h}{f_b} = n \tag{3.3-2}$$

where "m" means the row or column number of the matrix for the fundamental frequency (f_o). Similarly, "n" means the row or column number for harmonic frequency (f_h). For instance, "m" will be "10" if the fundamental frequency (f_o) is 50Hz and the base frequency (f_b) is 5 Hz. Even though, the size of matrix will be increased if the number of used harmonics in the modeling is increasing, the calculation time of HTF can be reduced by using the sparse matrix [35] or by selecting the specific harmonics to be studied.

The simulation results and their HTF are shown in Figure 3-22, where 10 Hz in RSC and the 50 Hz in GSC are applied to analyze the frequency coupling. Similar to the 50 / 50 Hz case, the same simulation schedules are applied to HTF (10 / 50 Hz) in order to validate the transient behavior. The results show a similar behavior with HTF (50 / 50 Hz) except the different frequencies at RSC. Furthermore, a different characteristic of the HTF can be found in Figure 3-22 which has low admittance at 10 Hz and different shapes in other frequency range as well, while Figure 3-21 shows a low admittance at 50 Hz. The HTF are, thus, coupled by the 10 Hz sampled frequency response as shown in Figure 3-22. It is worth to note that the input frequency of the RSC and magnitude may affect the frequency response of the whole HTF of BtB converter. Furthermore, this varying behavior of the BtB converter can not be explained in the LTI model.

*Table 3-IV.Errors between HSS / PLECS simulation and experiment*

		HSS/PLECS (%)	Experiment (%)	$\frac{HSS-Exp}{HSS} \times 100$ (%)
Grid side Current	5th	5	7	40
	7th	1.2	1.5	20
Conv. side Current	5th	18	20	11
	7th	20	21	5
DC Current	6th	1	1.5	50
	12th	0.3	0.5	66

The experimental results using the same procedure like in Figure 3-20 are also analyzed with the HTF simulation results as well as time-domain simulations (PLECS) as shown in Figure 3-23 and Table 3-IV, where the same system parameters are used for the simulations as well as the experiments and main harmonic components are only compared in the table. The HTF simulation results show almost matched results with PLECS simulations as shown in Figure 3-23-(b). The distorted grid current on both RSC and GSC sides due to the frequency coupling between them are shown in both results. Additionally, the dc current is also showing almost the same harmonic content. The identical results mean that the HTF is useful to mimic the frequency coupling between the RSC and GSC sides. Furthermore, the experimental results also show the same behavior with the simulation results as shown in Figure 3-23-(a). Even though the results seem to be well matched, it includes some small errors. First, because of the effect of the dead time, where the dead time generates other harmonics, and it will be coupled with other harmonics through the modulation. Secondly, the numerical error driven by FFT and the calculation of the state space equation may also case errors. The parasitic values of the real passive components in the experimental set up as well as the nonlinearities

of them are not considered in the time-domain simulation and in the HSS simulation as well. The errors can be reduced by increasing the number of harmonics and time steps or by measuring the parasitic components.

3.3.3. CONCLUSION

This section proposes a new HSS model of the back to back converter for the analysis of harmonic interaction and their instability. The simulation results from the PLECS as well as the experimental results show identical harmonic interaction with the simulation results from the HSS model. The representative features of the HSS modeling is that it is a linearized model according to the time varying trajectories by using the number of harmonics and Fourier series. Furthermore, the HSS model can give multiple HTF which can be used in the analysis of harmonic interaction and their coupling. As a result, the HTF can explain the coupling behavior between the RSC and the GSC in one domain, where the traditional LTI approach can not show this characteristic simultaneously at a single domain.
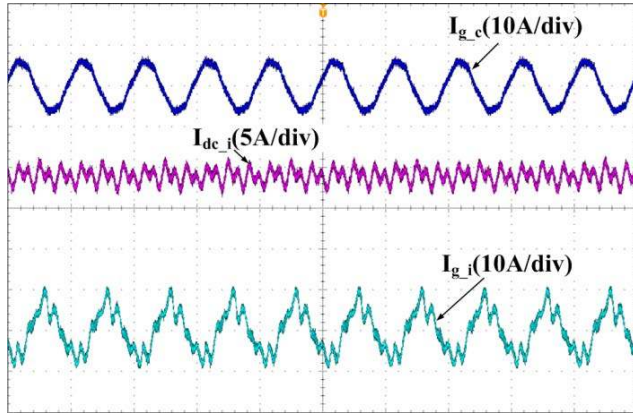
(a)
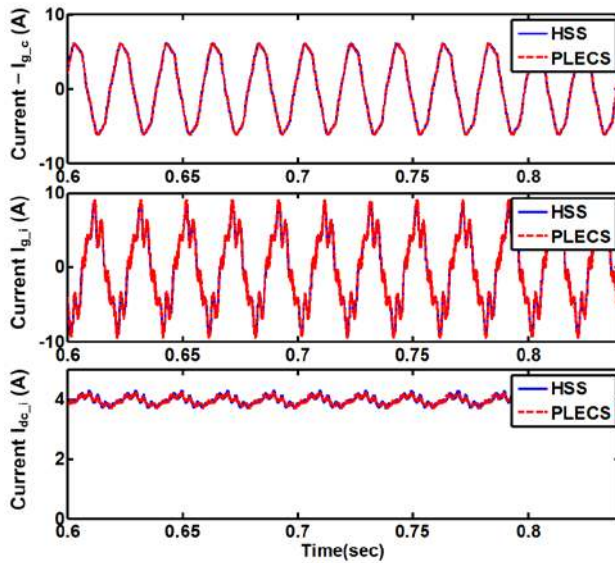
(b)

Figure 3-23. "Simulation and experimental results at 3 kW power rating using HSS modeling and PLECS, RSC : L_{gen} = 620 uH, L_{fc} = 1.7 mH, C_{fc} = 6 uF, C_{dc-c} = 1000 uF, $V_{in(line-line)}$ = 380 V, switching frequency = 6 kHz, GSC : L_{fi} = 3 mH, L_{gi} = 1 mH, C_{fi} = 4.7uF, C_{dc-i} = 1000 uF, $V_{pcc(line-line)}$ = 380 V, switching frequency = 10 kHz

- Grid side inductor current simulation (harmonic = -40th ~40th) waveform (a) Experimental results (blue = grid side current (I_{g_i}), cyan= converter side current (I_{g_c}), purple = dc current (I_{dc_i})),(b) Simulation results (grid side current (I_{g_i}), converter side current (I_{g_c}), dc current (I_{dc_i}))"[91]

3.4. HSS MODELING OF MULTIPLE CONNECTED VSC SYSTEMS

This section introduces a new model structure for multi-parallel connected power converters by using the HSS modeling. First, the whole procedure for single converters is explained briefly based on the introduced theory in Chapter 2. The representative characteristics are then described such that the harmonic impedance of each converter is varying according to the operating point. Second, the HSS model for multi-parallel connected converters is implemented by using the HSS model of single 3-phase converter as well as the HSS model of power cable. Furthermore, the Cigre-Bench mark model for low voltage micro-grid is adapted as a case [99] to verify the modeling results with the real cases. The impedance coupling at steady-state and dynamics between the multiple converters are then analyzed by using the HD and the HTF. The analyzed results using the HSS model are finally compared with time-domain simulations as well as experimental results.

3.4.1. MODELING PROCEDURE

A. System Description

A Cigre benchmark model [99] is considered as the model cases to emulate the time-varying behavior based on the well-known systems. The whole single line diagram of the Low Voltage (LV) network is depicted in Figure 3-24, where five power electronic converters are connected to control and manage the renewable energy source, and LV cables are considered between the converters and the feeder by using a PI-section model. However, the impedances of circuit breaker and contactor are not considered in the modeling procedure in order to focus on the interaction between cables and converters. The converters (A~E) in Figure 3-24-(a) are assumed to be 3-phase PWM converters to control the renewable energy sources, but other combinations are also available depending on the structures of the LV network. The main system parameters including the filter parameters and switching frequencies are described in Table 3-III, where the LCL filter is chosen for the connection of the five power converters in the same grid. The more detailed parameters of each controller part including the low pass filter ($H_1(s), H_2(s)$) in Figure 3-24-(a), the PI controller (PI(s)) and the Proportional Resonant Controller (PR(s)) are explained in the verification part.
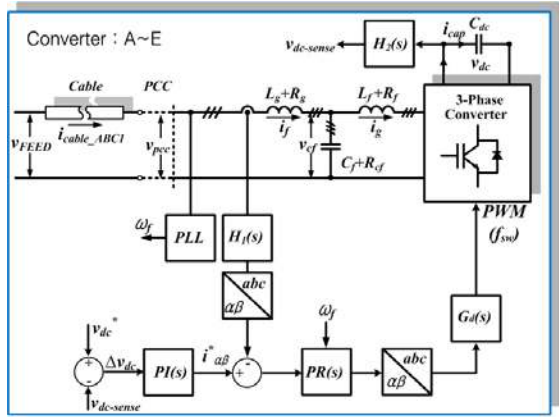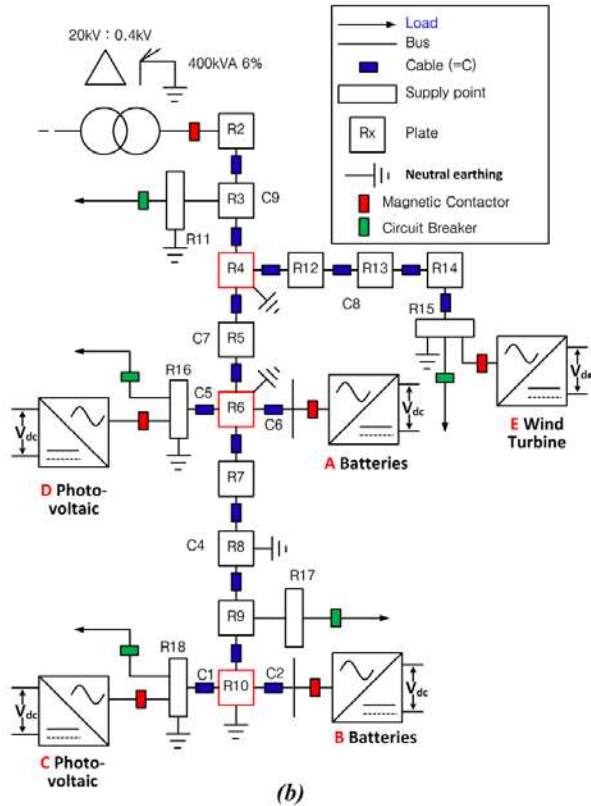
Figure 3-24. "Cigre benchmark model for the low voltage μ-grid [99]

(a) Block diagram for the grid connected converter model (Converter A~E) (b) Single line diagram of LV micro-grid network model" [100]

Table 3-V. "System parameter for benchmark model (see Figure 3-24)" [100]

Conv.	A	B	C	D	E
P_{rate}	35 kVA	25 kVA	3 kW	4 kW	10 kW
L_f (mH)	0.87	1.2	5.1	3.8	0.8
R_{Lf} (mΩ)	11.4	15.7	66.8	49.7	10
C_f (uF)	22	15	2	3	15
R_{Cf} (mΩ)	7.5	11	21.5	14.5	11
L_g (mH)	0.22	0.3	1.7	1.3	0.2
R_{Lg} (mΩ)	2.9	3.9	22.3	17	2.5
V_{dc} (V)	750	750	750	750	750
C_{dc} (uF)	1000	1000	500	500	800
R_{dc} (Ω)	10	10	10	10	10
f_{sw} (kHz)	10	10	16	16	10

B. 3-phase grid connected converter

A 3-phase grid connected PWM converter can be modeled based on (2-15), where the detailed procedure for the controller part and their connection to the topology are following the procedure described in [42]. The HSS model for the topology part is described in (3.4-1) - (3.4-3), where, "I" means the identity matrix, "Z" is the zero matrix and "N" is the dynamic matrix, where the size of matrix is dependent on the number of harmonics defined from the beginning. The PWM switching behavior in time-domain can have the same properties by transforming it into a Toeplitz (Γ) [31] matrix to perform a convolution in the frequency domain as described in Figure 3-25 (red box). The small letter used in Figure 3-24-(a) describes the time domain signal and the capital letters in Figure 3-25 and (3.4-1) means the harmonic vector from the Fourier series. The topology part of final HSS model for the 3-phase grid connected PWM converter is shown in Figure 3-25.

$$
\begin{bmatrix} \dot{I}_{g-abc}(t) \\ \dot{I}_{f-abc}(t) \\ \dot{V}_{cap-abc}(t) \\ \dot{V}_{dc}(t) \end{bmatrix} =
$$

$$
\begin{bmatrix} \frac{-R_g}{L_g}I - N & 0 & \frac{-1}{L_g}I & 0 \\ 0 & \frac{-R_f}{L_f}I - N & \frac{1}{L_f}I & -\frac{\Gamma[SW^T]}{L_f} \\ \frac{1}{C_f}I & \frac{-1}{C_f}I & -N & 0 \\ 0 & \frac{\Gamma[SW]}{C_{dc}} & 0 & -N \end{bmatrix} \begin{bmatrix} I_{g-abc}(t) \\ I_{f-abc}(t) \\ V_{cap-abc}(t) \\ V_{dc}(t) \end{bmatrix} + \begin{bmatrix} \frac{1}{L_g}I \\ 0 \\ 0 \\ 0 \end{bmatrix} [V_{pcc-abc}(t)] \qquad (3.4-1)
$$
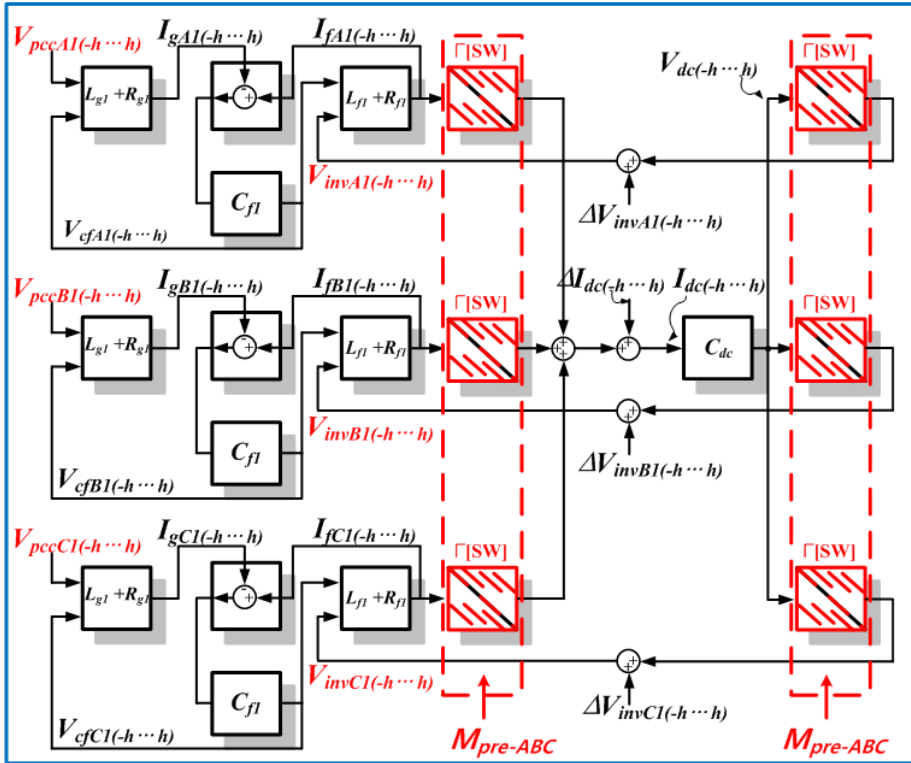
Figure 3-25. "A single 3-phase PWM converter (topology) using HSS modeling."[100]

The harmonic vector from PCC ($V_{pccABC1(-h...h)}$) is being the input of the LCL-filter. The harmonic vector at the converter side filter current ($I_{fABC1(-h...h)}$) is connected with the dc-side through a linearized switching harmonic vector ($\Gamma[SW]$) for the convolution. The summation of three phase currents ($I_{g\_ABC1(-h...h)}$) will be the harmonic vector of a dc current ($I_{dc1(-h...h)}$). The harmonic vector of dc voltage ($V_{dc1(-h...h)}$) can then be obtained through the convolution with the dc network harmonic vector (C_{dc}). The results are then convoluted again with the switching harmonic vector ($\Gamma[SW]$) to generate the harmonic vector at the inverter output voltage ($V_{invABC1(-h...h)}$). The derived results are combined again with the LCL – filter, repetitively, in order to achieve the harmonic vector of the filter current. The overall procedure will be repeated to update any variation from controllers as well as disturbances.

C. Low voltage cable

The HSS model of LV cable is also developed to consider the interaction between cables and converters as well. A PI-section model is adapted to consider further the effect of cable to the converters according to the length instead of using a simple inductance or resistance model for simplicity. Even though the PI model is still

linear and does not have the time-varying component at their basic structure, the HSS modeling theory in (2-15) is again used to have the same structure with the topology model as shown in Figure 3-26.
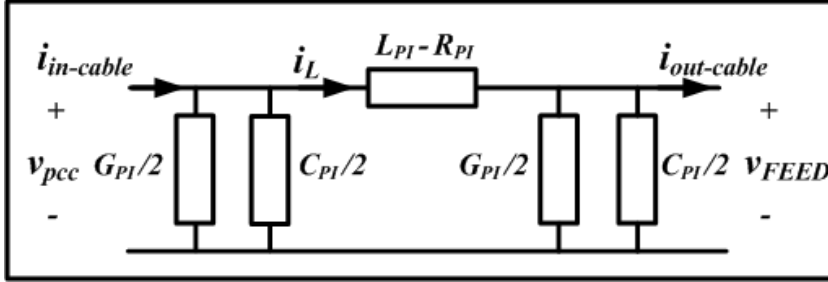

Figure 3-26. "PI section model for 1-phase cable." [100]

The $G_{PI}, C_{PI}, L_{PI}, R_{PI}$ are conductance, capacitance, inductance and resistance of the PI-section model, respectively. However, the conductance is not considered as the parameters, and the capacitance is chosen based on assumptions, where the value of capacitance in LV cable is very small. The cable model for single-phase can be achieved as described in Figure 3-26, (3.4-2). Additionally, the acronyms, subscripts and letters in (3.4-2) have also identical meanings with (3.4-1). The obtained HSS model of the cable can finally be connected to the HSS model of other converters as shown in Figure 3-24. (C1 - C9). Furthermore, the HSS structure of the PI section model can also be used for the other phases. The considered cable data are as follows [101]:

- Current rating / length : 200A / 100 m (C1~C9) (<u>assumed</u>)
- Cable Type : 3-Conductor A1-PVC (material) 185mm^2
- Resistance / Inductance : 0.152 mΩ/meter , 0.237 uH/meter
- Capacitance : 2 pF/meter (<u>assumed</u>)

$$
\begin{bmatrix} \dot{V}_{pcc}(t) \\ \dot{V}_{FEED}(t) \\ \dot{I}_L(t) \end{bmatrix} =
$$

$$
\begin{bmatrix} diag\left(-\frac{G_{PI}}{C_{PI}}\right) - N & Z & diag\left(-\frac{2}{C_{PI}}\right) \\ Z & diag\left(-\frac{G_{PI}}{C_{PI}}\right) - N & diag(\frac{2}{C_{PI}}) \\ diag\left(\frac{1}{L_{PI}}\right) & diag\left(-\frac{1}{L_{PI}}\right) & diag\left(-\frac{R_{PI}}{L_{PI}}\right) - N \end{bmatrix} \begin{bmatrix} V_{in}(t) \\ V_{out}(t) \\ I_L(t) \end{bmatrix} +
$$

$$
\begin{bmatrix} diag\left(\frac{2}{C_{PI}}\right) & Z \\ Z & diag(-\frac{2}{C_{PI}}) \\ Z & Z \end{bmatrix} \begin{bmatrix} I_{in-cable}(t) \\ I_{out-cable}(t) \end{bmatrix} \qquad (3.4-2)
$$

3.4.2. SIMULATION AND EXPERIMENTAL RESULTS

MATLAB and PLECS are selected as tools for the time and frequency domain simulations to validate the HSS model and their analysis results of the parallel connected converters. Three 3-phase voltage source converters are only considered

in the experimental validation to mimic the behavior of multiple connected converters, where five converters are considered in the case of simulation. All controllers are implemented by using the dSPACE system (DS1107), where the harmonic compensators are not included in the controller in order to investigate the pure harmonic interaction within topologies, cables and controllers. Furthermore, the harmonic vector of ideal grid voltage is assumed in this section to focus on the pure harmonic interactions among the converters.

A. Simulation from the HTF (Harmonic Transfer Function)

The harmonic coupling at steady state between 5-parallel converters is shown in Figure 3-27 based on (2-17). A dot (▪) shows the existence of certain harmonic impedance as well as the Jacobian values of them. The five harmonics are considered in this mapping because of the visibility of the harmonic coupling map. However, it is to note that the number of harmonics in the HSS model can be adjusted according to the interested harmonics.

The harmonics coupling map can thus show intuitively how the harmonics of the input grid voltage are correlated with the output harmonics of each converter through the multiplication with harmonics impedance, where the minus (-) and plus (+) signals in the harmonic vector mean the complex conjugates. Additionally, they also mean the positive, negative and zero sequence of harmonics and it can be decomposed for the model reduction as well. It is worth to note that the output harmonics will have balanced outputs if the converters are under a balanced condition. Hence, even if there are impedances in the harmonic coupling map, they can be canceled out with each other due to the characteristics of the harmonic conjugate. However, the harmonic impedance of the sequence components may not be neglected under an unbalanced condition. Based on the introduced characteristics of the harmonic coupling map, the steady-state results are shown in Figure 3-27.

A. Simulation from the HTF (Harmonic Transfer Function)

The harmonic coupling at steady state between 5-parallel converters is shown in Figure 3-27 based on (2-17). A dot (▪) shows the existence of certain harmonic impedance as well as the Jacobian values of them. The five harmonics are considered in this mapping because of the visibility of the harmonic coupling map. However, it is to note that the number of harmonics in the HSS model can be adjusted according to the interested harmonics.

The harmonics coupling map can thus show intuitively how the harmonics of the input grid voltage are correlated with the output harmonics of each converter through the multiplication with harmonics impedance, where the minus (-) and plus (+) signals in the harmonic vector mean the complex conjugates. Additionally, they also mean the positive, negative and zero sequence of harmonics and it can be decomposed for the model reduction as well. It is worth to note that the output harmonics will have balanced outputs if the converters are under a balanced conditi-
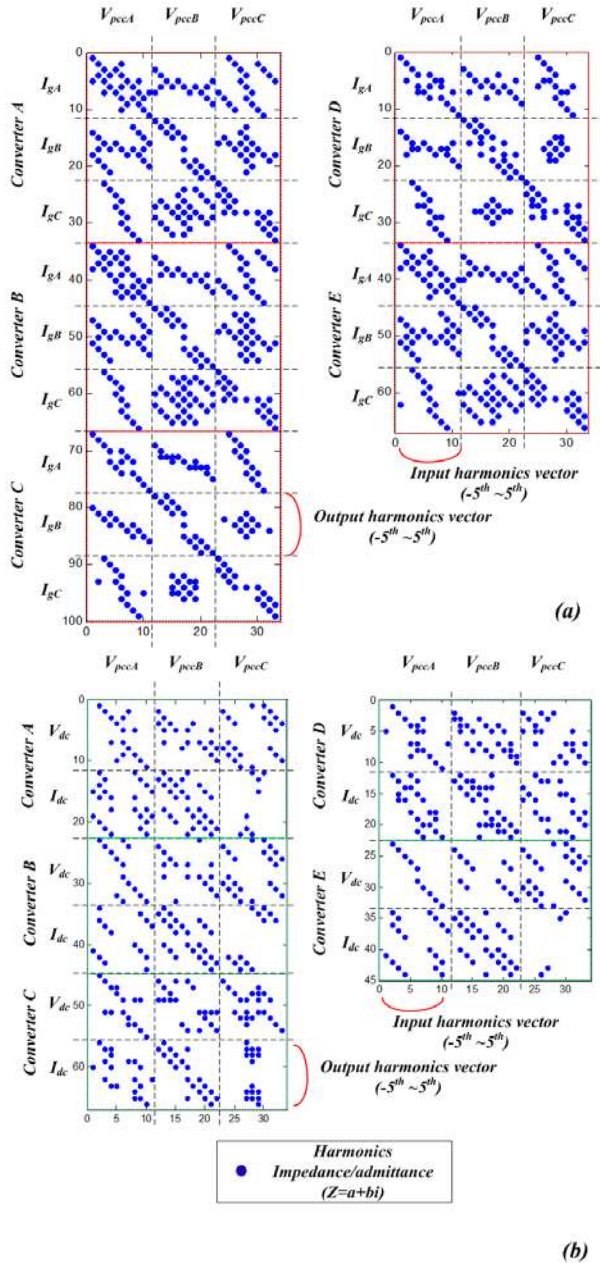
Figure 3-27. "Jacobian sparse matrix (Harmonic domain) for 5 grid converters, where X and Y axis is the harmonic vector (-5th ~ 5th), (a) Harmonic coupling of grid voltage ($V_{line-ABC}$) to grid current (I_{g-ABC}),(b) Harmonics coupling of grid voltage ($V_{line-ABC}$) to dc voltage (V_{dc}) and dc current (I_{dc})" [100].

on. Hence, even if there are impedances in the harmonic coupling map, they can be canceled out with each other due to the characteristics of the harmonic conjugate. However, the harmonic impedance of the sequence components may not be neglected under an unbalanced condition. Based on the introduced characteristics of the harmonic coupling map, the steady-state results are shown in Figure 3-27.

The HTF of 5 parallel converters are then depicted in Figure 3-28 by using (2-17) to analyze the dynamics of each harmonics. It can be found that the converters from #1 to #5 show different HTF based on the system parameter in Table 3-IV. The features of the HTF are also different according to the load conditions as shown in Figure 3-28-(c), (d). Furthermore, the characteristic of the HTF is changed in the range of 50 Hz~100 Hz (red circle), and it affects the transient behavior of the dc circuit and the grid voltage as well. Note that they show a different feature with the LTI model, which does not take into account both the variation of input information as well as the effect of dc side. It is investigated further that the dynamic characteristics of each phase are also different in the range between 50 Hz and 100 Hz (red-circle) as shown in Figure 3-28-(a), (b).

The time-varying harmonics vector from the HTF can then be converted into the time domain signals by rotating them. Five parallel connected 3 phase converters are evaluated based on the parameters in Table 3-III, and the simulation results from HTF are shown in Figure 3-29. The results from 0.4 sec to 0.5 sec show the identical results with the waveforms from the harmonic coupling map (harmonic domain) in Figure 3-27. The transient behaviors at 0.5 sec are obtained from the HTF in Figure 3-28 since the harmonic domain can not mimic the dynamics of the HSS model. The dc voltage, current and grid current of each converter in Figure 3-29 thus show different dynamics because of the different HTF of each converter in Figure 3-28. Note that the influence of HTF in each converter is different with each other since the dominant HTF of each converter is different, and it brings different dynamics of each converter as well. Furthermore, the HTF can have different properties as shown in Figure 3-28-(c) and Figure 3-28-(d) because of the time-varying behavior.

B. Experimental validation

Three parallel connected grid converters are considered in the set up in order to compare the proposed model with experimental results as shown in Figure 3-30, but the cables are not taken into account in the validation. The hardware part is interfaced with the controller through dSPACE, where all sensing signals from analog circuits are sampled by dSPACE Control Desk (yellow line). The PWM signals (red-line) for the switching of 3 converters can then be generated through the control algorithm shown in Figure 3-24. The data communication (green-line) between Control Desk and the dSPACE are performed by a Giga-bit LAN cable.

(a)

(b)
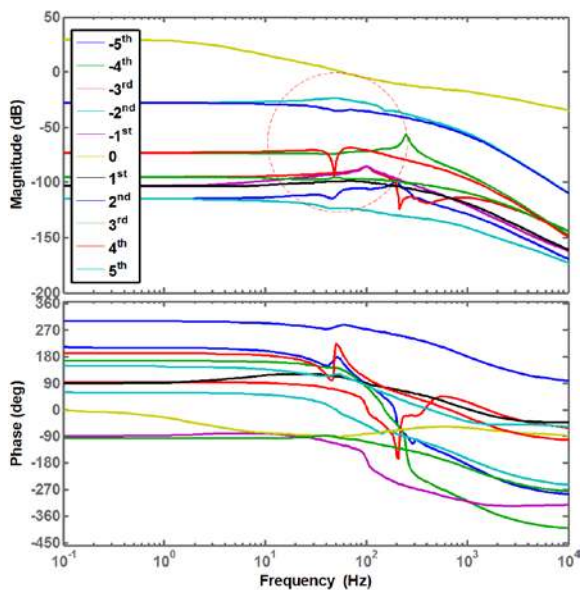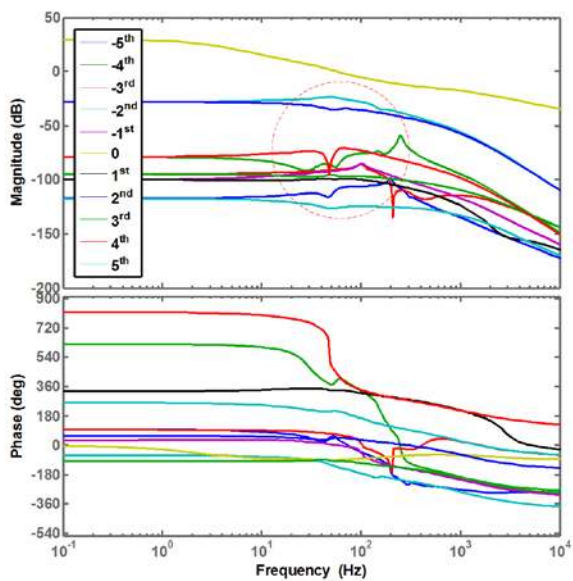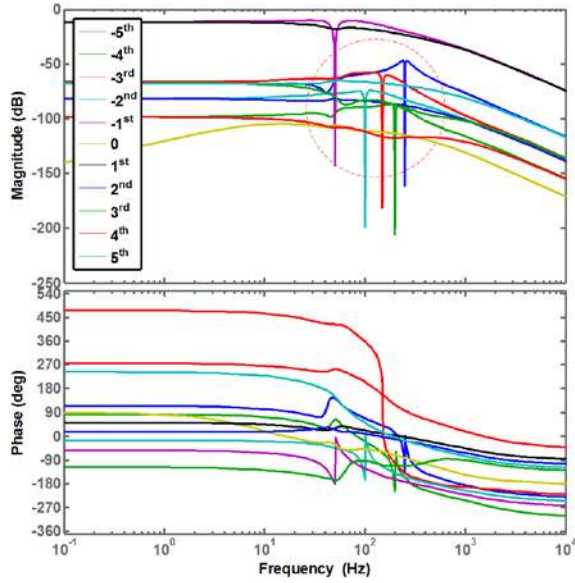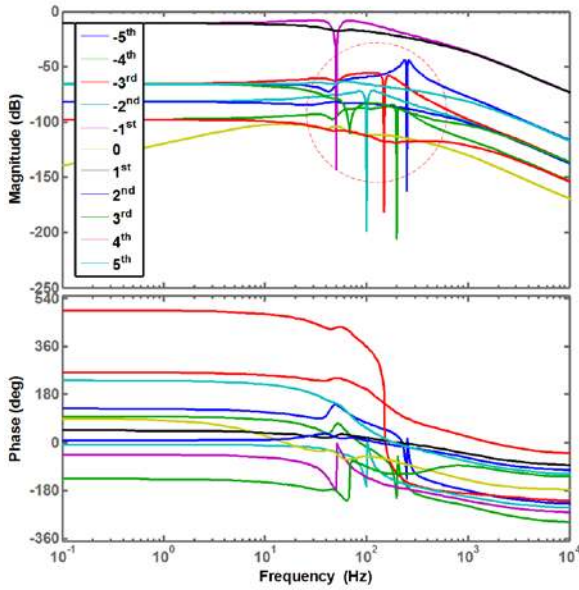
Figure 3-28. "Closed loop Harmonic Transfer Function of 5 paralleled converters (parameters are given in Table 3-IV), (a) Converter - A (I_{g-A}/V_{pcc-A}), (b) Converter - A (I_{g-B}/V_{pcc-B}), (c) Converter – A (V_{dc-A}/V_{pcc-A}), $I_{dc-load} = 75\ A_{dc}$, (d) Converter – A (V_{dc-A}/V_{pcc-A}), $I_{dc-load} = 13\ A_{dc}$" [100]

(a)

(b)
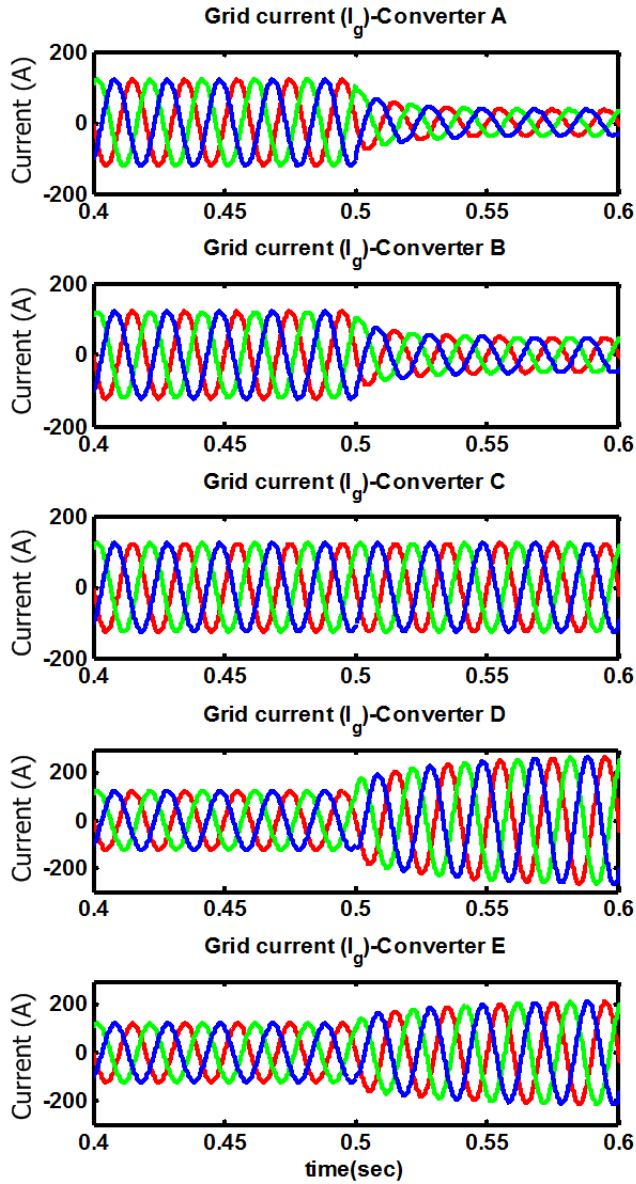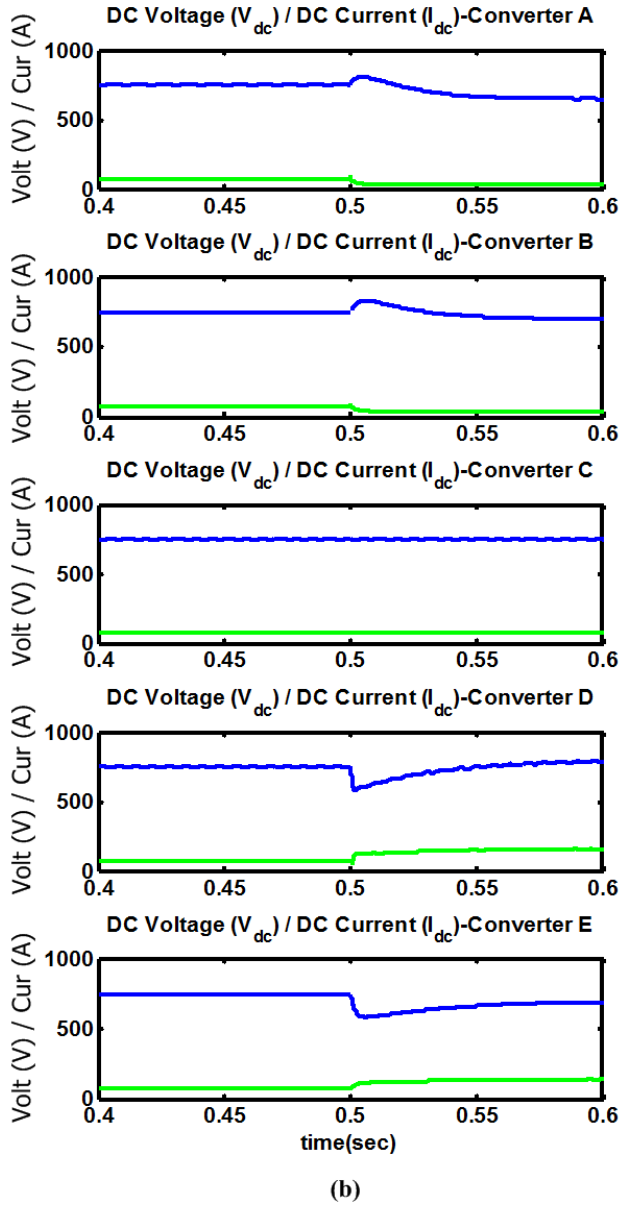
Figure 3-29. "Time domain simulation results from the Harmonic Transfer Function (h= -5th~5th), (a) Grid current (I_g) of Converter A,B,C,D,E, (b) DC voltage (V_{dc}) and DC current (I_{dc}) of Converter A,B,C,D,E, (From 0.4~0.5 sec, the parameters are same with Table 3-IV. The dc load current and dc voltage reference are changed at 0.5 sec : Converter A (V_{dc}* =650 / R_{dc}=50 ohm), Converter B (V_{dc}* =700 / R_{dc}=20 ohm), Converter C (V_{dc}* =750 / R_{dc}=10 ohm), Converter D (V_{dc}* =800 / R_{dc}=5 ohm), Converter E (V_{dc}* =700 / R_{dc}=5 ohm)), where R_{dc} is the dc load."[100]

Most papers are talking about measurement of the impedance from the experimental set up by using the frequency analyzer to verify their analytical models through the perturbation, but the different ways are adapted in this chapter to verify the model. The proposed model in (3.4-1) - (3.4-3) thus used only their measured signals to validate the developed model for specific period since the structure of HTF has multiple transfer functions and the measurement of them would be a challenge. The test flow is described in details as follows:
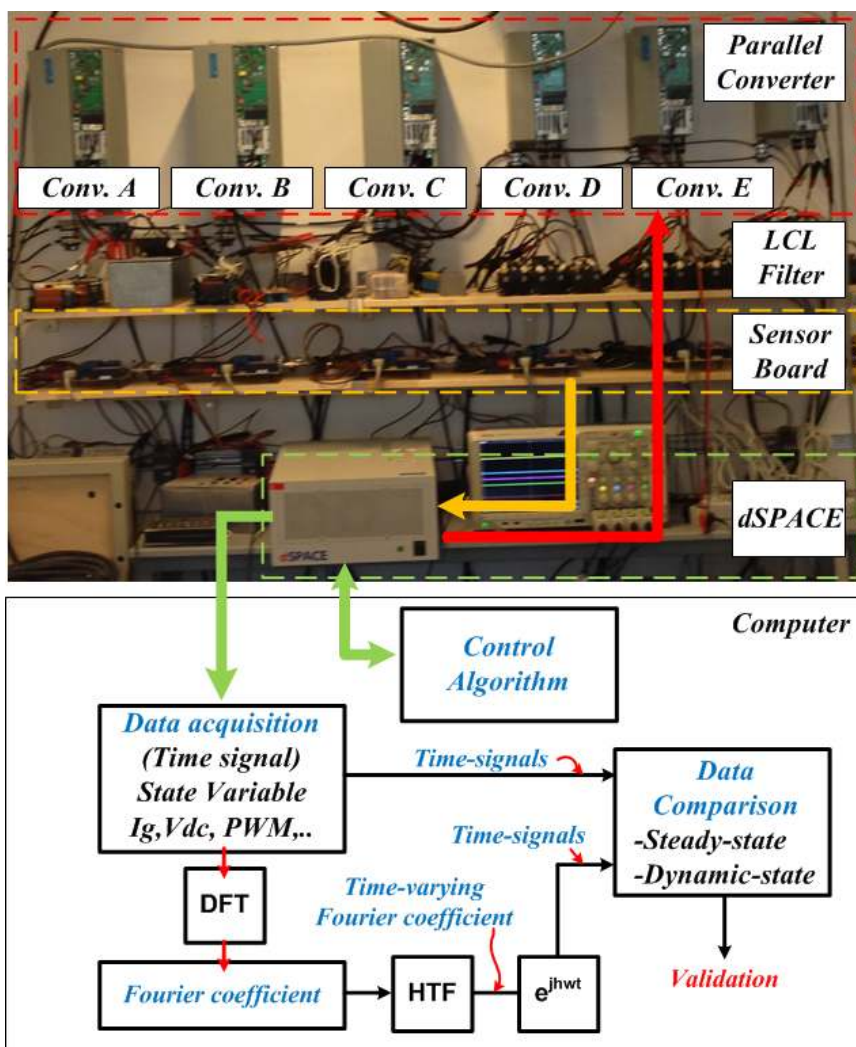
Figure 3-30. "Experimental set up and the sequence for validation of the harmonic transfer function" [100]

1. The periodic signals are required to perform the FFT from the measured signals. Thus, the signals are obtained when the test object operates at steady state.

2. All signals that have the state variables in the HSS model need to be measured. Hence, the grid current (i_g), the converter side current (i_f), the voltage of the filter capacitor (v_f), and the previous state of the current controller as well as the voltage controller etc., are measured by using the data record function in dSPACE.

3. The measured steady-state signals can then be transformed into the Fourier coefficient through the Discrete Fourier Transform (DFT), and they will be included in the developed HSS model to be the part of an initial value or a nominal value. It is critical that the synchronization among signals is the most significant condition that a user has to take care of in the measurements to obtain more accurate results.

4. The developed HSS model can then be simulated again based on the measured nominal values to achieve the dynamic response of each harmonics in the model. The final time-varying behavior of the obtained Fourier coefficient can then be converted into the time-domain signals by rotating them at the same frequency with their phasor.

5. The final time-domain signals from the developed HSS model can be compared with the experimental waveforms from the oscilloscope. Both can be compared in the time-domain as well as in the frequency domain.

Both the HTF model using the initial state from the experimental data and the experimental waveforms are compared based on the introduced procedure for verification, where the simulations as well as the experiments are performed by the parameters described in Figure 3-31 and . The comparisons with PLECS and the experimental waveforms are shown in Figure 3-31. The comparison shows that both results are matched well in the time-domain. However, small errors are appearing in terms of the magnitude of the harmonic components as well as the specific harmonics. The dead-time function is not considered in the HSS model as well as in the PLECS model while the dead-time (2 us) is considered in the experimental set up to avoid a short-circuit. Additionally, the parasitic values of passive components in the experimental set-up are not considered in the HSS simulation because of the difficulties of the measurement. The introduced two reasons principally affect the magnitude and the content of harmonics at the end. The ratio of errors and their components can thus be reduced by including two reasons in the HSS model.

3.4.3. SUMMARY AND CONCLUSION

This section has developed the model for multiple frequency response of multiple connected grid converter by using the HSS theory. Furthermore, the harmonic

coupling in steady state and their dynamic interaction are analyzed by using the HSS modeling approach. The modeling results in the frequency domain and their time-domain results show how harmonics under the control bandwidth ($< 20^{th}$) interact with other harmonics of other parallel connected converters. Hence, the coupling of steady-state harmonics can also be explained by using the harmonic coupling map from the developed HSS model. Besides, it is worth to note that the dynamic behaviors of each converter are not governed by a single operating point. The analyzed multiple HTF show that the dominant HTF and its operating point also affects the overall dynamic performances of the grid current as well as the dc voltage, and more HTF can be involved in the dynamics according to the conditions of converters. The results show exactly that the consideration of HTF and their coupling with others are important in order to achieve more accurate results in the analysis. The single transfer function from the conventional approach would not be enough as the complexity of converter systems is increasing. As a conclusion, the time-varying behavior, the frequency coupling and the Switching Instant Variation (SIV) are important criteria that have to be considered in the modeling procedure, and the multiple frequency response including them i.e. HSS model should be used for complex systems.
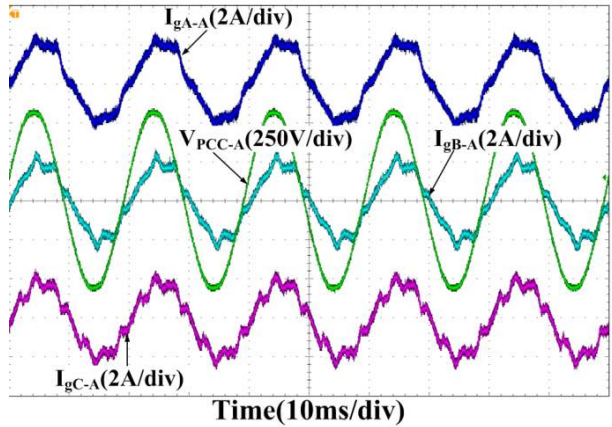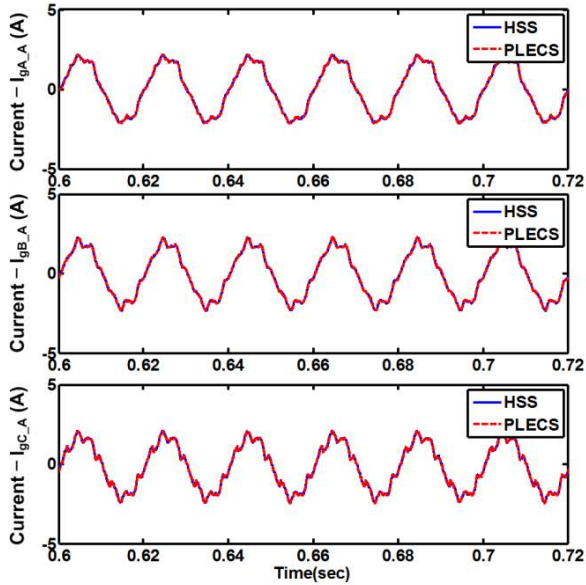
Figure 3-31. "Simulation and experimental results at 1kW Power rating using HSS modeling and PLECS

Converter-1 : L_f = 3 mH, L_g = 1 mH, C_f = 4.7uF, C_{dc} = 450 uF, $V_{pcc(line-line)}$ = 380 V, switching frequency = 10 kHz, ***Converter-2*** : L_f = 1.5 mH, L_g = 1.5 mH, C_f = 4.7uF, C_{dc} = 450 uF, $V_{pcc(line-line)}$ = 380 V, switching frequency = 10 kHz, ***Converter-3*** : L_f = 0.7 mH, L_g = 0.3 mH, C_f = 4.7uF, C_{dc} = 450 uF, $V_{pcc(line-line)}$ = 380 V, switching frequency = 10 kHz

- Grid side inductor current simulation (harmonic = -40th ~40th) waveform (a) Experimental results (blue = grid side current (I_{gA-A}), cyan= grid side current (I_{gB-A}), purple = grid side current (I_{gC-A}), green=grid voltage (v_{pcc-A})), (b) Simulation results (grid side current (I_{gA-A}), grid side current (I_{gB-A}), grid side current (I_{gC-A}))"[100]

CHAPTER 4. HSS MODELING OF OTHER APPLICATIONS

This chapter presents two applications of the HSS modeling, especially for dc systems and the diode rectifier. The background and previous research are also reviewed as well as explained why the time-varying behavior is important and how it can be included in the HSS model. The achieved models show how harmonics of two applications are involved in the performance at the steady-state as well as the dynamic behavior. All modeling results of each applications are implemented by using MATLAB and compared with nonlinear time-domain simulation. Futhermore, the obtained results are verified in the expereimental set-up by using dSPACE.

4.1. HSS MODELING OF DC GRID

The dc systems based on power electronics are being widely used since they have more advantages than ac systems like high efficiency and lower losses, i.e, electric ship, aircraft, home network, medical systems, and dc micro-grid are principal applications considered in the dc systems [23], [67], [102], [103]. The problems are that the multiple connections between dc systems and their interaction [12] may bring frequency coupling in the dc power electronic based systems. The unexpected instability as well as unknown harmonics can be generated due to them. Furthermore, they may introduce complex EMI problems because of the coupling at high-frequency [104], [105], and they also disturb the efficiency of dc systems due to a frequency coupling at low-frequency [106]. The analysis of harmonics and frequency coupling in the dc systems with the ac systems is, thus, new challenges since ac-dc converters originally generate the dc to the dc network. Hence, the dc components may also include the harmonics from the ac systems, i.e. 100 Hz, 200 Hz. An accurate tool is necessary to investigate the interactions by using the modeling, and to mimic the similar behavior through the simulation. A nonlinear time simulation can be used as an alternative to analyze the introduced problems. However, there are several difficulties in the analysis for large complex systems. In the switch model, a large memory for computation and long-term simulation time are necessary in the nonlinear simulations because the time-step should be varied in each simulation step in order to find an optimal point for convergences. Several linearized models have been introduced to overcome the introduced difficulties in the analysis.

For the past few decades, the development of an advanced modeling method for dc-dc converters has been an issue too. The State-Space AVeraging (SSAV) was first introduced in the dc-dc converters [12] to linearize the discontinuous switching behavior of dc-dc converters through the moving averaging filter. The developed

method has been widely applied to stability analysis as well as controller design based on the assumption that the ripples of the switching signals are relatively small and can be neglected, and the switching harmonics may not affect the control bandwidth. They may bring an inaccurate result in the case of low pulse-ratio converters because the dynamic interactions, which happen between the low frequency and low switching frequency, can be overlooked. The average model in [17] has an advanced performance compared to the traditional SSAV method by considering the effect of the time-varying effect from the modulation. It is thus critical to include the effect of time-varying components including the frequency coupling to the model in order to analyze the dynamic interaction accurately.

Several advanced methods have been introduced by considering the effect of the time-varying component partially in the converter models in order to overcome the limitations. The Generalized AVeraging (also known as dynamic phasor) (GAV) and multi-frequency averaging technique were firstly studied to take the influence of harmonics into account in the modeling procedure [21], [22], [37]. However, the model itself turns into a nonlinear model if it wants to include multi-harmonic components since the number of state variable inputs may be different. The advanced procedure for linearization and model-reduction is thus required to linearize it. As an alternative, the Describing Function (DF) is adapted to linearize the non-linear equation in [21] by using double Fourier series. It transforms the response as SISO (Single Input Single Output) system at the end. Furthermore, it can not mimic the coupled frequency responses because the MIMO (Multiple Input Multiple Output) structure is required to do it. Secondly, the average models based on the ripple theorem have been developed for some special applications and it may be difficult to get the linearized model through the SSAV [107], [108]. The converters are modeled by SIMO (Single Input Multiple Output) structures in [108] through the ripple theorem. The inductor ripples in each switching period are separated into several sections, and they are averaged by considering the ripples in the switching signals. The results come out with more accurate response than the traditional SSAV. However, the ripple theorem is also obtained from the averaging theory, and the problems are similar with the GAV. The coupling between the switching signals and others are may be difficult to investigate because of the averaged switching information.

The sampling based model [109], [110] is studied to characterize the SIMO model in the dc system by introducing the buck converter as an example. A single perturbation to the buck converter is appeared as multiple output frequency in the model. The research found that the traditional SSAV is mainly focusing on the perturbation at low frequency while the method is considering the range of high frequencies as well. The traditional SSAV may thus have limitations to investigate the behavior at high-frequency. However, the proposed method has difficulties in the analysis of the frequency coupling if the input has multiple information and the effects of them are significant in the final results.

The HSS modeling, Extended Harmonic Domain (EHD) [88], and Harmonic Transfer Function (HTF) [4] are introduced based on the theory of Harmonic Domain (HD) [35] to consider the time-varying behavior of the converters [31], [36], [48], which can not be included by the traditional approach [40]. They could directly explain that each frequency is coupled with other elements and interact through the frequency components in the controller as well as the passive circuit. It is noted that the linearized HSS method has multiple LTI (Linear Time Invariant) systems linearized from the LTP (Linear Time-varying Periodic) systems. The final structure will thus be MIMO (Multiple Input Multiple Output) systems to mimic the interaction between the input signals and the output signals.

This section develops the dc systems through the HSS modeling to simulate the frequency interaction of dc power electronic systems. First, the detailed procedures for modeling are described from topologies to controllers for closed loop systems. Second, the HSS models from the single converter are connected into multiple to reflect the frequency transfer between them. Full HSS models for the dc systems are then simulated to study the steady-state and dynamic characteristics of the converters. Furthermore, several cases are defined to study the frequency coupling characteristic within the HSS models. All results are fully verified through the nonlinear time-domain simulations as well as the frequency-domain simulations.
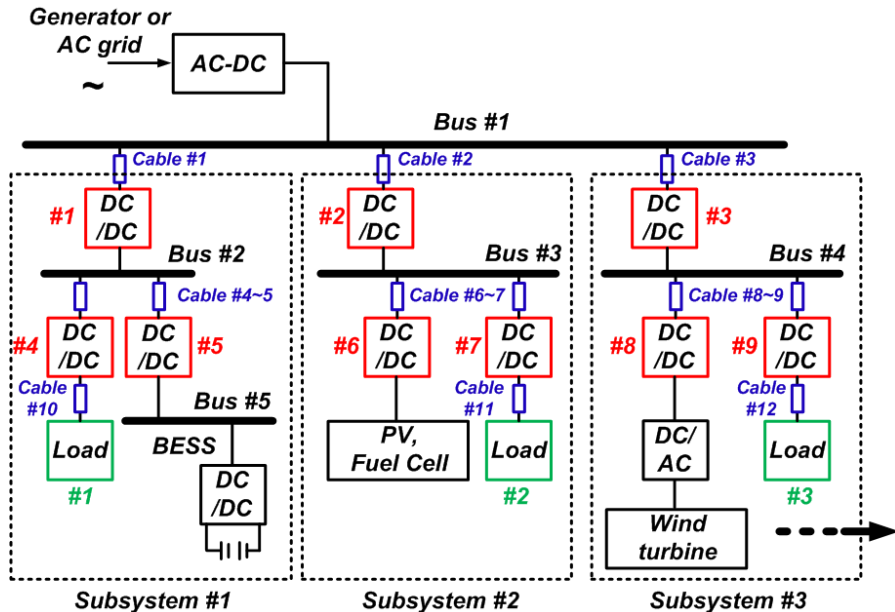

Figure 4-1. "Multi-converter dc power electronics system (9 dc-dc converters (#1~#9) with 3 dc loads (#1~#3)). BESS (=Battery Energy Storage System)" [111]

4.1.1. MODELING PROCEDURE

A. Topology modeling

All components of multi dc power electronic systems in Figure 4-1 can be transformed into the HSS model, but only the dc-dc converters (#1~#9) and dc loads (#1~#3) are modeled in this chapter. A bi-directional dc-dc converter or PWM converter are regarded as constant dc sources to focus on the interaction between the dc-dc converters. Three basic topologies, i.e. Buck, Boost, Buck-Boost, are taken into account based on the HSS theory in [40], [42]. More advanced dc-dc converters such as full bridge and, interleaved may be practically used in the applications, but they are basically from these three models. Each topology can thus be HSS model based on (2-13)-(2-15) as shown in Table 4-I and (4.1-2)-(4.1-4). It is noted that "*N*" in (4.1-1) is from the derivative of (2-15), "diag(·)" is the diagonal term of matrix and "Z" is the zero-matrix

$$N = \mathrm{diag}[-\mathrm{jk}\omega_0 \ldots - j\omega_0, 0, j\omega_0, \ldots jk\omega_0] \qquad (4.1\text{-}1)$$

The harmonic components in a switching should have the Toeplitz matrix ($\Gamma(.)$) to reflect the multiplication of two signals in the time-domain. It is additionally noted that the small variation of switching ($\Gamma(SW)$) will be updated when the state variable of the controller is changed in every step. Furthermore, the number of harmonics considered in the modeling procedure may decide the accuracy as well as the calculation time. A proper selection of the harmonics vector is thus critical to achieve faster and more accurate results. A 50 Hz is selected as the fundamental frequency (f_o) to study the frequency coupling at the low frequency. Hence, the number of harmonics selected is up to the 20th order harmonics. The coupling phenomena in the high-frequency region are also investigated as well.
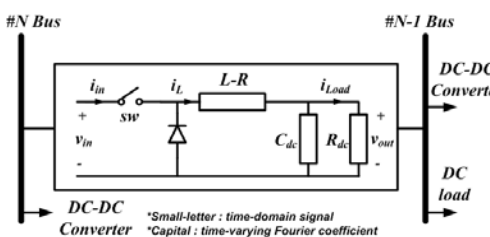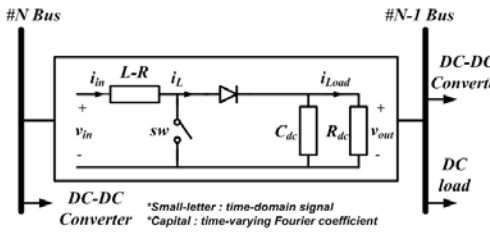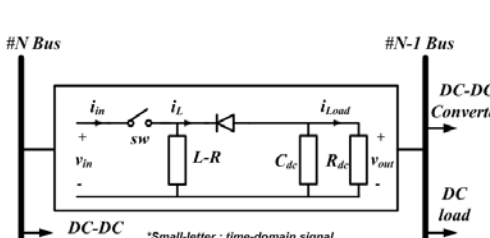
The harmonic transfer of the buck converter is described in Figure 4-2 as an example to know how the harmonics flow and affect to the other components during operation. It can be found that the harmonics from the other connected devices can also affect their components in the same way. It is noted that the small letter in Table 4-I (a)~(c) describes a time-domain signal while the capital letters in Figure 4-2 and Table 4-I (4.1-2)~(4.1-4) means the harmonic coefficient components in the frequency domain.

Furthermore, each HSS model in Figure 4-2 has their input vector (U) as well as their output (Y) vector. The buck converter module can be defined as three parts, namely, "L-R Circuit", "R-C Circuit", "Switch Circuit". To convolute two signals into the frequency domain, the harmonic vector of the switching function is transformed into a Toeplitz (Γ) [31] matrix as shown in Figure 4-2 (SW). The harmonic vector of dc voltage input (V_{in}) is then convoluted with the Toeplitz matrix (SW) of the switching. The results can be the input vector (V_1) in the "L-R circuit and the output vector of the "R-C Circuit" will be another input vector (V_{out}) of the "L-R Circuit". The output vector (I_L) of the "L-R Circuit" is then connected to the input vector of the "R-C Circuit" to include the harmonic impedance of the load (R). The harmonic vector of the inductor current (I_L) is again convoluted with the

Toeplitz matrix (SW) to generate the harmonic vector of the input current (I_{in}). All blocks and their harmonic vectors will continuously be corrected to a new vector as shown in Figure 4-2.

Table 4-I. "Circuit diagram and HSS modeling of dc-dc converters used in dc-grid." [111]

(a) Buck converter, (b) Boost converter, (c) Buck-boost converter, where Z is zero matrix

(a)	$$\begin{bmatrix} \dot{I}_L(t) \\ \dot{V}_{out}(t) \end{bmatrix}$$ $$= \begin{bmatrix} -N & diag(-\frac{1}{L}) \\ diag(\frac{1}{C_{dc}}) & -N \end{bmatrix} \begin{bmatrix} I_L(t) \\ V_{out}(t) \end{bmatrix}$$ $$+ \begin{bmatrix} \frac{\Gamma(SW)}{L} & Z \\ Z & diag(-\frac{1}{C_{dc}}) \end{bmatrix} \begin{bmatrix} V_{in}(t) \\ I_{Load}(t) \end{bmatrix}$$ (4.1-2)
(b)	$$\begin{bmatrix} \dot{I}_L(t) \\ \dot{V}_{out}(t) \end{bmatrix}$$ $$= \begin{bmatrix} -N & -\Gamma(1-SW) \\ \frac{\Gamma(1-SW)}{C_{dc}} & -N \end{bmatrix} \begin{bmatrix} I_L(t) \\ V_{out}(t) \end{bmatrix}$$ $$+ \begin{bmatrix} diag(\frac{1}{L}) & Z \\ Z & diag(-\frac{1}{C_{dc}}) \end{bmatrix} \begin{bmatrix} V_{in}(t) \\ I_{Load}(t) \end{bmatrix}$$ (4.1-3)
(c)	$$\begin{bmatrix} \dot{I}_L(t) \\ \dot{V}_{out}(t) \end{bmatrix}$$ $$= \begin{bmatrix} -N & -\frac{\Gamma(1-SW)}{L} \\ \frac{\Gamma(1-SW)}{C_{dc}} & -N \end{bmatrix} \begin{bmatrix} I_L(t) \\ V_{out}(t) \end{bmatrix}$$ $$+ \begin{bmatrix} \frac{\Gamma(SW)}{L} & Z \\ Z & diag(-\frac{1}{C_{dc}}) \end{bmatrix} \begin{bmatrix} V_{in}(t) \\ I_{Load}(t) \end{bmatrix}$$ (4.1-4)

In [23], the similar applications are modeled by applying the GAV to reduce both the simulation time and the model complexity. However, the GAV selects only the largest harmonics for the modeling. It is thus difficult to analyze the whole interaction between the harmonics of multiple converters. It is worth to note that the full consideration of harmonics may be critical when the dc systems are multiply connected with an ac-dc systems, i.e. in wind turbines, photovoltaics, micro

turbines, and ac-loads. However, the proposed HSS model can look inside the systems and map how the harmonics are correlated through each component as shown in Figure 4-2 and Table 4-I.
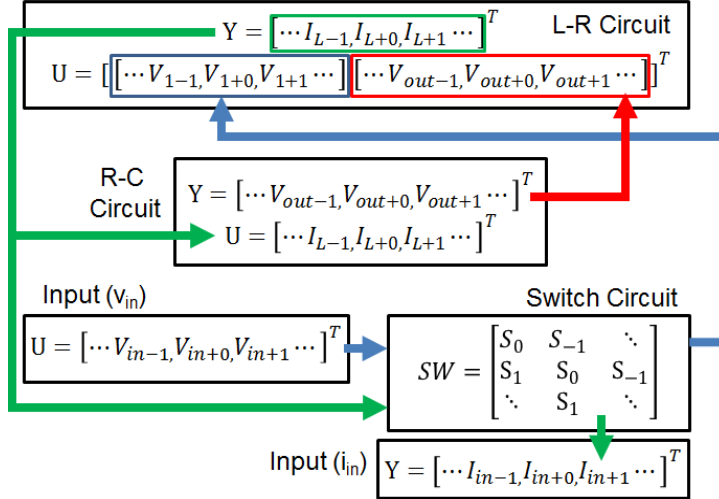
Figure 4-2. "Block diagram of the harmonics vector flow for calculation of buck converter shown in Figure 4-1" [111], where final input is vector V_{in}, and the output vector can be chosen from the states space format

B. Controller modeling

The dc voltage of each converter is simply controlled to focus on the interaction between the topology and single controller of the dc-dc converter. Hence, the controller should also be linearized similar, which was used in the linearization of the topology model in Figure 4-2, to include the small-signal dynamics caused by nonlinear switching.

The procedure for the linearization can be compared with the nonlinear behavior of time-domain. The multiplication of two time-domain signals can first be described as given in (4.1-5).

$$out(t) = u(t) \cdot in(t) \tag{4.1-5}$$

where, in(t), out(t) are the input and output signals in the time-domain respectively, and u(t) is the transfer signals in the time-domain to transform the input. For instance, a switching signal *sw(t)* can be u(t). However, the linearized behavior of time-varying signal in (4.1-5) can be represented as a harmonic vector in the HSS model to reflect the variation of the nonlinear behavior of u(t) as shown in (4.1-6).

$$\Delta OUT(t) = U_{base} \cdot \Delta IN(t) + \Delta U(t) \cdot IN_{base} \tag{4.1-6}$$

where, the U_{base}, IN_{base} are the nominal values (the previous state) of the harmonic vector and the $\Delta IN(t), \Delta U(t)$ are the small variation of the input and output harmonics vector, which are referring to the time-domain signal $IN(t), U(t)$. The division of two signals in the time-domain can also be linearized similarly with the linearization of the multiplication as shown in (4.1-5) and (4.1-6).

(a)   (b)
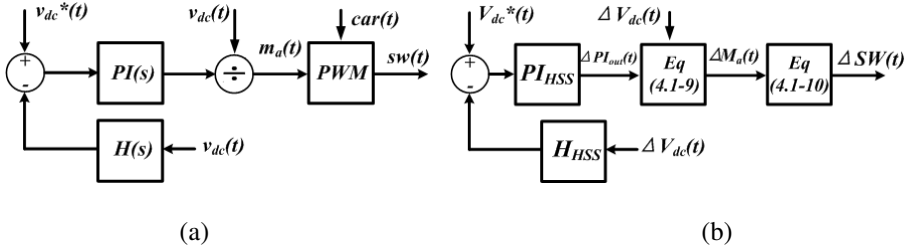
Figure 4-3. "Block diagram of a generalized controller for the dc-dc converter. (a) Nonlinear simulation model for the time-domain signals, (b) Linearized simulation model for the HSS model, where the capital means the harmonic vector"[111]

The simple block diagram for a dc-voltage controller is depicted in Figure 4-3. It is noted that the small letters mean the time-domain signals while the capital letters imply the harmonics vector containing up to the 20th order harmonics as well as the harmonics in the high-frequency range ($0.5f_{sw} ..., 2f_{sw}, 3f_{sw} ...$). The nonlinear time-domain model in Figure 4-3-(a) can thus be linearized into the MIMO frequency domain model by using the linearization procedure of the HSS model as shown in Figure 4-3-(b) based on the introduced theory in (4.1-5) and (4.1-6). The linearized controller (PI_{HSS}), the low-pass filter (H_{HSS}) and their related signals through the HSS method are given in (4.1-7) -(4.1-10).

$$
PI_{HSS} = \begin{bmatrix} PI(s - jh\omega_0) & & & & \\ & \ddots & & & \\ & & PI(s) & & \\ & & & \ddots & \\ & & & & PI(s + jh\omega_0) \end{bmatrix} \tag{4.1-7}
$$

where, $PI(s) = K_p + K_i/s$, K_p is the proportional gain, K_I is the integrator gain and PI_{HSS} means the HSS formulation of $PI(s)$.

$$
H_{HSS} = \begin{bmatrix} H(s - jh\omega_0) & & & & \\ & \ddots & & & \\ & & H(s) & & \\ & & & \ddots & \\ & & & & H(s + jh\omega_0) \end{bmatrix} \tag{4.1-8}
$$

where, $H(s) = 1/(s \cdot K_{lpf} + 1)$ with K_{lpf} as the bandwidth of the low pass filter and H_{HSS} is the HSS formulation of $H(s)$.

$$\Delta M_a(t) = -\frac{PI_{out}^b}{(V_{dc}^b)\Gamma(v_{dc}^b)}\Delta V_{dc}(t) + \frac{1}{V_{dc}^b}\Delta PI_{out}(t) \tag{4.1-9}$$

where, the V_{dc}^b, PI_{out}^b are the nominal values (the previous state) and the $\Delta V_{dc}(t), \Delta PI_{out}(t), \Delta M_a(t)$ are the small variation of the harmonic vector in the dc voltage, the output of PI controller and the modulation index.

$$\Delta SW(t) = \Gamma(SW_n - SW_{n-1})\Delta M_a(t) \tag{4.1-10}$$

where, the SW_n, SW_{n-1} are the present and previous status of the harmonics vector in the PWM switching. The harmonic vectors of Figure 4-3-(b) are continuously updated to the harmonic state vector of the dc-dc converter. The same procedures are applied to the other converters, which are having different topologies, controller gain and reference. The different controllers, i.e. Proportional Resonant (PR) controller etc, can also be transformed into the HSS method through a similar procedure. The low pass filter used in the sensing part is to eliminate the switching ripple of dc voltage since the PI controller in Figure 4-3 is normally tuned to have a high dc-gain at a dc frequency. Additionally, the motivation to scale down the controller output by dividing it by v_{dc} is to compare the output signal of the controller with the carrier waveform. The sensed signals through the low pass filter are generally adjusted in order to make it the same with the magnitude of other signals. The general scheme of the applied controller can be modified in various ways.

Table 4-II. "Circuit diagram and HSS modeling of low-voltage dc cable

Circuit diagram of Cable model (PI section), where Z is the zero matrix"[111] and its model.

$$\begin{bmatrix} \dot{V}_{in}(t) \\ \dot{V}_{out}(t) \\ \dot{I}_L(t) \end{bmatrix} = \begin{bmatrix} diag\left(-\frac{G_{PI}}{C_{PI}}\right) - N & Z & diag\left(-\frac{2}{C_{PI}}\right) \\ Z & diag\left(-\frac{G_{PI}}{C_{PI}}\right) - N & diag\left(\frac{2}{C_{PI}}\right) \\ diag\left(\frac{1}{L_{PI}}\right) & diag\left(-\frac{1}{L_{PI}}\right) & diag\left(-\frac{R_{PI}}{L_{PI}}\right) - N \end{bmatrix}\begin{bmatrix} V_{in}(t) \\ V_{out}(t) \\ I_L(t) \end{bmatrix}$$
$$+ \begin{bmatrix} diag\left(\frac{2}{C_{PI}}\right) & Z \\ Z & diag(-\frac{2}{C_{PI}}) \\ Z & Z \end{bmatrix}\begin{bmatrix} I_{in}(t) \\ I_{out}(t) \end{bmatrix} \tag{4.1-11}$$
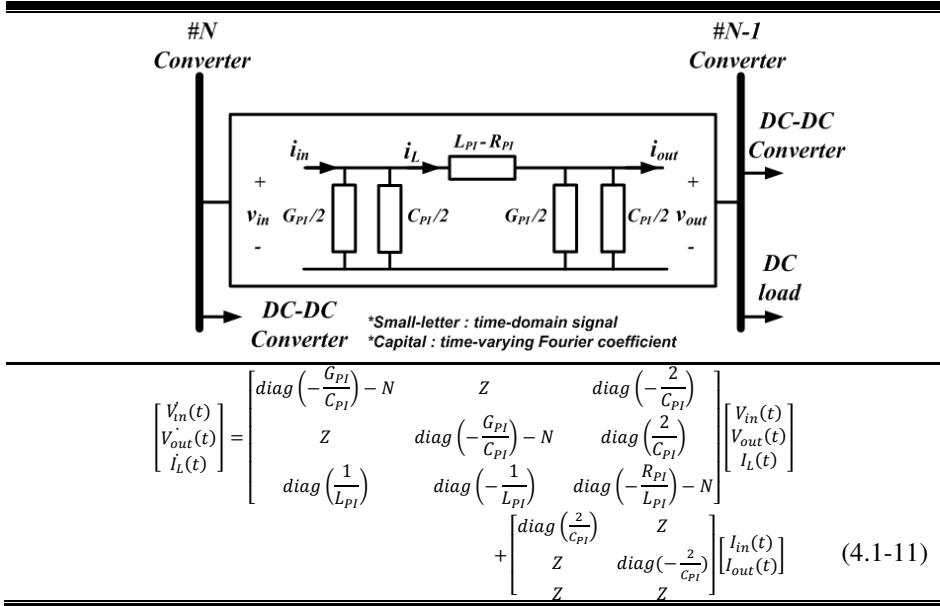
D. Low voltage dc-cable modeling

A low voltage cable is also transformed into the HSS model in order to take into account the interaction between cables and converters. The PI-section model is applied to extend a simple inductance or resistance model based on the length of the cable. The HSS structure of the cable model is shown in Table 4-II according to the HSS modeling theory in (2-13) ~ (2-15) in order to contain the harmonics of the model, where $G_{PI}, C_{PI}, L_{PI}, R_{PI}$ are conductance, capacitance, inductance and resistance of the PI-section cable model. The small and capital letters used in (4.1-11) have also the same meaning as (4.1-2) ~ (4.1-4). The final HSS model for the cable can then be connected with other converters and loads as shown in Figure 4-1. (Cable #1 ~ Cable #12). The parameters of an ac-cable are used in this section to apply practical data in the validation. The details of the cable are following [101], where the conductance is neglected from the parameters and the capacitance is assumed to be 2 pF/meter. However, the capacitance can be removed for simplicity since the reactive power from the capacitance of the cable may not affect to the dc systems. The capacitance appeared at the transient is not considered in the model.

4.1.2. SIMULATION AND EXPERIMENTAL RESULTS

MATLAB and PLECS are selected for time domain as well as frequency domain simulation to compare the two different methods, where all simulations are performed on the i7-4800MQ CPU (2.7 GHz). The developed HSS models are applied to validate the interaction among the dc power electronic systems.

A. Simulation parameters

The switching frequency of each dc-dc converter is defined to be 5 kHz to analyze the switching ripple in the simulations as well. Furthermore, the Bus #1 in Figure 4-1 is assumed to be 200 V_{dc}. The dc voltage is first increased through the dc-dc converters (#1 ~ #3) from the input dc-voltage of the main bus (Bus #1). The buck converters (#4, #9) then decrease the voltage at the loads (#1, #3). The buck-boost converters (#5, #6) are then controlling the output dc-voltage to reflect a time varying dc voltage (BESS, PV, Fuel Cell) to the systems. The boost converters (#7, #8) are finally considered to increase the voltage of both a wind turbine and the load as depicted in Figure 4-1. The outputs from the renewable energy source are simplified to be a constant dc voltage to focus on the analysis of the introduced dc-systems. Additionally, the resistive loads are only used in the validation. The loads are composed of passive componenets as well as active components. Even though the parts (the effect of renewable energy source, etc) of simulations are neglected for the simplicity, the proposed HSS model can be connected to other systems as well, i.e. constant voltage loads, constant power loads and other RLC loads.

B. HSS module connection

The input and output harmonics vector of each developed modes from the previous section then need to be linked into a final model. Three examples are shown in

Figure 4-4 to describe the procedure of how the each module can be linked with other modules. Each dc-dc converter can have final input vectors, which are defined as the dc voltage reference (V_{dc}^*), the input voltage (V_{in}) and the output load current (I_{load}). Additionally, the output harmonics vector will be the output voltage (V_{out}) and input current (I_{in}). The input and output harmonic vectors of cables and other components can also be decided similarly. It is worth to note that the input and output can be determined by the user based on the purpose of the modeling and the analysis.

As an example, the cable and single converters can be linked as shown in Figure 4-4-(a) by connecting the output voltage of the cable into the input voltage of the dc-dc converters. The current input vector of the converters has additionally be linked with the output vector of the cable model. Similar to the first example, the dc-dc converter can also be connected with the load model as shown in Figure 4-4-(b). It is worth to note that a node distribution matrix ($Dist_{node}$) is necessary to separate the combined current /voltage signals simultaneously as depicted in Figure 4-4-(c) if parallel connections of the converters or cables are required. The general structure to distribute the vectors can be given as (4.1-12).

$$Dist_{node} = [eye(k)_1, eye(k)_2, \dots eye(k)_n] \qquad (4.1\text{-}12)$$

where, the eye($\cdot$) means the identity matrix, and the harmonic components (k) of the matrix decides the size of the matrix. The "n" means additionally the number of nodes, which is dependent on the connected module. The other connections in series and parallel can also be taken into account by connecting the module to other modules as described in Figure 4-4,.
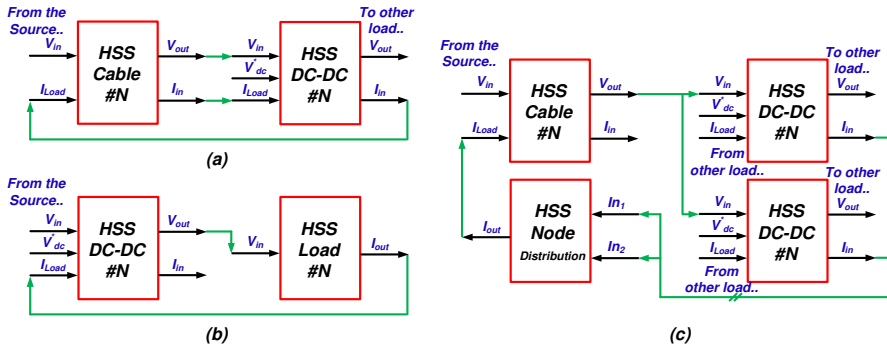
Figure 4-4. *"Block diagram for the connection of each HSS module into a full simulation cases. (a) dc-dc converter connection with single cable, (b) dc-dc converter connection with single load, (c) 2- parallel connected dc-dc converters connected with a single input cable"[111]*

C. Simulation (Steady-state /dynamic)

The simulation results based on the given parameters are compared as shown in Figure 4-5. It is noted that the harmonic vectors from the simulation can be

transformed into the time-domain signals by rotating the harmonic frequency as given (2-15). Each rotated harmonics in time-domain can then be a single time-domain signal as shown in Figure 4-5. The simulation results finally show that the results from the HSS model are identical with the results from the non-linear time-domain simulations (PLECS) as shown in Figure 4-5.

(a)

(b)

(c)

(d)
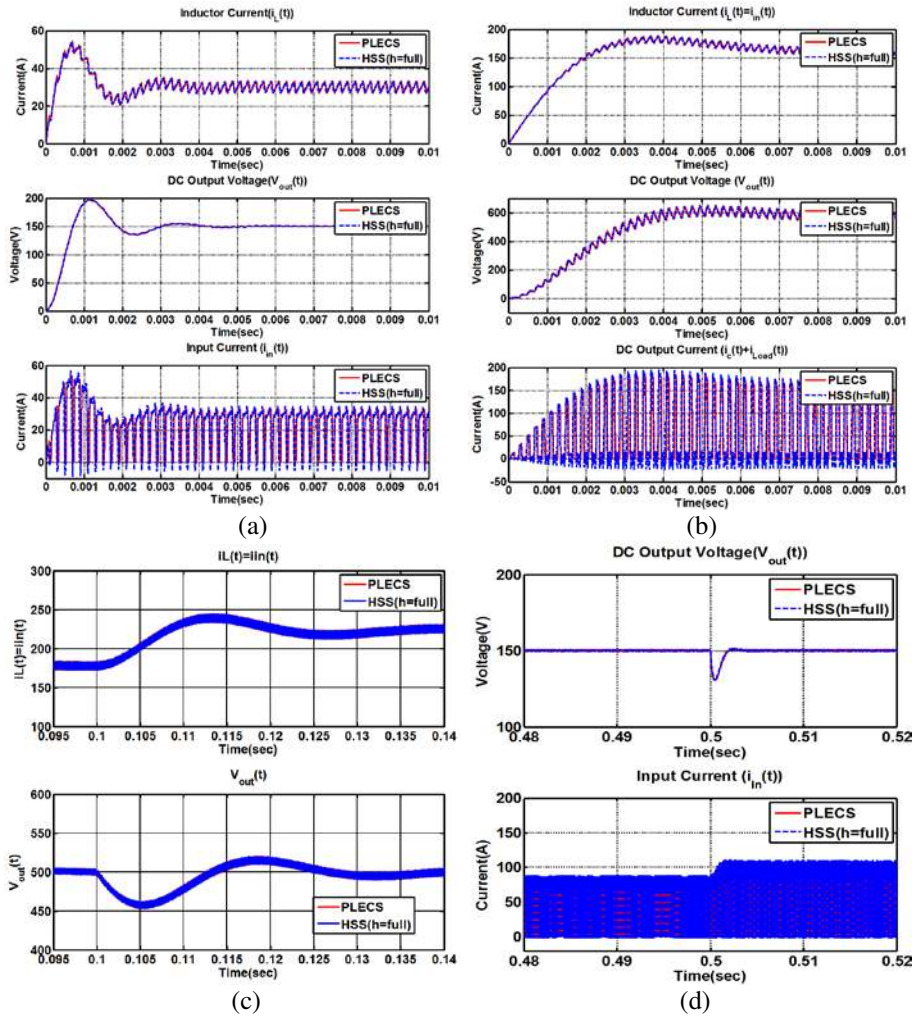
Figure 4-5. "Comparison of simulation results using PLECS and HSS modeling (a) buck converter in Table 4-I-(a), (b) boost converter in Table 4-I-(b), (c) 20% dc-load (load converters) step of boost converter #5 at t=0.1 ($i_L(t)$=inductor current, $v_{out}(t)$=dc output voltage), (d) 10% input-voltage reduction of buck converter #4 at t=0.5 ($i_{in}(t)$=input current, $v_{out}(t)$=dc output voltage)" [111].

Two cases are tested in the simulation. A transient behavior from the initial state is first simulated to verify whether the simulation converge from its "zero" initial state or not. Second, the behavior in steady-state is varied to simulate the dynamics of switching instant as well as the state change from the previous state. Additionally, the accuracy of the simulation result is compared with the discussion. The constant dc voltage (200 V_{dc}) is defined as the base of the input dc voltage and it is decreased into 150 V_{dc} through the buck converter as shown in Figure 4-5-(a). Furthermore, the main dc bus (Bus #1) is stepped up into 500 V_{dc} by using a boost converter as shown in Figure 4-5-(b). The 500 V_{dc} is then stepped down into 250 V_{dc} through the buck-boost converter. The simulation results show the dynamic behavior from the initial state and the convergence of the simulation. The dynamic behavior takes place as well when the buck and boost converters at the steady-state are connected with the other devices (@ t=0.1). It is worth to note that the results from the HSS model show the same performance with the PLECS as shown in Figure 4-5-(c). The output dc voltage is converging according to the varying loads while the load current is increased. The output is also chasing the reference as shown in Figure 4-5-(d) while the input current is varied to sustain the same power, even if the disturbance occurrs during the operation.
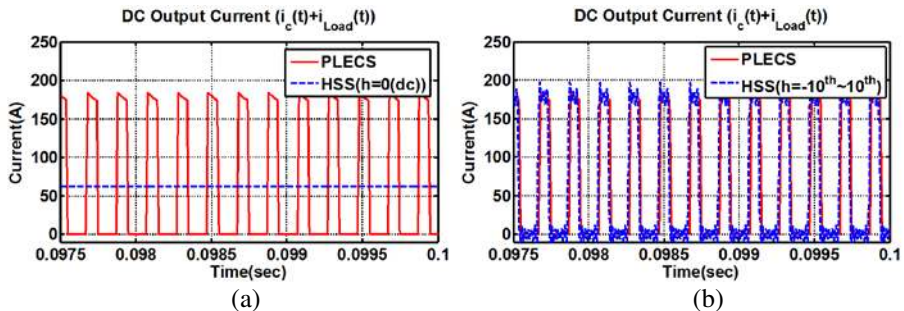
Figure 4-6. "Comparison of simulation precision according to the number of harmonics used ($i_c(t)$=capacitor current, $i_{Load}(t)$=output load current), (a) Comparison of PLECS and HSS (h=0(dc)), (b) Comparison of PLECS and HSS (h= -10th ~ 10th)"[111]

It is noticeable that the simulation accuracy of the HSS model depends on the number of harmonics considered in the model as well as the precision of the Fourier series while the PLECS and the other modeling methods are not related with them. The simple simulations for PWM switching are performed to compare the results as shown in Figure 4-6-(a), (b), where the accuracy can be improved by including more harmonics in the calculation. However, it will increase the matrix size as well as the calculation time. Additionally, even though PLECS shows faster simulation time than the HSS model when a single converter is simulated, the HSS model can mimic the same behavior. Furthermore, the simulation time of the HSS model may be much faster that the PLECS when the number of circuits increase. It has been found that the long-term simulation time for the HSS model is also shorter than the PLECS as given in Table 4-III.

Table 4-III. "Simulation time comparison using PLECS and HSS model" [111]

Simulation Condition (module/simulation time)	PLECS	HSS
1 converter / 1 sec	6 sec	7 sec
9 converter 3 load / 1sec	50 min	4 min

* Controllers are all included in the module.
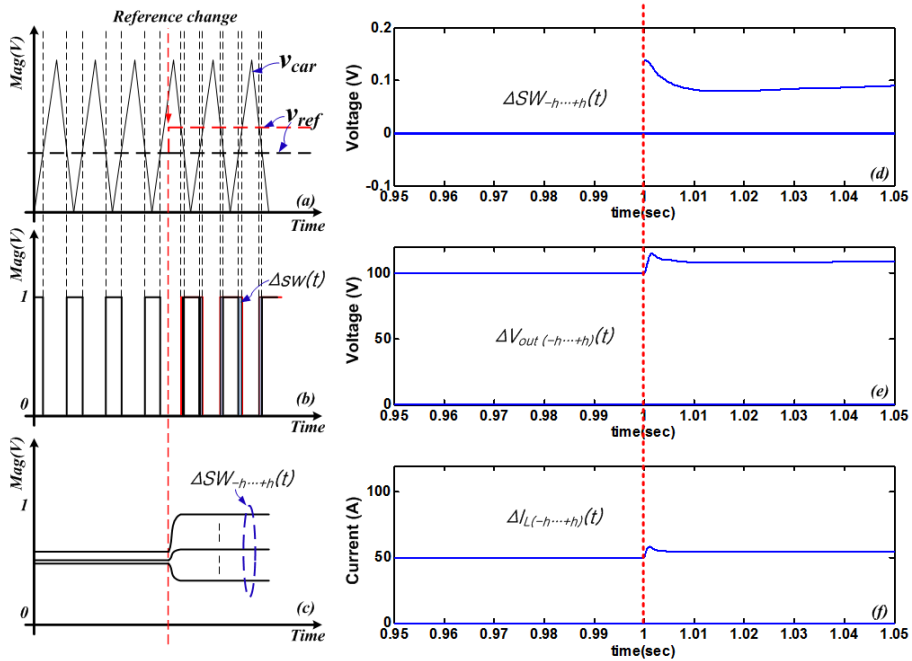
Figure 4-7. "Detailed description of the small-variation (Δ) behaviors of buck converter(a) Time domain representation of carrier signal (v_{car}) and reference signal (v_{ref}), where the changed reference is in red color, (b) Time domain representation of PWM signal and small variation of switching signal ($\Delta sw(t)$), (c) HSS direct simulation of switching instant variation, where all signals are varying harmonics (-h…h), (d) Direct HSS simulation result of switching instant variation ($\Delta SW_{-h…+h}(t)$), (e) Direct HSS simulation result of dc-voltage variation ($\Delta V_{out(-h…+h)}(t)$), (f) Direct HSS simulation result of inductor current variation ($\Delta i_{L(-h…+h)}(t)$))" [111]

D. Detailed dynamic behavior of harmonic vectors

The details about how the small variation of dc voltage (ΔV_{out}) can be related with the small variations of the switching instant (ΔSW) are explained. The nonlinear behavior of (4.1-5) is first described in details by using Figure 4-7-(a), (b). The carrier waveform (v_{car}) is compared with the output signal of controller (v_{ref}) to generate the PWM signal as depicted in Figure 4-7-(b). The small perturbation to the reference signal may also perturb the switching signal ($\Delta sw(t)$) as shown in Figure

4-7-(b). Even though the small variation can be achieved in the PLECS through the iterative calculation to find an optimized convergence, the number of test object for the simulation may increase the calculation time due to the iteration. The HSS model in (4.1-6) can be used to simulate the same behavior of (4.1-5), where "base" implies the nominal values (the previous state). The small variation of the switching instant can be emulated in the HSS model by perturbing the multiple harmonics as shown in Figure 4-7-(c). It is worth to note that all harmonics of $\Delta sw(t)$ can be decomposed as the $\Delta SW_{-h...h}(t)$. The small variation of time domain signals in the dc-dc converters, i.e. dc voltage, inductor current and control output, can be described as time-varying multiple harmonics by using (4.1-6). The separated harmonic vectors of the buck converter are simulated by using the HSS model in Figure 4-7-(d)~(f) to investigate all varying harmonics, where the controller reference is varied from 100 V to 120 V at 1 sec. According to (4.1-6), the state variables of the dc voltage as well as the inductor current are varied through the linearized harmonic vector of the switching signal to mimic the transient behavior due to the nonlinear switching. Even though the variation of harmonics is small to be neglected in Figure 4-7-(d)~(f), they can be involved to transfer the frequency from input to other nodes depending on the situations, where all varying harmonics of this section are using (4.1-5), (4.1-6) for the consideration of switching instant.

E. Discussion about frequency coupling

To explain how the frequency coupling can be included in the HSS model, the detailed behavior of the buck converter is analyzed as an example, where the parameters of the buck converter (#4) in Figure 4-1 are used for the simulation. It is assumed that the input or output of the dc-dc converter is connected with the ac-dc converter to mainly focus on the frequency coupling at the low order frequency. It is noted that the single phase ac-dc converter transforms the fundamental component (f_s) at the ac-side into even order harmonics $(2f_s, 4f_s ...)$ at the dc-side while 6th order harmonics $(6f_s, 12f_s ...)$ are generated at the dc-side of the three phase converter because of the modulation and the frequency coupling. Several methods have been studied to mitigate the original harmonics, which are dependent on the topology as well as the modulation scheme. For instance, the PR controller is adopted in the dc circuit to mitigate the low-order harmonics of the ac-side. However, it may bring unexpected harmonics or disturb the stable behavior of the system [112], [113]. Hence, understanding the principles of the low-frequency coupling between the ac systems and the dc systems is necessary for stable operation of the dc systems.

It is assumed that the low-frequency oscillation (100 Hz) exists in the input voltage with having 10 % magnitude of p.u value. Additionally, the single phase ac-dc converter is connected to the input source of the buck converter. The modulation scheme between the two systems can then be simplified as given in (4.1-13), where $v_{dc_{in}}(t)$ is input voltage, $d(t)$ is modulation ratio, ω_s is the low-frequency component of the input voltage, ω_d is the low-frequency component in modulation and $v_{out}(t)$ is the assumed output voltage through modulation, respectively. Additionally, high frequency components are simplified as "…" and β, α are the small ratio of low frequency component to explain the varying modulation index.
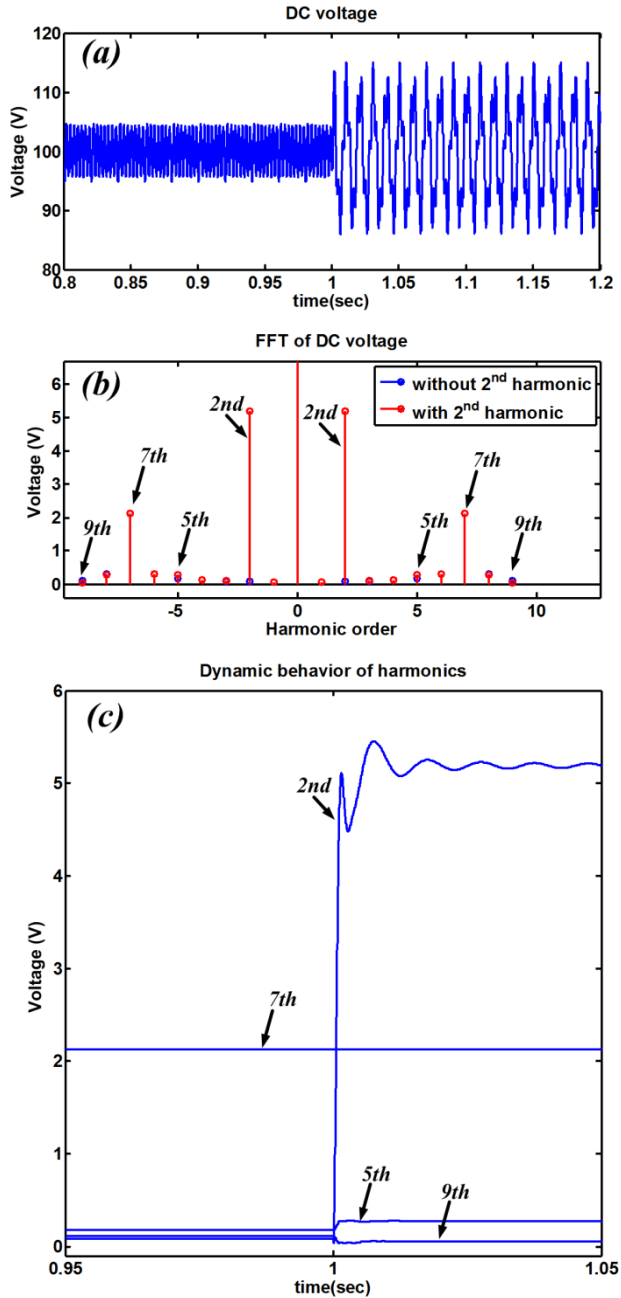
Figure 4-8. "Buck converter simulation for frequency coupling effect, (a) HSS simulation result of dc output voltage, (b) FFT result of dc output voltage, (c) Dynamic behavior of harmonics in dc voltage"[111]

$$v_{out}(t) = [d(t) \cdot (1 + \alpha \cdot \cos(\omega_d t) + \cdots)] \cdot \left[v_{dc_{in}}(t) \cdot (1 + \beta \cdot \cos(\omega_s t) + \cdots) \right]$$
$$(4.1\text{-}13)$$

(4.1-13) can be a basic relationship between input and output of dc converter if α, β are equal to "0". However, α, β should be defined to analyze the frequency coupling that α is dependent on the load condition and β is dependent on the converter, which is linked to the dc input. The other frequency range can also be considered in (4.1-13) based on the fundamental relationship. The final output signal of the dc converters can then be reorganized as shown in (4.1-14)~(4.1-16), where $v_{out_{dc}}(t)$ is the dc signal of (4.1-13), $v_{out_{low}}(t)$ is the low frequency range and $v_{out_{cross}}(t)$ is the coupled frequency through the multiplication of two signals.

$$v_{out_{dc}}(t) = v_{dc_{in}}(t) \cdot d(t) \qquad (4.1\text{-}14)$$

$$v_{out_{low}}(t) = v_{dc_{in}}(t) \cdot d(t) \cdot \alpha \cdot \cos(\omega_d t) + v_{dc_{in}}(t) \cdot d(t) \cdot \beta \cdot \cos(\omega_s t) \qquad (4.1\text{-}15)$$

$$v_{out_{cross}}(t) = (v_{dc_{in}}(t) \cdot d(t) \cdot \alpha \cdot \beta)/2 \cdot [\cos((\omega_d + \omega_s)t) + \cos((\omega_d - \omega_s)t)]$$
$$(4.1\text{-}16)$$

Additionally, the frequency coupling occurred by other frequencies can also be analyzed in the same way. However, it is worth to note that (4.1-14) ~ (4.1-16) mean the nonlinear time-varying behavior and the emulation of them through a conventional approach may be difficult since the LTI system (single input and single output) mainly average all signals. On the contrary to the conventional methods, the HSS model of the buck converter are simulated under the same conditions that 100 Hz (2nd order) components came out with the switching harmonics as well as the dc term as shown in in Figure 4-8, where they are generated by the modulation with the input frequency. It is assumed that the switching signal already contains 7th order harmonic before small perturbations (2nd order harmonics) is happened in the dc-dc converter. The 2nd order harmonic is perturbed with small magnitude at 1 sec, and it shifts the other low order harmonics (5th and 9th) as shown in Figure 4-8, where the 5th harmonic is increased while 9th harmonic is decreased as analyzed in (4.1-13)~(4.1-16). It is worth to note that all harmonics have their dynamics based on their own frequency response. Furthermore, the transformation of Figure 4-8-(c) into the time-domain signal by rotating the phasors shows identical waveforms with Figure 4-8-(a). It is thus remarkable that nonlinear relationships between converters in (4.1-14) ~ (4.1-16) can be accurately analyzed by using the HSS method and the LTP theory.

The HSS method is basically following the assumptions that all signals and parameters used in the model are periodic signals. The HSS method thus has a limiation to be used in the model, when it does not have a periodic status. However, almost all power electronic systems have a periodic behavior [31], [36], [46], [48], [114] and they cause the frequency coupling behavior through the switching and the modulation. Furthermore, the HSS (HD) method [115], [116] has been used in the analysis of inter-harmonics in the ac-dc application by reducing the periodicity of 0.1 Hz or 0.5 Hz etc. Hence, the system, which operates at periodic states, can be

analyzed through the HSS method, even if the test object has an asynchronous behavior.

4.1.3. SUMMARY AND CONCLUSION

This section has presented a way to develop the model of dc power electronic systems through the HSS method and how to validate the accuracy of the model in simulations. Each HSS model is modulized to combine them with other converters. The HSS models are analyzed with a PLECS to validate the accuracy and the frequency coupling between the converters and the loads. The simulation results from the HSS model show identical behavior with the PLECS. Thus, the frequency responses of the HSS model are more appropriate to mimic the dynamics of harmonics than the traditional ways, e.g., SSAV or GAV. Furthermore, it is verified, compared with the simulation time that the HSS model has better possibility to be extended in the case of multiple connected systems and thereby used in complicated future power electronic based power systems. Additionally, the proposed HSS model can be extended to the studies of the compensator design for harmonic mitigation or the stability assessment including the effect of the time-varying components.

4.2. HSS MODELING OF DIODE RECTIFIER

Diode based rectifiers are popular because of their simplicity, reliability, and cost effectiveness. These advantages have been proven in various applications for telecommunications, front-end AC drives and fluorescent lamps [117]. However, these widely used topologies have problems in respect to power quality. Hence, much research have been done to provide optimized power quality solutions according to international standards [118]. The multi-pulse applications are proposed for the high power applications by using a combination of the 3-phase diode rectifier topology and some passive elements. An analytical model in the time-domain considering either continuous mode or a discontinuous mode has also been proposed to explain details about input harmonics [119]. Furthermore, the small-signal input impedance model was also proposed by means of Harmonic Linearization to use a developed model for the stability analysis of 3-phase voltage source converter [27], [84], [120]. However, most research have overlooked the phase-dependence impedance profile, where the impedance at harmonic frequencies varies when the phase of the harmonics in the grid voltage changes. This changing profile could be significant and give new guidelines for the design of passive filters or harmonic compensators in controllers.

The phase dependence of impedance was first treated in HVDC applications where tensor linearization of the HVDC converter [65], [121], [122] was introduced. Though the linearization of the converter to frequency dependent impedance is a simple step due to an averaging procedure, it is difficult to linearize the nonlinearity of a diode rectifier by a single frequency response. Hence, [65], [121], [122] start to investigate how nonlinearity of the rectifier can be linearized by multiple frequency responses. Furthermore, the representation by a single complex number, which is mostly used by the single frequency dependent impedance, is not enough to linearize generally the nonlinear or time variant devices to the equivalent impedance. Additionally, the complex value of the impedance can depend upon the phase angle of the current flowing. Hence, the principal reasons of the phase dependent impedance are due to the nonlinear behavior caused by the time variant switching and frequency coupling between the ac and dc side. Hence, to represent these characteristics and to make an analytical impedance model, various iteration modeling methods have been proposed.

In this section, the Harmonic Domain based model is chosen as a solution to represent the phase dependence impedance of 3-phase diode rectifier. First an analytical model of a 3-phase diode rectifier in the Harmonic State-Space (HSS) framework is described. It is noted that the Harmonic Domain (HD) impedance can be achieved from the HSS modeling results, where the derived impedance includes the effect of frequency coupling and Switching Instant Variation (SIV). Next, the algorithm of tensor linearization [65], [121], [122] will be explained to represent

multiple complex values in 2 dimensions and how they can be extracted from the final HD impedance.

Also, the phase dependence impedance measured from a commercial time-domain simulation will be compared with the phase dependent impedance from the analytical model and both results will be compared with the experimental results as well verifying the existence of phase dependent impedance in the rectifier. Additionally, the measurement procedure will also be explained by a sequence diagram.
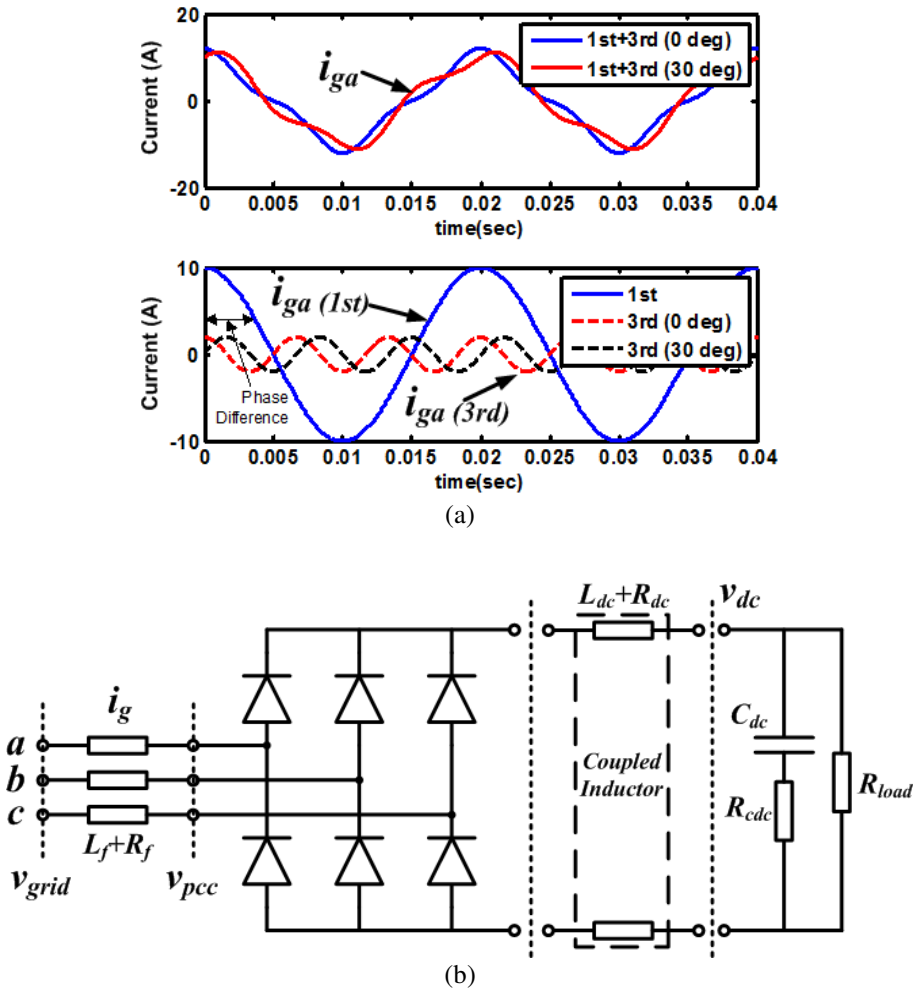

(a)

(b)

Figure 4-9. "3-phase diode rectifier, (a) Current waveform changed by phase difference of harmonics (3rd order harmonics), (b) General 3 phase diode rectifier topology used in the modeling, simulation and experiments for the HSS modeling" [123]

4.2.1. ANALYTICAL MODEL OF 3-PHASE DIODE RECTIFIER USING HSS MODELING

According to the basic theory in (2-15), the HSS model for a 3 - phase diode rectifier can be obtained. The general procedure for the modeling of the diode rectifier in the HSS method is discussed in [46], [48]. The whole modeling procedure will not be treated in this section, because this section focuses on the method verifying the phase dependence impedance from the analytical model, simulation, and experiment. The 3-phase diode rectifier is shown in Figure 4-9-(b), where L_f and R_f are grid side inductance and resistance, L_{dc} and R_{dc} are filter inductance and resistance at dc-side, C_{dc} and R_{cdc} are the filter capacitance and its parasitic resistance in the dc-link and R_{load} is the assumed load resistance, which is used to adjust the power rating of Constant Power Load (CPL). According to the introduced theory in the Chapter 2, the 3-phase diode rectifier is modeled in this section. The system is divided as three sections, where they are separated as ac-side subsystem, dc-side subsystem and switching subsystem. Each subsystem is correlated with each other through the harmonic vector to transfer the behavior of other subsystems. The effects, which can vary the switching instant of the diode during operation, are considered in each subsystems to reflect the phenomenon at the time-domain to the frequency domain.
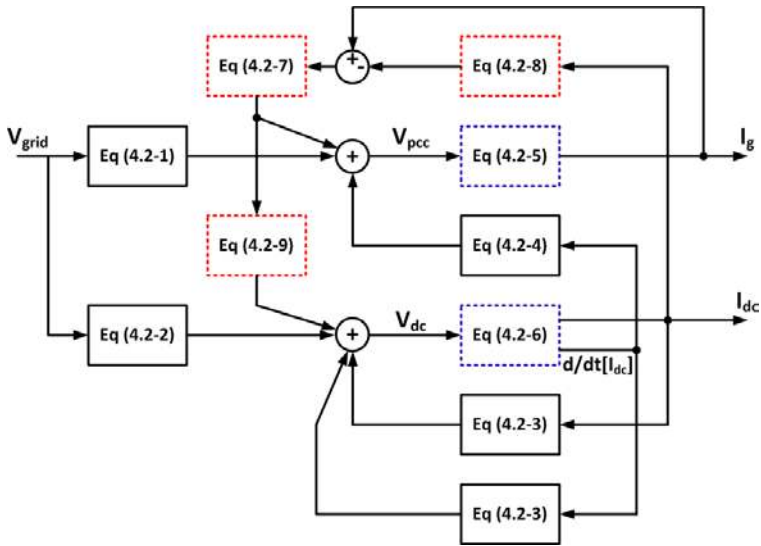
Figure 4-10. Block diagram of small-signal model for 3-phase diode rectifier. (black box=steady-state frequency transfer matrix, red box=matrix for the switching instant variation, blue box=HSS matrix of the dc-circuit and ac-circuit)

The complete block diagram for the frequency domain model of 3-phase diode rectifier is shown in Figure 4-10, where the equation number in Figure 4-10 are matched with the explanations of the equations below. The harmonics of the ac-side

voltage is fundamentally transferred to the harmonics of the dc-side voltage through the switching function. Similarly, the harmonics of dc-side current are transferred into the ac-side current by using another switching function. It is noted that the switching functions of voltage and current transfers are different compared with the voltage source converter since the switching instant of the diode is disturbed according to the variation of voltage and current at both ac and dc-side. Hence, their dynamic behavior should be completely considered to represent the correct behavior of harmonics in the model.

The proposed model is separated into two parts as they can be classified into "base part (=steady state)" and "dynamic part" to perturb the base case at the operating point. Firstly, the switching function in frequency domain is given in (4.2-1) ~ (4.2-4) where the equation can be regarded as the Fourier coefficients of each switching function, which is referred to as the considered harmonics. "m", which is used in whole equations, means harmonic vectors and subscript "0" of acronym means the base value that is the same with the base operating point, where the model is linearized. Furthermore, the acronyms in Figure 4-9 are represented as capital letters in Figure 4-10 to clarify the difference between time-domain and frequency domain signals. According to the rule that the multiplication of two time-domain signals can be represented as the convolution of two frequency-domain signals, (4.2-1) ~ (4.2-4) formulate the Toeplitz matrix to achieve a same behavior as with the results in time-domain. It is worth to note that the results of multiplication or convolution in (4.2-1) ~ (4.2-4) mean the steady-state results and still do not include the dynamic behavior of the converter.

$$\text{FTM}_1 = \frac{\mu_0}{2\pi} + \sum_m \frac{1}{m\pi} \sin\left(\frac{m\mu_0}{2}\right)\left[e^{-jm\left(\frac{\pi}{3}+\frac{\mu_0}{2}\right)} + e^{-jm\left(\frac{2\pi}{3}+\frac{\mu_0}{2}\right)} - e^{-jm\left(\frac{\pi}{3}+\frac{\mu_0}{2}-\frac{k2\pi}{3}\right)} - \right.$$
$$\left. e^{-jm\left(\frac{2\pi}{3}+\frac{\mu_0}{2}-\frac{k4\pi}{3}\right)}\right] \quad (4.2\text{-}1)$$

$$\text{FTM}_2 = \sum_m \left[\frac{6}{m\pi}\sin\left(\frac{m\pi}{3}\right) + \frac{6}{m\pi}\sin\left(\frac{m\mu_0}{2}\right)\sin\left(\frac{m\pi}{3}\right) e^{-j\left(m\frac{\mu_0}{2}+\frac{\pi}{2}\right)}\right] \quad (4.2\text{-}2)$$

$$\text{FTM}_3 = 1 + \frac{3\mu_0}{2\pi} + \sum_m \left[-\frac{12}{m\pi}\sin\left(\frac{m\mu_0}{2}\right)e^{\frac{-jm\pi}{6}} + \frac{9}{m\pi}\sin\left(\frac{m\mu_0}{2}\right)e^{\frac{-jm\pi}{6}}\right] \quad (4.2\text{-}3)$$

$$\text{FTM}_4 = \sum_m \frac{2}{m\pi}\left[\sin\left(\frac{m\pi}{3}\right) + \sin\left(\frac{m\mu_0}{2}\right)\sin\left(\frac{m\pi}{3}\right)e^{-j\left(\frac{m\mu_0}{2}+\frac{\pi}{2}\right)}\right] \quad (4.2\text{-}4)$$

The main role of (4.2-1) ~ (4.2-4) is to transfer the frequency components to their output, where the formulation of each Toeplitz matrix can be renamed as the Frequency Transfer Matrix (FTM). The general procedure of harmonic transfer starts from the grid voltage so the variation of the grid voltage may affect the behavior of the pcc voltage and dc-voltage as shown in Figure 4-9. Hence, equation (4.2-1) is the base FTM to transfer the harmonics of the grid voltage (v_{grid}) to the pcc-voltage (v_{pcc}) in Figure 4-9 and (4.2-2) is the FTM to transfer the harmonics of the grid voltage (v_{grid}) to the dc-voltage (v_{dc}). In the case of dc-current (i_{dc}), it also affects the variation of the dc-voltage and it should be considered in the procedure of

using the FTM (4.2-3). Furthermore, it also influences the variation of pcc-voltage (v_{pcc}) and it may be transferred by means of (4.2-4). Based on the described base operating point in (4.2-1) ~ (4.2-4), the variation of small-signal in somewhere of the system can be taken into account by using a small-signal analysis. Secondly, the dynamic behavior of the ac-side impedance can be represented as (4.2-5), where the acronyms are same with Figure 4-9 and Figure 4-10. Additionally, the dc-network of a 3-phase diode rectifier can also be included by using (4.2-6), where the used acronyms are following Figure 4-9 and Figure 4-10. The small variation of pcc-voltage and dc-voltage will affect other signals according to (4.2-5) and (4.2-6).

$$G_{ac} \rightarrow [\dot{I_g}] = \left[-\frac{R_f}{L_f} + jm\omega_0\right][I_g] + \left[\frac{1}{L_f} \quad -\frac{1}{L_f}\right]\begin{bmatrix} V_{grid} \\ V_{PCC} \end{bmatrix} \tag{4.2-5}$$

$$G_{dc} \rightarrow \begin{bmatrix} \dot{I_{dc}} \\ \dot{V_{out}} \end{bmatrix} = \begin{bmatrix} A_{11} & A_{12} \\ A_{21} & A_{22} \end{bmatrix}\begin{bmatrix} I_{dc} \\ V_{out} \end{bmatrix} + \begin{bmatrix} \frac{1}{L_{dc}} \\ 0 \end{bmatrix}[V_{dc}] \tag{4.2-6}$$

where,

$$A_{11} = -\left(\frac{R_{dc}}{L_{dc}} - \frac{R_{cdc}}{L_{dc}} \cdot \frac{R_{load}}{R_{load}+R_{cdc}}\right) + jm\omega_0, \ A_{12} = -\frac{1}{L_{dc}} \cdot \frac{R_{load}}{R_{load}+R_{cdc}},$$
$$A_{21} = \frac{1}{C_{dc}}\left(\frac{R_{load}}{R_{load}+R_{cdc}}\right) + jm\omega_0, \quad A_{22} = -\frac{1}{C_{dc}} \cdot \frac{1}{R_{load}+R_{cdc}}$$

However, the problem is that the inputs of (4.2-5) and (4.2-6) are affected by the grid current (i_g) and the dc-current (i_{dc}) and it changes the switching instant in the time-domain model. The nonlinear behavior in the time-domain should be included in the frequency domain model in order to achieve an accurate small-signal model for the harmonic analysis and their effect on the stability. The "dirac-comb" function is used to take into account the small variation of the ac-current as shown in (4.2-7).

$$\Delta\mu_{0-ac} = \sum_m \frac{1}{T}\left[e^{-jm\mu_0} + e^{-jm(\mu_0+\pi)}\right] \tag{4.2-7}$$

The small variation of "μ" from the base case "μ_0" will affect the pcc-voltage as the shape of the impulse response. Then, the effect can be included by using the periodic impulse train and (4.2-7) is the formulation of dirac-comb function in the frequency domain. The multiplication of the ac-current and the impulse train in the time-domain will give the voltage impulse, which will be the additional information to reflect the small-signal behavior of the ac-current. Furthermore, the small variation of the dc-current (i_{dc}) influences the variation of ac-current as well because the dc-current is connected with other two phase current during the conduction period and the commutation period. Hence, it should also be included by means of the dirac-comb function as given in (4.2-8), where the equation is the formulation for the frequency domain and it is using the Toeplitz formulation.

$$\Delta\mu_{0-ac2} = \sum_m[e^{-jm\mu_0}] \tag{4.2-8}$$

Simultaneously, a small variation of the pcc voltage affects the variation of dc-voltage. Hence, it should also be reflected in the modeling procedure as given by (4.2-9).

$$\Delta\mu_{0-dc} = \sum_m [\, e^{-jm\mu_0}\,] \qquad\qquad (4.2\text{-}9)$$

The voltage impulse at the pcc-voltage will influence the part of the dc-voltage which will mainly change the voltage drop due to the commutation angle (μ) of the diode rectifier. As a conclusion, the overall structure of the frequency domain model has both a feedback and a feedforward structure. The small variation of each signal will simultaneously affect the other correlated signals according to the operation of 3-phase diode rectifier. The challenge of modeling this behavior is how to linearize the nonlinear behavior in the modeling procedure. The traditional averaging based model can not demonstrate the same behavior due to the averaging procedure. However, the HSS model decomposes the nonlinear and discontinuous behavior by the Fourier coefficients and investigates the small variation of each considered harmonics. Finally, the reconstruction of the dynamic behavior to the time-domain by using (2-15) will show the same small signal dynamics with the nonlinear behavior in the time-domain.

4.2.2. ALGORITHM FOR MEASUREMENT OF PHASE DEPENDENT IMPEDANCE
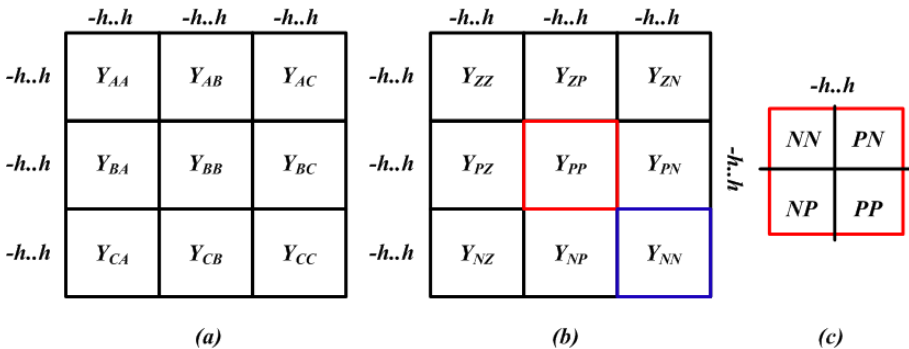
Figure 4-11. "Harmonic domain of 3-phase diode rectifier, (a) Frequency domain (Harmonic Domain) of three phase (A,B,C), (b) Frequency Domain (Harmonic Domain) of phase sequence (Z,P,N), (c) Structure of frequency domain (Y_{PP})" [123]

The harmonic analysis in the frequency domain can make it possible to analyze the harmonic frequency separately by using the principle of superposition. Besides, the complex phasor in the rectangular or polar form make it possible to obtain the frequency dependent impedance. The problem is that a phase angle of harmonics in the grid current is actually varying as shown in Figure 4-9-(a). As a result, the small variation of magnitude and phase in the grid voltage bring the nonlinear change of harmonics in the current due to the nonlinearity of the diode rectifier, where this means an impedance of the diode rectifier that can not be represented by a single frequency response. However, this behavior can be represented as multiple coupled frequency responses or tensor representations, which are obtained from the small linear region around the operating point. Hence, this can be achieved by injecting a

small-signal harmonic voltage distortion to the rectifier in order to obtain the perturbed current.

The division of the two partial derivatives gives the admittance value at the harmonic frequency as given in (4.2-11), where "m" and "n" mean harmonic frequency of current (I) and voltage (V). This can be done in all harmonic frequencies as given in (4.2-10), which is a part of the HD shown in Figure 4-11-(a) or (b) and it is noted that if the resolution of harmonics is increased at the diagonal axis of (4.2-10), then it is the same method as with frequency response used in the averaged modeling. As a result, the frequency coupling impedance may have a formulation as shown in Figure 4-11-(a) or (b), where Figure 4-11-(a) means coupled ABC phase impedance in the frequency domain, Figure 4-11-(b) means the coupled sequence impedance in frequency domain and –h…h means frequency from negative to positive. However, the admittance value in (4.2-11) is not enough to study the phase dependence. The pair impedance representing the negative frequency is required to represent the phase dependence impedance. In reality, the frequency response is composed by (+) frequency side as well as (-) frequency side as given in (4.2-12) and Figure 4-11-(c), where "*" in (4.2-12) means the conjugate terms of admittance.

$$
\begin{bmatrix}
\dfrac{\sigma I_1}{\sigma V_1} & \dfrac{\sigma I_1}{\sigma V_1} & \dfrac{\sigma I_1}{\sigma V_1} & \cdots & \dfrac{\sigma I_1}{\sigma V_1} \\
\dfrac{\sigma I_1}{\sigma V_1} & \dfrac{\sigma I_1}{\sigma V_1} & & & \\
\dfrac{\sigma I_1}{\sigma V_1} & & \dfrac{\sigma I_1}{\sigma V_1} & & \\
\vdots & & & \ddots & \vdots \\
\dfrac{\sigma I_1}{\sigma V_1} & & & \cdots & \dfrac{\sigma I_1}{\sigma V_1}
\end{bmatrix}
\tag{4.2-10}
$$

$$
Y_{m,n} = \frac{\sigma I_m}{\sigma V_n} = \frac{\Delta I_m}{\Delta V_n}
\tag{4.2-11}
$$

$$
\begin{bmatrix} \Delta I_+ \\ \Delta I_- \end{bmatrix} = \begin{bmatrix} Y_1 & Y_2 \\ Y_1^* & Y_2^* \end{bmatrix} \begin{bmatrix} \Delta V_+ \\ \Delta V_- \end{bmatrix}
\tag{4.2-12}
$$

The voltage and current in the positive frequency and the admittance Y_1 and Y_2 in (4.2-12) are used in the calculation of the phase dependent impedance. Hence, the decomposed matrix (4.2-13) from (4.2-12) can be achieved, where acronym "r" means a real value of $\Delta V, \Delta I$ and "i" means an imaginary value of $\Delta V, \Delta I$.

$$
\begin{bmatrix} \Delta I_r \\ \Delta I_i \end{bmatrix} = \begin{bmatrix} Y_{11} & Y_{12} \\ Y_{21} & Y_{22} \end{bmatrix} \begin{bmatrix} \Delta V_r \\ \Delta V_i \end{bmatrix}
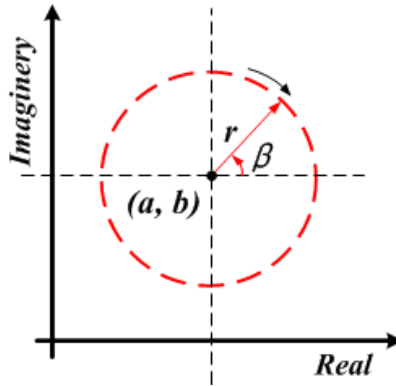\tag{4.2-13}
$$

Figure 4-12. "Tensor of complex admittance for phase dependence impedance" [123]

It is noted that the phase dependency has 3D information (harmonic phase, impedance magnitude and impedance phase) and the Tensor is a good tool to represent the phase dependency in the 2D domain. Hence, a complex admittance value $Y_{11}, Y_{12}, Y_{21}, Y_{22}$ in (4.2-13) can be converted as shown in Figure 4-12 and (4.2-14), where

$$a = \frac{1}{2}(Y_{11} + Y_{22}), \ b = \frac{1}{2}(-Y_{12} + Y_{21}) \tag{4.2-14}$$

$$r = \frac{1}{2}\sqrt{(Y_{11} - Y_{22})^2 + (Y_{12} + Y_{21})^2}, \ \beta = \tan^{-1}\left(\frac{Y_{12}+Y_{21}}{Y_{22}-Y_{11}}\right)$$

In an analytical model, the method to obtain complex conjugate impedance is to use a HD based modeling method, where this modeling is considering the properties in the negative frequency as well as the cross coupled frequency response in a single domain. However, the averaging based modeling method can not consider these effects. Describing both steady-state and dynamic harmonic coupling is possible by means of (2-15), where this can be converted into the harmonic transfer function as shown in (2-17). When "s" is equal to "0", it can also show the steady-state harmonic coupling status and the achieved matrix (s=0) has the same formulation as given in Figure 4-11-(a) or (b). For instance, the "Y_{AA}" of Figure 4-11-(a) or the "Y_{PP}" of Figure 4-11-(b) has the same structure as (2-20), where the input as well as output vector have the same formulation, since it is composed by "-h…h".

Additionally, the final positive and negative impedance from (2-20) are the "Jacobian" values as shown in Figure 4-11-(c). As a conclusion, the phase dependence property of the complex admittance (*Y*), which is obtained from the analytical model in (2-20), can be directly drawn by means of (4.2-12), (4.2-13) and Figure 4-12, when "s" of (2-20) is equal to "0". In a similar way, the phase dependent impedance can be measured from the time-domain simulations and the experimental set up by using an inverse matrix of (4.2-12), (4.2-13) and use the perturbed signals ($\Delta V, \Delta I$).

4.2.3. SIMULATION AND EXPERIMENT RESULT

MATLAB and PLECS are used to compare the analytical modeling results with the non-linear time domain simulations. The 3-phase rectifier in Figure 4-9-(b) is used in experimental validation as well.
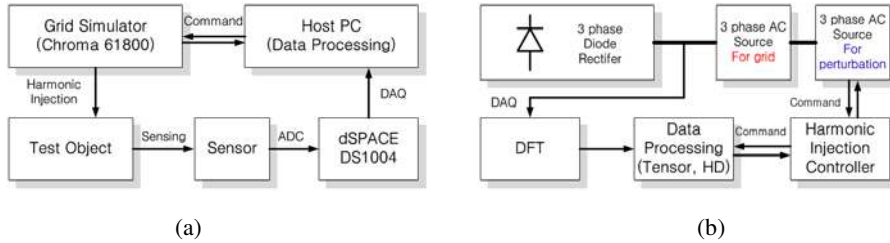

(a)   (b)

Figure 4-13. "Diagrams for phase dependent impedance measurement (a) Block diagram for measurement in the time domain simulation tool, (b) Block diagram for measurement in the experimental set up" [123].

First, a block diagram for the phase dependent measurement in the time domain simulation is shown in Figure 4-13-(a), where all parameters and filter structures are the same as shown Figure 4-9-(b). A small-signal perturbation technique is required to calculate the phase dependent impedance. Hence, an additional 3-phase source is connected with an ac source in series as shown in Figure 4-13-(b). It is noted that the main purpose of an additional source is to perturb a switching instant of the diode and it is controlled by an internal algorithm. At first stage, the specific harmonic injection starts from 0 degree and the phase angle of the injected harmonics is increased by up to 180 degree. Both the 3-phase voltage and current are measured simultaneously by means of a sensing block given by the simulation tool according to the variation of phase angle. The measured data are directly transformed into frequency information by using Discrete Fourier Transform (DFT). The gathered frequency data of the 3-phases are transformed into sequence components in order to decompose the coupling among the three phases (A, B, C) and the obtained data are converted again to a Tensor representation by means of (4.2-12), (4.2-13) and Figure 4-12 to describe the phase dependent impedance in two dimensions. Another harmonic perturbation starts to be injected by varying the phase angle of the perturbed signals to measure the input phase dependent impedance after finishing the measurement of the previous harmonics injection.

The experimental validation can be performed in a similar way. A grid simulator (Chroma 61800) is used to inject small harmonic signals, where the harmonics have a variable phase (0 degree ~180 degree) by controlling the grid simulator from a Host PC. Hence, the test object, which is shown in Figure 4-13-(a), can operate in a perturbed ac grid condition. In the same way, the 3-phase input current of the test object, which reflects the SIV, and the perturbed 3-phase grid voltage are measured at the same time by means of a sensor box as shown in Figure 4-13-(a). The scaled

signals are transferred into dSPACE (DS1007) through an ADC box, where the dSPACE is used to perform the data processing instead of using a DSP. Finally, the gathered data experiences the same procedure with the method used in the time domain simulations. The 3-phase data is transformed into sequence data and converted into frequency information by using DFT. The obtained frequency information at the specific harmonic frequency can be converted into a Tensor formulation by using (4.2-12), (4.2-13) and Figure 4-12 in order to represent the phase dependences in two dimensions.

A comparison of the three results is shown in Figure 4-14, where the Tensor from the HSS model, time domain simulation and experimental setup are compared in one domain. It is noted that blue "O" in Figure 4-14 means the phase dependent impedance at 0 degree phase difference and this harmonic impedance is the same with the impedance derived from the averaging method at the same frequency. For the visibility, the phase dependent impedance among the same harmonic frequency is only measured from the experimental set up. The results show that the 3 results are matched well and how the impedance at the harmonic frequency can be varied according to the phase variance. The magnitude and phase of the impedance at 0 degree phase are shown in Figure 4-14-(b) and these values are derived from blue "O" of Figure 4-14-(a). It is worth to note that the magnitude and phase value in Figure 4-14-(b) is the same as the impedance result, which is derived from the average model of a 3-phase diode rectifier. The averaged model is averaging all harmonic contents on both dc and ac sides by using a moving average filter and it mainly considers the averaged value to represent the basic dynamic behavior. However, it can be found in Figure 4-14 that the impedance values from the averaged model are part of the impedance, which is represented as Tensor format or HSS model in (2-20).

The magnitude and phase plot of other cases are also plotted in Figure 4-15, where the magnitude and phase are represented by using the same method introduced in Figure 4-14-(b). The impact of phase dependency is relatively large in case of 5th, 7th, 11th, 13th harmonics as shown in Figure 4-14-(a), where the large circle means that the real and imaginary values of the impedance are varying according to the different phases of the input signal. In case of 3rd, 17th, the effect of phase dependence can be neglected since the circle is very small and it means that the output signal of the power converter will not take care about the phase difference of the input signal. The same analysis can be found in Figure 4-15, where the magnitude and phase of the 5th, 7th, 11th, 13th, are mainly varying. However, other frequencies show a small difference according to the phase variation of the input signals. The case is dependent on the filter type in the dc-side or ac-side of a diode rectifier as well as on the operating point of the diode rectifier whether the rectifier is in continuous conduction mode or discontinuous conduction mode.
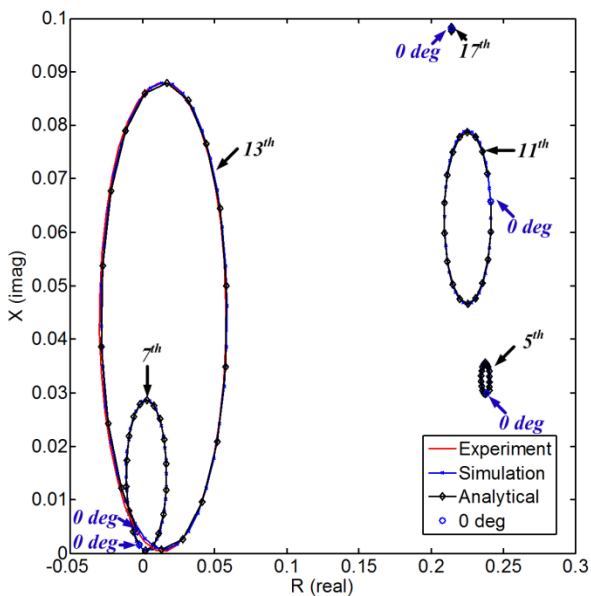
(a)
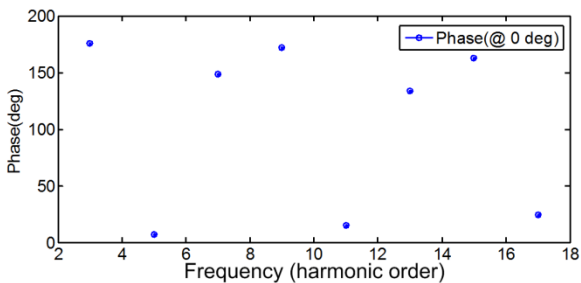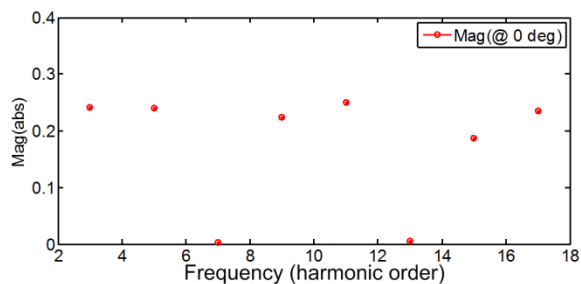
(b)

Figure 4-14. "Comparison of phase dependence impedance (Positive sequence) (a) Phase dependent impedance (0 degree – 180 degree) at discontinuous conduction mode, (b) Phase dependent impedance profile at 0 degree" [123]
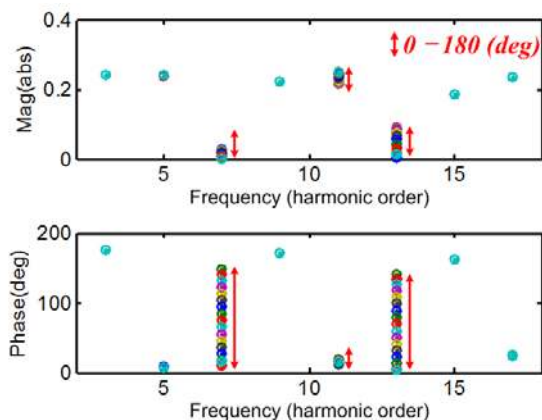
Figure 4-15. "Phase dependence impedance plot in magnitude and phase when the phase of input frequency is perturbed from 0 degree to 180 degree"[123]

It is worth to note that the impedance map in Figure 4-14 or Figure 4-15 is critical in respect to the harmonic analysis of the diode or thyristor application. The impedance representation in Figure 4-14 and Figure 4-15 is derived by using (4.2-12) – (4.2-13), (2-17)~(2-20) and it means that input harmonic signals is not the multiplication of single impedance as normally done in the averaged model. The accurate linearized impedance has a MIMO characteristic and the input harmonic frequency is multiplied by multiple harmonic impedances as shown in Figure 4-15. Even though the effect of a phase dependent impedance in Figure 4-14 and Figure 4-15 is only considered for the same perturbed harmonic frequency, the phase dependent impedance between different frequencies are also critical in order to achieve the correct harmonic components of the diode or thyristor applications, since it has also the same relationship with (2-20) and it will affect the final harmonic frequencies if they have a phase dependent impedance.

4.3. SUMMARY AND CONCLUSION

This section has demonstrated a phase dependent impedance of the widely used 3-phase diode rectifier by using an analytical model, simulations and also an experimental set up. It has been neglected in the conventional modeling since the effect of them in the voltage source converter has been small. However, as the voltage source converter operating at the low switching frequency as well as the diode based converters is increasing in numbers, the influence of the phase dependency is becoming more critical. First, the HD based modeling method (HSS modeling method) is used to make a model of 3-phase diode rectifier by considering SIV and the interaction of the ac and dc impedance. Furthermore, the HD impedance profile, which is derived from the analytical model, is used to extract the impedance at negative frequency. Besides, a Tensor formulation is used to represent multiple complex numbers in a single domain through the HD impedance profile. The results

from the analytical model show that the impedances of harmonic frequency have a phase dependent characteristic. Additionally, these are also verified by time-domain simulations and experimental set ups, where these results could be important in order to be able to analyze impedance interactions or to design a passive filter as well as harmonic compensators in the grid.

CHAPTER 5. ANALYSIS OF HARMONIC INSTABILITY

The modeling of power converters and their linearization have been studied more than a few decades in the field of power electronics. Especially, resonances and unexpected harmonics in the power electronic based systems are being more issues as the number of converters is increasing, and a proper modeling approach is urgent to deal with in order to exactly estimate their behavior in the design as well as in system analysis. The Voltage Source Converters (VSC) in electric railway networks [4] and microgrids [96] recently show the unexpected harmonics, the damped resonance, and the unstable oscillations at the wide range of frequency from few hundreds of hertz to kHz [4]. They have been investigated that the control dely and their interaction between converters and other connected devices may mainly bring the unexpected phenomena during the operation.

However, their interactions and unexpected operation has not been estimated properly since the estimated resonances are shifted through the frequency coupling, and the unestimated resoanaces are appearing because several time-varying signals are multiplied inside. Thus, the principal challenges are how to deal with the time-varying behavior in the modeling of power converters. It is noted that the differences among several modeling approaches, i.e. State Space Averaging (SSAV), DQ rotational frame (DQ), Generalized Averaging (GAV) [21], Multi-frequency Averaging (MAV) [6], Harmonic Linearization (HL) [26] and Harmonic Domain (HD) based method [35], [40], etc, are how they can simply mimic the time-varying behavior in their procedure [4]. Therefore, it is worth to note that they can be classified into two categories as Linear Time Invariant (LTI) and Linear Time Periodic (LTP) models, though they have been introduced with slightly different procedures. However, the introduced methods are difficult to understand regarding their time-varying behavior as well as the limitation, and it prevents the selection of model from being properly adapted in the stability analysis of power converters.

The effect of time-varying components have already been discussed in several studies so that the frequency-coupling of the converter transform the estimated resonances, unexpected harmonics and instabilities [4], [6], [11], [124]. Furthermore, the oscillations at a low frequency have been investigated in the Static VAr Compensators (SVC) and High-Voltage Direct Current (HVDC) [11], [124]. The harmonics at low frequency have increased due to the low admittance of the ac system, and they are then coupled with the admittance in dc side through the switching. At the end, they make the converters unstable at unexpected frequencies. Hence, the time-varying component should be linearized in the modeling, and models being able to include them are urgently required in order to estimate the unstable behavior precisely.

This chapter compares the differences between LTI and LTP models to use them properly for the stability analysis of power converter. Firstly, the source of the time-varying component is discussed to understand their effect. The structures of LTI and LTP models are then introduced by comparing the principal modeling methods in the field of power electronics. Additionally, the reasons, why the time-varying components are necessary to get an accurate model, are explained including the difficulties to include them in the model. Secondly, a comparison of two models is verified by using simulations in the frequency domain as well as in the time domain using the canonical LTP model. The single-phase grid connected converter is used as an example to show the different stability point according to the time-varying behavior. Furthermore, the limitation and the advantages of them are presented at the end to use them appropriately for the stability analysis.

(a) (b)
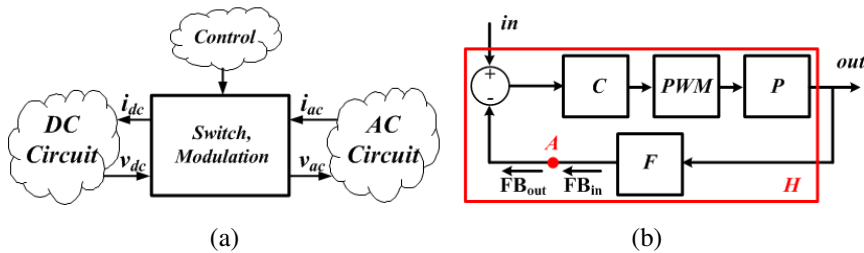
Figure 5-1. "Frequency coupling and coupled feedback systems, (a) General structure of power converter, (b) Generalized block diagram of power converter, where "C" is controller, "PWM" is modulation and time delay, "P" is plant (filter) and "F" is feedback gain."[125]

5.1. STRUCTURE AND STABILITY ANALYSIS OF LTI AND LTP MODEL

A. Basic structure of LTI and LTP model

A structure of LTI and LTP model can be defined by (2-19) and (2-20). Fundamentally, the HTF at zero frequency ($H_0(s)$) has the same structure as SSAV and shows Single Input and Single Output (SISO) characteristic [12]. It can be the result when the procedure of traditional modeling does not consider the varying ac information as well as the impedance at dc circuit. However, the DQ [126], [127] models are considering the shifted frequency response ($H_0(s + j\omega)$) since the overall stability of the ac circuit is ruled by the fundamental frequency according to their basic assumptions. Furthermore, the influence of admittance at negative frequency may not affect too much if the three phase system is operating under the balanced conditions. It is worth to note that the d-axis transfer function of the DQ model has the same structure as the real part of $H_0(s + j\omega)$ (= $\text{Re}[H_0(s + j\omega)]$) and the imaginary part of $H_0(s + j\omega)$(=$\text{Im}[H_0(s + j\omega)]$) has the same formulation as with the q-axis transfer function. Recently, [128] discussed the effectiveness of the negative frequency in the DQ model through the complex transfer function. Two complex transfer functions are thus considered in this analysis of unsymmetrical system by shifting the transfer function at zero frequency into the range of positive

frequencies ($\text{Re}[H_0(s+j\omega)]$, $\text{Im}[H_0(s+j\omega)]$) and a range of negative frequencies ($\text{Re}[H_0(s-j\omega)]$, $\text{Im}[H_0(s-j\omega)]$). Based on the introduced structure of the LTP model, it can be found that the DQ is a part of the LTP model. Furthermore, the coupling in the DQ model means that the real and the imaginary part of the impedance at the fundamental frequency are coupled with each other. Hence, the DQ model has the identical characteristics like the frequency shifting of the SSAV model.

However, the GAV (=Dynamic Phasor) [21] has the same structure with $H_1(s)$ as well as $H_{-1}(s)$ in the LTP model by including the influence of the negative frequency. Additionally, the GAV linearizes the nonlinear part in the modeling procedure by using a Describing Function (DF), while the DQ model is using the small signal perturbation for the linearization. Even though the GAV tries to include more parts of time-varying components in its procedure, the part of the LTP model ($H_{-1}(s) \ldots H_1(s)$) are only taken into account to reduce the order of model results based on the assumption that the fundamental frequency may affect the overall behavior of the systems.

The HL model [26], which is recently introduced to analyze unbalance systems, is also a part of the LTP model in (2-20). Similary to the GAV model, it tries to extract only two transfer functions by using the DF and the assumption used in the "Harmonic Balanced (HB)" method. It can be found that both the GAV and the HL are trying to include the effect of frequency coupling in the nonlinear model for their final formulation. However, the characteristics of DF and HB make the final results of the two methods to a single transfer funcion by eliminating the influence of higher harmonics. Though the results could be enough to analyze a single system, it may bring inaccurate results [44] when the number of systems is increasing since the effect of frequency coupling at high frequency can be more important.

On the other hand, the HD model [35], [48], which is also called the Harmonic State Space (HSS) modeling, is recently studied to include the whole time-varying components and it has a full structured LTP model given in (2-20). It is fundamentally linearizing the time-varying components by using Fourier Series. Furthermore, the accuracy of the HD model is determined by the number of harmonic components in the modeling procedure. The basic structure of the HD model (HSS) itself has been used as a canonical model of the LTP system [40]. Various applications have been developed in the field of mechanical engineering by using the HSS model. However, similar strudies have simultaneously been performed in the field of power system with the name MAV [129] or "Multivariable dq-reference frame (MDQ)" [126] in order to consider more time-varying components than other introduced methods. The differences between them are whether they manage the real and imaginary part of the multi-frequency response with the average value or not.

The modeling methods used in the power systems can be divided into the LTI and LTP model. It is noted that the LTI model is a special case of the LTP model, when

the time-varying components are just assumed to be a constant value. The DQ, the GAV, and the HL are also a small part of the LTP model at the fundamental frequency or a kind of reduced order model of LTP structure. However, the MAV, the MDQ and the HSS model can be classified into the full framework of the LTP model as given in (2-20). A full model in (2-20) is the most important to include for all time-varying behaviors of the system. However, it can also make the analysis of the system difficult due to the impedance coupling as shown in (2-20). Hence, a proper selection of the modeling approach is carefully required. However, at least for the ac system, the DQ model should be used in the analysis to take into account the positive frequency part of the fundamental component, while a simplified SSAV can not properly investigate the time-varying behavior of the analysis. Furthermore, the HD (HSS) model has more possibility to take a look the details of each frequency component depending on the applications.

B. Stability analysis of LTI and LTP model

The linearization should be done in advance by different approaches in order to get the LTI or the LTP frequency response, when the small-signal stability of the feedback system in Figure 5-1-(b) is required for the analysis.
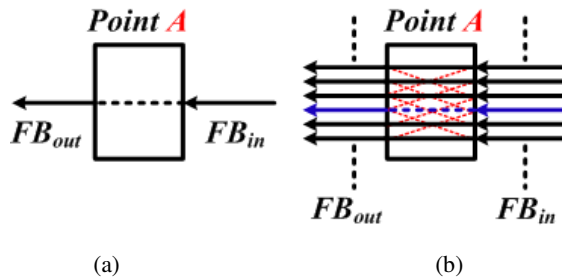
Figure 5-2. "Perturbation point of modeling method in LTI and LTP model of Figure 5-1-(b), (a) LTI view of "point A", (b) LTP view of "point A"" [125]

A single perturbation having a small magnitude has been injected into the traditional method in order to achieve a single transfer function. It is noted that the frequency response obtained by the single perturbation has a single magnitude and phase angle referring to the perturbed frequency. Hence, the single frequency response can only be used for the stability analysis at the single operating point, which is normally the dc operating point. As a result, if the contour of the LTI Nyquist plot does not encircle (-1,0), the LTI system has a stable operation. For instance, the SSAV model can be analyzed by using a SISO-LTI Nyquist plot according to the introduced procedure for the linearization and perturbation. The structure of the LTI feedback loop is shown in Figure 5-2-(a) that it is needed to inject the perturbation by cutting off the feedback loop (A) in Figure 5-1-(b) in order to be able to analyze the open-loop transfer function by using the Nyquist plot. The single-frequency can firstly be perturbed to the input (FB_{in}) in the case of LTI perturbation in Figure 5-2-(a) by

obtaining a responding single frequency (FB_{out}). A single Nyquist-plot can be depicted as the result of such analysis.

On the other hand, the reduced order LTP systems (the DQ, the GAV, the HL) can be analyzed through the generalized Nyquist criterion for MIMO (Multi Input Multi Output) systems [130], where the contours of the multiple eigenvalues may not encircle the point "(-1,0)" if the system is stable. Hence, the way to perturb the systems should also be performed by another method due to the coupling behavior, when the system is considered as the LTP model. The "point A" in Figure 5-1-(b) can be regarded as shown in Figure 5-2-(b) for the perturbation of LTP system since it is the multiple coupling with a number of inputs and outputs. The multiple inputs and outputs can be regarded as multiple decomposed signals at frequencies from a single signal in the time domain, where the number of them depends on the truncated size of (2-20). The "blue-line" in Figure 5-2-(b) can then be disconnected to inject multiple perturbations. The output vector (FB_{out}) of Figure 5-2-(b) will bring the multiple output even if the user injects a single perturbation ("blue line") to input vector (FB_{in}) as shown in Figure 5-2-(b) due to the coupling behavior of the LTP model. The introduced coupling can then result in different stability points.

In the case of a full-order LTP model, the LTP Nyquist plot can be obtained by considering the system as a "sampled system" instead of drawing the contour of multiple eigenvalues. The frequency range (ω) of each contour should vary from $\omega = -\omega_p/2$ to $\omega = +\omega_p/2$ according to [45] to draw the LTP Nyquist plot having a CCW (Counter Clock Wise) encirclement. For the convenience of stability analysis and their interpretation, the inverse LTP Nyquist diagram can also be drawn. If the feedback gain of Figure 5-1-(b) is assumed as "k", the encirclement of "–k" point will be considered in the judgement of stable operation instead of using the "-1/k" as the normal Nyquist plot [45].

5.2. SIMULATION COMPARISON OF LTP MODEL

A comparison of the different stability points between the LTI and LTP model is simulated using the same conditions by using the MATLAB. Firstly, the canonical LTP model "*Lossy Mathieu equation*" [40], which has been widely studied in mechanical engineering, is selected as the basic example of the simulation in order to distinguish the differences between the LTI and LTP model. Secondly, a single-phase grid-connected converter is modeled by using the HSS model, and it is analyzed based on the introduced LTP theory as well as the LTP Nyquist plot.

A. LTP stability in "Lossy Mathieu equation."

The canonical model of the LTP system in (5-1) is used to compare the simple behavior of LTP and LTI model, where the canonical model is a second order differential equation having the periodic time-varying behavior through "a, b, ω_p". It is noted that (5-1) can be regarded as the LTI model if "b" is "0". Furthermore, the

formulation of the canonical model is the modulated converter system since the time-varying behavior $(a + 2b\cos(\omega_p t))$ in (5-1) can be regarded as the modulation in Figure 5-1-(b). Furthermore, the overall behavior of (5-1) may be similar with the grid connected single-phase system if the input of (5-1) is assumed as a cosine function, which is rotating at the same frequency as with "ω_p".

$$\ddot{x}(t) + 2\zeta\dot{x}(t) + \big(a + 2b\cos(\omega_p t)\big)x(t) = I\cos(\omega t) \qquad (5\text{-}1)$$

(5-1) can be transformed into the HSS model as shown in Figure 5-3 by using MATLAB, and the open-loop Nyquist plot can be obtained by cutting off at the point "A". The plant part "G_p" of (5-1) is $1/(s(s + 2\zeta))$, where "ζ" is defined as "0.2" in the simulation. Additionally, the input magnitude is assumed to be "1", and the period of ω_p is defined as "2", where the frequency is "$1/\pi$". However, the "b" and "K" are varied based on several conditions to emulate the influence of the time-varying elements in (5-1). As a result, the LTP Nyquist plot and the LTI Nyquist plot are compared in order to show their difference when considering the time-varying component for the overall stability.
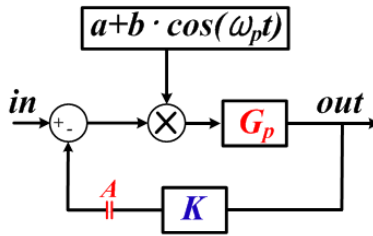
Figure 5-3. "Canonical LTP model from Figure 5-1-(b), where the effect of the PWM is regarded as cosinus function"[125].

The LTI Nyquist plot and LTP Nyquist plot from (5-1) are compared in Figure 5-4. The results show that the LTI and LTP models draw the same contour in Figure 5-4-(a) and (b) when "b" is equal to "0", even if the block diagram of Figure 5-3 has the same internal structure as the LTP model given in (2-19). Thus, the results from the time-domain simulation using LTI and LTP model show the same dynamics as shown in Figure 5-4-(c). It is noted that both models are stable since the feedback gain "-K" point is encircled by the contour according to the introduced definition of the inverse Nyquist plot. However, the different features start to appear as the modulation factor "b" is varying. It is remarkable that the LTP Nyquist plot starts to have a symmetric ripple because of the time-varying behavior as shown in Figure 5-4-(d). It is worth to note that the time-varying component in the modulated system shows a different contour with the LTI Nyquist plot. It draws the same contour as shown in Figure 5-4-(a) even "b" is varied though. Additionally, the stable region of the LTP Nyquist plot is becoming to be separated, and the stable region also becomes to be reduced than the Figure 5-4-(b) as "b" is increasing. Furthermore, the different results are shown in Figure 5-4-(e), where the time-varying behavior generates a dc-offset in the time domain simulation of the LTP model. However, the

time response of both models can still show convergence since "-K" of both models are in the stable area. It shows that the stability by using the LTI model can be approximated, even if the system parameters are varying. However, the errors of the estimation may increase more as the parameters are varying. The feedback gain "K" is increased to "1.2" to verify the stable region in Figure 5-4-(d) as well as their time-domain simulation. The magnified part of Figure 5-4-(d) is shown in Figure 5-4-(f), where the LTI model is stable because "-K (=-1.2)" is still inside of the stable region. However, the time-domain simulations of the LTP model start to diverge exponentially as shown in Figure 5-4-(g), where "-K (= -1.2)" is not encircled by contour as shown in Figure 5-4-(f).
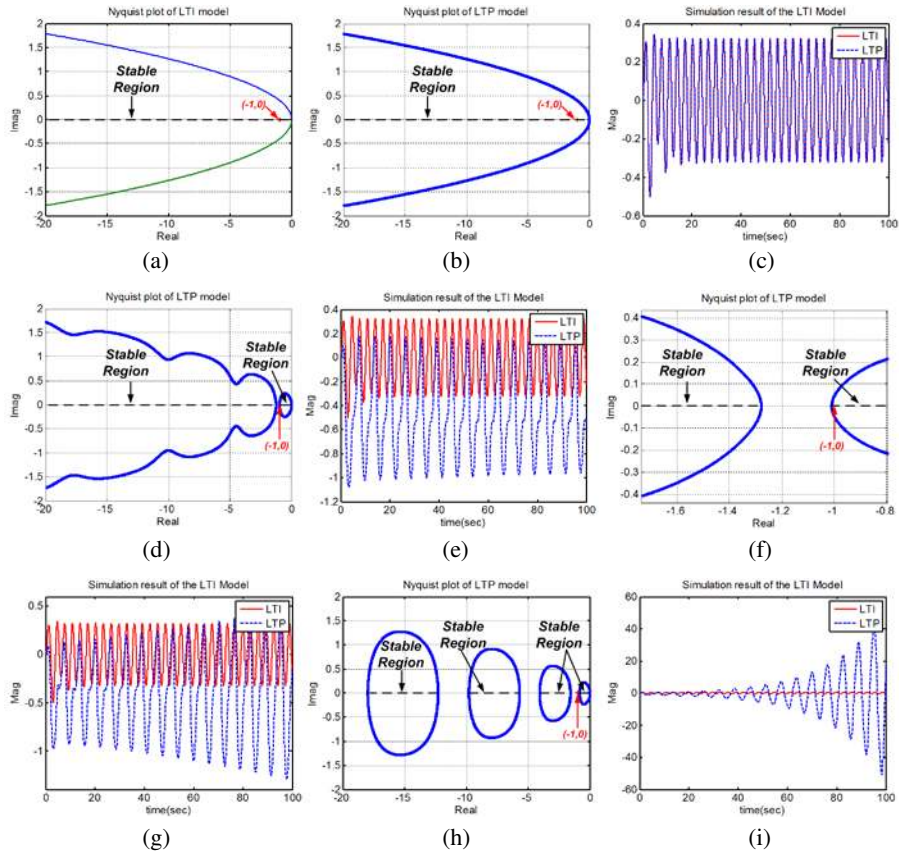
Figure 5-4. "*Comparison of stability analysis in LTI and LTP model (a) Nyquist plot (@ Point A of Figure 5-3) of LTI model, (b) Nyquist plot (@ Point A) of LTP model, when a=1 ; b=0 , (c) Time-domain simulation of LTI and LTP model, when a=1; b=0, (d) Nyquist plot (@ Point A) of LTP model, when a=1 ; b=0.4 ; K=1 , (e) Time-domain simulation of LTI and LTP model, when a=1 ; b=0.4 ; K=1, (f) Magnified Nyquist plot (@ Point A) of LTP model, when a=1 ; b=0.4 ; K=1 , (e) Time-domain simulation of LTI and LTP model, when a=1 ; b=0.4 ; K=1.2, (d) Nyquist plot (@ Point A) of LTP model, when a=1 ; b=0.5 ; K=1 , (e) Time-domain simulation of LTI and LTP model, when a=1 ; b=0.5 ; K=1"[125]*

The LTP Nyquist plot starts to make several circles as shown in Figure 5-4-(h) as "b" is increasing, and the stable region is more separated as a result. The "-K" is thus not encircled any more as shown in Figure 5-4-(h). Hence, the results in Figure 5-4-(i) show unstable operation as well. However, it is noted that the LTI Nyquist plot and their time-domain simulations still estimate the same behavior even if the modulation factor is changed. Besides, the results of LTP model in Figure 5-4-(d) ~ (i) show different behavior according to the varying signal, and they can not be seen in the LTI model.

B. LTP stability in a "Single-phase grid-connected converter"

The single-phase grid-connected converter is selected as an example to study the influence of time varying components to the stability region based on the knowledge from the stability analysis of the LTP canonical model. A block diagram of a single-phase grid-connected converter with a simple ac-filter (L_f, R_f) is shown in Figure 5-5. Additionally, a simple L-C circuit (L_g, R_g, C_f) is considered to emulate the grid impedance. A sensed dc-voltage ($v_{dc-sense}$) of the capacitance (C_{dc}) and dc-load (R_{dc}) through a low-pass filter (H_{LPF}) is controlled by using a PI controller to operate the converter in rectifier mode. The current reference (i_f^*) from the PI controller ($|i_f^*|$) and PLL ($\cos_{PLL}(\cdot)$) is then controlled by the PR-controller. The output of the current controller (PR) is then compared with a carrier waveform to generate the PWM. The behavior of the PLL is simplified in the LTP model as a cosine function, which is synchronized with the grid voltage (v_g). Furthermore, the harmonic compensator, i.e. Proportional Resonant (PR) controller, is not implemented in the ac circuit as well as in the dc-circuit to analyze the influence of harmonics. Hence, basically, the ac current includes the odd order harmonics and the dc voltages contains the even order harmonic in the waveform.
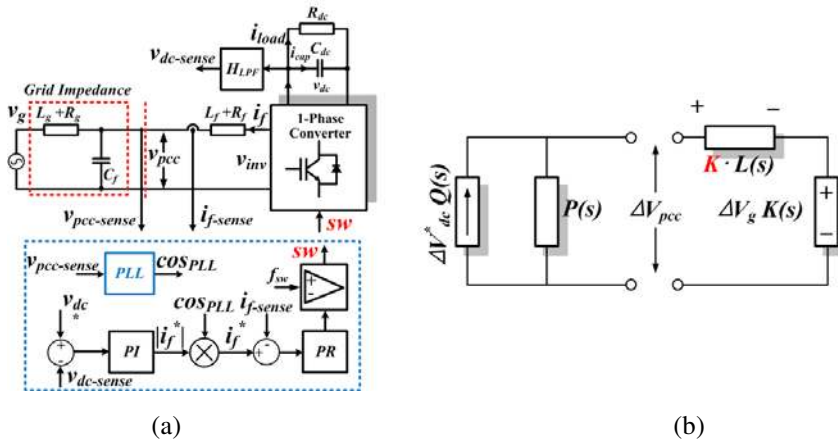

(a)   (b)

Figure 5-5. "Single-phase grid-connected converter with grid impedance (a) Block diagram of topology and control system, (b) Impedance representation of single-phase grid-connected converter"[125]

The HSS model of a single phase grid connected converter in Figure 5-5-(a) is achieved by using the LTP theory [41]. The switching operations can be regarded as the main time-varying components in the HSS model. However, other components in the converter have also possibilities to be considered as the time-varying components depending on the applications. Furthermore, the final structure has a formulation of a Multiple Input Multiple Output (MIMO) - LTI systems since all signals are composed by harmonic vectors, which refer to the matrix formulation of the HSS model. As a result, the interaction between the converter admittance (P(s)) and the grid admittance (L(s)) can be represented as shown in Figure 5-6-(b) based on the circuit diagram in Figure 5-5-(a) in order to analyze the overall LTP stability of the single phase grid connected converter. All transfer functions in Figure 5-5-(b) are constructed by a matrix, where Q(s) means the MIMO matrix (dc-voltage reference (Δv_{dc}^*) / ac-current (Δi_f)) and K(s) is also the MIMO matrix (PCC-voltage (Δv_{pcc}) / the grid-voltage (Δv_g)), where harmonics from the -10th to 10th order are considered in the LTP Nyquist plot

Based on the introduced theory, the LTP Nyquist plot of the loop gain (P(s)/L(s)) is considered to analyze the LTP stability. Furthermore, the modulation signal is mainly varied to mimic the time-varying behavior of the converter as it is verified in the canonical model of the LTP system in Figure 5-3 and Figure 5-4. Two cases (1 kW and 0.1 kW) are analyzed to consider the behavior of varying modulation. The results of the time domain simulations are shown in Figure 5-7-(a), where the power reference is changed at 0.4 sec from 1 kW and 0.1 kW. It can be seen in Figure 5-7-(a) that the harmonics of both cases are changed since the change of the power reference varies the modulation behavior of the converter. However, the converter is still under stable operation as shown in Figure 5-6-(a) and (b). It is noted that the different colors in the Nyquist plot of Figure 5-6-(a) and (b) mean the contours drawn by the different HTF based on the LTP theory, where both contours are drawn at different operating points. Additionally, the unstable regions (black line) are moved as the power reference is changed. Also, the different sizes of contours are shown in Figure 5-6-(b), which shows the influence of the time-varying element. This time-varying behavior in the converter has the same meaning by varying the "b" value in Figure 5-3 and Figure 5-4.

The unstable operation can be found by increasing the feedback gain "K" to be "30". Two LTP Nyquist plots, which are having different conditions, are compared as shown in Figure 5-6-(c) and (d), where the contour in Figure 5-6-(c) can be obtained when "K" is "1". The time-domain simulations in the same condition in Figure 5-7-(b) from 0 sec to 0.4 sec show stable operation since the "-K (=-1)" point is still in the stable region. However, the converter is becoming unstable as "K" is increasing to "30" because "-K" in the LTP Nyquist plot of Figure 5-6-(d) is in the unstable region and it results in instability in the time domain as shown in Figure 5-7-(b). Note that the contours are governed by each HTF, and they change the stable region according to the time-varying component (=modulation) of the systems.

Inverse Nyquist plot of LTP model

(-1, 0)

Unstable Region

(a)

Inverse Nyquist plot of LTP model

(-1, 0)

Unstable Region

(b)

(c)

(d)
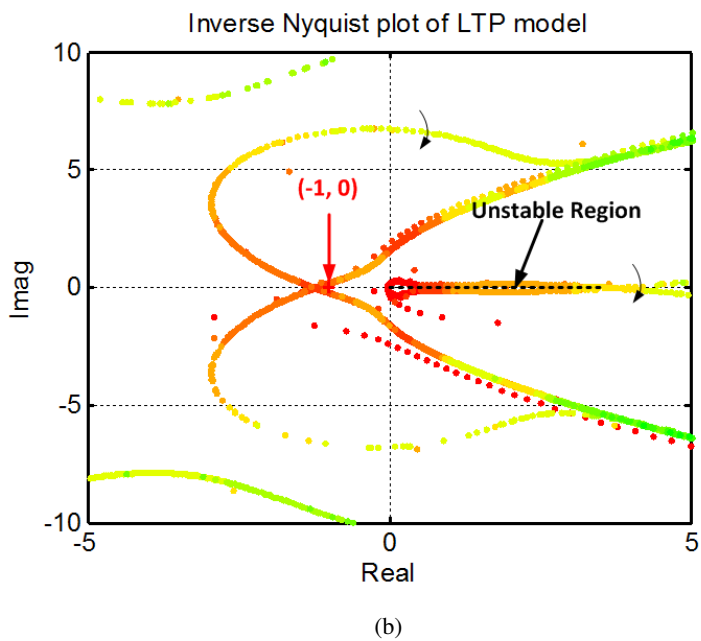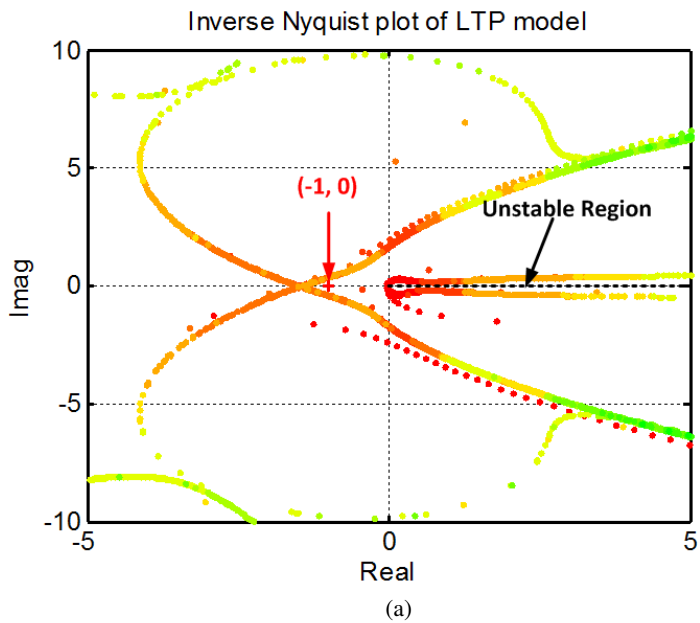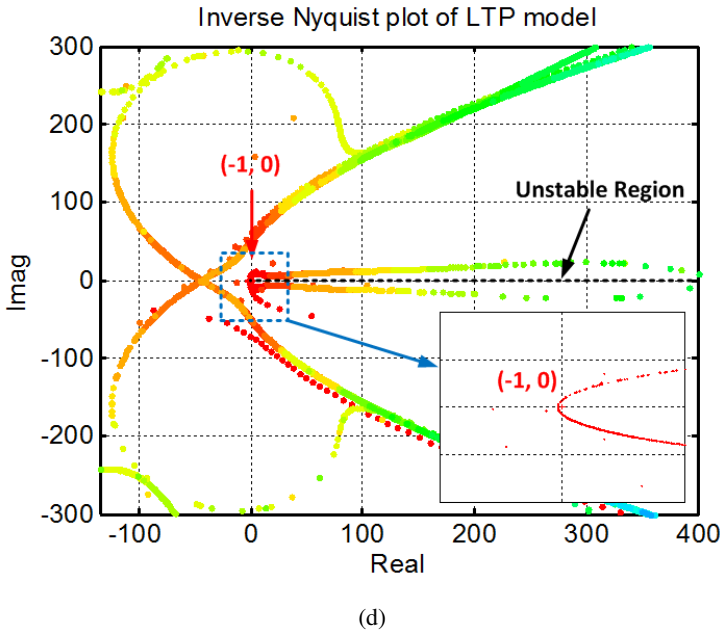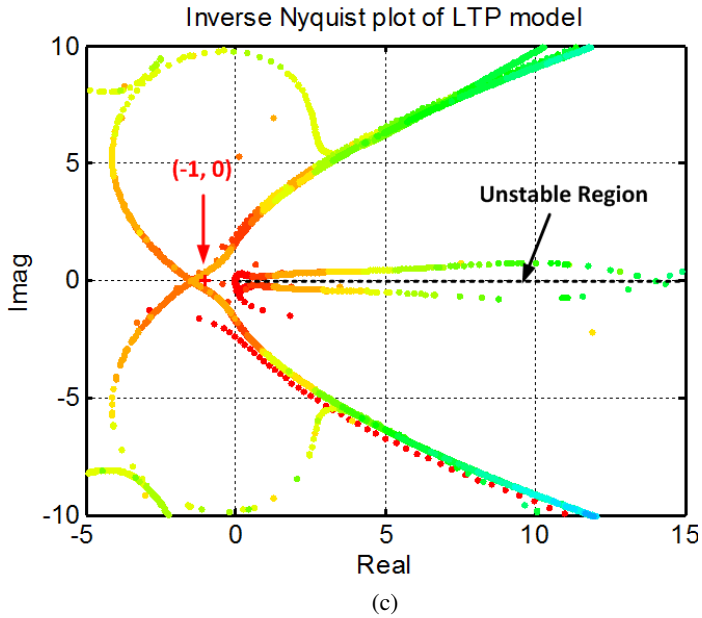
Figure 5-6. "Nyquist plot of Loop gain ($P(s)/L(s)$) of single phase grid connected converter (a) LTP Nyquist plot of Loop gain (1 kW), (b) LTP Nyquist plot of Loop gain (0.1 kW), (c) LTP Nyquist plot of Loop gain (1 kW, K=1) , (d) LTP Nyquist plot of Loop gain (1 kW, K=30)"[125]
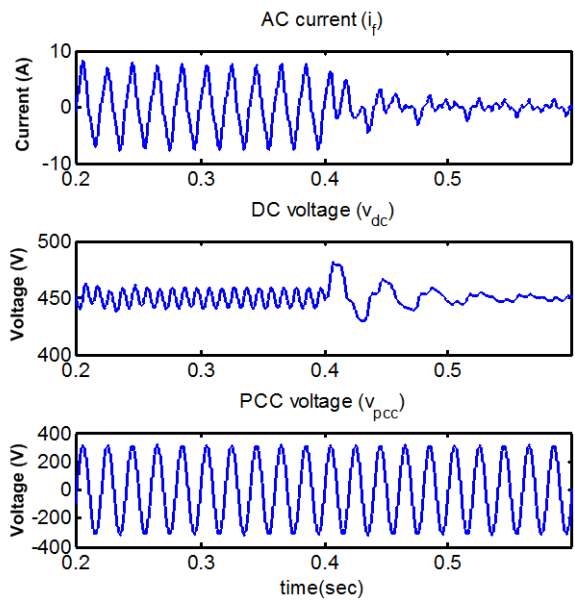
(a)
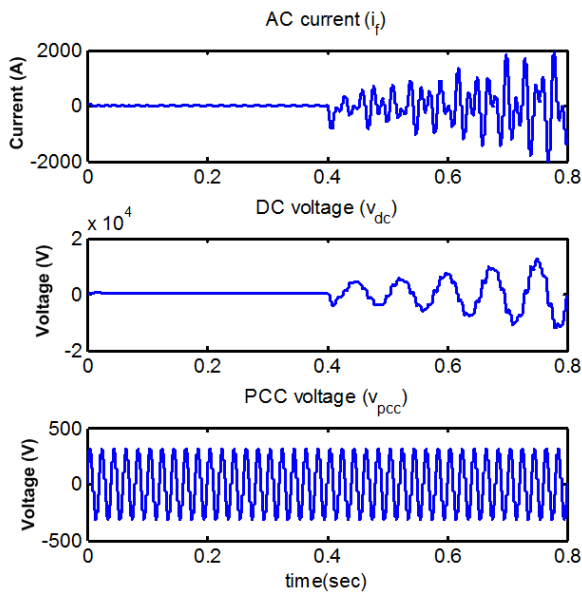
(b)

Figure 5-7. "Time domain simulation results of Figure 5-5 (a) Power variation from 1 kW to 0.1 kW at 0.4 sec, (b) Grid impedance variation at 0.4 sec" [125]

C. Discussion regarding the importance of harmonics

It is verified through a simple example as well as in the applications of power electronic systems that the time-varying components may significantly affect the stability analysis as the stability regions are disturbed according to the magnitude and phase of the time-varying components. Additionally, it is worth to note that the numbers of HTF decides the accuracy of model properties since the LTP system can be regarded as sampled systems. Furthermore, Figure 5-6 may have a similar meaning with the DQ model, or the GAV model. The reduced LTP model (DQ, GAV, HL) may include the effect of time-varying components by averaging it as a constant value. However, the reduced LTP model may generate an error in terms of stability analysis since they are including just a part of the full LTP model. It is recommended that considering at least the 10th order to the LTP model in order to achieve more accurate results in the stability analysis since the eigenvalues of other HTF can affect the dominant HTF. The two simple examples are studied in this chapter, where the consideration of more harmonics may increase the resolution of the stability analysis, if the systems have multiple varying components or they operate with low pulse ratio. Furthermore, the inclusion of harmonics and the LTP stability can be more critical for the parameter dependent systems like "diode" or "thyristor" applications.

5.3. SUMMARY AND CONCLUSION

This chapter compares the LTI and LTP model to distinguish their differences and usages for stability analysis. The analysis and the background of the theory are validated through a simple canonical model as well as a simple power converter. It is verified that the well-known conventional methods are the part of the LTP model. Even though they could be enough to analyze the stability of the power converters, an accurate analysis will be more difficult as the number of test objects is increasing. Furthermore, the influence of time-varying components may be more severe as the user considers more time-varying components in the analysis. The analysis results through the LTP and LTI Nyquist plot shows that the LTP model is more useful for the power converters having the time-varying components since they can not be taken into account in the analysis of the LTI model.

CHAPTER 6. CONCLUSION AND FUTURE WORK

The purpose of this chapter is to summarize the results, which have been achieved throughout the PhD project and to emphasize the achieved main contributions presented. Finally, topics for the future work are also discussed.

6.1. SUMMARY AND CONCLUSION OF THESIS

This project has performed research on the HSS modeling and its analysis method to investigate the harmonic interaction and the Linear Time varying Periodically (LTP) stability of power electronic based systems.

Power electronic based systems are being employed in many fields, and the analysis of complex dynamics and harmonic coupling is essential in order to maintain both stable operation and good power quality. Problems related to the frequency coupling are an issue since instability can arise and unexpected frequencies can appear in complex networks. An accurate model, which can cover all the components in one single domain and provide some insights into the system interactions, is required because the time-varying behaviors and trajectories can not be considered in the traditional way. Hence, the main time-varying components have been reviewed with well-known modeling methods in power electronics in order to investigate their effects on the model accuracy.

New model results of single-phase, three-phase, back-to-back grid-connected converter and multi parallel converters are developed by using the HSS modeling method. The obtained frequency responses show the steady-state harmonic coupling in the harmonic matrix as well as the dynamic coupling between the ac and dc circuit. It shows that the stable or unstable behavior of grid-connected converter is correlated with the frequency coupling. These characteristics can normally not be considered in the conventional modeling method, which is based on LTI (Linear Time Invariant) model. However, the HSS model derived from LTP (Linear Time varying Periodically) theory can consider these MIMO (Multi Input Multi Output) characteristics in the same domain. First, the full HSS modeling procedure is provided to show the difference with the conventional modeling methods. Second, the results from the developed model are compared with the nonlinear time-domain simulation results in order to show the validity of the HSS model. As a result, it shows well-matched results with a commercial simulation tool and also with the experimental results. Third, the HSS model is used as a tool to analyze the steady-state harmonic interaction as well as the dynamic harmonic interaction. The result shows how harmonics are transferred in the model and which impedances are effective to generate the harmonics.

Additionally, the dc power electronic systems are also studied by using an HSS modeling approach. Each component as well as the dc-dc converters are modularized to connect them with other models. The selected converters are analyzed and validated by means of the proposed method. To verify the validity of the HSS model, the HSS simulation results are compared with the nonlinear time-domain simulations. Also, the frequency coupling between the source of the power converters and the output of power converters is also analyzed. The overall results derived from the HSS model show the same performance, which means the transfer function derived from HSS model has more accurate characteristics than the conventional modeling method. Besides, the whole dc-dc converters are simulated by using the HSS method for the large scale network. The result shows that the HSS can provide faster simulation time with the same result as with nonlinear simulation.

Furthermore, the widely used 3-phase diode rectifier has been modeled and validated by using an analytical model, simulation and experiments. First, the HD (Harmonic Domain) based modeling method (=HSS modeling method) is adapted to make a model of 3-phase diode rectifier by considering SIV (Switching Instant Variation) and the interaction of ac and dc impedance. Furthermore, the HD impedance profile, which is derived from an analytical model, is used to extract the impedance at positive and negative frequency. Besides, a Tensor is used to represent multiple complex numbers in a single domain by means of HD impedance profile. The results from the analytical model show that the impedances at harmonic frequency have a phase dependence characteristic. Additionally, these are also verified by time-domain simulations and experiments, where the results are important to analyze impedance interactions or to design a passive filter as well as harmonic compensators.

Last, the nature of the LTI and LTP model has been presented for the stability analysis of power converters. The main criteria and difficulties in the modeling procedure are introduced by including that the original behavior of a power converter is a nonlinear time-periodic system and also illustrated how the difficulties can be covered through the LTI and LTP theory. The classification of the conventional model is also performed in order to know whether the time-varying components of power electronic systems are taken into account in their modeling procedure or partially considered in the procedure. A simple model from mechanical system is adapted explicitly to explain the differences between the LTI and LTP model in the frequency domain and time domain. The results show that the stability analysis based on the LTP theory is more acceptable for power converters, as the time-varying behavior can not be considered in the LTI model. Furthermore, the results show that LTI model is a part of the LTP model, when the time-varying components are regarded as averaged values or some constant values. Even though the LTI model could be enough to analyze the systems based on some assumptions, the LTP model should be considered in order to find out the hidden regions for the stability analysis. This characteristic is important as the number of considered systems is increasing.

As a conclusion, the power electronic based systems are urgently required to achieve the needs for the renewable energy source. Hence, the advanced modeling methods are mandatory in order to analyze and design the systems properly since the frequency coupling and harmonics bring in unknown phenomena due to the time-varying behavior and it disturbs the overall stability of the power electronic based power systems. It is thus found in this project that the proposed HSS model can only include the detail time-varying behavior of each system, and it shows also the different aspects to find the hidden properties of the systems. The final achieved results in this study will provide new perspectives into the future power systems in order to achieve "Advanced Harmony".

6.2. CONTRIBUTIONS

The main contributions of this project from the author`s point of view are highligted in the following;

1. Review and comparison of LTI and LTP model

- The well-known modeling methods in the field of power electronics are classified into two categories based on the mathematical proof and their background theory. The generalized averaging, state-space averaging, dq-domain model, harmonic linearization, and harmonic domain based methods are mainly compared with simulations. A comparison and review of these methods can be used to understand the difference among them as well as their limitations in order to be used for the analysis of power electronic based power systems.

2. Development of LTP model for VSC applications

- Several VSC applications are developed by using the LTP theody and the HSS modeling method. The developed models are including the frequency coupling between ac and dc side. Furthermore, the switching instant variation is considered in the modeling procedure, where two aspects have not been considered in the conventional modeling methods or simply included based on several assumptions.

-The 3-phase VSC model can explain how the positive and negative sequence harmonics are coupled with zero sequence in the dc circuit. The single phase VSC model also shows how even order harmonics and odd order harmonics are dynamically transferred on both the ac and dc sides. The developed back-to-back VSC can be used to analyze the effect of varying input frequency in generator (rotor) side converter. The different frequency responses based on different rotor frequencies precisely show why the time-varying components should be considered for accurate analysis. Furthermore, the model of 6-parallel converters are used to analyze the harmonic interaction among them and to see the dynamic interaction between converters and cables.

3. Development of LTP model for dc power electronic based systems

- The LTP model for dc micro grid can be used for the analysis of frequency coupling between the ac and dc systems. The developed MIMO frequency responses are successfully analyzed and demonstrated how frequency in dc and ac systems are transferred to the other ac- or dc- side.

- A large dc micro-grid is simulated by using the developed LTP model. The MIMO frequency responses mimic the coupled frequency as well as the dynamics at the transient behavior. The simulation time is drastically reduced compared to the time-domain simulation and this advantage can be used for the simulation of a large dc systems without neglecting some information due to the simplifications.

4. Measurement and analysis of phase dependancy impedance

- The grid dependent swtiching in a 3-phase diode rectifier is modeled by using the introduced LTP theory. The developed MIMO frequency responses explain how harmonics in the ac grid affects to the dc side throughout the switching.

- The phase dependent impedance is measured by using the grid simulator in the laboratory and it is compared to the analytical model. The extracted phase dependent impedance from the analytical model can be used to explain why harmonics are changed by the phase variation of the input and also to analyze the varying impedance according to the phase variation of the input. Furthermore, the analyzed results show why the LTP model is more accurate that the averaged diode model.

5. Analysis of LTP stability

- Based on the developed models, the analysis for LTP stability is adapted to investigate the hidden stability criterion. The method can exactly show the effect of the time-varying components and how it can influence to the stability criterion of LTP stability. The basic theory is verified in the single phase grid connected VSC, where the results show that the stability region is changed by the varying modulation. The approach can be extended to analysis of other power electronic based systems in order to find out the effect of the time-varying components on the stabilty.

6.3. FUTURE WORK

Some other interesting and relevant topics are identified during the process of the research work. The important research topics that could be considered for further investigations are listed as follows;

1. Measurement of Harmonic Transfer Function (HTF) for verification

The developed frequency responses for the analysis of harmonic interaction in this thesis are mainly veified by using the time-domain simulation. The spectrum analyzer can be used to obtain the MIMO frequency response from the experimental set-up. The results can be compared with the frequency responses from the analytical HSS model for the validation of the frequency coupling.

2. Consideration of other time-varying components in the modeling

The modulation and their behavior are mainly investigated as the time-varying components of power electronic based systems. Additionally, the varying frequency at the rotor side of wind power converter is also considered in order to achieve different frequency responses using the conventional model. However, the varying ac grid voltage and other periodic elements can be studied in order to map different frequency responses.

3. Measurement of LTP Nyquist plot for verification

The LTP Nyquist plot can show different stability criteria, which can not be considered in the LTI model. The measurement of the LTI Nyquist plot was well known in several publications, where it can be measured throughout the simple perturbation. However, the LTP Nyquist plot is coupled with each other and new rules for perturbations are required in order to measure it from the experimental setup. The derived results can consider the hidden region of LTI stability criteria.

4. Considering nonlinear characteristics in inductor, transformer and cable

The introduced LTP model can include the nonlinear characteristic of inductor, transformer and cable when they have the periodic characteristics like a hysterisis curve. The characteristics can be linearized by using the Fourier series or double Fourier series. The considered nonlinear characteristics could affect the frequency coupling and also the stability analysis of the system.

5. More benchmarking between the different modeling methods

Each modeling method used in the power converters has their own assumptions and limitations. They should be selected depending on the purpose of modeling as introudeced in this thesis. Hence, more benchmarking between them through the experimental validation would be interesting topic for a future research.

REFERENCES

[1]   "Harmony - Research Project leader by Aalborg University - Aalborg University." [Online]. Available: http://www.harmony.et.aau.dk/. [Accessed: 30-Mar-2016].

[2]   Christian Flytkjaer Jensen, "Harmonic Assessment in a Modern Transmission Network," presented at the HARMONY Symposium 2015, Aug-2015.

[3]   Chen Liang, "Simulation Analysis on Harmonics Pollution of Large-Scale Wind System Accessed to Grid," in *Advanced Materials Research*, 2014, vol. Vol. 997, pp. 795–599.

[4]   E. Mollerstedt and B. Bernhardsson, "Out of control because of harmonics-an analysis of the harmonic response of an inverter locomotive," *IEEE Control Syst.*, vol. 20, no. 4, pp. 70–81, Aug. 2000.

[5]   "Wiley: Power System Harmonics, 2nd Edition - Jos Arrillaga, Neville R. Watson." [Online]. Available: http://eu.wiley.com/WileyCDA/WileyTitle/productCd-0470851295.html. [Accessed: 30-Mar-2016].

[6]   S. Lissandron, L. D. Santa, P. Mattavelli, and B. Wen, "Experimental Validation for Impedance-Based Small-Signal Stability Analysis of Single-Phase Interconnected Power Systems With Grid-Feeding Inverters," *IEEE J. Emerg. Sel. Top. Power Electron.*, vol. 4, no. 1, pp. 103–115, Mar. 2016.

[7]   B. Wen, D. Boroyevich, R. Burgos, P. Mattavelli, and Z. Shen, "Small-Signal Stability Analysis of Three-Phase AC Systems in the Presence of Constant Power Loads Based on Measured d-q Frame Impedances," *IEEE Trans. Power Electron.*, vol. 30, no. 10, pp. 5952–5963, Oct. 2015.

[8]   M. Bollen, J. Meyer, H. Amaris, A. M. Blanco, A. Gil de Castro, J. Desmet, M. Klatt, L. Kocewiak, S. Ronnberg, and K. Yang, "Future work on harmonics - some expert opinions Part I - wind and solar power," in *2014 IEEE 16th International Conference on Harmonics and Quality of Power (ICHQP)*, 2014, pp. 904–908.

[9]   J. Meyer, M. Bollen, H. Amaris, A. M. Blanco, A. Gil de Castro, J. Desmet, M. Klatt, Ł. Kocewiak, S. Rönnberg, and K. Yang, "Future work on harmonics - some expert opinions Part II - supraharmonics, standards and measurements," in *2014 IEEE 16th International Conference on Harmonics and Quality of Power (ICHQP)*, 2014, pp. 909–913.

[10]   H. Liu and J. Sun, "Modeling and analysis of DC-link harmonic instability in LCC HVDC systems," in *2013 IEEE 14th Workshop on Control and Modeling for Power Electronics (COMPEL)*, 2013, pp. 1–9.

[11]   A. E. Hammad, "Analysis of second harmonic instability for the Chateauguay HVDC/SVC scheme," *IEEE Trans. Power Deliv.*, vol. 7, no. 1, pp. 410–415, Jan. 1992.

[12]   R. D. Middlebrook, "Small-signal modeling of pulse-width modulated switched-mode power converters," *Proc. IEEE*, vol. 76, no. 4, pp. 343–354, Apr. 1988.

[13]   P. T. Krein, J. Bentsman, R. M. Bass, and B. C. Lesieutre, "On the use of averaging for the analysis of power electronic systems," *IEEE Trans. Power Electron.*, vol. 5, no. 2, pp. 182–190, Apr. 1990.

[14]   A. F. Witulski and R. W. Erickson, "Extension of state-space averaging to resonant switches and beyond," *IEEE Trans. Power Electron.*, vol. 5, no. 1, pp. 98–109, Jan. 1990.

[15]   X. Wang, F. Blaabjerg, and W. Wu, "Modeling and Analysis of Harmonic Stability in an AC Power-Electronics-Based Power System," *IEEE Trans. Power Electron.*, vol. 29, no. 12, pp. 6421–6432, Dec. 2014.

[16]   A. Griffo and J. Wang, "State-space average modelling of synchronous generator fed 18-pulse diode rectifier," in *13th European Conference on Power Electronics and Applications, 2009. EPE '09*, 2009, pp. 1–10.

[17]   D. J. Perreault and G. C. Verghese, "Time-varying effects and averaging issues in models for current-mode control," *IEEE Trans. Power Electron.*, vol. 12, no. 3, pp. 453–461, May 1997.

[18]   J. Shen, S. Schroder, H. Stagge, and R. W. De Doncker, "Impact of Modulation Schemes on the Power Capability of High-Power Converters with Low Pulse Ratios," *IEEE Trans. Power Electron.*, vol. 29, no. 11, pp. 5696–5705, Nov. 2014.

[19]   P. Mattavelli, A. M. Stankovic, and G. C. Verghese, "SSR analysis with dynamic phasor model of thyristor-controlled series capacitor," *IEEE Trans. Power Syst.*, vol. 14, no. 1, pp. 200–208, Feb. 1999.

[20]   J. R. C. Orillaza and A. R. Wood, "Linearized harmonic domain model for three-phase thyristor controlled reactor," in *Proc. of Australasian Universities Power Engineering Conference. AUPEC '08.*, pp. 1–5.

[21]   S. R. Sanders, J. M. Noworolski, X. Z. Liu, and G. C. Verghese, "Generalized averaging method for power conversion circuits," *IEEE Trans. Power Electron.*, vol. 6, no. 2, pp. 251–259, Apr. 1991.

[22]   F. Yahyaie and P. W. Lehn, "On Dynamic Evaluation of Harmonics Using Generalized Averaging Techniques," *IEEE Trans. Power Syst.*, vol. 30, no. 5, pp. 2216–2224, Sep. 2015.

[23]   A. Emadi, "Modeling and analysis of multiconverter DC power electronic systems using the generalized state-space averaging method," *IEEE Trans. Ind. Electron.*, vol. 51, no. 3, pp. 661–668, Jun. 2004.

[24]   X. Guo, Z. Lu, B. Wang, X. Sun, L. Wang, and J. M. Guerrero, "Dynamic Phasors-Based Modeling and Stability Analysis of Droop-Controlled Inverters for Microgrid Applications," *IEEE Trans. Smart Grid*, vol. 5, no. 6, pp. 2980–2987, Nov. 2014.

[25]   C. Liu, A. Bose, and P. Tian, "Modeling and Analysis of HVDC Converter by Three-Phase Dynamic Phasor," *IEEE Trans. Power Deliv.*, vol. 29, no. 1, pp. 3–12, Feb. 2014.

[26]   M. Cespedes and J. Sun, "Impedance Modeling and Analysis of Grid-Connected Voltage-Source Converters," *IEEE Trans. Power Electron.*, vol. 29, no. 3, pp. 1254–1261, Mar. 2014.

[27]   Z. Bing, K. J. Karimi, and J. Sun, "Input Impedance Modeling and Analysis of Line-Commutated Rectifiers," *IEEE Trans. Power Electron.*, vol. 24, no. 10, pp. 2338–2346, Oct. 2009.

[28]   J. J. Rico, M. Madrigal, and E. Acha, "Dynamic harmonic evolution using the extended harmonic domain," *IEEE Trans. Power Deliv.*, vol. 18, no. 2, pp. 587–594, Apr. 2003.

[29]   M. Madrigal and E. Acha, "Harmonic modelling of voltage source converters for HVDC stations," in *AC-DC Power Transmission. Seventh International Conference on (Conf. Publ. No. 485)*, 2001, pp. 125–131.

[30]   G. N. Love and A. R. Wood, "Harmonic State Space model of power electronics," in *Proc. of 13th International Conference on Harmonics and Quality of Power. ICHQP 2008*, pp. 1–6.

[31]   J. R. C. Orillaza and A. R. Wood, "Harmonic State-Space Model of a Controlled TCR," *IEEE Trans. Power Deliv.*, vol. 28, no. 1, pp. 197–205, Jan. 2013.

[32]   J. Sun, D. M. Mitchell, M. F. Greuel, P. T. Krein, and R. M. Bass, "Averaged modeling of PWM converters operating in discontinuous conduction mode," *IEEE Trans. Power Electron.*, vol. 16, no. 4, pp. 482–492, Jul. 2001.

[33]   W. Keyin, L. Dezhi, O. Yangbing, Z. Xiaofei, and Y. Ming, "State-space average-value model of 3-phase 4-wire diode-bridge rectifier," in *IEEE International Symposium on Industrial Electronics, 2009. ISIE 2009*, 2009, pp. 1634–1638.

[34]   E. Acha, A. Semlyen, and N. Rajakovic, "A harmonic domain computational package for nonlinear problems and its application to electric arcs," *IEEE Trans. Power Deliv.*, vol. 5, no. 3, pp. 1390–1397, Jul. 1990.

[35]   J. Arrillaga and N. R. Watson, "The Harmonic Domain revisited," in *Proc. of 13th International Conference on Harmonics and Quality of Power. ICHQP 2008*, pp. 1–9.

[36]   M. S. Hwang and A. R. Wood, "Harmonic State-Space modelling of an HVdc converter," in *2012 IEEE 15th International Conference on Harmonics and Quality of Power (ICHQP)*, 2012, pp. 573–580.

[37]   J. Mahdavi, A. Emaadi, M. D. Bellar, and M. Ehsani, "Analysis of power electronic converters using the generalized state-space averaging approach," *IEEE Trans. Circuits Syst. Fundam. Theory Appl.*, vol. 44, no. 8, pp. 767–770, Aug. 1997.

[38]   A. Yazdani and R. Iravani, "A generalized state-space averaged model of the three-level NPC converter for systematic DC-voltage-balancer and current-controller design," *IEEE Trans. Power Deliv.*, vol. 20, no. 2, pp. 1105–1114, Apr. 2005.

[39]   A. M. Stankovic, P. Mattavelli, V. Caliskan, and G. C. Verghese, "Modeling and analysis of FACTS devices with dynamic phasors," *IEEE Power Eng. Soc. Winter Meet.*, vol. 2, pp. 1440–1446, 2000.

[40]   N. M. Wereley and S. R. Hall, "Linear Time Periodic Systems: Transfer Function, Poles, Transmission Zeroes and Directional Properties," in *Proc. of American Control Conference*, pp. 1179–1184.

[41]   J. B. Kwon, X. Wang, F. Blaabjerg, C. L. Bak, A. R. Wood, and N. R. Watson, "Harmonic Instability Analysis of Single-Phase Grid-Connected Converter using Harmonic State Space (HSS) modeling method," *IEEE Trans. Ind. Appl.*, vol. PP, no. 99, pp. 1–1, 2016.

[42]   N. M. Wereley and S. R. Hall, "Frequency response of linear time periodic systems," in *Proc. of the 29th IEEE Conference on Decision and Control*, vol. 6, pp. 3650–3655.

[43]   S. R. Hall and N. M. Wereley, "Generalized Nyquist Stability Criterion for Linear Time Periodic Systems," in *Proc. of American Control Conference*, pp. 1518–1525.

[44]   E. Mollerstedt and B. Bernhardsson, "A harmonic transfer function model for a diode converter train," in *IEEE Power Engineering Society Winter Meeting, 2000*, 2000, vol. 2, pp. 957–962.

[45]   J. R. Orillaza, M. S. P. Hwang, and A. R. Wood, "Switching Instant Variation in Harmonic State-Space modelling of power electronic devices," in *Proc. of the 20th Australasian Universities Power Engineering Conference (AUPEC)*, pp. 1–5.

[46]   M. S.-P. Hwang and A. R. Wood, "A new modelling framework for power supply networks with converter based loads and generators - the Harmonic State-Space," in *Proc. of 2012 IEEE International Conference on Power System Technology (POWERCON)*, pp. 1–6.

[47]   C. D. Collins, N. R. Watson, and A. R. Wood, "Unbalanced SSSC modelling in the harmonic domain," *7th Int. Power Eng. Conf. IPEC 2005*, vol. 2, pp. 705–710, Nov. 2005.

[48]   J. Kwon, X. Wang, C. L. Bak, and F. Blaabjerg, "Harmonic instability analysis of single-phase grid connected converter using Harmonic State Space (HSS) modeling method," in *2015 IEEE Energy Conversion Congress and Exposition (ECCE)*, 2015, pp. 2421–2428.

[49]   S. B. Kjaer, J. K. Pedersen, and F. Blaabjerg, "A review of single-phase grid-connected inverters for photovoltaic modules," *IEEE Trans. Ind. Appl.*, vol. 41, no. 5, pp. 1292–1306, Sep. 2005.

[50]   J. He, Y. W. Li, D. Bosnjak, and B. Harris, "Investigation and resonances damping of multiple PV inverters," in *2012 Twenty-Seventh Annual IEEE Applied Power Electronics Conference and Exposition (APEC)*, 2012, pp. 246–253.

[51]   D. G. Infield, P. Onions, A. D. Simmons, and G. A. Smith, "Power quality from multiple grid-connected single-phase inverters," *IEEE Trans. Power Deliv.*, vol. 19, no. 4, pp. 1983–1989, Oct. 2004.

[52]   E. P. I. Association, "Global market outlook for photovoltaics (Available : http://www.epia.org)," 2013.

[53]   K. O. Kovanen, "Photovoltaics and power distribution," *Renew. Energy Focus*, vol. 14, no. May/Jun, 2013.

[54]   K. Ogimoto, I. Kaizuka, Y. Ueda, and T. Oozeki, "A Good Fit: Japan's Solar Power Program and Prospects for the New Power System," *IEEE Power Energy Mag.*, vol. 11, no. 2, pp. 65–74, Mar. 2013.

[55]   C. Winneker, "World`s solar photovoltaic capacity passes 100-gigawatt landmark after strong year (Available : http://www.epia.org/news/)."

[56]   J. He, Y. W. Li, D. Bosnjak, and B. Harris, "Investigation and Active Damping of Multiple Resonances in a Parallel-Inverter-Based Microgrid," *IEEE Trans. Power Electron.*, vol. 28, no. 1, pp. 234–246, Jan. 2013.

[57]   X. Wang, F. Blaabjerg, and P. C. Loh, "Virtual RC Damping of LCL-Filtered Voltage Source Converters With Extended Selective Harmonic Compensation," *IEEE Trans. Power Electron.*, vol. 30, no. 9, pp. 4726–4737, Sep. 2015.

[58]   X. Wang, Y. Pang, P. C. Loh, and F. Blaabjerg, "A Series-LC-Filtered Active Damper With Grid Disturbance Rejection for AC Power-Electronics-Based Power Systems," *IEEE Trans. Power Electron.*, vol. 30, no. 8, pp. 4037–4041, Aug. 2015.

[59]   D. B. W. Abeywardana, B. Hredzak, and V. G. Agelidis, "A Rule-Based Controller to Mitigate DC-Side Second-Order Harmonic Current in a Single-Phase Boost Inverter," *IEEE Trans. Power Electron.*, vol. 31, no. 2, pp. 1665–1679, Feb. 2016.

[60]   S. Bala, T. Tengner, P. Rosenfeld, and F. Delince, "The effect of low frequency current ripple on the performance of a Lithium Iron Phosphate (LFP) battery energy storage system," in *2012 IEEE Energy Conversion Congress and Exposition (ECCE)*, 2012, pp. 3485–3492.

[61]   R. Bojoi, L. R. Limongi, D. Roiu, and A. Tenconi, "Enhanced Power Quality Control Strategy for Single-Phase Inverters in Distributed Generation Systems," *IEEE Trans. Power Electron.*, vol. 26, no. 3, pp. 798–806, Mar. 2011.

[62]   A. Kulkarni and V. John, "Mitigation of Lower Order Harmonics in a Grid-Connected Single-Phase PV Inverter," *IEEE Trans. Power Electron.*, vol. 28, no. 11, pp. 5024–5037, Nov. 2013.

[63]   C. Liu and J.-S. Lai, "Low Frequency Current Ripple Reduction Technique With Active Control in a Fuel Cell Power System With Inverter Load," *IEEE Trans. Power Electron.*, vol. 22, no. 4, pp. 1429–1436, Jul. 2007.

[64]   B. C. Smith, N. R. Watson, A. R. Wood, and J. Arrillaga, "A Newton solution for the harmonic phasor analysis of AC/DC converters," *IEEE Trans. Power Deliv.*, vol. 11, no. 2, pp. 965–971, Apr. 1996.

[65]   N. Kroutikova, C. A. Hernandez-Aramburo, and T. C. Green, "State-space model of grid-connected inverters under current control mode," *IET Electr. Power Appl.*, vol. 1, no. 3, pp. 329–338, May 2007.

[66]   X. Wang, F. Blaabjerg, and W. Wu, "Modeling and Analysis of Harmonic Stability in an AC Power-Electronics-Based Power System," *IEEE Trans. Power Electron.*, vol. 29, no. 12, pp. 6421–6432, Dec. 2014.

[67]   Y. Tang, W. Yao, P. C. Loh, and F. Blaabjerg, "Design of LCL Filters With LCL Resonance Frequencies Beyond the Nyquist Frequency for Grid-Connected Converters," *IEEE J. Emerg. Sel. Top. Power Electron.*, vol. 4, no. 1, pp. 3–14, Mar. 2016.

[68]   E. Twining and D. G. Holmes, "Grid current regulation of a three-phase voltage source inverter with an LCL input filter," *IEEE Trans. Power Electron.*, vol. 18, no. 3, pp. 888–895, May 2003.

[69]   M. Liserre, F. Blaabjerg, and S. Hansen, "Design and control of an LCL-filter-based three-phase active rectifier," *IEEE Trans. Ind. Appl.*, vol. 41, no. 5, pp. 1281–1291, Sep. 2005.

[70]   K. Zhou, Z. Qiu, N. R. Watson, and Y. Liu, "Mechanism and elimination of harmonic current injection from single-phase grid-connected PWM converters," *IET Power Electron.*, vol. 6, no. 1, pp. 88–95, Jan. 2013.

[71]   J. H. R. Enslin and P. J. M. Heskes, "Harmonic interaction between a large number of distributed power inverters and the distribution network," *IEEE Trans. Power Electron.*, vol. 19, no. 6, pp. 1586–1593, Nov. 2004.

[72]   X. Wang, F. Blaabjerg, M. Liserre, Z. Chen, J. He, and Y. Li, "An Active Damper for Stabilizing Power-Electronics-Based AC Systems," *IEEE Trans. Power Electron.*, vol. 29, no. 7, pp. 3318–3329, Jul. 2014.

[73]   S. T. Tentzerakis and S. A. Papathanassiou, "An Investigation of the Harmonic Emissions of Wind Turbines," *IEEE Trans. Energy Convers.*, vol. 22, no. 1, pp. 150–158, Mar. 2007.

[74]   A. Petersson, T. Thiringer, L. Harnefors, and T. Petru, "Modeling and experimental verification of grid interaction of a DFIG wind turbine," *IEEE Trans. Energy Convers.*, vol. 20, no. 4, pp. 878–886, Dec. 2005.

[75]   S. Liang, Q. Hu, and W. J. Lee, "A Survey of Harmonic Emissions of a Commercially Operated Wind Farm," *IEEE Trans. Ind. Appl.*, vol. 48, no. 3, pp. 1115–1123, May 2012.

[76]   J. Sun, "Small-Signal Methods for AC Distributed Power Systems : A Review," *IEEE Trans. Power Electron.*, vol. 24, no. 11, pp. 2545–2554, Nov. 2009.

[77]   X. Feng, J. Liu, and F. C. Lee, "Impedance specifications for stable DC distributed power systems," *IEEE Trans. Power Electron.*, vol. 17, no. 2, pp. 157–162, Mar. 2002.

[78]   S. R. Kaprielian, A. E. Emanuel, R. V. Dwyer, and H. Mehta, "Predicting voltage distortion in a system with multiple random harmonic sources," *IEEE Trans. Power Deliv.*, vol. 9, no. 3, pp. 1632–1638, Jul. 1994.

[79]   X. Wang, F. Blaabjerg, and Z. Chen, "Autonomous Control of Inverter-Interfaced Distributed Generation Units for Harmonic Current Filtering and Resonance Damping in an Islanded Microgrid," *IEEE Trans. Ind. Appl.*, vol. 50, no. 1, pp. 452–461, Jan. 2014.

[80] S. Vesti, T. Suntio, J. Á. Oliver, R. Prieto, and J. A. Cobos, "Effect of Control Method on Impedance-Based Interactions in a Buck Converter," *IEEE Trans. Power Electron.*, vol. 28, no. 11, pp. 5311–5322, Nov. 2013.

[81] J. Sun, "Impedance-Based Stability Criterion for Grid-Connected Inverters," *IEEE Trans. Power Electron.*, vol. 26, no. 11, pp. 3075–3078, Nov. 2011.

[82] J. Sun, Z. Bing, and K. J. Karimi, "Input Impedance Modeling of Multipulse Rectifiers by Harmonic Linearization," *IEEE Trans. Power Electron.*, vol. 24, no. 12, pp. 2812–2820, Dec. 2009.

[83] J. Sun and Z. Bing, "Input impedance modeling of single-phase PFC by the method of harmonic linearization," in *Proc. of Twenty-Third Annual IEEE Applied Power Electronics Conference and Exposition. APEC 2008*, pp. 1188–1194.

[84] K. Ilves, A. Antonopoulos, S. Norrga, and H. P. Nee, "Steady-State Analysis of Interaction Between Harmonic Components of Arm and Line Quantities of Modular Multilevel Converters," *IEEE Trans. Power Electron.*, vol. 27, no. 1, pp. 57–68, Jan. 2012.

[85] X. Yuan and A. Lovett, "Dc-link capacitance reduction in a high power medium voltage modular wind power converter," in *Proc. of 15th European Conference on Power Electronics and Applications (EPE)*, pp. 1–10.

[86] Y. Zhang and Y. W. Li, "Investigation and Suppression of Harmonics Interaction in High-Power PWM Current-Source Motor Drives," *IEEE Trans. Power Electron.*, vol. 30, no. 2, pp. 668–679, Feb. 2015.

[87] B. Vyakaranam, M. Madrigal, F. E. Villaseca, and R. Rarick, "Dynamic harmonic evolution in FACTS via the extended harmonic domain method," in *Proc. of Power and Energy Conference at Illinois (PECI), 2010*, pp. 29–38.

[88] D. G. Holmes and T. A. Lipo, *Pulse Width Modulation for Power Converters: Principles and Practice*. Wiley-IEEE Press, 2003.

[89] R. Teodorescu and F. Blaabjerg, "Flexible control of small wind turbines with grid failure detection operating in stand-alone and grid-connected mode," *IEEE Trans. Power Electron.*, vol. 19, no. 5, pp. 1323–1332, Sep. 2004.

[90] J. Kwon, X. Wang, C. L. Bak, and F. Blaabjerg, "Analysis of harmonic coupling and stability in back-to-back converter systems for wind turbines using Harmonic State Space (HSS)," in *2015 IEEE Energy Conversion Congress and Exposition (ECCE)*, 2015, pp. 730–737.

[91] J. Kwon, X. Wang, C. L. Bak, and F. Blaabjerg, "Harmonic interaction analysis in grid connected converter using Harmonic State Space (HSS) modeling," in *2015 IEEE Applied Power Electronics Conference and Exposition (APEC)*, 2015, pp. 1779–1786.

[92] H. Sandberg, E. Mollerstedt, and Bernhardsson, "Frequency-domain analysis of linear time-periodic systems," *IEEE Trans. Autom. Control*, vol. 50, no. 12, pp. 1971–1983, Dec. 2005.

[93]   N. Pogaku, M. Prodanovic, and T. C. Green, "Modeling, Analysis and Testing of Autonomous Operation of an Inverter-Based Microgrid," *IEEE Trans. Power Electron.*, vol. 22, no. 2, pp. 613–625, Mar. 2007.

[94]   C. Meyer, M. Hoing, A. Peterson, and R. W. D. Doncker, "Control and Design of DC Grids for Offshore Wind Farms," *IEEE Trans. Ind. Appl.*, vol. 43, no. 6, pp. 1475–1482, Nov. 2007.

[95]   Y. Lei, A. Mullane, G. Lightbody, and R. Yacamini, "Modeling of the wind turbine with a doubly fed induction generator for grid integration studies," *IEEE Trans. Energy Convers.*, vol. 21, no. 1, pp. 257–264, Mar. 2006.

[96]   J. L. Agorreta, M. Borrega, J. López, and L. Marroyo, "Modeling and Control of -Paralleled Grid-Connected Inverters With LCL Filter Coupled Due to Grid Impedance in PV Plants," *IEEE Trans. Power Electron.*, vol. 26, no. 3, pp. 770–785, Mar. 2011.

[97]   F. C. Sayas and R. N. Allan, "Generation availability assessment of wind farms," *Transm. Distrib. IEE Proc. - Gener.*, vol. 143, no. 5, pp. 507–518, Sep. 1996.

[98]   J. Skea, D. Anderson, T. Green, R. Gross, P. Heptonstall, and M. Leach, "Intermittent renewable generation and maintaining power system reliability," *Transm. Distrib. IET Gener.*, vol. 2, no. 1, pp. 82–89, Jan. 2008.

[99]   C. T. Force, "Benchmark Systems for Network Integration of Renewable Energy Resources," 2011.

[100]   J. Kwon, X. Wang, C. L. Bak, and F. Blaabjerg, "The modeling and harmonic coupling analysis of multiple-parallel connected inverter using Harmonic State Space (HSS)," in *2015 IEEE Energy Conversion Congress and Exposition (ECCE)*, 2015, pp. 6231–6238.

[101]   S. Anand and B. G. Fernandes, "Reduced-Order Model and Stability Analysis of Low-Voltage DC Microgrid," *IEEE Trans. Ind. Electron.*, vol. 60, no. 11, pp. 5040–5049, Nov. 2013.

[102]   J. B. Kwon, X. Wang, C. L. Bak, and F. Blaabjerg, "Modeling and simulation of DC power electronics systems using Harmonic State Space (HSS) method," in *2015 IEEE 16th Workshop on Control and Modeling for Power Electronics (COMPEL)*, 2015, pp. 1–8.

[103]   K. J. Karimi, A. Booker, and A. Mong, "Modeling, simulation, and verification of large DC power electronics systems," in *, 27th Annual IEEE Power Electronics Specialists Conference, 1996. PESC '96 Record*, 1996, vol. 2, pp. 1731–1737 vol.2.

[104]   K. K. Tse, H. S.-H. Chung, S. Y. R. Hui, and H. C. So, "A comparative study of carrier-frequency modulation techniques for conducted EMI suppression in PWM converters," *IEEE Trans. Ind. Electron.*, vol. 49, no. 3, pp. 618–627, Jun. 2002.

[105]   J. Balcells, A. Santolaria, A. Orlandi, D. Gonzalez, and J. Gago, "EMI reduction in switched power converters using frequency Modulation techniques," *IEEE Trans. Electromagn. Compat.*, vol. 47, no. 3, pp. 569–576, Aug. 2005.

[106] W. Yan, W. Li, and R. Liu, "A Noise-Shaped Buck DC #x2013;DC Converter With Improved Light-Load Efficiency and Fast Transient Response," *IEEE Trans. Power Electron.*, vol. 26, no. 12, pp. 3908–3924, Dec. 2011.

[107] V. Vorperian, "A ripple theorem for PWM DC-to-DC converters operating in continuous conduction mode," in *Power Electronics Specialists Conference, 2004. PESC 04. 2004 IEEE 35th Annual*, 2004, vol. 1, p. 28–35 Vol.1.

[108] P. Patra, A. Patra, and N. Misra, "A Single-Inductor Multiple-Output Switcher With Simultaneous Buck, Boost, and Inverted Outputs," *IEEE Trans. Power Electron.*, vol. 27, no. 4, pp. 1936–1951, Apr. 2012.

[109] X. Yue, F. Wang, S. Yang, F. Zhuo, and Y. Pei, "Modeling for input impedance of buck converters and its application analysis," in *2015 IEEE Energy Conversion Congress and Exposition (ECCE)*, 2015, pp. 2400–2406.

[110] X. Yue, Y. Zhu, S. Yang, Y. Chen, F. Zhuo, and Y. Pei, "A modulation and sampling based modeling method for the nonlinearities of power converters and its application analysis," *17th Eur. Conf. Power Electron. Appl. EPE15 ECCE-Eur.*, pp. 1–10, Sep. 2015.

[111] J. Kwon, X. Wang, F. Blaabjerg, and C. Bak, "Frequency Domain Modeling and Simulation of DC Power Electronic Systems Using Harmonic State Space (HSS) Method," *IEEE Trans. Power Electron.*, vol. PP, no. 99, pp. 1–1, 2016.

[112] A. G. Yepes, F. D. Freijedo, O. Lopez, and J. Doval-Gandoy, "Analysis and Design of Resonant Current Controllers for Voltage-Source Converters by Means of Nyquist Diagrams and Sensitivity Function," *IEEE Trans. Ind. Electron.*, vol. 58, no. 11, pp. 5231–5250, Nov. 2011.

[113] J. Kwon, X. Wang, and F. Blaabjerg, "Impedance based analysis and design of harmonic resonant controller for a wide range of grid impedance," in *2014 IEEE 5th International Symposium on Power Electronics for Distributed Generation Systems (PEDG)*, 2014, pp. 1–8.

[114] J. J. Rico, E. Acha, and T. J. E. Miller, "Harmonic domain modelling of three phase thyristor-controlled reactors by means of switching vectors and discrete convolutions," *IEEE Trans. Power Deliv.*, vol. 11, no. 3, pp. 1678–1684, Jul. 1996.

[115] G. N. Bathurst, N. R. Watson, and J. Arrillaga, "Adaptive frequency-selection method for a Newton solution of harmonics and interharmonics," *Gener. Transm. Distrib. IEE Proc.-*, vol. 147, no. 2, pp. 126–130, Mar. 2000.

[116] A. Ramirez, "The Modified Harmonic Domain: Interharmonics," *IEEE Trans. Power Deliv.*, vol. 26, no. 1, pp. 235–241, Jan. 2011.

[117] Robert W. Erickson, Dragan Maksimovic, *Fundamentals of Power Electronics*. Springer US, 2001.

[118] Jos Arrillaga and Neville. R Watson, *Power System Harmonics, Second Edition*. Wiley-IEEE Press, 2004.

[119] P. Pejovic and J. W. Kolar, "Exact Analysis of Three-Phase Rectifiers With Constant Voltage Loads," *IEEE Trans. Circuits Syst. II Express Briefs*, vol. 55, no. 8, pp. 743–747, Aug. 2008.

[120] J. Sun and K. J. Karimi, "Small-signal input impedance modeling of line-frequency rectifiers," *IEEE Trans. Aerosp. Electron. Syst.*, vol. 44, no. 4, pp. 1489–1497, Oct. 2008.

[121] A. Semlyen, "Steady-state analysis of nonlinear dynamic systems with periodic excitation based on linearization in harmonic space," *Can. Electr. Eng. J.*, vol. 11, no. 3, pp. 114–117, Jul. 1986.

[122] G. N. Bathurst, B. C. Smith, N. R. Watson, and J. Arrillaga, "Modelling of HVDC transmission systems in the harmonic domain," *IEEE Trans. Power Deliv.*, vol. 14, no. 3, pp. 1075–1080, Jul. 1999.

[123] Kwon. J., Wang. X., Bak. C. L., Blaabjerg. F., Hwang. M., Wood. A. R., Watson. N. R., and Esparza. M., "Measurement of Phase Dependent Impedance for 3-phase Diode Rectifier," in *2016 IEEE 42nd Annual Conference of IEEE Industrial Electronics Society (IECON 2016)*, 2016, pp. 1–8.

[124] E. V. Larsen, D. H. Baker, and J. C. McIver, "Low-order harmonic interactions on AC/DC systems," *IEEE Trans. Power Deliv.*, vol. 4, no. 1, pp. 493–501, Jan. 1989.

[125] J. Kwon, X. Wang, F. Blaabjerg, and C. L. Bak, "Comparison of LTI and LTP models for stability analysis of grid converters," in *2016 IEEE 17th Workshop on Control and Modeling for Power Electronics (COMPEL)*, 2016, pp. 1–8.

[126] T. Messo, A. Aapro, and T. Suntio, "Generalized multivariable small-signal model of three-phase grid-connected inverter in DQ-domain," in *2015 IEEE 16th Workshop on Control and Modeling for Power Electronics (COMPEL)*, 2015, pp. 1–8.

[127] J. Shen, S. Schroder, H. Stagge, and R. W. De Doncker, "Precise modeling and analysis of DQ-frame current controller for high power converters with low pulse ratio," in *2012 IEEE Energy Conversion Congress and Exposition (ECCE)*, 2012, pp. 61–68.

[128] L. Harnefors, "Modeling of Three-Phase Dynamic Systems Using Complex Transfer Functions and Transfer Matrices," *IEEE Trans. Ind. Electron.*, vol. 54, no. 4, pp. 2239–2248, Aug. 2007.

[129] V. A. Caliskan, G. C. Verghese, and A. M. Stankovic, "Multi-frequency averaging of DC/DC converters," in *, IEEE Workshop on Computers in Power Electronics, 1996*, 1996, pp. 113–119.

[130] S. C. Chung, S. R. Huang, J. S. Huang, and E. C. Lee, "Applications of describing functions to estimate the performance of nonlinear inductance," *Sci. Meas. Technol. IEE Proc. -*, vol. 148, no. 3, pp. 108–114, May 2001.